UNIVERSITY OF SOUTHAMPTON

DEPARTMENT OF PHYSICS AND ASTRONOMY

School of Science

Characterisation of Novel Flexoelectric Bimesogens

Matthew John Clarke

Thesis for the degree of Doctor of Philosophy

April 2004

UNIVERSITY OF SOUTHAMPTON

ABSTRACT

DEPARTMENT OF PHYSICS AND ASTRONOMY
SCHOOL OF SCIENCE

Doctor of Philosophy

CHARACTERISATION OF NOVEL FLEXOELECTRIC BIMESOGENS

by Matthew John Clarke

The research presented in this thesis relates to the flexoelectro-optic switching effect observed in bimesogenic chiral nematic liquid crystal materials. By coupling flexoelectrically to an applied electric field it is possible for the optic axis of a chiral nematic liquid crystal material to be rotated, inducing a change in the optic properties of the material. This rotation of the optic axis is fast, in-plane, and the magnitude of rotation is proportional to the amplitude of the applied field. As well as being dependent on the applied field amplitude, the flexoelectro-optic switching process has no threshold, resulting in 'v-shaped' switching.

The bimesogenic nematic liquid crystal materials studied in this work have been found to be particularly suited for flexoelectro-optic switching, producing extremely high optic axis rotation (> 45°) and fast response times (< 1 ms). By using bimesogenic liquid crystals, it is possible to have both high dipole moments and a low dielectric anisotropy, increasing the potential for flexoelectric coupling and decreasing the undesirable effects of dielectric coupling, respectively. The ratio of the effective flexoelectric coefficient to the average of the splay and bend elastic constants, $\bar{e}/K$, serves as a figure of merit for a material's suitability for flexoelectro-optic switching. Typically, for a chiral nematic monomesogenic material, the ratio $\bar{e}/K$ is less than 0.6 C N^{-1} m^{-1}; however, for the bimesogenic materials studied in this work the ratio ranges from 0.8 to 2.35 C N^{-1} m^{-1}.

Table of Contents

Declaration

This thesis is the result of work done by the author whilst in registered postgraduate candidature at the University of Southampton. The work is entirely original except where due reference is made and no portion of the work referred to in this thesis has been submitted in support of an application for another degree or qualification at this or any other university or institute of learning. Results obtained in collaboration with others are clearly indicated and may be submitted by them for another degree.

Matthew John Clarke

Acknowledgements

Firstly, I would like to thank my supervisor Professor Coles. Thanks Harry for your constant encouragement, for always seeing the positive side when things went wrong and for always having a good idea for me to try.

This work would not have been possible with out the help and advice of both Marcus Coles and Bronje Musgrave.

I am extremely grateful to Marcus for taking me under his wing when I joined the group and for always supplying useful advice and suggestions.

I would like to thank Bronje for instructing me in the ways of flexoelectricity, her support and for being a proof-reader extraordinaire.

Special thanks to:

Steve Morris for his physical property measurements in Chapters 3 and 6.
Jon Willmott for his rotating analyser measurements shown in Chapter 7.
Andrew Blatch for producing the bulk of the liquid crystals studied in this work.
Steve Perkins for synthesising the initial materials studied in Chapter 5.

I would like to thank the following members of the liquid crystal group, past and present, for their help: Chris Noot, Dean Shoosmith, Anna Remnant, Piers de Hondt, Petra Lehmann, Mikhail Pivnenko, Yong-il Cho, Cecile Schott and Leona Hope.

I am grateful to the EPSRC for their financial support.

Finally, I would like to thank my mum and sister for their continued support and encouragement.

Chapter One

1 Introduction to the Thesis

1.1 Preamble

This Ph.D. project is concerned with the effects of flexoelectricity in bimesogenic liquid crystals and the potential of these systems.

Initially it was thought that there were only three phases of matter: solid, liquid and gas. However, this is not correct, as there is a certain class of materials that do not directly undergo a transition from solid to liquid, but pass though a number of intermediate phases before becoming liquid. These special phases exhibit some of the properties of both liquids and solids and are known as mesophases ('middle' phases) or more often as liquid crystals.[1] The molecules of these mesophases possess varying degrees of positional and orientational order. Molecules in liquid crystal phases are fluid, but unlike isotropic liquids, the mesophases have anisotropic physical attributes. It is these properties that are responsible for the many interesting and useful features of the liquid crystal phase. This thesis is mainly concerned with the optical properties of liquid crystals and the effects of an electric field on these properties. The focus of this work is the relatively recently discovered electro-optic switching process known as the flexoelectro-optic effect.[2] The work herein expands on the relatively small amount of research that has been produced concerning the flexoelectro-optic effect and the influence of molecular shape. An outline of the thesis is presented below.

1.2 Outline of the thesis

In Chapter 2, a cross-section of the theoretical background of liquid crystal science is presented. The science discussed is that which is relevant to the experimental work presented in this thesis.

In Chapter 3, the experimental techniques and apparatus used in the experimental work are introduced and discussed. Additionally, a study of the flexoelectric properties of a simple monomesogen is described.

Chapter 4 compares and contrasts directly two very different methods for determining the flexoelectric properties of a nematic liquid crystal.

In Chapter 5, a homologous series of oxy-fluorobiphenyl bimesogens are introduced. The flexoelectro-optic properties of mixtures between members of the homologous series are then studied. The effect on the flexoelectro-optic properties of increasing or reducing the chirality of the system is examined.

A homologous series of non-symmetric bimesogens is introduced in Chapter 6. The homologues comprise an oxy-fluorobiphenyl mesogenic unit and an oxy-cyanobiphenyl mesogenic unit. The flexoelectro-optic properties of the homologous series are studied. Also, a series of mixtures between two of the homologues is examined. Finally, as in Chapter 5, the effects of chirality on the flexoelectro-optic properties are investigated.

In Chapter 7, the effect on the flexoelectric properties of introducing an ester-linking group into the molecular structure of the symmetric bimesogens is examined. An attempt is made to optimise the flexoelectro-optic properties of these ester-based bimesogens by combining them with a selection of different liquid crystal materials. This work was carried out on mixtures with the non-symmetric bimesogens studied in Chapter 6 and with a selection of commercially available liquid crystalline materials.

Chapter 8 concludes the thesis by summarising the experimental observations made in Chapters 4 to 7. Some suggestions for the direction of future work are also presented.

References

1 Lehmann, O., Z. Physikal. Chem. **4** 462 (1889)

2 Patel, J. S., and Meyer, R. B., Phys. Rev. Lett. **58(15)** 1538 (1987)

Chapter Two

2 Theory

2.1 Introduction

This body of work is concerned with thermotropic liquid crystal phases. Thermotropic liquid crystalline phases occur as a function of temperature, they can be enantiotropic (exhibiting the same phase sequence on heating or cooling) or monotropic (exhibiting a different phase sequence on cooling).

For a molecular material to be a thermotropic liquid crystal its molecules have to be geometrically anisotropic (e.g. rod-like or disc-like in shape), have permanent dipolar groups and have a high anisotropy of polarisability. Depending on the molecular geometry and composition, the system may exhibit one or more types of liquid crystal mesophase before becoming an isotropic liquid. The work in this thesis is concerned only with rod-shaped or calamitic molecules. In a liquid crystal phase, rod-shaped molecules tend to prefer to align with their long axes parallel to those of neighbouring molecules. Generally the ratio of length to width of the molecules is four to one or higher. The structure of a typical thermotropic liquid crystal (See Figure 2.1) is made up of two or more aromatic rings, a bridging group (A-B) and two terminal groups (X and Y).

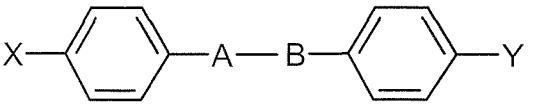

Figure 2.1 Typical Thermotropic Liquid Crystal Structure.

Generally, X would be a polar group and Y would be an alkyl chain. By adjusting the alkyl chain length, the bridging group, or the polar group, it is possible to change the major properties of the liquid crystal. A molecular unit that, when substituted on to a non-mesogenic chemical species, introduces liquid crystallinity is known as a mesogenic unit

or mesogen. Molecules containing a singular mesogenic unit are known as monomesogens, while molecules containing two mesogenic units separated by a spacer unit are known as bimesogens. In other work, bimesogens have been called mesogenic twin molecules, bismesogens, dimesogens or dimers; but in this work they will only be referred to as bimesogens. Molecules are not limited to containing one or two mesogenic units; For example, polymeric liquid crystals may contain many mesogenic groups.

This chapter comprises a number of sections that introduce the theory relevant to this work. In Section 2.2 the concept of the order parameter is introduced; the order parameter is used to quantify the order of a liquid crystal phase. The nematic liquid crystal phases are briefly introduced in Section 2.3. A number of smectic liquid crystal phases are discussed in Section 2.4. The nematic phase is discussed in greater detail in Section 2.5, as the concepts of elastic deformation of the director field and the free energy density of the nematic phase are introduced. In Section 2.6, the chiral nematic liquid crystal phase is discussed in greater depth. Section 2.7 discusses the optical properties of the chiral nematic phase. The effects of an applied electric field on the chiral nematic phase, including the effects of flexoelectricity, are examined in Section 2.8. Finally, in Section 2.9 the key points of the chapter are summarised.

2.2 The order parameter

In a crystalline solid, the constituent molecules are generally perfectly aligned (i.e. on a lattice). Conversely, in a liquid the molecules are randomly orientated. The arrangement of the molecules in a liquid crystalline material shows similarities to both liquids and solids. The anisotropically-shaped liquid crystal molecules generally prefer to be orientated in roughly the same direction; the vector along the average orientation direction is defined by the vector **n**. The director does not give any indication of the orientational order of the phase. To quantify the degree of orientational order an order parameter,[1] S, is defined by a thermal average over the molecular ensemble:

$$S = \frac{1}{2}\left\langle 3\cos^2\Theta - 1\right\rangle, \qquad (2.1)$$

where θ is the angle between the long axis of an individual molecule and the director of the liquid crystal. It is clear that the order parameter relates to the orientation order of the phase. If the molecules are aligned perfectly with no thermal fluctuations, as in a

crystalline solid, then S = 1. In an isotropic liquid where the molecules are randomly orientated (S = 0). Typically, a liquid crystal has a value of S lying between 0.3 and 0.9.

2.3 The nematic phase

The nematic phase, denoted N, is the least ordered of the liquid crystal phases. It is characterised by long range orientational ordering and the random location of the molecules. The molecules are free to move in any direction, but their long axes are, on average, orientated parallel to each other (see Figure 2.2(a)). The preferred direction of orientation is given by the director **n**, and the director is non-polar in the nematic phase, i.e. **n** = **-n**. The phase has complete rotational symmetry about the director. For nematics, the order parameter usually has a value between 0.3 and 0.7.

Mesogenic molecules can contain chiral centres, with the result that these molecules can collectively form chiral structures. A chiral structure is defined as a structure that lacks mirror symmetry. The least ordered phase formed by chiral molecules is the chiral nematic phase, denoted N*. In the chiral nematic phase there exists an in-plane rotation of the director (see Figure 2.2(b)), this rotation can produce a left- or right-handed helical director configuration. The helical pitch, P, is defined as the distance over which the director rotates by 360° (see Figure 2.2(c)). The director planes themselves possess no long range positional order (as in the nematic phase), thus the director is non-polar, i.e. **n** = **-n**.

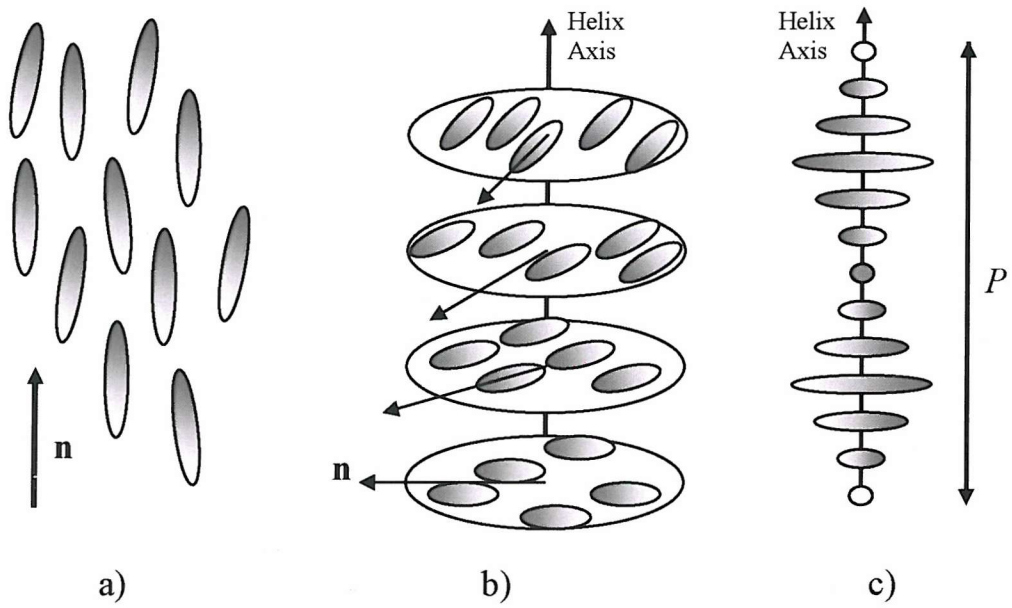

Figure 2.2 A diagrammatic representation of the a) nematic phase, b) the chiral nematic phase and c) the definition of pitch.

It is possible to make an achiral nematic into a chiral nematic by doping it with a chiral additive; this relies on the interaction between the adjacent molecules.[2] Conversely, an achiral material can be formed from a mixture of chiral molecules with left- and right-handed chirality.

The chiral nematic phase has different optical properties to those of the achiral nematic phase because of its helical director structure. The bulk of work in this thesis is concerned with the optical and physical properties of chiral nematics, which are discussed in much greater detail later in this chapter.

2.4 The smectic phases

Smectic liquid crystal phases have a diffused layered structure. Thus, as well as having orientational order, the smectic liquid crystal phases have some degree of positional order. The interactions between adjacent molecules within a layer are much stronger than the interactions between molecules in adjacent layers: this makes it possible for the layers to slide past each other easily.[3] There are many different smectic phases and they are defined by the director arrangement within the layers. In this work, only the most common smectic phases are discussed.

The least ordered of the smectic liquid crystal phases is the smectic A phase, commonly denoted S_A. In the smectic A phase, the director lies normal to the layer planes, **k**, as shown in Figure 2.3. The phase possesses rotational symmetry about the director. The layers spacings can vary from approximately half to twice the length of an individual molecule[3,4] depending on the material. It is possible to consider each layer as an individual two-dimensional liquid, as it is difficult for molecules to diffuse between layers.

As with the nematic phase, a smectic A phase may be composed of achiral or chiral molecules. Smectic A phases containing chiral molecules are denoted smectic A* or S_A*. Even containing chiral centres, the smectic A phase cannot display a continuous dislocation-free helical structure. As a result of this, there is no difference in the optical properties between unperturbed achiral and chiral smectic A liquid crystal phases. However, the application of an electric field orthogonally the director of a chiral smectic A material induces a tilting of the molecules in the plane normal to the field. This gives rise to an optical effect known as electroclinic switching.[5]

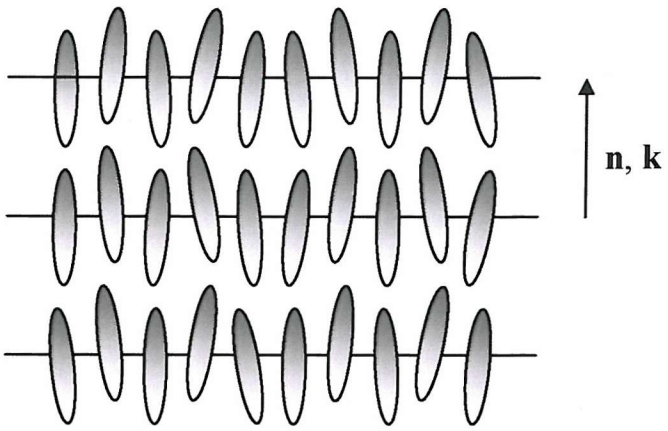

Figure 2.3 A diagrammatic representation of the smectic A phase.

Another commonly encountered smectic phase is the smectic C phase, denoted S_C. In this phase the director in each smectic layer is aligned at an angle to the layer normal. This is illustrated in Figure 2.4(a). As with the smectic A phase, the smectic C phase can be considered as a two-dimensional liquid. There is also a chiral form of this mesophase, known as the smectic C* or S_C* phase. The smectic C* phase is illustrated in Figure 2.4(b). The chirality of the molecules imposes a helical structure on the phase as the director precesses about a cone from one layer to the next. The cone angle is defined as the angle between the layer normal and the director. For a smectic A or C phase the order parameter, S, has been seen to be as high as 0.9.[3]

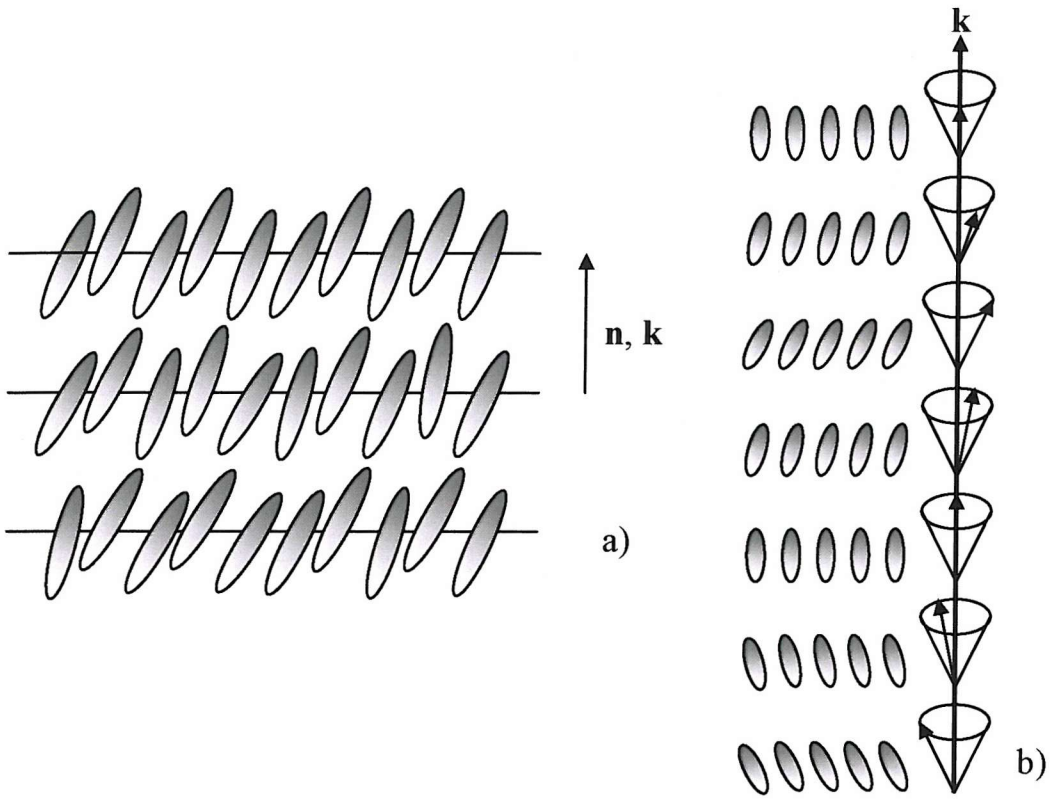

Figure 2.4 A diagrammatic representation of a) the smectic C phase and b) the chiral smectic C phase.

There are many other smectic phases, such as the hexatic phases illustrated in Figure 2.5. These phases possess additional degrees of positional order within the layer planes. The higher order phases are of little relevance to this work, and will not be discussed further.

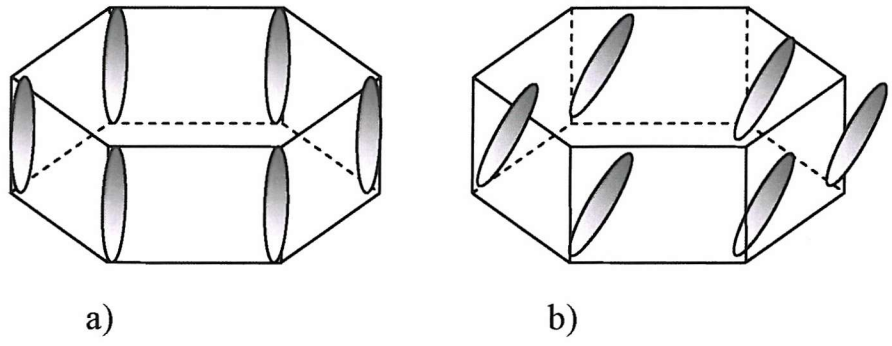

Figure 2.5 A representation of the in-plane structure of two hexatic smectic phases.

2.5 The free energy of a nematic system

The molecules in a mesophase can have their arrangement altered by external forces. These external forces are usually the result of a mechanical change, e.g. inducing the liquid

crystal to flow, or by applying an electromagnetic field. The free energy of a nematic medium in its equilibrium state is usually derived using the Eriksen-Leslie method,[3] where the elastic deformations of the director are considered in a continuous medium. Frank's theory[6] results in the following equation for the elastic free energy $f_{elastic}$ of a nematic in its equilibrium state:

$$f_{elastic} = \frac{1}{2}K_{11}(\nabla \cdot \mathbf{n})^2 + \frac{1}{2}K_{22}(\mathbf{n} \cdot \nabla \times \mathbf{n})^2 + \frac{1}{2}K_{33}(\mathbf{n} \times \nabla \times \mathbf{n})^2, \qquad (2.2)$$

where K_{11} is the splay elastic constant, K_{22} is the twist elastic constant and K_{33} is the bend elastic constant. The free terms in the elastic free energy equation represent splay, twist and bend deformations of the director field, respectively. These three deformations are represented pictorially in Figure 2.6. Any elastic deformation of a nematic liquid crystal can be represented by a combination of these three deformations.

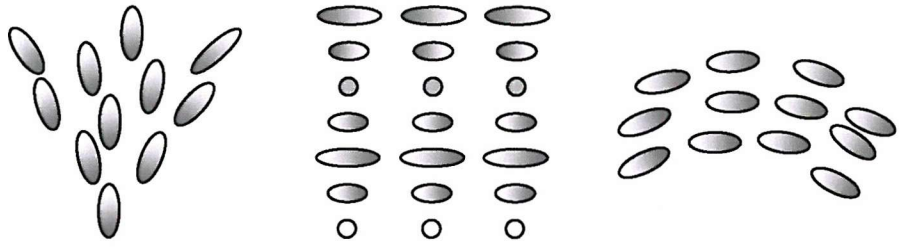

Figure 2.6 A pictorial representation of the splay, twist and bend deformations that can be exhibited by a nematic liquid crystal.

The elastic constants are always positive as the undeformed nematic phase must possess a minimum free energy. Typically, the elastic constants have values of the order of 10^{-11} N. The splay elastic constant is generally very slightly smaller than the bend elastic constant. The twist elastic constant tends to be the smaller of the three.[3] The elastic constants decrease rapidly as the temperature of the sample increases but the ratios of the constants only vary slightly with temperature.[4]

2.6 The chiral nematic phase

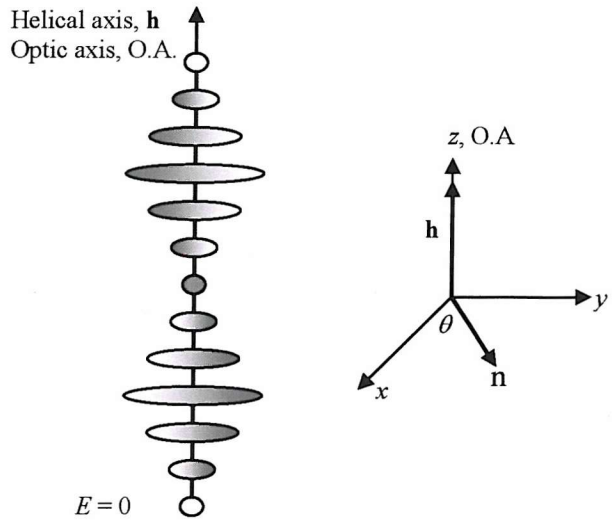

Figure 2.7 The director orientation in the chiral nematic phase defined in a Cartesian reference frame.

The chiral nematic phase was introduced briefly in Section 2.3. The director arrangement of a chiral nematic liquid crystal can be described in a Cartesian reference frame, where the helix axis **h** lies parallel to the z-axis (see Figure 2.7). This means that the director **n**, is confined to the xy-plane. The director is defined as

$$\begin{aligned} n_x &= \cos\theta, \\ n_y &= \sin\theta, \\ n_z &= 0. \end{aligned} \tag{2.3}$$

The angle θ between the director in successive xy-planes is taken to be zero when the director is parallel to the x-axis, and it is given by

$$\theta = \frac{2\pi}{P} z = kz . \tag{2.4}$$

The variable k is the modulus of the helical wavevector of the material and P is the pitch, as was introduced in Section 2.3. The sign of P is defined as being positive for a right-handed helix.

Generally the pitch has a reciprocal relationship to the temperature of the chiral nematic sample.[7] As the temperature increases the angle θ between successive *xy*-planes increases; thus reducing the pitch of the phase. In the less common cases where the pitch increases with T, variations in molecular packing arrangements are generally considered to the cause of the unusual behaviour.[8] An example of this is twist inversion, where a helix unwinds and then reforms with opposite handedness. This generally occurs over only a narrow temperature range, and manifests itself as a sudden decrease in pitch. Most of the interesting optical properties of chiral nematic liquid crystals, including those in this work, are a result of the helical pitch.

2.7 The optical properties of the chiral nematic phase

The chiral nematic phase can have a significant effect on the propagation of light through the material. The nature of this effect depends on both the properties of the light (i.e. wavelength and polarisation) and the properties of the chiral nematic phase. The relative direction of travel for the light compared to the helix axis of the chiral nematic phase is also of great importance.

2.7.1 Selective reflection and optical rotation

When light of a certain wavelength propagates along a direction parallel to the helix axis, it may be selectively reflected by the chiral nematic liquid crystal. An overview of the theory derived to describe the selective reflection properties of the chiral nematic phase was presented by both Kats[9] and Nityananda.[10] They proposed that light propagating through the chiral nematic phase can be considered to be interacting with a series of ellipsoid molecules in a spiral arrangement, with pitch equal to the helical pitch length of the phase and a repeat length of *P*/2. The geometry of the system was defined to match that of Figure 2.7, the molecules spiral about the *z*-axis though an angle θ between successive *xy*-planes as defined in Equation 2.4. Only the key results of this theoretical treatment are outlined here.

The theory shows that there is a wavelength of light, λ_0, which is selectively reflected by the chiral nematic liquid crystal, is related to the properties of the chiral nematic phase by the equation

$$\lambda_0 = \bar{n}P, \qquad (2.5)$$

where $\bar{n}$ is the average refractive index of the phase and P its helical pitch. Clearly the selective reflection wavelength is directly proportional to the helical pitch of the chiral nematic material. It is also shown that there is a reflection band centred on the selective reflection wavelength, given by

$$\Delta\lambda = P\delta n, \tag{2.6}$$

where δn is the microscopic refractive index anisotropy. The form of the spectrum reflected by a sample of semi-infinite thickness illuminated by light at normal incidence parallel to the helix axis, is shown in Figure 2.8.

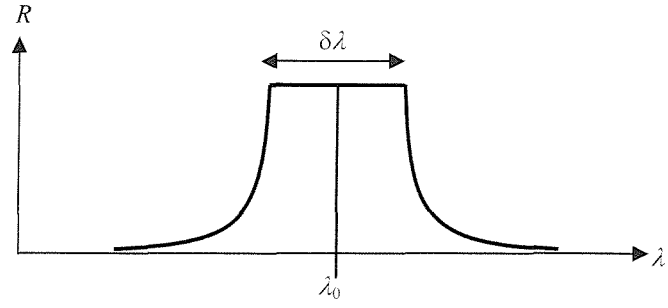

Figure 2.8 The theoretical form of the reflected spectrum of light for a chiral nematic liquid crystal. The illuminated light is at normal incidence, parallel to the helix axis.

For a real physical sample of finite thickness, the reflection spectrum is centred on λ_0 but possesses additional sidebands outside the main reflection band.[3,11]

The theory also shows that for a right-handed helix, right-circularly polarised light is reflected while left-circularly polarised light is transmitted through the sample. The left-circularly polarised light is transmitted because the electric field vector rotates in the same direction as the sample director along the $+z$-axis. However right-circularly light has its electric field vector rotating in the opposite direction to that of the sample's director and is hence reflected.

The chiral nematic material is also optically active, inducing a rotation in the plane of polarisation of incident light. Theory suggests that the rotary power on light of wavelength λ is governed by the following equation:

$$\rho = \frac{\pi P(\delta n)^2}{4\lambda^2\left[1-\left(\lambda^2/\lambda_0^2\right)\right]}. \qquad (2.7)$$

This behaviour has been confirmed experimentally.[12,13] The form of the optical rotatory power of the chiral nematic phase as a function of λ is illustrated in Figure 2.9.

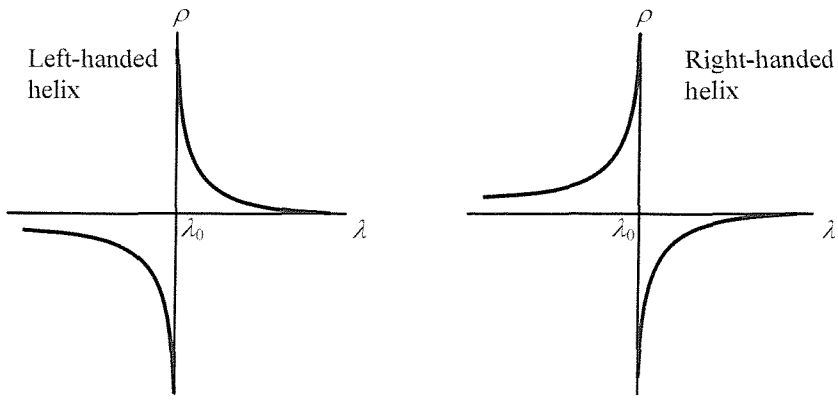

Figure 2.9 The optically rotary power of chiral nematic liquid crystal, acting on light of wavelength λ passing through it.

The optical rotary power at $\lambda = \lambda_0$ is zero and it can be seen that the sign of optical rotary power changes. For $\lambda >> \lambda_0$ the rotary power tends towards zero, while for $\lambda << \lambda_0$ it tends to $\pi P(\delta n)^2/(4\lambda^2)$.

When observing a chiral nematic material at an angle that is not quite parallel to the direction of the helix axis a variation in the selectively reflected colour is observed. A theoretical description of light propagating at an angle that is not parallel to the helical axis would be complex to derive, and no analytical solution has been found to date. It is possible to approximate this complex reflection process by considering the chiral nematic phase as a periodic layered structure (with a repeat distance of $P/2$). Bragg reflection from these "layers" can then be considered.[14] Though it is not of relevance to this work, for completeness the derived equation for a first order reflection is reproduced here

$$\lambda = \bar{n}P\cos\left[\frac{1}{2}\left(\sin^{-1}\left(\frac{\sin\theta_i}{\bar{n}}\right)+\sin^{-1}\left(\frac{\sin\theta_r}{\bar{n}}\right)\right)\right], \qquad (2.8)$$

where θ_i and θ_r are the external angles of incidence and reflection, respectively. This approximation holds for small angles and it is worth noting that for normal incidence ($\theta_i = \theta_r = 0$) this equation becomes $\lambda = \bar{n} P$, as seen earlier in Equation 2.5.

2.7.2 Macroscopic birefringence of chiral nematics

A birefringent material is one that exhibits different refractive indices depending on the direction of propagation and the polarisation of the incident light. Thus a beam incident on a birefringent material can be split into two separate beams of orthogonal polarisations.

The liquid crystal materials considered in this work are uniaxially birefringent; this means that they possess a single axis of symmetry known as the optic axis. As there is a circular symmetry about the optic axis, the orthogonal components of light propagating along the optic axis do not experience different refractive indices and hence there is no double refraction. However, when light propagates in a direction at an angle to the optic axis there is double refraction. The refractive index normal to the optic axis is called the ordinary refractive index, while the refractive index parallel to the optic axis is known as the extraordinary refractive index. For light incident at an angle to the optic axis, the electric field vector can be resolved into components along the optic axis and normal to it. The component normal to the optic axis will experience the ordinary refractive index, n_o, while the component parallel to the optic axis experiences the extraordinary refractive index, n_e. As a result of the difference in the refractive indices, the components will propagate with different phase velocities in the material.

The refractive indices of a uniaxially birefringent material can be represented pictorially by considering wavelets in the crystal, as shown in Figure 2.10. The birefringence of a material is defined by:

$$\Delta n = n_e - n_o. \qquad (2.9)$$

If $n_e > n_o$, the material is called positively birefringent and has an ordinary component with a faster phase velocity than that of the extraordinary component. If $n_e < n_o$ then the material is negatively birefringent, with the extraordinary component having a faster phase velocity.

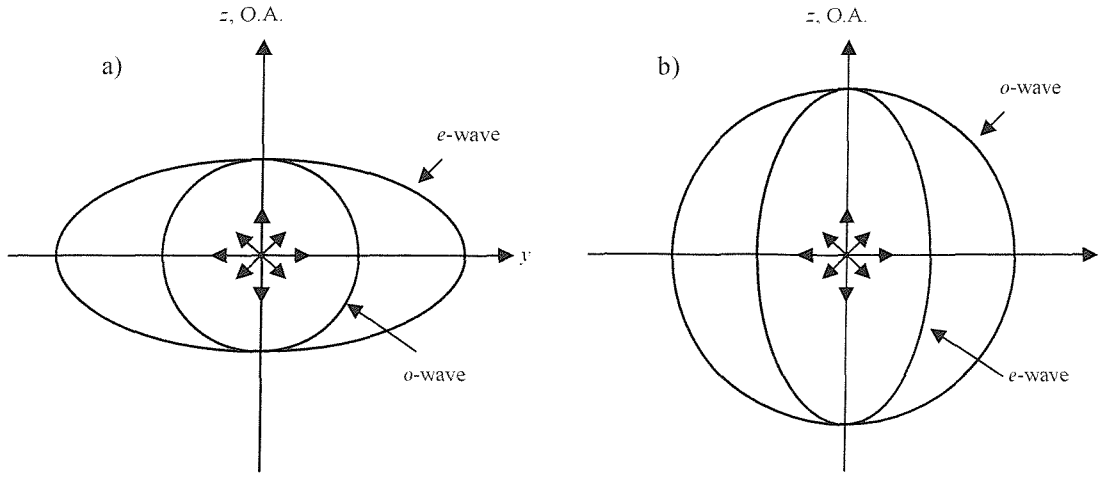

Figure 2.10 A representation of wavelets in a uniaxially anisotropic material with a) positive birefringence and b) negative birefringence.

For light propagating in a direction normal to the optic axis of a birefringent material, the phase difference, $\Delta\phi$, between the ordinary and extraordinary rays is given by

$$\Delta\phi = \frac{2\pi}{\lambda} d\Delta n, \tag{2.10}$$

where λ is the wavelength of light and d is the thickness of the material along the direction of propagation.

For an achiral nematic material (and for a smectic A material) the bulk birefringence is positive provided the director points in the same direction throughout the sample. However, for a chiral nematic the birefringence of the bulk is negative because of the helical structure of the phase. Microscopic refractive indices ($n_{\parallel}$ and $n_{\perp}$) are defined in relation to the shape of the molecules. For an achiral nematic material $n_o = n_{\perp}$ and $n_e = n_{\parallel}$. However, in an undeformed chiral nematic material, the long axes of the molecules (and thus $n_{\parallel}$) lie normal to the helical axis. By symmetry this implies that the optic axis of the bulk material lies along the $n_{\perp}$ axis, which gives

$$n_e = n_{\perp}, \tag{2.11}$$

for chiral nematic materials. It has also been shown[15] for chiral nematic materials that the macroscopic ordinary refractive index is given by

$$n_o = \sqrt{\frac{1}{2}\left(n_{\parallel}^2 + n_{\perp}^2\right)}. \qquad (2.12)$$

The macroscopic birefringence Δn of the chiral nematic material is thus related to the microscopic refractive indices by

$$\Delta n = n_e - n_o = n_{\perp} - \sqrt{\frac{1}{2}\left(n_{\parallel}^2 + n_{\perp}^2\right)}. \qquad (2.13)$$

2.7.3 Blue phases and their optical properties

For liquid crystals exhibiting chiral nematic phases of sufficiently short pitch, there exist additional phases, often brightly coloured, between the chiral nematic phase and the isotropic phase. These colourful phases are known as blue phases (although they are not always blue).

There are three different kinds of blue phase, known as BP I, BP II and the 'fog' phase (sometimes called BP III). The number of blue phases that appear varies from material to material. The temperature range of the blue phases is generally less than a few degrees, although larger temperature ranges have been reported.[16] A typical chiral nematic material exhibiting all three blue phases would exhibit the transitional ordering shown in Figure 2.11.

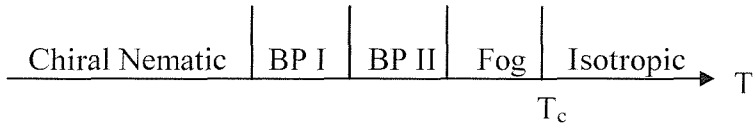

Figure 2.11 A typical phase diagram for a chiral nematic exhibiting three blue phases.

Unlike the chiral nematic phase, blue phases possess a periodic structure in three dimensions. The BPI and BPII phases exist when there is a balance between defect lines and the so-called "double-twist" structure.[4] The double-twist structure is formed when the chiral nematic phase alters to allow helix axes to twist in all directions perpendicular to a central axis. It is impossible for these structures to fit together in three-dimensional space without defects. Hence, they only form when the energy cost of the defects is low. This generally only occurs when the pitch is short and the sample temperature is near the

clearing temperature. As a general rule of thumb, for a chiral nematic material to exhibit a blue phase, its pitch has to be less than 500 μm.[17] The BPI and BPII phases are both cubic in structure,[18,19] with the BP I phase having a body centred cubic structure and the BP II phase being a simple cubic structure. There is a third blue phase, the fog phase, which has an amorphous structure. Optically, the blue phases have interesting properties. For example, they are optically active but are optically isotropic. The periodicity of the BP I and BP II phases results in Bragg reflection of incident light, which gives rise to their characteristic colourful appearance.

Many of the materials studied in this thesis exhibit one or more blue phases and their effects are discussed where relevant. There has been work on additional blue phases that only appear in the presence of an electric field:[20,21] these phases are not relevant to this work and will not be discussed further.

2.8 The effects of an electric field on the chiral nematic phase

2.8.1 Dielectric coupling

An electric field can couple to a liquid crystal via dielectric and flexoelectric coupling. Dielectric coupling usually dominates over flexoelectric coupling and therefore is the more commonly observed. The effects of dielectric coupling on the chiral nematic phase are discussed below.

The application of a sufficiently high electric field across a chiral nematic liquid crystal results in a change in the observed texture (provided that the liquid crystal has a non-zero dielectric anisotropy). The relative dielectric permittivity of a molecule is represented by an ellipsoid with $\varepsilon_{\parallel}$ and $\varepsilon_{\perp}$ being the permittivity along the long and short axes, respectively. The dielectric anisotropy of the molecule is defined as

$$\Delta\varepsilon = \varepsilon_{\parallel} - \varepsilon_{\perp}. \qquad (2.14)$$

By varying the amplitude of the applied electric field, various textures can be induced in the liquid crystal. The different textures are a result of the change in the director arrangement of the liquid crystal, which is caused by the applied field. These changes in texture tend to occur at certain critical voltages.

The free energy of a liquid crystal subjected to an electric field can be expressed as:

$$f = f_{elastic} + f_{dielectric} + f_{flexoelectric}. \qquad (2.15)$$

If it is assumed that the flexoelectric term is small compared to the other two terms, the theoretical form of the free energy is given by [4]

$$f = \left[\frac{1}{2}K_{11}(\nabla \cdot \mathbf{n})^2 + \frac{1}{2}K_{22}(\mathbf{n} \cdot \nabla \times \mathbf{n} + k)^2 + \frac{1}{2}K_{33}(\mathbf{n} \times \nabla \times \mathbf{n})^2\right] - \frac{\varepsilon_0 \Delta\varepsilon}{2}(\mathbf{E} \cdot \mathbf{n})^2. \qquad (2.16)$$

For chiral nematic with positive dielectric anisotropy aligned in the standing helix texture, the application of an electric field parallel to the helix axis produces a series of texture changes. These are illustrated in Figure 2.12.

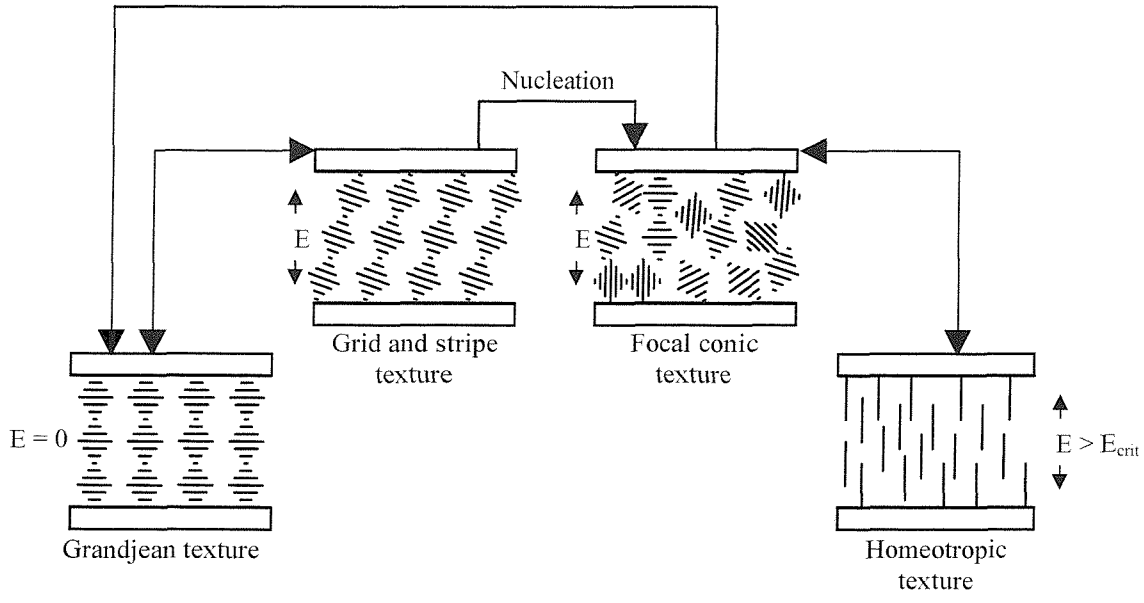

Figure 2.12 A representation of the texture changes exhibited by a short chiral nematic material as a function of applied field amplitude.

In the absence of an applied electric field, a chiral nematic material contained in a cell carrying planar alignment layers will adopt the Grandjean texture. The helix axis in this geometry is orthogonal to the walls of the cell. When an increasing electric field is applied in a direction normal to the walls, there is a critical voltage at which the Grandjean texture starts to change its appearance. This is the formation of the grid and stripe texture and it is observed as a consequence of a tilting in the helices induced by the applied field. The deformation is generally treated as being sinusoidal in form, as is represented in Figure

2.13. The stripe texture is formed when the deformation occurs in one dimension. The grid texture is formed when two orthogonal deformations of this nature form in the cell.[22] These deformations lead to local and visible variations in refractive index.

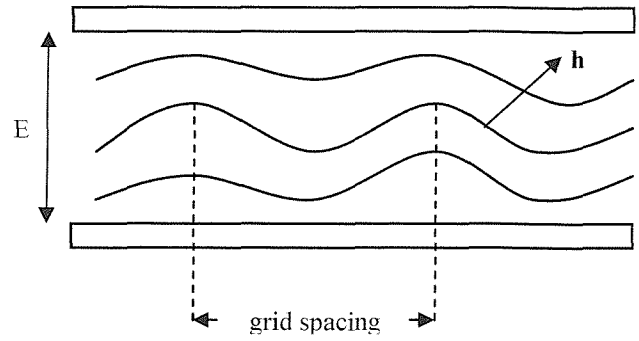

Figure 2.13 The sinusoidal deformation associated with the grid and stripe texture.

The one dimensional stripe texture is more likely to be formed rather than the two-dimensional grid texture when the ratio of the cell thickness to pitch length, d/P, is small.

When the grid and stripe texture forms, the focal conic texture tends to nucleate. The focal conic texture can also form directly from the Grandjean texture, if the applied field is sufficiently high. The behaviour of the focal conic texture upon the removal (or sufficient reduction) of the applied electric field depends on two parameters; the pitch and the thickness of the glass cell.[23,24] If the ratio of the cell thickness to pitch is small the focal conic texture will relax quickly (in a matter of seconds) back to the Grandjean texture. However, if the ratio d/P is large the chiral nematic material can stay in the focal conic texture permanently or relax slowly (taking minutes, hours or even days) back to the Grandjean texture.

If the applied field amplitude is increased incrementally, eventually the applied field will be sufficient to unwind the helix completely and the liquid crystal molecules will align with the applied field. The chiral nematic material adopts the appearance of a homeotropically aligned nematic, when viewed between crossed polarisers. The expression for the critical unwinding field has been derived from the theory of helical unwinding proposed by de Gennes[25] and is given by:

$$E_{crit} = \frac{\pi^2}{P}\sqrt{\frac{K_{22}}{\varepsilon_0 \Delta\varepsilon}}. \qquad (2.17)$$

At the critical field, the pitch increases to infinity as the helix unwinds completely. It is important to note that the helix-unwinding is in fact a continuous process as the field is increased.[4,26] Currently there is no theoretical description for the unwinding of the helix which includes all the experimentally observed phenomena; however, there are two descriptive models that provide an insight in to the process. Both descriptions are shown schematically in Figure 2.16. The process developed by de Gennes is shown in Figure 2.16(a). The suggestion here is that the regions where the directors are aligned along the applied field direction will expand as the field is increased. These unwound regions are separated by twist domains, which do not contract a great deal in the applied field because the untwisting of these regions would require too much energy. At the critical field, the separation of the twist domains becomes infinite.

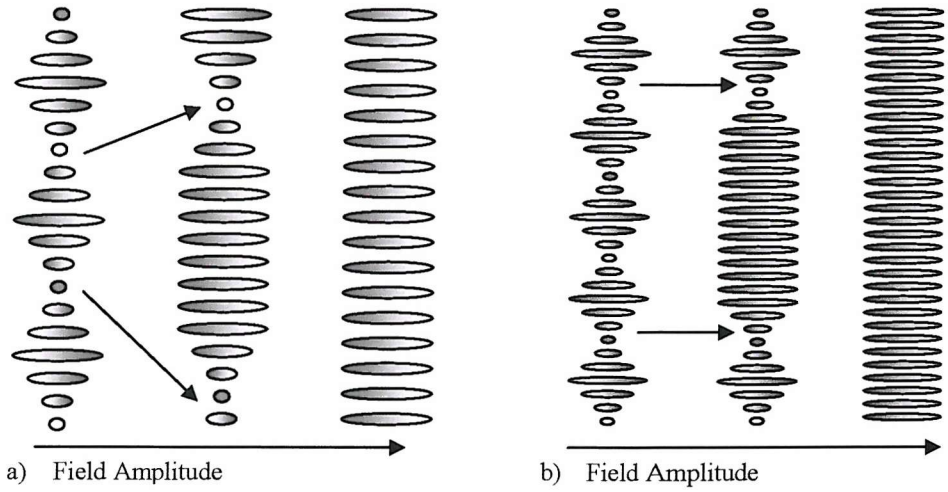

Figure 2.14 The theoretical models for helix unwinding proposed by a) de Gennes and b) Kawachi and Kogure.

The model of helix unwinding represented by Figure 2.14(b) was envisaged by Kawachi and Kogure,[27] and is based on their experimental observations of the field-induced helix-unwinding of a long pitch chiral nematic. The unwinding process was described in terms of the annihilation of the focal conic texture by disclinations. This was experimentally observed for a long pitch chiral nematic in a relatively thin cell, which results in a low number of turns in the standing helix. On nucleation, the focal conic texture forms in well-ordered stripes, with the helix lying in a single direction, the stripes themselves (which correspond to 180° turns of the helix) lie perpendicular to the helix axis. On the application of a field sufficient to unwind the helix fully, it was observed that the stripes disappear

from their end points. Kawachi and Kogure concluded that the disclinations play a major role in the unwinding of the helix.

Comparing and contrasting the two different models it can be seen that the de Gennes model allows for the experimentally observed gradual change in the helical structure when the applied field is increased; however, the Kawachi and Kogure model does not allow this. The de Gennes model, however, does not explain the experimental results observed by Kawachi and Kogure.

The complete unwinding of the helix is not permanent and only persists as long as the applied field is maintained. On reducing the amplitude of the applied field below the critical unwinding field, the focal conic texture re-forms and persists until the field is removed as discussed previously in this section.

2.8.2 Flexoelectric coupling

In the previous section, the effects of dielectric coupling between an electric field and a chiral nematic liquid crystal were discussed. In addition, it is possible for the electric field to couple to a liquid crystal material flexoelectrically. Flexoelectricity was originally called piezoelectricity in nematics by Meyer[28] because although it is a very different effect, it is analogous in many ways.

Piezoelectricity occurs when a strain applied across a material induces a polarisation in the material. The reverse is also true; when an electric field is applied across the material a deformation is created. Analogously, in a nematic liquid crystal curvature strains will result in a macroscopic flexoelectric polarisation and conversely, flexoelectric coupling between the material and field will induce a curvature strain.

The original theory proposed by Meyer[28] described flexoelectricity in terms of dipolar molecules. For dipolar flexoelectric coupling to occur, the liquid crystal molecules must be asymmetric in shape and have a permanent molecular dipole. In the absence of an electric field, the bulk material is non-polar (i.e. $\mathbf{n} = -\mathbf{n}$) and the constituent molecules are free to rotate about their long axes. On the application of a suitable electric (or magnetic) field, the molecular dipoles will preferentially align along the field direction resulting in a macroscopic polarisation, thus breaking the symmetry of the system. The asymmetric shape of the molecules induces a strain on the system that is relieved by a curvature of the director field. Conversely an imposed curvature couples to the shape asymmetry to induce a macroscopic polarisation.

The direction of the molecular dipole in relation to the long molecular axis is critical, as it determines which of the curvatures (splay or bend) will allow the induced polarisation. The molecular shape also affects the form of the flexoelectrically induced

curvature. There are two "pure" molecular shapes which allow either a purely splay or bend deformation[28] respectively. A splay deformation couples with pear (or raindrop) shaped molecules[28] and occurs when polarity is introduced to the system (i.e. $\mathbf{n} \neq -\mathbf{n}$).[29] The longitudinal components of the molecular dipoles no longer cancel, see Figure 2.15, instead they add constructively producing a macroscopic polarisation. The transverse components of the dipoles still cancel because the splay deformation has rotational symmetry about the director.

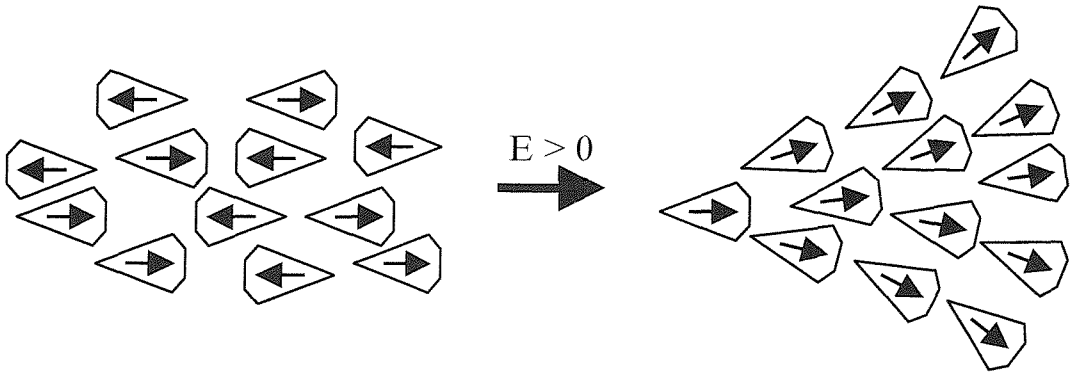

Figure 2.15 The flexoelectrically-induced pure splay deformation associated with pear-shaped molecules.

A pure bend deformation is generally associated with a banana-shaped molecule[28] as illustrated in Figure 2.16. When a bend deformation is induced, the non-polar nature of the system is not affected, i.e. $\mathbf{n} = -\mathbf{n}$.[29] The induced macroscopic polarisation lies normal to the local director and is a result of the transverse components of the dipole moments adding constructively.

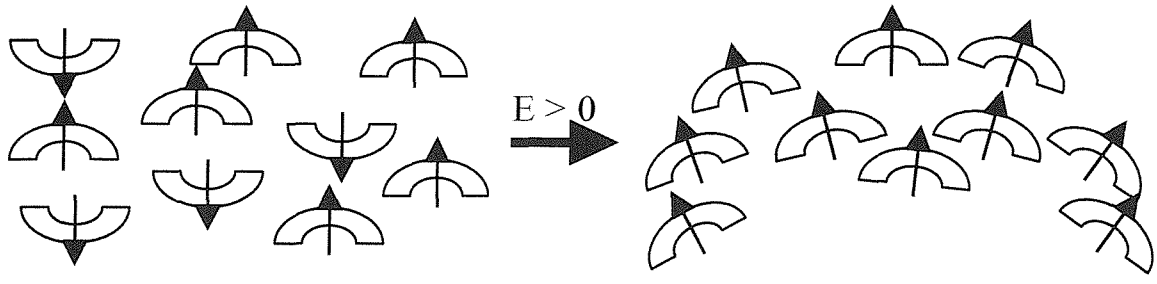

Figure 2.16 The flexoelectrically-induced pure bend deformation associated with banana-shaped molecules.

There cannot be flexoelectric polarisation due to a pure twist deformation, as there is always an axis perpendicular to the helix axis which has two-fold rotation symmetry and therefore there can be no polarisation along the helix axis.[29]

Now consider that case where the constituent asymmetric molecules are neither purely pear nor banana shaped, but rather a combination of the two. In an applied field the molecules will form a periodic pattern of splay and bend deformations (as illustrated in Figure 2.17). This was first described by Meyer[28] and has since been observed experimentally.[30]

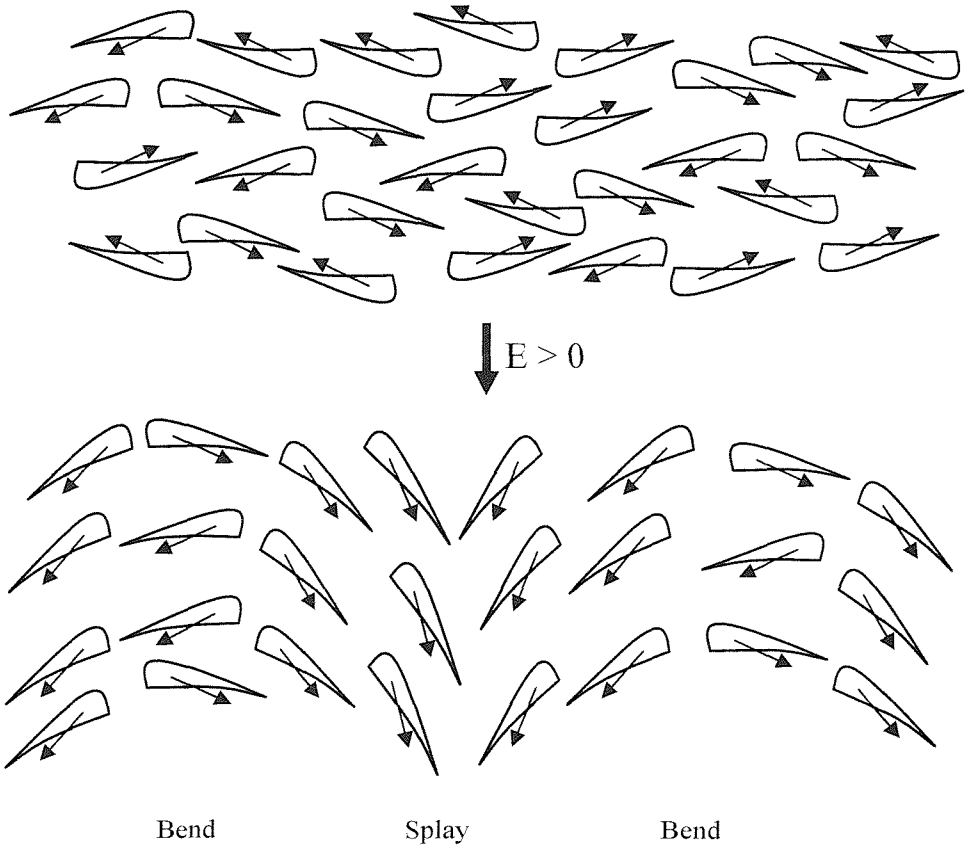

Figure 2.17 A representation of the periodic splay-bend pattern formed for molecules that are a combination of both pear and banana shapes.

As the flexoelectric deformation may be a combination of splay and bend components, it is possible to express the total flexoelectric polarisation density in a nematic as

$$\mathbf{P} = e_s \mathbf{S} + e_b \mathbf{B}, \qquad (2.18)$$

where e_s and e_b are the flexoelectric coefficients for splay (**S**) and bend (**B**) respectively. The sign convention (originally adopted by Rudquist and Lagerwall[29]) that is used in this work is illustrated in Figure 2.18.

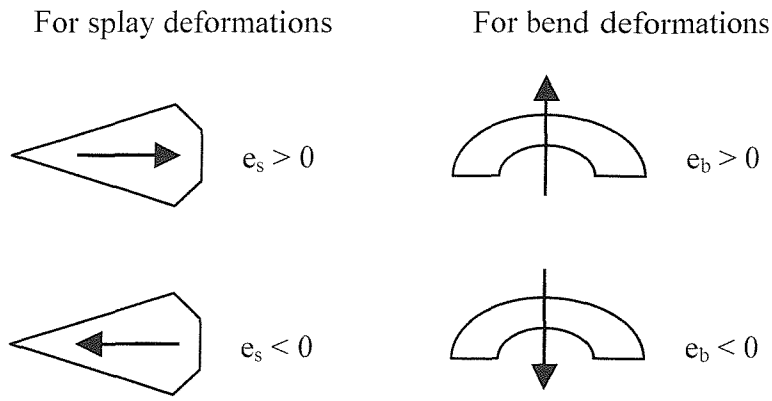

Figure 2.18 The sign conventions for relating splay and bend coefficients to molecular shape and direction of the dipole moment used in this work.

The equation for total flexoelectric polarisation density can be written in terms of the director of the liquid crystal molecules as

$$\mathbf{P} = e_s \mathbf{n}(\nabla \cdot \mathbf{n}) + e_b \mathbf{n} \times \nabla \times \mathbf{n}. \qquad (2.19)$$

Here it can be seen that only the projection of the molecular dipole onto **n** contributes to e_s, and similarly the dipolar contribution to e_b is due to the projection of the transverse component of the molecular dipole in the plane of the bend.

Flexoelectricity is not restricted just to asymmetric molecules with strong dipoles. Prost and Marcerou[31] showed that quadrupolar flexoelectric coupling was also possible; this does not require shape asymmetry or the presence of a permanent molecular dipole. As a result, this means that flexoelectricity is possible in all nematic materials. Figure 2.19 illustrates the effect of a splay deformation in a nematic material composed of non-polar symmetric molecules. It can be seen that the splay deformation of a group of quadrupoles creates an inhomogeneous charge distribution, leading to a macroscopic polarisation.

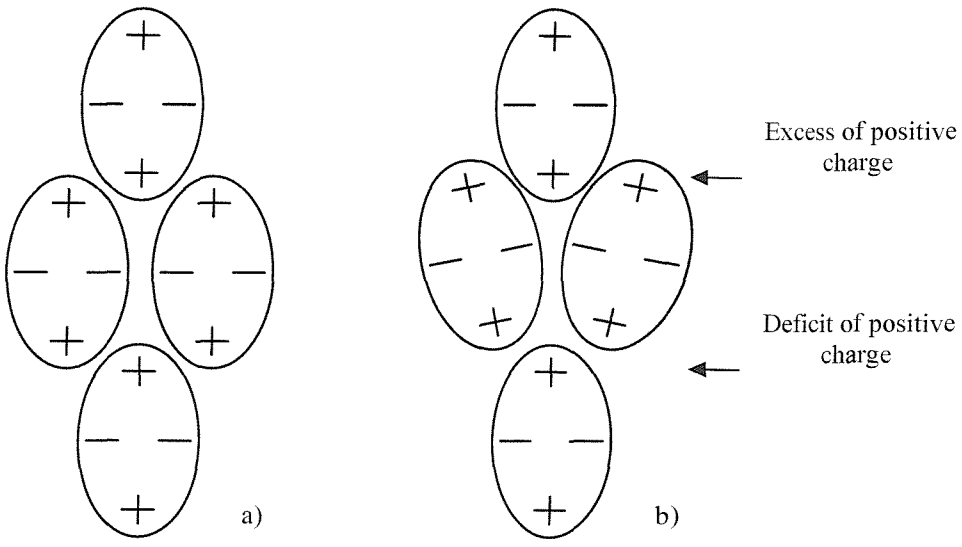

Figure 2.19 An illustration of quadrupolar flexoelectricity; a) shows the undeformed system, while b) shows a splay curvature.

It is also possible that higher order effects (such as octupoles) could have associated flexoelectricity; however, under normal circumstances the contributions would be very small.

There has not been a great amount of experimental and theoretical work on flexoelectricity to date, although the subject is now of greater interest. There have, however been a number of interesting findings, a selection of which will be summarised here.

A study was made by Lagerwall *et al.*,[32] examining the effects of *trans-cis* photoisomerism on flexoelectric coefficients. It was found that the flexoelectric coefficients increased by 40% on transformation to the *cis* isomer, which was believed to be due to an increase in the dipole moment of the molecule.

A large body of experimental work on flexoelectricity was performed by Maheswara Murthy *et al.*[33] They studied a range of monomesogenic materials, including phenylcyclohexanes, cyanobiphenyls and oxy-cyanobiphenyls. Their findings are summarised below:

- $(e_s+e_b)/2K_{22}$ is independent of chain length for members of homologous series of monomesogens.
- $(e_s+e_b)/2K_{22}$ is invariant as a function of temperature for most of the materials studied.

- (e_s+e_b) is proportional to the square of the order parameter (S^2), but may also have some component dependent upon S.

The work of Osipov[34] regarding the molecular theory of flexoelectricity showed that (e_s+e_b) should be determined from the contribution of dipolar flexoelectric coupling, while (e_s-e_b) should be determined from the quadrupolar contribution. In the case of dipolar flexoelectric coupling, the flexoelectric coefficients are predicted to scale with the square of the order parameter as a function of temperature, i.e. $e_{s,b}(T) \sim S^2(T)$. This theory therefore agrees, in part, with the experimental work of Maheswara Murthy *et al.*,[33] more so if K_{22} is also assumed to scale with the square of the order parameter, although this is not always a valid assumption.

Further theoretical work of Osipov[35] shows that flexoelectric coefficients may also vary linearly with the order parameter in cases where the molecular form has a high degree of conformational freedom; this is believed to explain the linear temperature dependence of (e_s+e_b) observed by Maheswara Murthy *et al.*,[33] for some nematic liquid crystal materials.

2.8.3 The flexoelectro-optic effect

In 1987, Patel and Meyer[36] were the first to observe an electro-optic switching effect in chiral nematics that was directly attributable to flexoelectricity; this is sometimes known as the "flexoelectro-optic effect." The nature of this optical effect and why it occurs is discussed here.

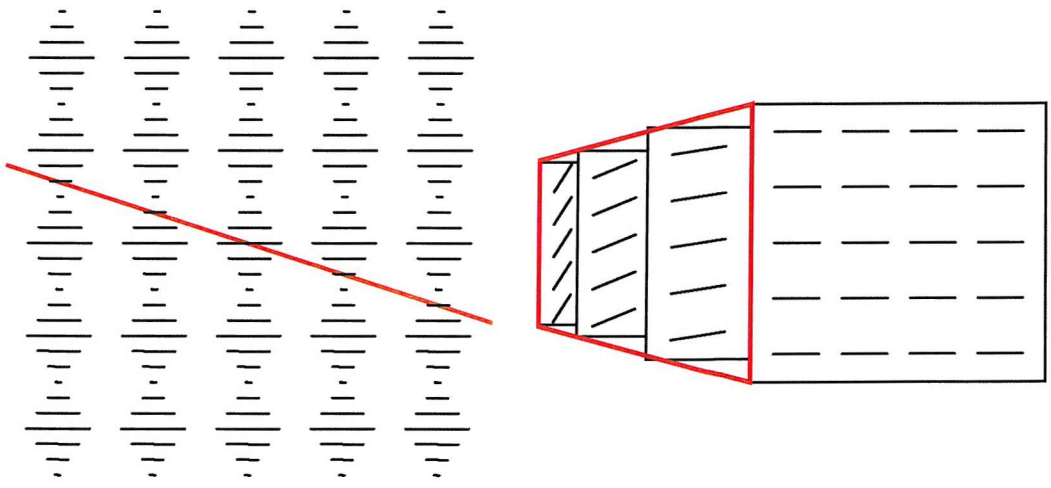

Figure 2.20 An illustration of a Bouligand slice in a chiral nematic liquid crystal.

It has been shown by Bouligand[37] that if an imaginary cut is made in a chiral nematic liquid crystal, at an angle to the helix axis, the director field in the plane of the cut forms a periodic pattern (see Figure 2.20). A periodic splay-bend deformation in the director field can be formed by rotating the director planes, such that the director lies in the plane of the cut. This is illustrated in Figure 2.21.

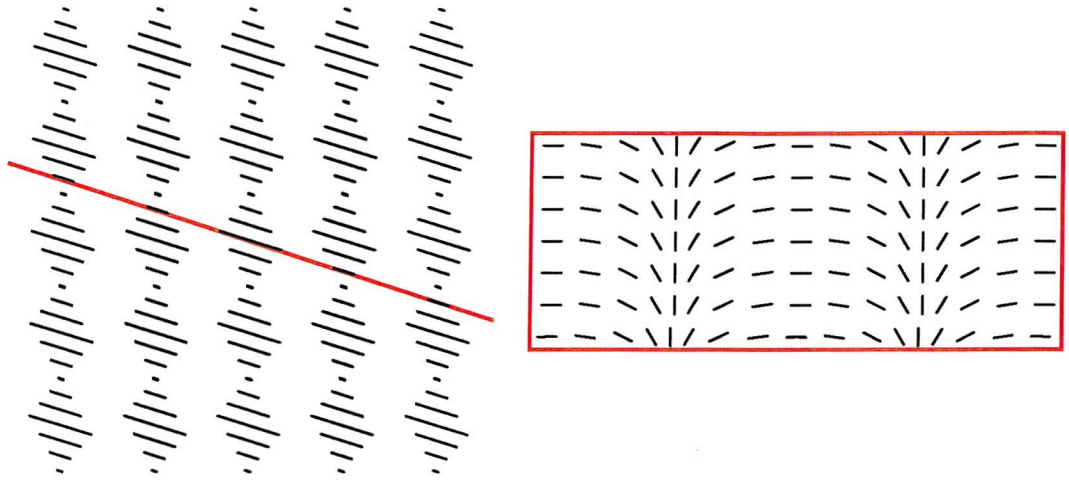

Figure 2.21 An illustration of the splay-bend deformation formed by a rotation of the director planes.

In a short-pitch chiral nematic, the optic axis of the material lies normal to the director planes. Hence, any rotation of the director planes results in an equal rotation of the optical axis. The application of a suitable electric field, in a direction normal to the helix axis, induces curvature strains as the molecular dipoles couple flexoelectrically to the field. The resulting rotation of the director planes through an angle ϕ means that the optic axis also rotates by the same angle. This flexoelectrically-induced rotation of the optic axis is known as the flexoelectro-optic effect, and is shown diagrammatically in Figure 2.22.

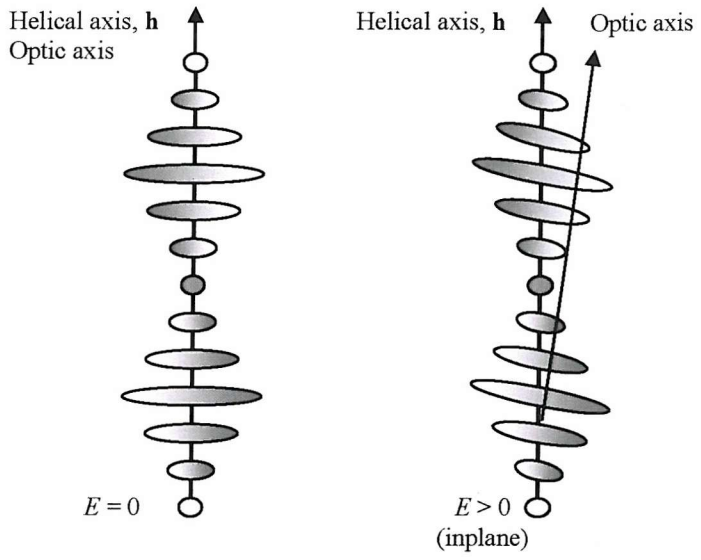

Figure 2.22 A representation of the flexoelectro-optic effect.

In order to observe the flexoelectro-optic effect, it is preferable to align a short-pitch chiral nematic in the uniform lying helix (ULH) orientation, in an electro-optic cell. This is illustrated in Figure 2.23.

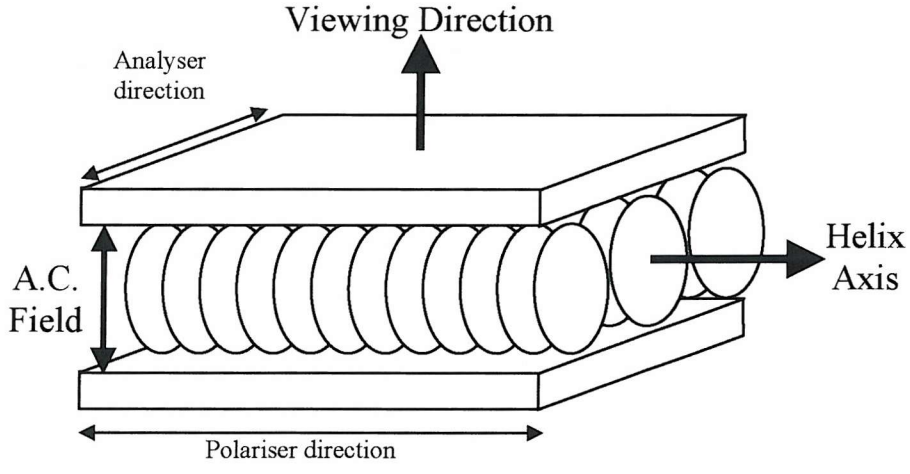

Figure 2.23 A representation of the uniformly lying helix (ULH) geometry in a glass cell. The optic axis rotates in the plane of the cell in a suitable applied electric field.

If the cell is of suitable thickness, the chiral nematic material behaves as a uniaxial optical waveplate, with its optic axis coinciding with its helix axis. On the application of an electric field across the cell, the molecular dipoles orientate to give a macroscopic polarisation in the direction of the field and a uniform rotation of the director around the field direction, resulting in the periodic splay-bend deformation. The macroscopic optic

axis is now perpendicular to the direction of the Bouligand cut in the plane of the director, thus the optic axis has rotated by an angle ϕ. When an electric field of opposite sign is applied, the direction of polarisation is reversed and the optic axis rotates by an angle $-\phi$.

The original theoretical treatment for the flexoelectro-optic effect was presented by Patel and Meyer.[36] It is from an interpretation of this theory by Rudquist[38] that the following theory is taken. The free energy density of a chiral nematic on the application of an electric field is composed of contributions from the elastic, dielectric and flexoelectric free energy densities, recall Equation 2.15:

$$f = f_{elastic} + f_{dielectric} + f_{flexoelectric}. \tag{2.15}$$

Recalling Equation 2.16 and adding a flexoelectric term gives

$$f = \left[\frac{1}{2}K_{11}(\nabla\cdot\mathbf{n})^2 + \frac{1}{2}K_{22}(\mathbf{n}\cdot\nabla\times\mathbf{n}+k)^2 + \frac{1}{2}K_{33}(\mathbf{n}\times\nabla\times\mathbf{n})^2\right] - \frac{\varepsilon_0\Delta\varepsilon}{2}(\mathbf{E}\cdot\mathbf{n})^2 - \mathbf{E}\cdot\mathbf{P}_{flex}, \tag{2.20}$$

where

$$-f_{flexoelectric} = \mathbf{E}\cdot\mathbf{P}_{flex} = e_s(\mathbf{E}\cdot\mathbf{n}(\nabla\cdot\mathbf{n})) + e_b(\mathbf{E}\cdot\mathbf{n}\times\nabla\times\mathbf{n}). \tag{2.21}$$

It can be seen that the dielectric contribution to the total free energy density is quadratic in terms of $\mathbf{E}$, whereas the flexoelectric term is linear in $\mathbf{E}$. This means that at low fields, provided that the dielectric anisotropy of the material is small, the flexoelectric term dominates over the dielectric term. Assuming that the amplitude of the electric field is low and that the dielectric anisotropy is small:

$$\begin{aligned} f &= f_{elastic} + f_{flexoelectric} \\ &= \left[\frac{1}{2}K_{11}(\nabla\cdot\mathbf{n})^2 + \frac{1}{2}K_{22}(\mathbf{n}\cdot\nabla\times\mathbf{n}+k)^2\,\frac{1}{2}K_{33}(\mathbf{n}\times\nabla\times\mathbf{n})^2\right] - \left[e_s(\mathbf{E}\cdot\mathbf{n}(\nabla\cdot\mathbf{n})) + e_b(\mathbf{E}\cdot\mathbf{n}\times\nabla\times\mathbf{n})\right] \end{aligned} \tag{2.22}$$

A new expression for the director co-ordinates is required in terms of the rotation of the director planes. The director planes are rotated though an angle ϕ about the applied field

direction. the x-axis is defined to lie along the direction of the applied field and thus the rotation of the director planes can be treated as a rotation of the y- and z-axes about the x-axis by an angle $-\phi$ to y'and z'. The new director components as functions of x, y and z are given by:

$$\begin{aligned}\mathbf{n} &= (\cos\theta, \sin\theta\cos\phi, -\sin\theta\sin\phi) \\ &= \mathbf{i}\cos kz + \mathbf{j}\sin kz\cos\phi - \mathbf{k}\sin kz\sin\phi,\end{aligned} \tag{2.23}$$

where $\theta = kz = 2\pi z/P$ gives the rotation of successive director planes, due to the chirality of the liquid crystal, measured from the x-axis. The angle θ is positive for an anticlockwise rotation with increasing z and is taken to be zero at the origin. The rotation of the optic axis as a result of flexoelectric coupling is defined to be positive for an anticlockwise rotation about the x-axis in the yz-plane. From this, the following expressions are derived:

$$\begin{aligned}&\nabla\cdot\mathbf{n} = -k\cos kz\sin\phi, \\ &\nabla\times\mathbf{n} = -\mathbf{i}k\cos kz\cos\phi - \mathbf{j}k\sin kz, \\ &\mathbf{n}\cdot\nabla\times\mathbf{n} = -k\cos\phi, \\ &\mathbf{n}\times\nabla\times\mathbf{n} = \mathbf{i}\left(-k\sin^2 kz\sin\phi\right) + \mathbf{j}\left(k\cos kz\sin\phi\cos\phi\right) + \mathbf{k}\left(-k\sin kz\cos kz\sin^2\phi\right), \\ &\mathbf{n}(\nabla\cdot\mathbf{n}) = -k\cos kz\sin\phi(\mathbf{i}\cos kz + \mathbf{j}\sin kz\cos\phi - \mathbf{k}\sin kz\sin\phi), \\ &(\mathbf{n}\times\nabla\times\mathbf{n})^2 = k^2\sin^2 kz\sin^2\phi.\end{aligned} \tag{2.24}$$

When the expressions given in Equation 2.24 are substituted into Equation 2.22 together with $\mathbf{E} = -E\mathbf{i}$, the following expression is obtained:

$$\begin{aligned}f = &\frac{1}{2}K_{11}\left(k^2\cos^2 kz\sin^2\phi\right) + \frac{1}{2}K_{22}k^2(1-\cos\phi)^2 + \frac{1}{2}K_{33}\left(k^2\sin^2 kz\sin^2\phi\right) \\ &- Ek\sin\phi\left(e_b\sin^2 kz + e_s\cos^2 kz\right).\end{aligned} \tag{2.25}$$

To derive the average free energy density over the whole helical structure, f must be averaged with respect to kz ($=\theta$). A standard mathematical result is $\langle\sin^2\theta\rangle = \langle\cos^2\theta\rangle = \frac{1}{2}$, and thus the average free energy density becomes

$$\langle f \rangle = \frac{1}{4} K_{11} \left(k^2 \sin^2 \phi \right) + \frac{1}{2} K_{22} k^2 (1 - \cos \phi)^2 + \frac{1}{4} K_{33} \left(k^2 \sin^2 \phi \right) - \frac{1}{2} Ek \sin \phi (e_b + e_s). \tag{2.26}$$

The following definitions are made:

$$K = \frac{(K_{11} + K_{33})}{2} \tag{2.27}$$

and

$$\bar{e} = \frac{(e_s + e_b)}{2} \tag{2.28}$$

where $\bar{e}$ is the effective flexoelectric coefficient and K is the average of the splay and bend elastic constants. The average free energy becomes

$$\langle f \rangle = \frac{1}{2} Kk^2 \sin^2 \phi + \frac{1}{2} K_{22} k^2 (1 - \cos \phi)^2 - \bar{e} Ek \sin \phi. \tag{2.29}$$

Finally, this expression is minimised by taking the derivative with respect to ϕ and setting the result equal to zero, giving

$$\frac{\partial \langle f \rangle}{\partial \phi} = k^2 \sin \phi \cos \phi (K - K_{22}) + K_{22} k^2 \sin \phi - \bar{e} Ek \cos \phi = 0, \tag{2.30}$$

which can be rearranged to give

$$\tan \phi = \frac{\bar{e} E}{k K_{22}} - \sin \phi \frac{K - K_{22}}{K_{22}}. \tag{2.31}$$

If it is assumed that the induced tilt angles of the optic axis are small, then a small angle approximation can be made, i.e. $\sin\phi \approx \tan\phi$. This gives a more useful expression, namely

$$\tan \phi = \frac{\bar{e} E}{kK} = \frac{\bar{e} E}{K} \frac{P}{2\pi}. \tag{2.32}$$

This expression has been successfully fitted to data where the tilt angle is as high as 35°.[39]

From Equation 2.32, it can be seen that $\tan\phi$ has a linear dependence on the applied field. This linear dependence is very significant, as it means that the magnitude of ϕ can be directly controlled by the amplitude of the applied field.

As with any electro-optic effect, the speed of response when an electric field is applied is of great importance. For a theoretical treatment of the response time, the "switch" is considered to be a perturbation in the orientation of the optic axis. The time taken to relax back to the equilibrium position is defined as the response time. From thermo-dynamical theory, the equation for this relaxation after perturbation[40] can be written as

$$\frac{\partial\phi}{\partial t} = \frac{1}{\gamma}\frac{\partial\langle f\rangle}{\partial\phi}, \tag{2.33}$$

where γ is the effective viscosity associated with the helix distortion. This equation shows that the response time is related to the change in free energy density with respect to the tilt angle. Substituting into Equation 2.29 gives

$$\gamma\frac{\partial\phi}{\partial t} = k^2\sin\phi\cos\phi(K - K_{22}) + K_{22}k^2\sin\phi - \bar{e}Ek\cos\phi. \tag{2.34}$$

If it is assumed that ϕ is small, then the approximations that $\sin\phi \approx \phi$ and $\cos\phi \approx 1$ can be made resulting in

$$\gamma\frac{\partial\phi}{\partial t} - Kk^2\phi = \bar{e}Ek. \tag{2.35}$$

Consider the case when sufficient field is applied such that the rotation of the optic axis is maximised, i.e. $\phi = \phi_{max}$. When the perturbing field is removed at t = 0 then the solution is of the form

$$\phi = \phi_{max}e^{-\frac{t}{\tau}}. \tag{2.36}$$

If this solution is substituted in to Equation 2.35, this gives

$$-\frac{\gamma}{\tau}\phi_{\max} + Kk^2\phi_{\max} = 0, \tag{2.37}$$

at t = 0. Equation 2.37 can be rearranged to give the following solution for the response time of the material:

$$\tau = \frac{\gamma}{Kk^2} = \frac{\gamma}{K}\frac{P^2}{4\pi^2}. \tag{2.38}$$

From this derivation, it can be seen that the response time is independent of the applied field amplitude, at least to a first approximation. Qualitatively this can be explained[41] by considering that as the field is increased there is a proportional increase in the torque exerted on the molecules. The molecules must respond to the increased torque by rotating through a greater angle; however, the increased field also proportionately increases the rotational speed of the molecules. Thus the increase in rotation angle balances the proportional increase in the rotational speed of the molecules and hence the response time remains unchanged by changes in the applied field amplitude.

The viscosity coefficient, γ, is taken to be of the order of the rotational viscosity coefficient γ_1. Typically γ_1 ranges from 0.01 to 0.1 kg m^{-1} s^{-1} in nematic liquid crystal materials.[41] Substituting typical values for the rotational viscosity coefficient (0.1 kg m^{-1} s^{-1}), the elastic coefficient (~10^{-11} N) and pitch length (400 nm) into Equation 2.38 would give an impressive response time of less than 50 μs.

Equation 2.38 shows that the flexoelectro-optic response time can be optimised by using a material with short pitch, low effective viscosity and high mean splay-bend elastic constant. Compare this to Equation 2.32, where it can be seen that a large effective flexoelectric coefficient, a long pitch and a low mean elastic constant are required for a large tilt angle per unit field. There are clearly some compromises required between the response time and the maximum tilt angle per unit field, regarding the pitch and mean splay-bend elastic constant when choosing an "ideal" material. Regardless of response times and tilt angles, the pitch should be short enough so that the fingerprint texture is not formed. It is important to note that the tilt angle per unit applied field is linearly proportional to the pitch, while the response time increases with the square of the pitch; this would suggest that response time considerations should take preference with regards to choosing helical pitch. In the "ideal" material the effective flexoelectric coefficient and

effective viscosity are optimised, i.e. maximised and minimised respectively, then the mean splay-bend elastic constant and pitch values are of less importance. Of course there are other factors that must be taken in to consideration when determining "ideal" values for the various co-efficients. For example, to maximise the critical field for helix-unwinding a large value for K_{22} is required. However, as K_{22} is generally lower than K_{11} and K_{33}, to have a high K_{22} may result in the mean splay-bend elastic constant being large, which would be a disadvantage.

2.8.4 Molecular structure and its effects on the flexoelectro-optic properties

As has already been discussed, molecular structure is very important for flexoelectricity, and hence has a large effect on the flexoelectro-optic properties. For a high effective flexoelectric coefficient, an asymmetric shape with a strong permanent dipole is required. Meyer's original theory[28] suggested that molecules with a banana shape and a transverse dipole, or molecules with a pear shape and a longitudinal dipole, have maximised flexoelectric coefficients. However, the strength and direction of the permanent dipole also contribute to the dielectric anisotropy. This means that the banana-shaped molecules will have negative dielectric anisotropy and the pear-shaped molecules have positive dielectric anisotropy. Hence, banana-shaped molecules with large transverse dipoles would preferentially align normal to the applied field and pear-shaped molecules with large longitudinal dipoles would align along the applied field direction. Neither molecular shape in combination with such large dipoles would be potential candidates for flexoelectro-optic switching; the banana-shaped molecules would not adopt the necessary lying helix geometry in an applied field, while for the pear-shaped molecules the field required for helix unwinding would be small. For non-symmetric molecular shapes with some angle between the long axis of the molecule and the direction of the dipole moment, the contribution to the dielectric anisotropy from the transverse and longitudinal components can be similar in magnitude. It has been suggested by Rudquist[38] that a material with a combined pear-banana shape and a molecular dipole at ~45° to the molecular long axis is likely to have a low dielectric anisotropy, while still possessing a strong molecular dipole and high shape asymmetry. As a result of its hybrid shape and its dipole moment, the molecule will have non-zero values for both the splay and bend flexoelectric coefficients.

Recent work[42,43,44] has suggested that bimesogenic liquid crystals offer a very significant improvement in flexoelectro-optic properties. Bimesogens can be synthesised to have both strong molecular dipoles and low dielectric anisotropy. The individual dipole moments of

the two mesogenic groups oppose one another, to a certain extent, giving a material with low dielectric anisotropy.

2.9 Summary

In this chapter, descriptions are given of the physical, optical and electro-optical properties of chiral nematic liquid crystals. The concept of helical pitch for a chiral nematic was introduced and its effect on the optical properties of the phase was discussed. A chiral nematic material has two mechanisms for coupling to an applied electric field – namely, dielectrically and flexoelectrically. The effects of dielectric coupling on the chiral nematic phase were discussed in terms of the induced texture changes and the process of helix unwinding. The mechanism of flexoelectric coupling was discussed in detail, and a consequence of flexoelectric coupling known as the flexoelectro-optic effect was introduced. The theory of the flexoelectro-optic switching process derived by Patel and Meyer[36] was described in some detail. It was shown that the magnitude of the tilt angle increases linearly with applied field amplitude and is also dependent on the pitch length and the ratio of the average flexoelectric coefficient to the average splay-bend elastic constant. The magnitude of the response times were found to be independent of the applied electric field amplitude (to a first approximation) but showed a strong dependence on pitch length and effective rotational viscosity. The predicted and measured effects of molecular structure on the flexoelectric properties were also discussed.

References

1 Tsvetkov, V., Acta Physiochim (USSR) **16** 132 (1942)

2 Lisetski, L. N., and Tomalchev, A. V., Liq. Cryst. **5(3)** 877 (1989)

3 Chandrasekhar, S., Liquid Crystals, Cambridge University Press, Cambridge (1992)

4 de Gennes, P. G., and Prost, J., The Physics of Liquid Crystals, 2nd edition, Oxford Science Publications, Oxford (1993)

5 Garoff, S., and Meyer, R. B., Phys. Rev. Lett. **38** 848 (1977)

6 Frank, F. C., Disc. Faraday Soc. **25** 19 (1958)

7 Fergason, J., Goldberg, N., and Nadalin, R., Mol. Cryst. **1** 315 (1966)

8 Blatch, A. E., Fletcher, I. D., and Luckhurst, G. R., J. Mater. Chem. **7(1)** 9 (1997)

9 Kats, E. I., Sov. Phys. JETP **32** 1004 (1971)

10 Nityananda, R., Mol. Cryst. Liquid. Cry. **21** 315 (1973)

11 Coles, H. J., Chapter 4 in The Handbook of Liquid Crystals, vol 2A. (editors: Demus, D., Goodby, J., Gray, G. W., Spiess, H. W., and Vill, V.), Wiley-VCH, Weinheim (1998)

12 Chandrasekhar. S and Shashidhara-Prasad J., Mol. Cryst. Liquid. Cryst. **14** 115 (1971)

13 Martin, J. C. and Cano, R., C. R. Acad. Sci. **B278** 219 (1974)

14 Fergason, J. L., Molecular Crystals **1** 293 (1966)

15 Dreher, R., and Meier, G., Phys. Rev. A **8** 1616 (1973)

16 Kikuci, H., Yokota, M., Hisakado, Y., Yang, H., and Kajiyama, T., Nature Materials **1** 64 (2002)

17 Stegemeyer, H., Blümel, T., Hiltrop, K., Onusseit, H., and Porsch, F., Liq. Cryst. **1(1)** 3 (1986)

18 Meiboom, S., and Sammon, M., Phys. Rev. Lett. 44 882 (1980)

19 Grebel, H., Hornreich, R. M., and Shtrikman, S., Phys. Rev. A **28** 1114 (1983)

20 Pieranski, P., Cladis, P. E., and Barbet-Massin, R., J. Phys. Lett. **46** L-973 (1985)

21 Hornreich, R. M., and Shtrikman, S., J. Phys. (France) **41** 335 (1980)

22 Gerritsma, C. J., and van Zanten, P., Phys. Lett. **37A(1)** 47 (1971)

23 Nara, Y., Kobayashi, S., and Miyaji, A., J. Appl. Phys. **49(7)** 4277 (1978)

24 Komitov, L., Lagerwall, S. T., Stebler, B., and Strigazzi, A., J. Appl. Phys. **76(6)** 3762 (1994)

25 de Gennes, P. G., Solid-State Commun. **6** 163 (1968)

26 Rudquist, P., Komitov, L., and Lagerwall, S. T., Phys. Rev. E **50(6)** 4735 (1994)

27 Kawachi, M., and Kogure, O., Japan. J. Appl. Phys. **16(9)** 1673 (1977)

28 Meyer, R. B., Phys. Rev. Lett. **22(18)** 918 (1969)

29 Rudquist, P., and Lagerwall, S. T., Liq. Cryst. **23(4)** 503 (1997)

30 Dozov, I., and Penchev, I., J. Physique **47** 373 (1986)

31 Prost, J., and Marcerou, J. P., J. Physique **38** 315 (1977)

32 Hermann, D. S., Rudquist, P., Ichimura, K., Kudo, K., Komitov, L., Lagerwall, S. T. Phys. Rev. E **55(3)** 2857 (1997)

33 Maheswara Murthy, P. R., Raghunathan, V. A., and Madhusudana, N. V., Liq. Cryst. **14(2)** 483 (1993)

34 Osipov, M. A., Sov. Phys. JETP **58(6)** 1167 (1983)

35 Osipov, M. A., J. Physique Lett. **45** L-823 (1984)

36 Patel, J. S., and Meyer, R. B., Phys. Rev. Lett. **58(15)** 1538 (1987)

37 Bouligand, Y., J.Physique **30** C4-90 (1969)

38 Rudquist, P., Ph.D. thesis, Chalmers Technical University, Gothenburg (1997)

39 Rudquist, P., Buivydas, M., Komitov, L., and Lagerwall, S.T., J. Appl. Phys. **76(12)** 7778 (1994)

40 Lee, S. D., Patel, J. S., and Meyer, R. B., Mol. Cryst. Liq. Cryst. **209** 79 (1991)

41 Patel, J. S., and Lee, S. D., J. Appl. Phys. **66(4)** 1879 (1989)

42 Musgrave B., Ph.D. thesis, Southampton University, Southampton (1999)

43 Coles, H. J., Coles, M. J., Perkins, S., Musgrave, B., and Coates D., Bimesogenic Compounds and Flexoelectric Devices, EU Patent EP99119114 (1999)

44 Coles, H. J., Musgrave, B., Coles, M. J., and Willmott, J., J. Mater Chem. **11** 2709 (2001)

Chapter Three

3 Experimental Techniques

3.1 Introduction

This chapter describes the apparatus and experimental techniques used during the course of the work presented in this thesis. Section 3.2 provides a description of the equipment used to characterise the optical and electro-optical properties of the liquid crystal materials studied. The sample and cell preparation procedures used are explained in Section 3.3. Section 3.4 gives an explanation of the techniques used to study the intrinsic physical properties of liquid crystals in this work, while Section 3.5 discusses the techniques used to examine the electro-optic properties of the materials. In Section 3.6 the relevant properties of 7OCB are studied for use as a comparison to the work in this thesis.

3.2 The apparatus

3.2.1 General overview

The most extensively used piece of apparatus in this work is the polarising microscope. Samples to be examined are placed on a heating block, between the microscope's polarisers. The polarisers are normally arranged so that their transmission axes are aligned at 90° relative to each other (also known as 'crossed'). The crossed polarisers mean that light is only observed in the eyepieces if the sample is optically anisotropic and its optic axis is aligned appropriately. Polarising microscopy can be used to identify and characterise liquid crystal phases, as well as to determine phase transition temperatures and carry out electro-optic measurements. The general set-up of the apparatus used to characterise the liquid crystals properties via microscopy is shown in Figure 3.1. A heating block, upon which samples are placed, is attached to the rotation stage of the microscope, allowing temperature dependent measurements to be performed.

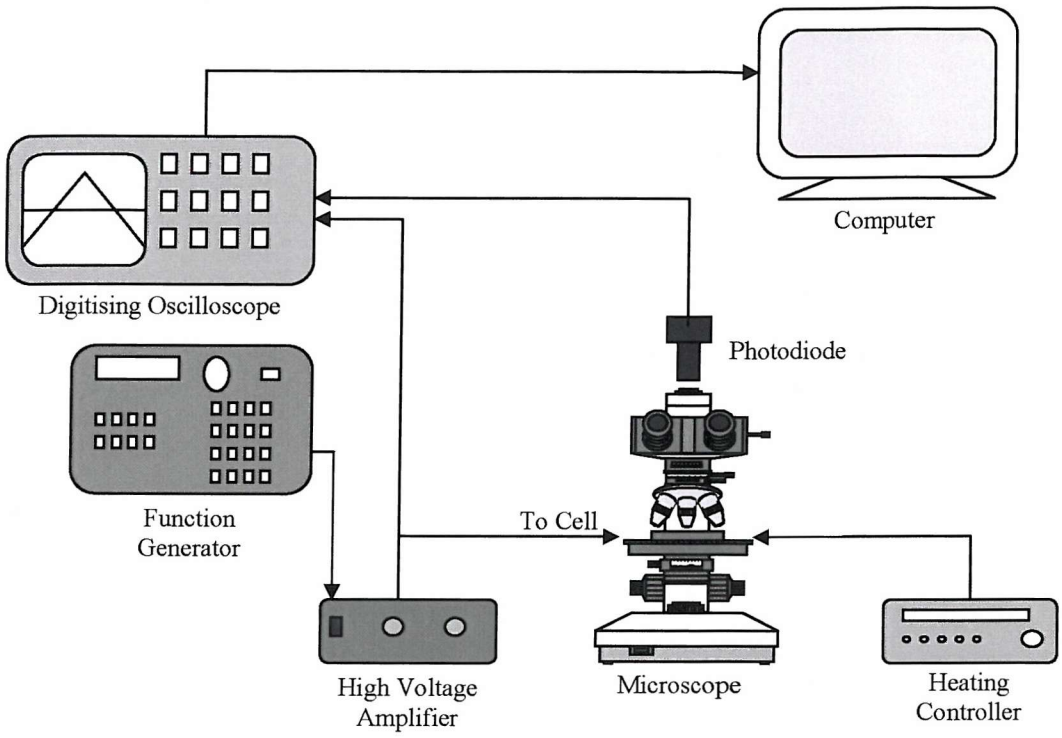

Figure 3.1 General experimental set-up for optical microscopy and electro-optic studies.

For the purpose of making electro-optic measurements, it is necessary to have the facility to apply electric fields to the sample; to do this a function generator is used. The signal from the function generator is amplified using a wide band voltage amplifier. It is also necessary to have some form of detector to analyse the intensity of the light transmitted through the sample; this is achieved using a photodiode. Both the applied electric signal and photodiode signal are monitored using a digital oscilloscope. The resultant data can be analysed using a computer connected to the oscilloscope.

There are further techniques used to examine liquid crystal materials in this work. The additional measurements are performed using the differential scanning calorimeter (DSC) and UV-Visible spectrometer.

3.2.2 The microscope and heating stage

The microscope used throughout this work for the observation of samples is an Olympus[1] BH-2 model, a schematic of which is shown in Figure 3.2.

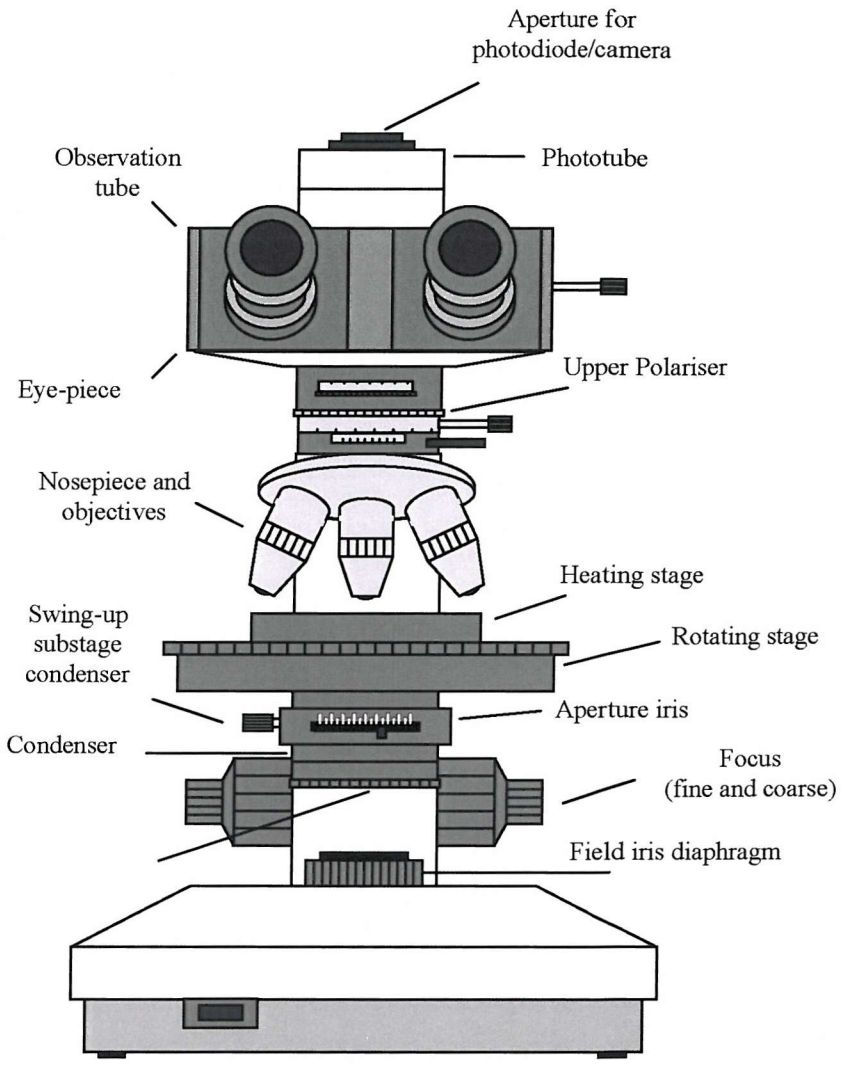

Figure 3.2 The Olympus BH-2 polarising microscope.

The objectives used are generally in the range of 4 to 50 times magnification strength, and they are infinity corrected so that additional optics can be placed in the phototube as necessary. The objectives are also of the "Plan" type, which means that the curvature of field is corrected and the image is focussed on to a flat plane. The numerical aperture of the condenser has to be adjusted to match that of the objective to obtain good resolution.

Both the upper and lower polarisers can be rotated as necessary. The upper polariser (or analyser) can be rotated in measurable increments of 0.1° whilst the lower polariser can be rotated in measurable increments of 5°. The upper polariser can be removed easily if it is not required for the observation. The observation tube itself has three settings, one to direct all the transmitted light to the eyepieces, one to direct all the light to the phototube and one that splits the light so that half goes to the eyepieces and the other

half to the phototube. The eyepieces on the observation tube increase the magnification of the image by a factor of ten. One of the eyepieces has a crosshair marked on it, which can be used to make measurements of length on the sample being observed. The phototube allows extra optics to be attached to the microscope; for the present work this is generally either a photodiode or a camera. It is also possible to insert a reflection arm below the observation tube, which illuminates the sample from above; this allows the samples to be view in reflection instead of in transmission. The reflecting arm also has slots to allow additional optical components to be inserted in the light path.

The sample being observed was generally placed on a Linkam[2] heating stage, which is mounted on the microscope's rotation stage. The rotation stage is marked in divisions of 1° and great care is taken to make sure the stage and heating block are centred so as to produce accurate angle measurements. The heating block is connected to a Linkam TP91 temperature controller, which can be used adjust the temperature of the heating block from room temperature to approximately 250°C in increments of 0.1°C. The temperature controller has a RS232 communications port which allows it to be connected to a computer. The heating stage has an easily removable window, which is used to insulate the sample from environmental effects (such as draughts). The window can be removed to allow physical interaction with the sample, e.g. shearing, if necessary. It is possible to cool the sample to temperatures below room temperature using a Linkam cooling system CS 196, which works by blowing cool nitrogen gas through the heating stage. It is possible to cool the sample down to below -150°C with this method. It is important that at temperatures below about 10°C the insulating window is used, otherwise moisture in the air condenses on the sample, making it impossible to view.

3.2.3 Applying an electric field

An electric field can be applied across the sample using a function generator. The function generator used in this work is a Thurlby Thandar[3] programmable function generator TG1304. The function generator is capable of producing square, triangular and sinusoidal waveforms, with a frequency range of 1 mHz to 13 MHz, and peak to peak voltages between 0.2 mV and 20 V. It is also possible to produce dc voltages from –10 V and +10 V in increments of 0.1 mV. The function generator signal can be amplified if necessary by using a wide-band high voltage amplifier, which was produced in-house. It is possible to amplify signals up to 240V peak to peak using this amplifier. The Thurlby Thandar function generator has an IEEE communications port that enables it to be connected to a computer.

The signals applied are monitored using a Hewlett-Packard[4] model 54503A 500 MHz digitizing oscilloscope. The oscilloscope has four input channels, four movable cursors for measuring voltages and time, and is capable of averaging 2 to 2048 waveforms (in increments of powers of 2). The oscilloscope has a number of useful in-built functions, such as auto-measuring the voltage in a number of different ways and computing signal fall and rise times, etc. The oscilloscope, like the function generator, also has an IEEE communications port for computer control.

3.2.4 The photodiode detector

To measure the light intensity through the observation tube of the microscope, a photodiode detector is used. The detector used is a Thorlabs[5] PDA55 switchable gain silicone photodetector; it has five discrete gain settings of 0, 10, 20, 30, 40 dB, a spectral range of 400-1100 nm and an active region of approximately 13 mm^2. For this work, the photodiode is set to the maximum gain. The photodiode is mounted in a holder designed to fit into the microscope's phototube. The signal from the photodiode is amplified and then displayed on the oscilloscope. The photodiode is used to measure change in light intensity in the phototube and this is the basis of all the electro-optic measurements made in this thesis. A simple test of the linearity of the photodiode's response is to measure the signal as a function of the angle of the top polariser relative to the bottom polariser. The results are shown in Figure 3.3, and it can be seen that the photodiode's response is linear.

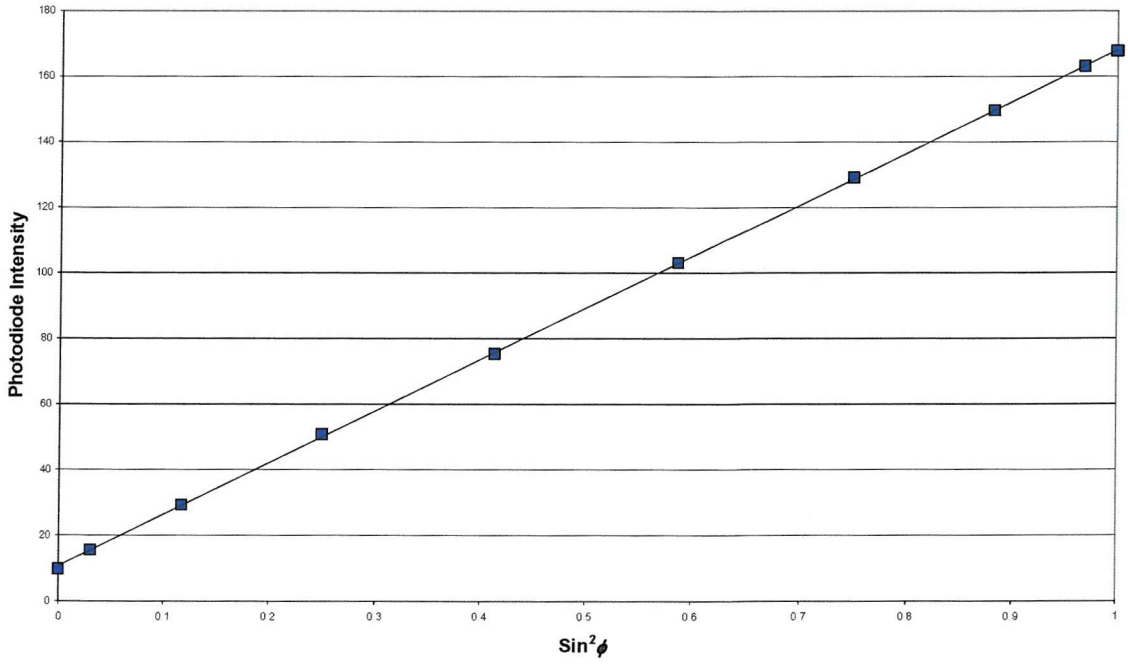

Figure 3.3 The photodiode response as a function of the angle of the polariser.

3.2.5 The computer

As the oscilloscope, heating stage and function generator can all be connected to a computer it seemed sensible to take advantage of this. The computer used is a standard IBM-style[6] computer running Microsoft Windows.[7] Agilent have produced a visual programming language called VEE[8] for the purpose of controlling instruments, which is immensely useful. The author has produced a number of VEE programs to control the oscilloscope and function generator for different tasks. The Linkam controller can be controlled through VEE using an additional program written by Marcus Coles. Three programs were used in the work described in this thesis; one to convert the oscilloscope display data into a file, another that records the response of the photodiode as the temperature is changed and finally a program that captures the photodiode response as the applied voltage is changed. The last two programs are automated and can be left to run on their own, whereas previously these measurements had to done manually and were time-consuming. The uses of these two programs are discussed later in this chapter.

3.2.6 The UV-visible spectrometer

For the purposes of measuring cell gaps and observing the absorption spectra of materials, a Hewlett-Packard model 8453 UV-Visible spectrometer is used. The ultraviolet and visible light for the spectrometer are produced by deuterium and tungsten lamps, respectively. The spectrometer's detector is a photodiode array, which has an operating range of 190 to 1100 nm and a resolution of 2 nm. The spectrometer is connected to a computer running software that can display either the absorbance or transmittance spectra produced by the spectrometer. It is possible with the software to measure the absorbance or transmittance at any wavelength, as well as identify the wavelengths at which peaks and troughs occur. Before a sample is placed in the spectrometer a reference spectrum is obtained.

It is also possible to make measurements as a function of sample temperature using the spectrometer. To do this, a Mettler[9] FP 82 heating stage is placed into the light path of the spectrometer. The stage is controlled by a Mettler FP 80 temperature controller, which has an accuracy of 0.1°C. The stage can be used to achieve temperatures from room temperature up to 120°C. Unlike the Linkam hot stage, where the sample sits on a heating block, the Mettler heating stage encloses the sample on both sides. The heating stage has a 2mm diameter aperture, through which the sample may be observed. This enclosure of the sample provides temperature stability and holds it in position when the stage is turned on its side and inserted in the light path of the spectrometer. The heating stage is held in place

by a retort stand and great care is taken to ensure that the sample surface lies normal to the direction of the light path. Before any measurements are made a reference spectrum is obtained using the empty heating stage.

3.2.7 The differential scanning calorimeter

The differential scanning calorimeter (DSC) used during this work is the Perkin-Elmer[10] DSC 7 model. In differential scanning calorimetry, a test sample is heated or cooled, together with a separate reference sample, at a certain rate, and the amount of heat required to keep the sample at the same temperature as the reference is measured. Phase transitions in the sample can be seen as peaks (endotherms) or troughs (exotherms) in the trace of the heat added plotted against temperature. Information about changes in intermolecular structure can be deduced from the relative sizes of the various peaks, although it is not possible to identify the liquid crystal phases themselves from the trace.

3.2.8 Cameras

Two types of camera were used during the work produced in this thesis. The more commonly-used camera was the JVC model KY-F50 CCD video camera[11] in conjunction with the Optimas 6.5 image processing software produced by Media Cybernetics.[12] On other occasions an Olympus C4040Z digital camera was used. Both cameras can be mounted on the phototube of the microscope. To focus the image on to the CCD array, a NFK photo-eyepiece is inserted into the phototube. The choice of photo-eyepiece determines the magnification of the image. For this work an Olympus 2.5 times photo-eyepiece is used.

3.3 Sample preparation

3.3.1 Cells and alignment layers

To make a rapid observation of a sample, the simplest method is to place the material on a glass microscope slide and place a cover slip over the top. This admittedly crude method (there are no alignment layers and no attempt to control sample thickness) allows phases and phase transitions to be examined, as a sample's texture changes as a function of temperature. A more elaborate cell is formed using glass slides with alignment layers on their inner surfaces. Alignment layers are applied to the surfaces of the slides to induce director alignment in the liquid crystal sample with respect to the cell walls, which allows characteristic textures to be observed. Homeotropic alignment is defined when the director of the phase is orientated orthogonally to the cell wall and planar alignment is defined when the director of the phase is orientated parallel to the cell wall. The alignment layers

are usually applied before the cell is constructed. It is often necessary to have cells of a known thickness, and this is usually achieved by using a spacer material to separate the walls of the cell. For the application of an electric field across the enclosed liquid crystal material, the inner surfaces of the cell may be coated with a conductive material before any surface alignment is applied. The various types of cell used in this work are described in detail below.

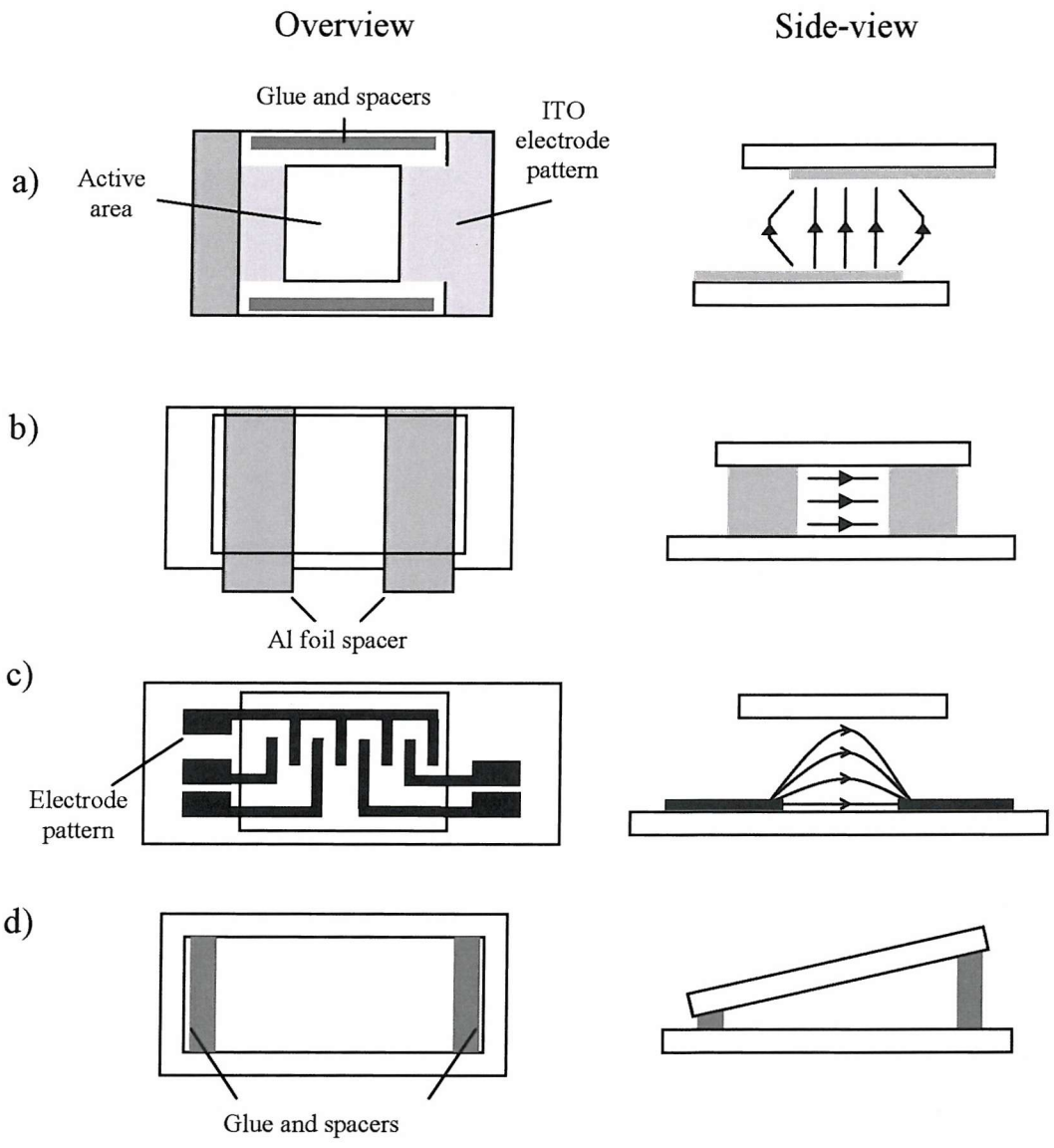

Figure 3.4 The cells used in this work for electro-optical studies.

The most commonly used cells were commercially manufactured cells,[13] illustrated in Figure 3.4(a). The cells are made of two glass sides with the inner surfaces coated with indium tin oxide (ITO), which is a transparent conductive coating. In these cells, there is a square region measuring 0.25 mm^2, in which the electric field affects the material. Wires

are soldered on to the ITO layers using indium. The cell can then be connected to a voltage source. Spacer beads of 5 μm or 7.5 μm diameter are contained in the glue that joins the cell walls together. The cells are capillary filled with a liquid crystal in its isotropic phase. A small quantity of the material is placed along an unsealed edge and it then starts to fill the cell by capillary action. Norland optical adhesive is used to seal the filled cells, and the optical adhesive is cured using ultra-violet light. The liquid crystal material may be photochemically altered by the UV light, so exposure is minimised in this process by using a mask. The cells generally carry a layer of rubbed polyimide on both inner surfaces, which acts as a planar alignment layer. The direction of rubbing on the inner surfaces can be parallel to each other (along one of the diagonals of the cell) or perpendicular (primarily for use with achiral nematics). The electro-optic measurements performed in this work are predominantly made using cells with parallel alignment layers

There were also commercially made cells available without alignment layers; these can be easily used to make homeotropic cells. The untreated cells are capillary-filled with a 1% solution of lecithin in chloroform; the chloroform rapidly evaporates leaving a layer of lecithin deposited on the inner surfaces. The cells are then "baked" for a minute at 70°C, to remove any trapped solvent. Lecithin alignment layers decompose at approximately 90°C, which means they have can not be used at higher temperatures. This method for rapidly making homeotropic cells produces good, uniform cells.

A number of home-made cells were also used. These cell were generally produced using glass slides; however to produce electro-optic cells, ITO-coated glass was used. To fabricate planar cells of reasonable quality, the alignment layers are simply deposited on to the surface of the glass substrate using a lens tissue. The direction of the easy axis forms in the rub direction of the alignment layer. The alignment layers are made of 1% aqueous solution of polyvinyl alcohol (PVA) which promotes reasonably strong planar alignment. It is possible to obtain improved alignment layers by depositing the PVA solution on to the glass substrate using the spin-coating technique, then rubbing the layer mechanically using a specially designed rubbing device produced in-house. Spin-coating is a technique whereby the alignment layer solution is dripped on to the substrate, which is rotating at high speed. Spin-coating is also a very good technique for applying a lecithin solution used for promoting homeotropic alignment.

While un-patterned ITO glass is used to make cells where the field is applied normal to the cell walls, it is sometimes necessary to make cells where the field is applied in-plane (or parallel to the cell walls). To make cells for applying in-plane fields, one of two methods was generally used. The first method is to make the cell using glass substrates and, for the electrodes two pieces of aluminium foil (or similar conductive material) are

used. The foil strips also act as spacers, as indicated in Figure 3.4(b). When fabricating such a cell, it is possible to roughly choose the electrode gap, and it is important to keep the electrode edges as parallel as possible. This method is difficult to implement successfully, as the actual construction of the cell can be troublesome and it can be difficult to fill the cell completely, so that air bubbles do not form between the electrode gap. The second method, illustrated in Figure 3.4(c), has an ITO-coated glass surface etched with an inter-digitated electrode pattern. The opposing substrate is made from standard glass and is joined to the first substrate using glue mixed with spacer beads. This construction is much easier to implement than that of the previous method. However, as illustrated in Figure 3.4(c,) there is some inhomogeneity in the field near the electrodes, which does not happen with the foil electrodes, see Figure 3.4(b). This method is the one predominantly used for generating in-plane fields in the present work, because the cells are easier to make, and the electrode gap and cell thickness can be controlled more easily.

There is one more kind of home-made cell used in this work and that is the wedge cell. In a wedge cell the opposing surfaces are not parallel, but are aligned at an angle to each other, as illustrated in Figure 3.4(d). To make a wedge cell, two mixtures of glue and spacer beads are used, where the spacer beads have different diameters in each mixture. One glue mixture is lightly spread on the edge of one glass surface and the other mixture is spread along the opposite edge. The second glass surface is lightly placed on the first. The interference fringes in the cell can then be used to judge the uniformity of the wedge. A good wedge cell should show equally-spaced interference fringes running parallel to the glued edges; if this is the case, the cell is placed in the UV oven to allow the glue to cure. Otherwise, the interference fringes in the cell can be adjusted by applying physical pressure. It is important not to use too much glue or it capillary-fills the cell.

The spacer beads used in this work are commercially available Dynospheres produced by Agar. The diameters of spacer beads range from 1 to 40 μm.

3.3.2 Characterisation of the cells

It is important to know the spatial properties of the cells used to characterise liquid crystals. For standard cells, where the field is applied in a direction perpendicular to the cell walls, the cell gap at the electrode area should be known (so that the field can be determined). This distance is measured using the UV-Visible spectrometer. The empty cell is mounted on the holder of the spectrometer normal to the light path. The holder's aperture is a slit of ~1mm width. The cell wall acts as an etalon, producing interference fringes which appear as peaks and troughs in the measured spectrum. For normal incidence, the interference spectrum is given by the equation below:

$$m\lambda_m = 2n_{cell}d\,, \tag{3.1}$$

where n_{cell} is the effective refractive index of the material in the cell (for an empty cell n_{cell} = 1), m is the order of the interference at the wavelength λ_m and d is the distance between the glass walls. By comparing the wavelengths at which successive peaks (or alternatively, troughs) occur, the cell gap can be determined from the following equation:

$$2d = \frac{\Delta m}{\Delta(1/\lambda_m)}. \tag{3.2}$$

This technique has an accuracy of 0.1 μm.

For cells in which the electric field is applied parallel to the cell walls, it is necessary to know both the cell thickness and the size of the electrode gap. For the cell using foil electrodes the cell gap is approximately equal to the thickness of the foil, while for the second type of cell (etched electrode pattern) the cell thickness can be measured using the UV-Visible spectrometer, as described above. The electrode gap can simply be measured using the crosshair with divisions in the eyepiece of the microscope.

Two methods were used to measure the wedge angle of a cell. The first way to calculate the wedge angle is to count the interference fringes across a certain length of the cell when it is placed under a sodium lamp (emission wavelength of 589nm). Then using the following equation it is possible to calculate the wedge angle ϕ_w:

$$\tan\phi_w = \frac{\lambda n}{x}, \tag{3.3}$$

where λ is the wavelength of the light used and n is the number of fringes in the distance x. The difficulty with this method is that the fringes can be too numerous to count accurately. For example, for a wedge angle of 0.1° the fringe spacing would be 0.34mm.

The second method used to measure the angle of the wedge cell is to use the UV-Visible spectrometer. The aperture of the spectrometer is a slit ~1mm wide. By measuring the cell width at various marked positions on the cell it is possible to calculate the wedge angle, ϕ_w, (see Figure 3.5, below) using the following simple equation:

$$\tan\phi_w = \frac{d_1 - d_2}{x}, \qquad (3.4)$$

where d_1 and d_2 are the cell widths measured at two positions separated by the distance x. The bulk of wedge angle measurements made in this work were made using this UV-Visible spectrometer method.

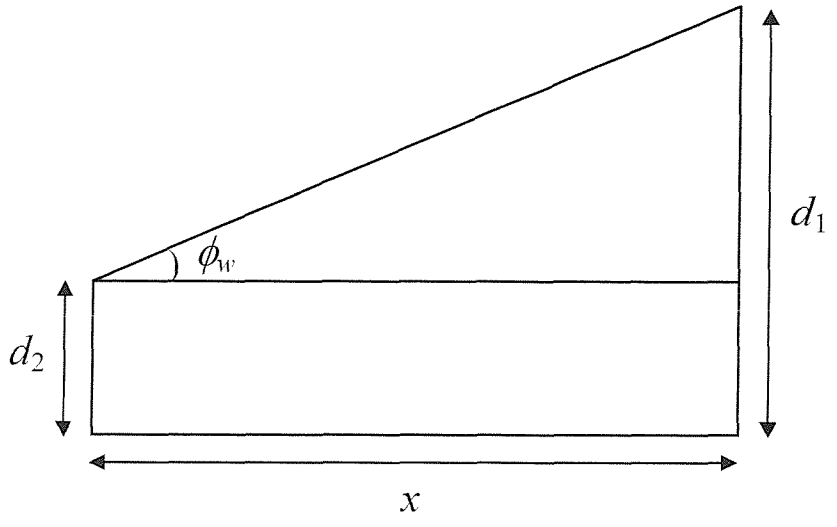

Figure 3.5 A diagrammatic explanation of the parameters given in equation 3.4.

3.3.3 Making mixtures

For almost all the work produced for this thesis, the liquid crystal materials used are mixtures, composed of two or more different materials. The quantities of the different materials used are given as weight percentages of the total weight of the mixture. The respective weights of the materials used are measured using a Mettler Toledo AG245 balance. The materials are usually measured into a bottle or similar sample holder; then heated into the isotropic phase to mix. The mixture is usually left for 48 hours or longer (depending on the mixture) in the isotropic phase, so that diffusion gives a well-mixed sample. For chiral nematic mixtures it is possible to make a visual estimation of the quality of mixture by observing the uniformity of the colour of the reflected light. The total weight of an individual mixture was usually in the region of 20 mg to 100 mg, depending on the availability of the component materials.

3.4 Characterisation of mesophases

3.4.1 Optical characterisation of liquid crystal phases

An effective and commonly-used method for identifying liquid crystal phases is by visual observation using a polarising microscope. The textures observed give an indication as to which phase the liquid crystal is in, and by using different alignment layers or shearing the sample, further clues as to the identity of the phase can be uncovered. The use of alignment layers can result in the formation of large well-aligned domains; this allows the effects of the anisotropy of the molecules to be viewed macroscopically. Sometimes a texture with smaller domains (a defect texture) can give more information about a phase than a well-aligned liquid crystal. However, if the domains are very small and there are many defects then a scattering texture is observed. This texture is generally not identifiable as belonging to a particular phase. By shearing such a sample it may be possible to promote the formation of larger domains, which give may help with identifying the phase. Phases may also be identified by applying an electric field (or magnetic field), and observing the behaviour of the sample in these external fields. There are many different liquid crystal phases in existence, but only a select few were observed in the course of this work. The observations and techniques used to identify these phases are described below.

The nematic phase can usually be identified with a polarising microscope by its schlieren, or brush textures. These textures usually form when a nematic is aligned in-plane and it has defect points; the molecules lie in-plane but the director does not have a uniform direction. At defect points, dark brushes appear where the nematic molecules are aligned with either of the microscopes crossed polarisers, see Figure 3.6. A nematic phase may exhibit either two or four brushes at a defect point; this is unique to a nematic and can serve as a method for identifying the phase.

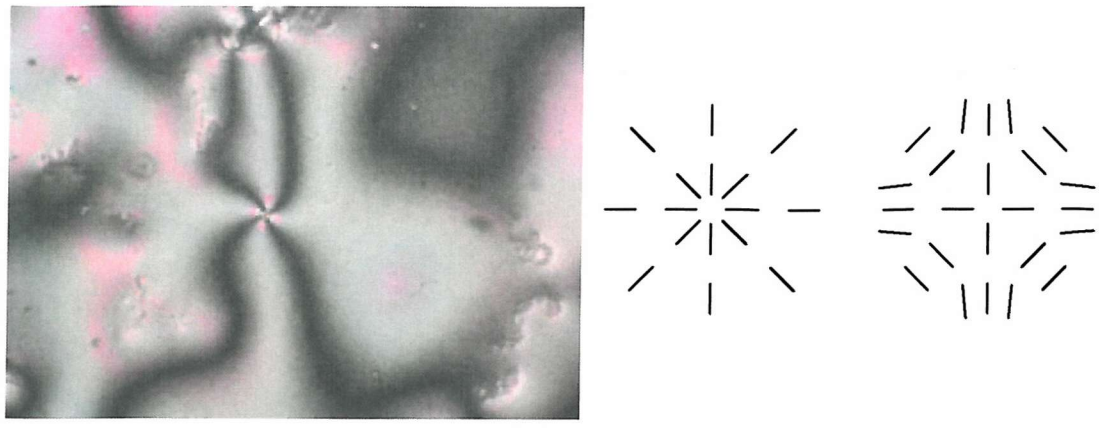

Figure 3.6 The schlieren (or brush) texture in a nematic liquid crystal and a schematic of the possible director configuration around two of the point defects that can cause this texture.

If a nematic liquid crystal is placed in a cell with parallel planar alignment layers, then the molecules will align in one direction and show no defect points. If the spacing of the cell is parallel then the cell will appear uniform in colour. If the cell walls are not parallel, a range of colours will be observed. This is a consequence of the variation in sample thickness, which causes a change in the wavelength-dependent phase retardation of polarised light. Photographs of a parallel-walled cell and a wedge-shaped cell containing a nematic liquid crystal are shown in Figure 3.7.

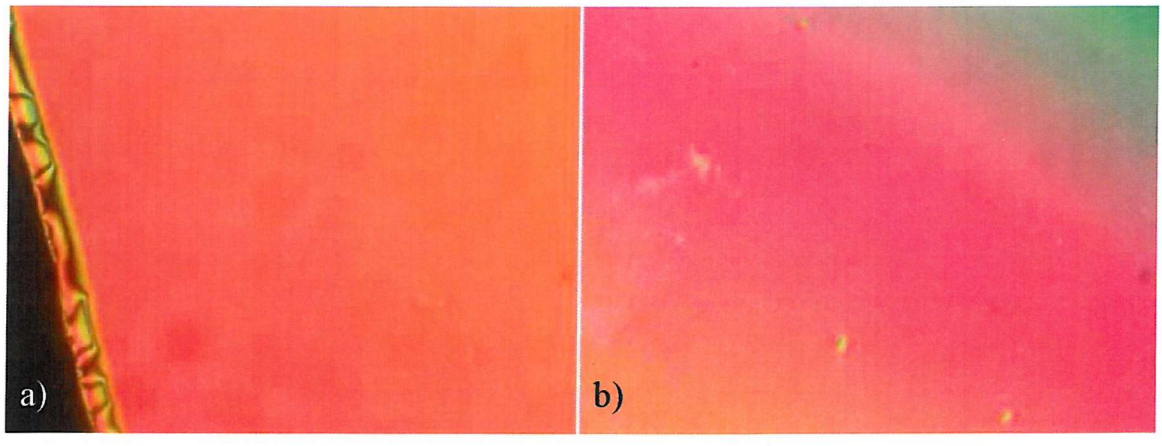

Figure 3.7 A nematic liquid crystal material in a) a parallel-walled glass cell and b) a wedge-shaped cell. Both cells carry planar alignment layers.

When a cell containing a nematic liquid crystal is physically compressed, there is always a flash of colour, indicative of a brief change in the retardation. If a nematic liquid crystal is

aligned homeotropically, the cell will appear black between crossed polarisers and will flash if the cell is momentarily compressed, as the molecular alignment is disturbed.

The chiral nematic phase is an easily recognisable liquid crystal phase, as it usually adopts the Grandjean texture in glass cells carrying planar alignment. The Grandjean texture is formed when the helical axis of the chiral nematic phase lies orthogonal to the surfaces of the cell walls. This texture forms when the liquid crystal molecules are constrained to lie in the plane of the cell walls. If such a cell is viewed between crossed polarisers, it generally appears uniform in colour. The colour of the Grandjean texture does not change on rotation of the sample when viewed between crossed polarisers as the optic axis of the phase lies parallel to the direction of propagation of the light.

It is common to observe oily streaks in the Grandjean texture of the chiral nematic phase. These oily streaks are defects caused by sections of the chiral nematic helical axis not aligning orthogonally to the surfaces of the cell. The oily streaks can be brought to extinction, when viewed between crossed polarisers, by rotating the cell so the optic axis of the oily streak is parallel to one of the polarisers.

If placed in a cell with homeotropic alignment layers, a chiral nematic liquid crystal can adopt a lying helix texture, with the helix axis lying in the plane of the cell. If the pitch is sufficiently long then the characteristic "finger-print" texture would be observed. For a chiral nematic liquid crystal with a shorter pitch, the material displays a focal conic texture. A typical Grandjean texture and focal conic texture are shown in Figure 3.8 below.

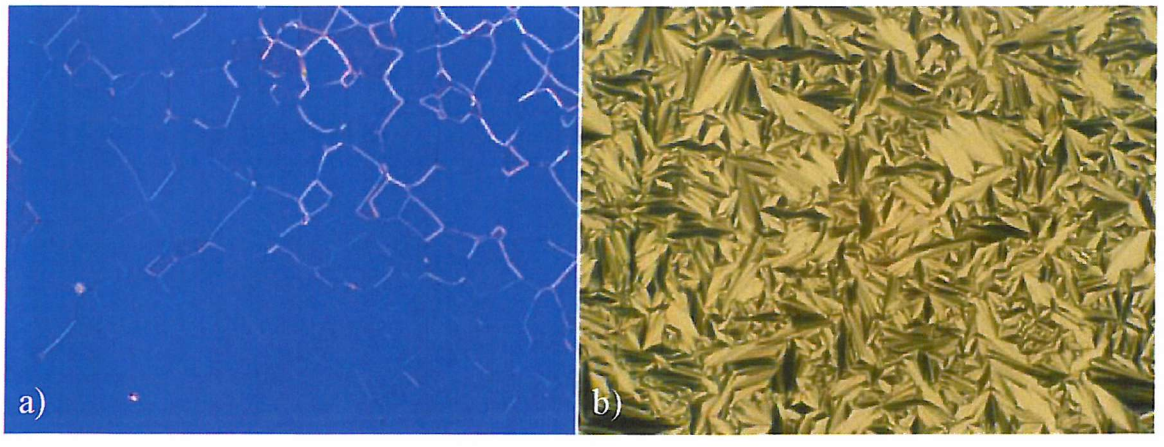

Figure 3.8 a) A typical Grandjean texture with oily streaks present and b) a typical focal conic texture, observed for a chiral nematic.

The smectic A phase is typically recognisable by its focal conic or fan-like texture, which occurs when the material is aligned in-plane, see Figure 3.9(a). The smectic A focal conic

texture is similar to that of the chiral nematic phase; however, the fans are sharper in appearance. When the smectic A phase is aligned homeotropically, it will appear black when viewed between crossed polarisers. Unlike the nematic phase, the homeotropically aligned smectic A phase does not flash when compressed. Shearing the smectic A phase when aligned in the focal conic texture can also induce the formation of the homeotropic texture. The chiral version of the smectic A phase shows no difference optically to the achiral version.

On cooling from the isotropic phase into the smectic A (or A*) phase, the mesophase forms as elongated batonnets. When compared to the nematic phases, which form from the isotropic phase in droplets, these batonnets are an indication of the higher order of the smectic phase.

The majority of the work carried out in this thesis is concerned with chiral nematics; the only observations of the smectic A* phase were made using materials with an over-lying chiral nematic phase. For the transition from the chiral nematic phase to the smectic A* phase to occur, it is required that the helix of the chiral nematic phase is unwound, enabling the molecules to form into the layers associated with the smectic phase. Thus, the presence of an underlying smectic A* phase can be identified by an increase in the sensitivity of the pitch of the chiral nematic phase to small changes in temperature. The pitch of the chiral nematic phase is most sensitive to changes in temperature near the chiral nematic to smectic A* phase transition.

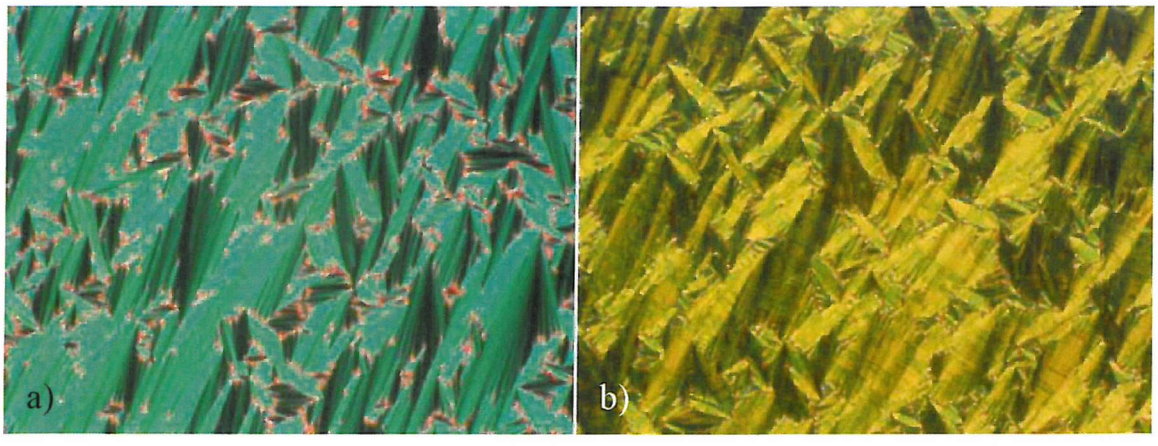

Figure 3.9 a) The "fan-like" focal conic texture of the SmA* phase and b) the "broken" focal conic texture of the SmC* phase.

The chiral smectic C phase is characterised by the "broken" focal conic texture. For the smectic C* phase, the fans appear less distinct than those of the smectic A focal conic texture, as shown in Figure 3.9(b). Due to the tilt in the layers the smectic C* phase cannot

be induced to align homeotropically; instead it forms a dark, cloudy texture. There are materials that exhibit a direct transition from the chiral nematic phase to the smectic C* phase. However, the presence of a smectic A* phase between the chiral nematic phase and the smectic C* phase is more common. The effects on the chiral nematic phase caused by an underlying smectic C* phase are similar to that observed in the presence of an underlying smectic A* phase. There is a rapid pre-transitional increase in the pitch length of the chiral nematic phase as the transition to the smectic C* phase is approached. It should be noted that the pitch of the chiral nematic phase close to the transition has no relation to the pitch of the smectic C* phase. There is an achiral smectic C phase, which differs in appearance to the chiral phase because it does not have any of the physical properties associated with chirality.

For the purpose of this work, only the properties of the chiral nematic phase are of interest. It is, however, very important to know whether a material has an underlying smectic phase as this can directly affect the properties of the chiral nematic phase.

3.4.2 Characterising the chiral nematic phase

The chiral nematic phase has various innate properties related to its helical structure. In this section the various methods used for quantifying these properties are outlined.

The chiral nematic phase exhibits selective reflection spectrum due to its helical pitch. Provided this reflected wavelength occurs in the visible spectrum, it is possible for the pitch of the chiral nematic phase to be measured optically using the Cano wedge technique. For this purpose, wedge-shaped cells of a known wedge angle and carrying parallel planar alignment layers are required. The planar alignment promotes the necessary standing helix configuration for these measurements and restricts the helix to having an integer number of half-turns. Disclination lines form in the Grandjean texture at the boundary where the number of half-turns in the helix increases or decreases by one. These disclinations appear at the edges of what are known as the Grandjean steps. These steps, in a uniform wedge-shaped cell, run parallel to the thin edge of the wedge and are equally-spaced.[14] If the wedge angle, ϕ_W, of the cell is known, then it is possible to calculate the pitch, P, by measuring the separation of the disclination lines, l, and applying the following equation:

$$P = 2l \tan \phi_w . \qquad (3.5)$$

An alternative method, not used in this work, for calculating the pitch length of the chiral nematic phase is to use the helical structure's periodicity as a diffraction grating for a laser. This technique could be used as a replacement for the previous technique described above, especially when it is impossible to make visual observations, such as when the selective reflection wavelength occurs at infra-red wavelengths.

The selective reflection wavelength for the chiral nematic phase, in the Grandjean texture, is directly related to the pitch by the average refractive index of the material. Selective reflection wavelength measurements are performed using the UV-Visible spectrometer, introduced in Section 3.2.6. A glass cell containing the chiral nematic liquid crystal material is mounted in a Mettler heating stage, to allow the selective reflection wavelength to be measured as a function of temperature. By measuring the transmission spectrum of the chiral nematic liquid crystal, a value for the selective reflection wavelength, λ, can be determined. The range of selective reflection wavelengths that can be measured is limited by the spectral range of the UV-Visible spectrometer, i.e. 190 to 1100nm. This actual measurable range tends to be narrower than this, due to noise near the upper limits of the spectra range and absorption by the glass cell at the lower limits.

Another measurable physical property of the chiral nematic phase is the handedness of the helix. There are two common methods for measuring this, one of which requires the use of a material of known handedness for comparison. Both methods are discussed below.

Consider a chiral nematic liquid crystal in the Grandjean geometry, placed between crossed polarisers and illuminated with white light. A selective reflection band, centred about the selective reflection wavelength, will be observed. For wavelengths outside this reflection band, the plane of polarisation of the light is rotated as it propagates through the chiral nematic liquid crystal. For a wavelength shorter than the selectively reflected band, the rotation of the plane of polarisation is in one direction and, if the wavelength is longer, the plane is rotated in the other direction. This optical effect is a direct result of the anomalous optical rotatory power of the phase, illustrated in Figure 2.9. A small rotation of the top polariser in one direction; brings the light that has been rotated in the same direction to extinction. The light that is now transmitted is the component of the light that was rotated in the opposite direction. For example, consider a left-handed helix: the plane of polarisation of wavelengths shorter than the selective reflection band will be rotated in the same direction as the helix, i.e. anti-clockwise. Longer wavelengths have their polarisation rotated in a clockwise direction, thus if the analyser is rotated in an anti-clockwise direction, a longer wavelength is transmitted. The reverse would be true for a

right-handed helix, i.e. a shorter wavelength would be transmitted. This effect, used to determine the handedness of the helix is summarised in Table 3.1.

Helix Handedness	Rotate Analyser Clockwise	Rotate Analyser Anti-clockwise
Left-handed	Shorter wavelengths transmitted	Longer wavelengths transmitted
Right-handed	Longer wavelengths transmitted	Shorter wavelengths transmitted

Table 3.1 A simple guide for measuring the handedness of the helix using a polarising microscope.

The second method to identify helical handedness is to use a contact preparation between the liquid crystal material of unknown handedness and a material of known handedness. If both materials have the same helicity then the pitch of the "unknown" material should be shortened by mixing with the "known" as the respective twist forces reinforce one another. In the converse case where the helicities of the two materials are conflicting, then the pitch will increase in length and it may be possible to form a region where the twist forces cancel out and an achiral nematic is formed. This method is especially useful when determining the handedness of materials which are not inherently liquid crystalline, such as chiral additives.

3.4.3 Determining the transition temperatures of liquid crystal materials

One method for the determining the transition temperatures of liquid crystal materials is by the use of differential scanning calorimetry (DSC). By comparing the heat required to match the temperature of a sample to that of a reference material as their temperatures are changed, it is possible to determine the temperature at which phase transitions occur in the sample. It is very important to note that phases cannot be identified from the DSC trace; only the temperature transitions can be determined. Once the phases have been identified by microscopy, the DSC data can be used to consolidate these observations.

The majority of samples used in this work have simple phase sequences with clear changes in texture at temperature transitions; as a result in most cases the temperatures quoted are those measured using observation from polarising microscopy. It is important to note that transition temperatures are influenced by their surroundings (e.g. by the presence of alignment layers). For example, the same material studied by DSC and observed in a glass cell on a microscope, may exhibit different transition temperatures. For an accurate

comparison of the transition temperatures for two different materials, using the DSC would be the recommended method.

Another technique used in this work was an adaptation of the microscopy method. The VEE language was used to create a program that records the output of the photodiode during an automated temperature scan. A plot of the photodiode response as a function of temperature is then produced for a liquid crystal material. The response of the photodiode is sensitive to any textural changes in the sample. This method can be used to complement DSC scans and, in some cases, was used to provide data about transitions that were unclear from the DSC.

Throughout this work, the reduced temperature of a material is often quoted in place of the absolute temperature. There are a number of differing definitions used for the reduced temperature; for the purpose of this work the reduced temperature is defined as:

$$T_{reduced} = T - T_{clearing}, \tag{3.6}$$

where $T_{clearing}$ is the temperature at which the isotropic phase transition occurs, upon heating.

3.5 Electro-optic properties

3.5.1 Critical fields and achieving the uniformly lying helix texture

The critical fields are defined as the electric field values at which geometrical changes in texture occur in the chiral nematic phase. Generally, the critical fields of chiral nematics materials with positive dielectric anisotropy were measured, with the material initially aligned in the standing helix/Grandjean geometry. The material is contained in a glass cell with planar alignment layers that is placed on the heating stage of the polarising microscope. For the purpose of this measurement the polarisers are uncrossed (parallel). The sample temperature is as close as possible to the clearing temperature of the material (taking into account any blue phases that may be present). The photodiode response is recorded as a function of the electric field applied across the glass cell. The process of recording the photodiode response and controlling the applied field is automated using the VEE programming language. A measurement temperature close to the clearing temperature is used, as it allows the lowest possible values of the critical fields to be measured. The critical values are at their lowest because the elastic constants and viscosities of the chiral nematic phase are near their minimum values.

As a function of applied field, the chiral nematic goes through the sequence of texture changes that were discussed in Section 2.8.1. A diagram of the photodiode response as a function of applied field is shown in Figure 3.10. The locations of the critical fields are marked.

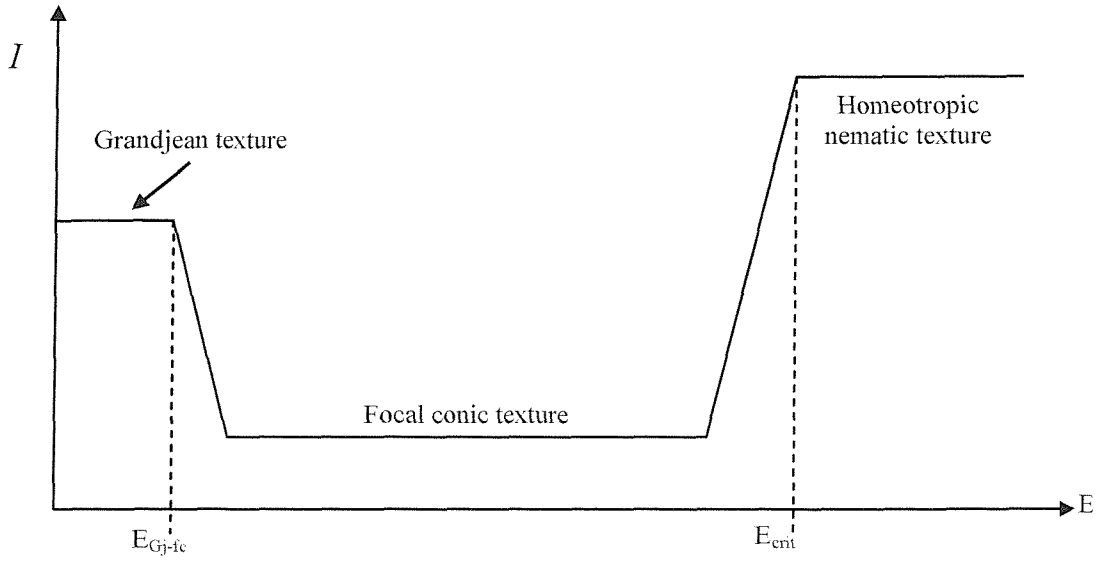

Figure 3.10 A diagram of the theoretical photodiode response, as a function of increasing electric field, for a chiral nematic that is initially planar aligned.

As the applied field is increased from zero, there occurs a critical field, $E_{Gj\text{-}fc}$, at which the grid and stripe texture starts to nucleate within the Grandjean texture. This is indicated by a decrease in the light intensity at the photodiode, which decreases further as the Grandjean texture is deformed. As the applied field is increased further, the light-scattering focal conic texture nucleates. At a higher applied field, the onset of helix unwinding will be signified by an increase in light intensity. When the helix is unwound totally, at E_{crit}, the light intensity detected will reach a maximum. On decreasing the field some hysteretic behaviour may be observed in the transition from the fully unwound helix state to the focal conic texture. The standing helix texture may or may not re-establish at fields close to zero: if not, the liquid crystal material will remain in the focal conic texture and the light intensity will not return to its initial value.

The rate at which the focal conic texture relaxes to the Grandjean texture depends on a number of factors, including: the material's viscosity; the anchoring energy of the alignment layers; the material's elastic constants; and the thickness of the sample.[15,16] The pitch of the material also has a significant effect on the relaxation time, with a shorter pitch material taking longer to relax than a longer pitch material.

The critical field at which the focal conic texture starts to nucleate is dependent on the presence of oily streaks in the Grandjean texture. In the presence of oily streaks, the focal conic texture will nucleate from these oily streaks. In the absence of oily streaks, the focal conic texture has to nucleate from defects in the cell walls or impurities within the sample.[17] Nucleation from defects or impurities tends to require a higher field than nucleation from oily streaks. As the presence of defects and impurities in uncontrollable, to produce consistent measurements of the $E_{Gj\text{-}fc}$ critical field (especially when comparing different materials), it is necessary to ensure the presence of an oily streak within the microscope field of view, because the oily streak defect acts as an easily observable nucleation point.

These critical field measurements are important to this work as they give an indication of the electric field range over which flexoelectro-optic switching may be performed. The upper limit for flexoelectro-optic switching is the point at which the helix starts to unwind just below the critical field E_{crit}, since this is equivalent to the point at which the uniformly lying helix texture starts to degrade. As the sample temperature is decreased, important parameters such as the viscosity and elastic constant increase, increasing the critical field for total helix unwinding. The critical field at which the scattering focal conic starts to nucleate is also important because it defines the minimum electric field required to achieve the uniformly lying helix texture. Flexoelectro-optic switching does occur for all non-zero applied fields below the field for total helix unwinding; however, in some cases if the field is too low to maintain the lying helix alignment, the texture will degrade as the material relaxes back to the Grandjean texture. This degradation is characterised by the appearance of "ribbons" of Grandjean texture in the uniformly lying helix texture.

In order to characterise flexoelectro-optic switching in a chiral nematic material, it is necessary to promote the formation of the uniformly lying helix texture. The texture can be considered as a variant of the focal conic texture, transformed into a monodomain birefringent texture, with its optic axis lying uniaxially in the plane of the cell. Typically, for a material with positive dielectric anisotropy, a combination of an electric field and shearing is required to promote the uniformly lying helix texture. The field has to be sufficient to induce the scattering focal conic texture, as this is necessary for the helix to lie in the plane of the cell. The process of shearing the cell (or creating a flow in the cell) causes the helices to lie with their axes uniformly aligned in a single direction. There are a number of novel techniques for achieving the uniformly lying helix without shearing the material, some of which are discussed in this work.

3.5.2 Electro-optic switching

The switching properties of interest to this work are the tilt angles and the response times associated with a flexoelectro-optically switched chiral nematic liquid crystal material. To observe the electro-optic switching properties of a liquid crystal material, it is usual to study the material between crossed polarisers.

Consider a material of birefringence Δn and thickness d, placed between crossed polarisers. The material's optic axis lies at an angle ψ to the transmission axis of the first polariser. The light intensity transmitted by the second polariser (called the analyser for clarity) is given by:

$$I(\psi) = I_0 \sin^2(2\psi) \sin^2\left(\frac{\Delta n d \pi}{\lambda}\right), \tag{3.7}$$

where I_0 is the intensity of the polarised light incident on the sample and λ is the wavelength of the light. This arrangement is shown schematically in Figure 3.11, together with a diagram showing transmitted intensity as a function of ψ.

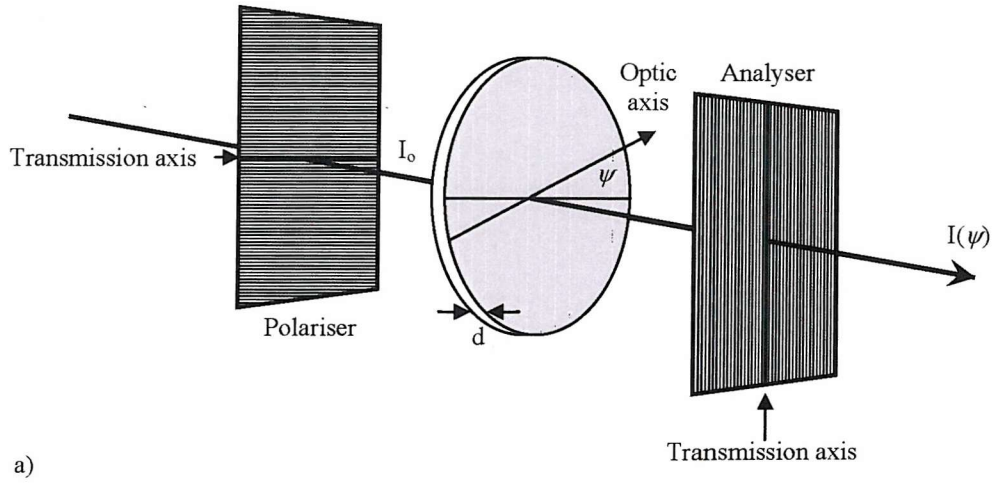

a)

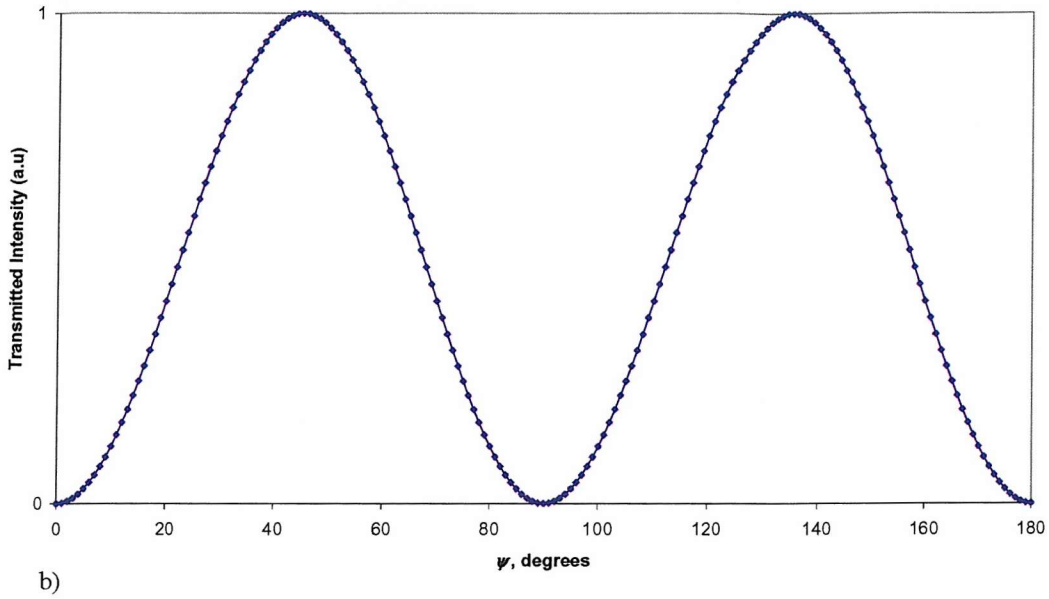

b)

Figure 3.11 a) A simple representation of light passing through a birefringent material placed between crossed polarisers and b) the transmitted intensity as a function of the angle between the optic axis of the material and the transmission axis of the first polariser.

When the direction of the optic axis is changed by some angle, ϕ, in the plane of the material, the intensity of the light transmitted becomes:

$$I(\psi,\phi) = I_0 \sin^2[2(\psi \pm \phi)]\sin^2\left(\frac{\Delta n d\pi}{\lambda}\right). \qquad (3.8)$$

From Equation 3.8 and Figure 3.11, it is clear that the greatest contrast between two states will be observed when the optic axis of the material is rotated from being parallel to either the polariser's (or analyser's) transmission axis to lie at an angle of 45° or 135°.

In this work, the tilt angle is defined as being the maximum angle the optic axis rotates away from the equilibrium position of the optic axis for a certain applied electric field, $\phi(E)$. The switching angle is defined as the angle between the two switched states, $2\phi(E)$. To measure the tilt angle, a monopolar field may be applied across the cell. However, it is more convenient to apply a bipolar field, which results in the optic axis sweeping through the switching angle $2\phi(E)$. Tilt angles are measured as a function of applied electric field and temperature, using the polarising microscope set-up described previously. The following method is used to measure the tilt angles:

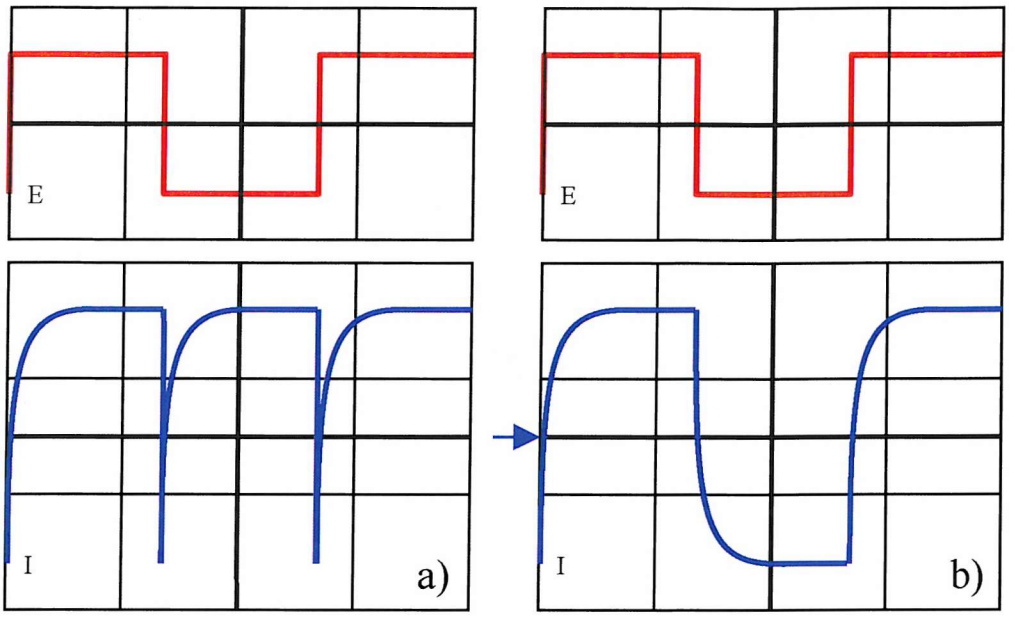

Figure 3.12 A diagrammatic representation of the photodiode response, for a bipolar square wave applied field, when the zero position of the optic axis is a) parallel and b) at 22.5° to the transmission axis of one of the polarisers.

1) Initially, the sample is rotated until the equilibrium position of the optic axis is aligned with the transmission axis of one of the polarisers, i.e. $\psi = 0°$, see Figure 3.12(a).
2) The sample is then rotated by 22.5°, so that $\psi = 22.5°$. The mid-point of the two switched positions is marked with a cursor on the oscilloscope, as shown on Figure 3.12(b).
3) The sample is then rotated until the maximum of one of the switched positions lies level with the cursor; the position of the rotation stage is then noted.
4) The sample is then rotated in the opposite direction until the maximum of the other switched positions lies level with the cursor; the new position of the rotation stage is noted. The tilt angle is equal to half the difference between the two noted positions.

This method is very accurate especially for small angles, as a small rotation of the optic axis close to $\psi = 22.5°$ produces a large change in light intensity. The tilt angles measured are accurate to 0.25°.

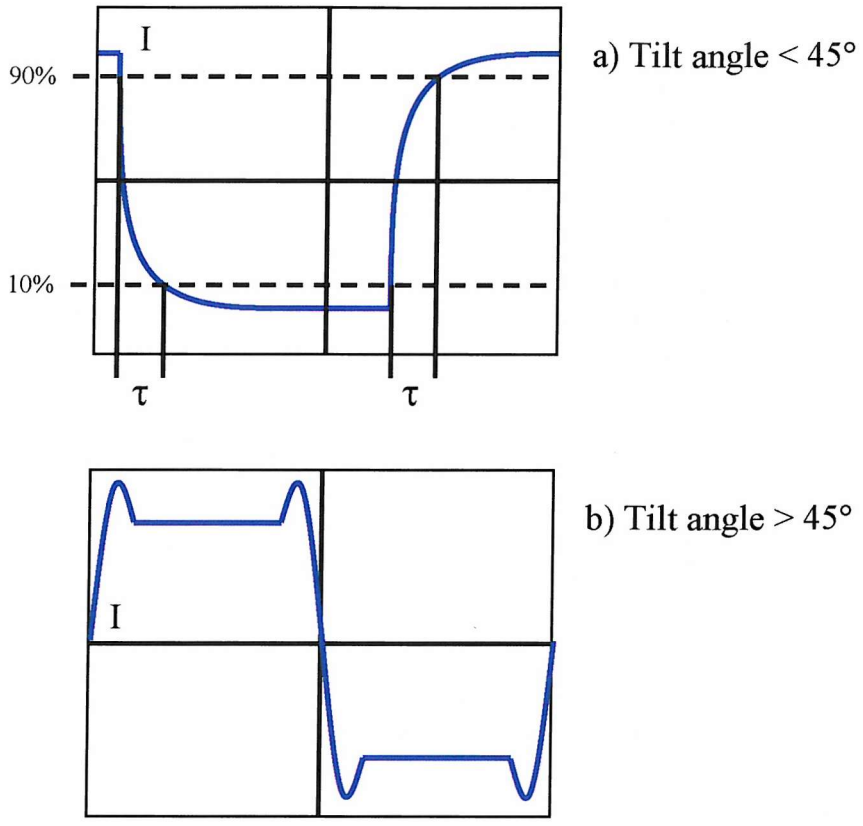

Figure 3.13 Diagrammatic representation of the typical photodiode response for a) tilt angles less than 45° and b) for tilt angles greater than 45°.

The response times of materials are measured as the time taken for the light intensity at the photodiode to change in intensity from 10% to 90% of the maximum intensity (or 90% to 10%) as a function of applied field. This is illustrated in Figure 3.13(a). The change of 10% to 90% was chosen as it negates any delay after the polarity of the field is switched. It should be noted for flexoelectro-optic switching there is no delay:[18] measuring an intensity change of 10% to 90% allows the flexoelectro-optic response times to be compared fairly to alternative switching regimes, which do exhibit a delay when the polarity of the field is switched. The response times are measured using a bipolar field square waveform and as a result of this, the response time measured is for the full switching angle, rather than the tilt angle.

The sample is aligned with its equilibrium optic axis at 22.5° to the transmission axis of one of the polarisers, i.e. $\psi = 22.5°$. Response times for tilt angles less than or equal to 22.5° are easily measurable using the method described with an uncertainty of less than 3%. However, larger tilt angles produce a more complicated electro-optic response, as illustrated in Figure 3.13(b). It is possible to measure these response times using the

polarising microscope, but the measurement is more complicated and thought to be less accurate.

3.6 The flexoelectric properties of a simple liquid crystal material

The flexoelectric properties of a simple monomesogen were examined to give a useful reference for the novel materials studied in this work. The material chosen for this was 7OCB, which is an alkylcyanobiphenyl.[19]

The chemical structure of 7OCB is shown in Figure 3.14.

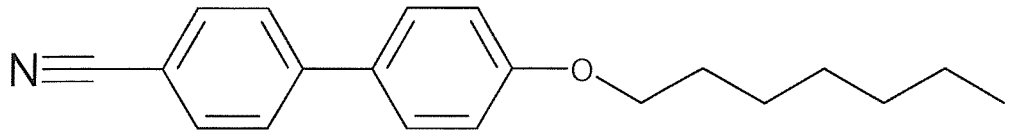

Figure 3.14 The chemical structure of 7OCB.

The transition temperatures of 7OCB are:

Crystal –(54°C)-> Nematic –(74°C)-> Isotropic.

The transition temperatures were taken from the Merck datasheet[20] for 7OCB. For completeness, the transition temperatures were measured for comparison using the differential scanning calorimeter. The following transition temperatures were observed:

Crystal –(48.3°C)-> Nematic –(74.8°C)-> Isotropic (On Heating)

To induce chirality in 7OCB and produce a chiral nematic phase, the monomesogen was mixed with a small quantity of the chiral additive BDH1281.[21,20] The flexoelectro-optic switching properties of the chiral mixture could then be studied.

Three different mixtures of BDH1281 in 7OCB were prepared; the concentrations of BDH1281 used were 2.20%, 2.95% and 3.91% (weight/weight). The transition temperatures of the three mixtures were measured using the differential scanning calorimeter. The results of this study are shown in Table 3.2 below.

Concentration of BDH1281 in 7OCB	On Heating
2.20%	**Crystal** -(46.3°C)-> **N***-(73.8°C)-> **I**
2.95%	**Crystal** -(45.7°C)-> **N***-(73.7°C)-> **I**
3.91%	**Crystal** -(44.2°C)-> **N***-(73.1°C)-> **I**

Table 3.2 The transition temperatures of 7OCB with various percentages of the chiral additive BDH1281 (all percentages are weight/weight) measured using DSC.

From Table 3.2 it can be seen that the transition temperatures decrease as the concentration of chiral dopant is increased. The clearing temperature for the 3.91% mixture, when compared to pure 7OCB, is lower by 1.7°C. When measured in glass cells, via optical microscopy, the difference in clearing temperatures for the three mixtures and pure 7OCB is negligible.

3.6.1 Flexoelectro-optic studies

2.20% BDH1281 in 7OCB

The first mixture to be studied was 2.20% BDH1281 in 7OCB (w/w). Initial visual observations show that the mixture undergoes the transition from the chiral nematic phase to the isotropic phase at 74°C. No blue phases were observed on either heating or cooling. The flexoelectro-optic switching properties of the mixture were studied with the mixture aligned in the uniformly lying helix geometry. The results of the measurements are shown in Figure 3.15.

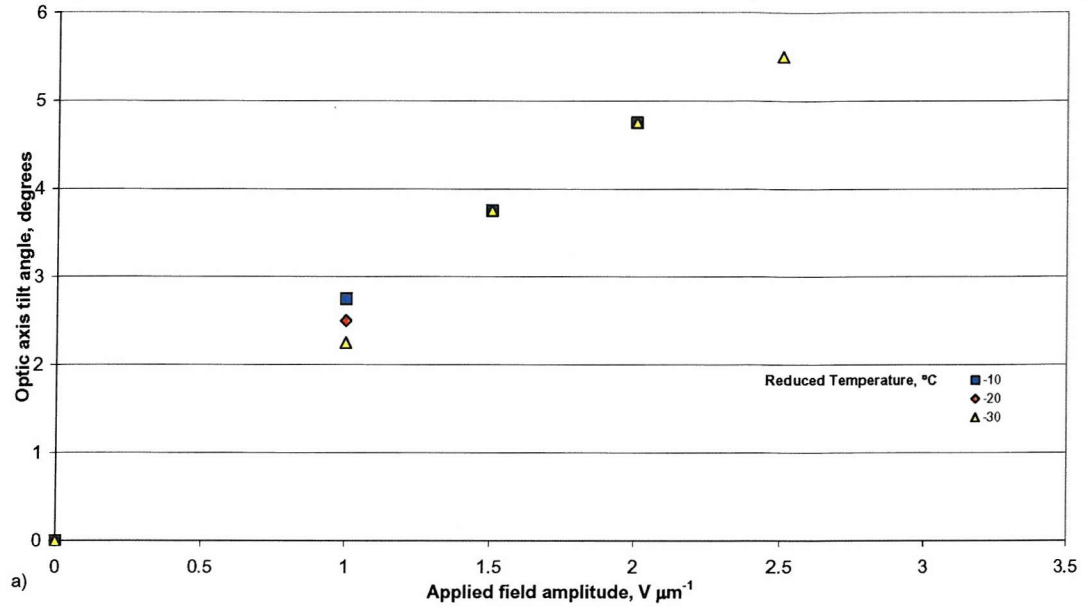

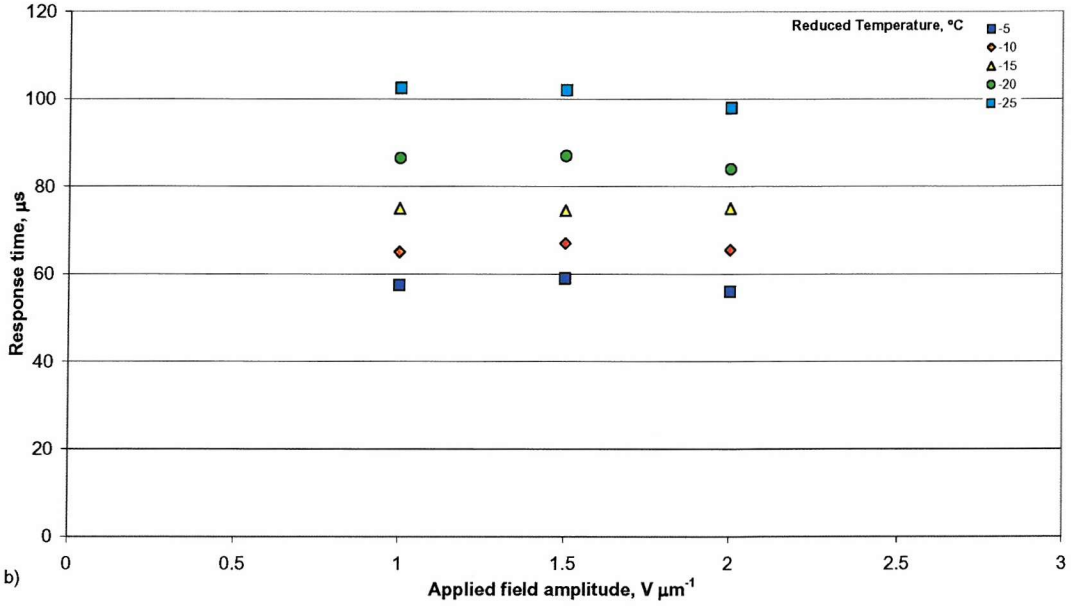

Figure 3.15 The flexoelectro-optic switching properties of a mixture of 2.20% BDH1281 in 7OCB (w/w). The graphs show, as a function of applied field amplitude, a) the induced tilt angles and b) the response times, measured across a range of reduced temperatures. The response times are measured for 10-90% of the full switch of the optic axis, i.e. twice the tilt angle. The measurements were made in a commercially-made cell, carrying planar alignment layers, with a thickness of 5.00μm.

From these results it can be seen that a maximum tilt angle of 6° is achievable. The application of higher electric fields than those shown, results in degradation of the

alignment; this is associated with the onset of full helix unwinding. The response times are fast (ranging from 50 to 110μs) and are comparable to the typical response times of a surface stabilised ferroelectric liquid crystal.[22]

The pitch and selective reflection wavelengths of the mixture were also measured, as a function of temperature. The wavelength at which selective reflection is observed is outside of the range measurable at lower temperatures. The selective reflection wavelength and pitch of the mixture is shown in Figure 3.16.

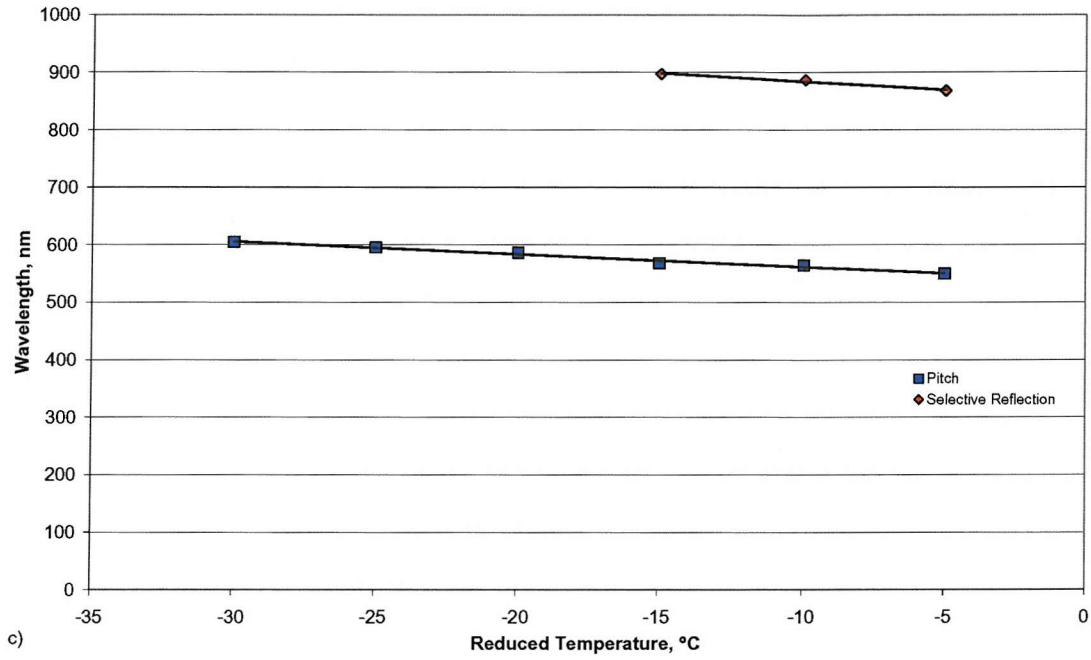

Figure 3.16 The selective reflection wavelength and pitch measurements for 2.20% BDH1281 in 7OCB. Trend-lines were added to guide the eye. The pitch was measured using a wedge cell of angle 0.042°.

In Chapter 2 it was shown that:

$$\tan\phi = \frac{\bar{e}E}{kK} = \frac{\bar{e}E}{K}\frac{P}{2\pi}. \qquad (2.32)$$

Rearranging this equation gives:

$$\frac{\bar{e}}{K} = \frac{\tan\phi}{E}\frac{2\pi}{P}, \qquad (3.9)$$

where P is the helical pitch; E is the applied electric field amplitude; ϕ is the flexoelectro-optic tilt angle; $\bar{e}$ is the effective flexoelectric coefficient; and K is the average of the splay and bend elastic constants. At a given temperature, the ratio $\tan\phi/E$ is measurable as the gradient of the tangent of ϕ against applied electric field, giving:

$$\frac{\bar{e}}{K} = \frac{\Delta \tan\phi}{\Delta E}\frac{2\pi}{P}. \qquad (3.10)$$

Using the measurements of tilt and pitch it is now possible to calculate the ratio of $\bar{e}/K$. This ratio of the effective flexoelectric coefficient and the average of splay and bend elastic constants is known, for convenience, as the "flexo-elastic" ratio. The flexo-elastic ratio gives a direct indication of the flexoelectric properties of a material, with higher values corresponding with better flexoelectric properties.

It is also possible to calculate the average refractive index of a material as a function of temperature, by using values measured for the selective reflection wavelength and pitch substituted into Equation 2.5:

$$\lambda_0 = \bar{n}P. \qquad (2.5)$$

The flexo-elastic ratio and values for the average refractive index are calculated for 2.20% BDH1281 in 7OCB. The results of these calculations are shown in Table 3.3.

Reduced Temperature, °C (Tc = 74°C)	Selective Reflection Wavelength, Nm	Pitch, nm	$\bar{n}$	$\Delta\tan\phi/\Delta E$, μm V^{-1}	$\bar{e}/K$, C N^{-1} m^{-1}
-5	868	550	1.58	0.0402	0.46
-10	887	564	1.57	0.0417	0.47
-15	897	568	1.58	0.0410	0.45
-20	-	586	-	0.0420	0.45
-25	-	596	-	0.0418	0.44

Table 3.3 A comparison of the values at different reduced temperatures for the ratio of $\bar{e}/K$ for 2.20% BDH1281 in 7OCB.

From these results it would appear that the flexo-elastic ratio remains relatively constant, as the temperature is decreased. Likewise, the average refractive index of the mixture appears relatively constant as a function of temperature.

2.95% BDH1281 in 7OCB

The second mixture studied was 2.95% BDH1281 in 7OCB (w/w). Initial visual observations show that the mixture undergoes the transition from the chiral nematic phase to the isotropic phase at 74°C. On cooling, at least one blue phase is observed between the isotropic phase and chiral nematic phase. The flexoelectro-optic switching properties of the mixture were studied with the mixture aligned in the uniformly lying helix geometry. The pitch and selective reflection wavelengths were also measured. All the results are shown in Figure 3.17.

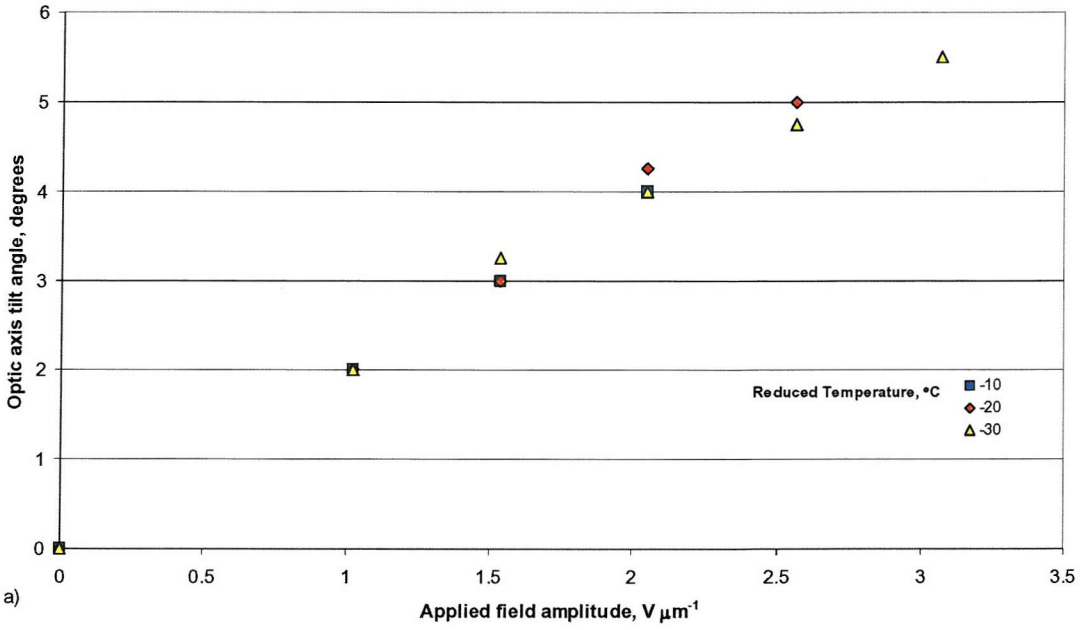

a)

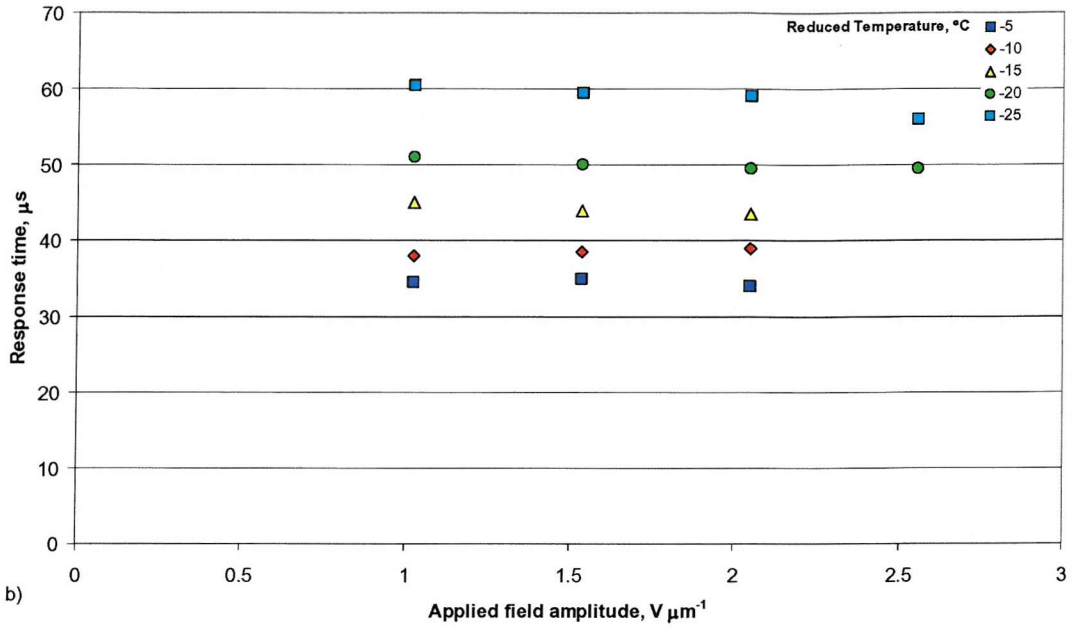

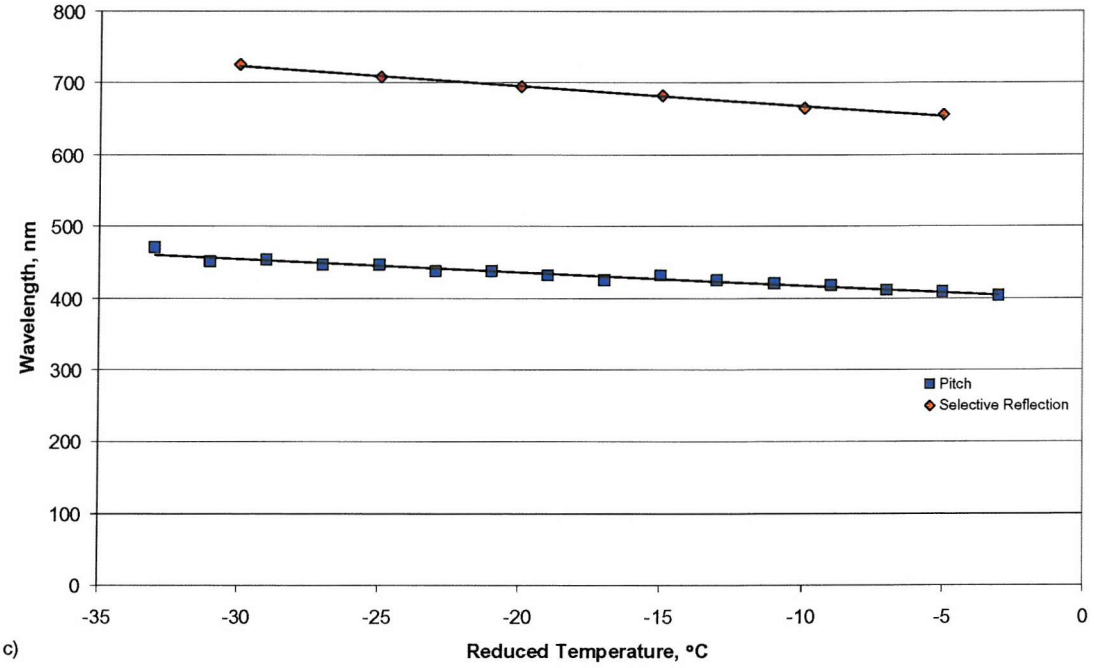

Figure 3.17 The properties of a mixture of 2.95% BDH1281 in 7OCB (w/w). The graphs show a) the induced tilt angles, b) the response times and c) selective reflection and pitch, all measured across a range of reduced temperatures. The response times are measured for 10-90% of the full switch of the optic axis, i.e. twice the tilt angle. The selective reflection properties were measured using a UV-visible spectrometer and the pitch was measured using a wedge cell of angle 0.033°.

Figure 3.17(a) shows that a maximum tilt angle of 5.5° is achievable before dielectric coupling starts to cause degradation in the lying helix alignment. The response times shown in Figure 3.17(b) are fast, ranging from 30 to 60μs.

From this data shown in Figure 3.17, it is possible to calculate the both the flexo-elastic ratio and the average refractive index. The results of these calculations are shown in Table 3.4.

Reduced Temperature, °C (Tc = 74°C)	Selective Reflection Wavelength, Nm	Pitch, nm	$\bar{n}$	$\Delta\tan\phi/\Delta E$, μm V^{-1}	$\bar{e}/K$, C N^{-1} m^{-1}
-5	656	409	1.60	0.0317	0.49
-10	666	419	1.59	0.0342	0.51
-15	683	432	1.58	0.0325	0.48
-20	695	435	1.60	0.0349	0.51
-25	709	446	1.59	0.0325	0.46

Table 3.4 A comparison of the values at different reduced temperatures for the pitch, selective reflection and the calculated values for the average refractive index and the ratio of the effective flexoelectric coefficient to the average of the splay and bend elastic constants. The material studied was 2.95% BDH1281 in 7OCB.

Two observations can be made from these results. Firstly, the average refractive index is relatively invariant (~1.59) over the temperature range measured and secondly the flexo-elastic ratio is also relatively invariant.

3.91% BDH1281 in 7OCB

The final mixture studied was 3.91% BDH1281 in 7OCB (w/w). Initial visual observations show that the mixture undergoes the transition from the chiral nematic phase to the isotropic phase at 74°C. On cooling, at least one blue phase is observed between the isotropic phase and chiral nematic phase. The mixture was aligned into the uniformly lying helix geometry and its flexoelectro-optic switching properties were measured. The pitch and selective reflection wavelengths of the mixture were also measured. All the results are shown in Figure 3.18.

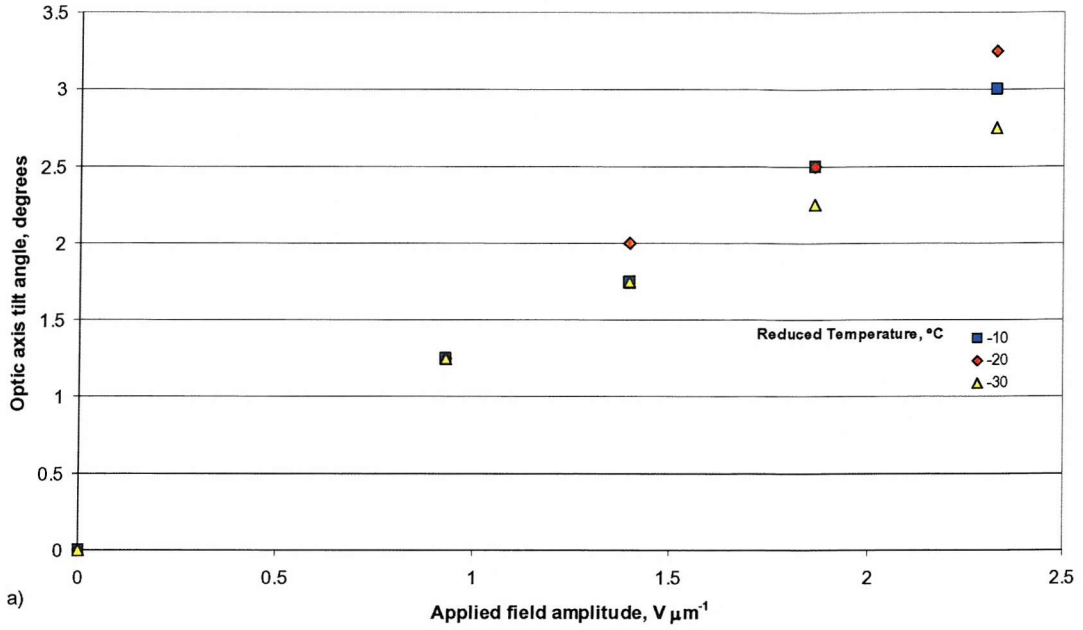
Optic axis tilt angle, degrees
3.5
3
2.5
2
1.5
1
0.5
0
0
0.5
1
1.5
2
2.5
Applied field amplitude, V µm-1
Reduced Temperature, °C
-10
-20
-30

a)

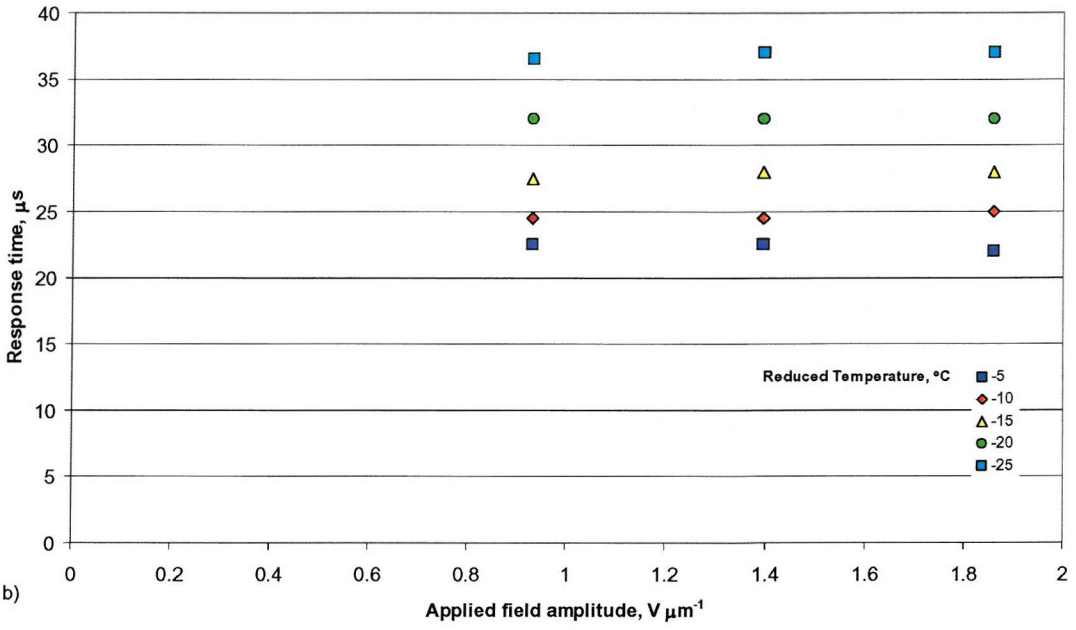
Response time, µs
40
35
30
25
20
15
10
5
0
0
0.2
0.4
0.6
0.8
1
1.2
1.4
1.6
1.8
2
Applied field amplitude, V µm-1
Reduced Temperature, °C
-5
-10
-15
-20
-25

b)

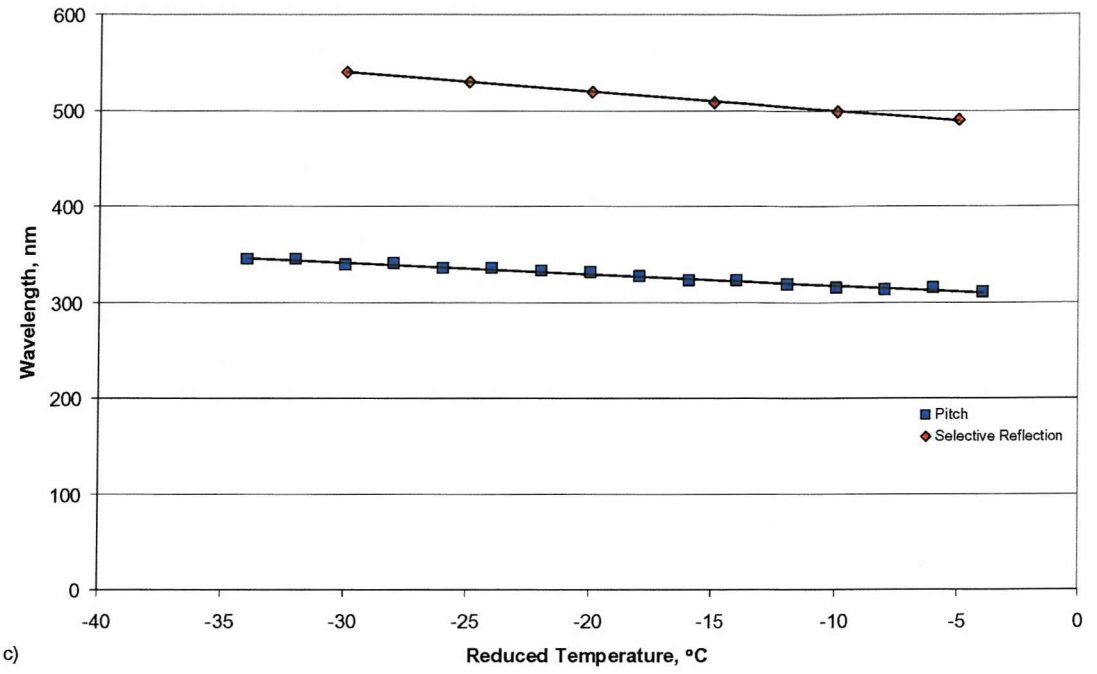

c)

Figure 3.18 The properties of a mixture of 3.91% BDH1281 in 7OCB (w/w). The graphs show a) the induced tilt angles, b) the response times and c) selective reflection and pitch, all measured across a range of reduced temperatures. The response times are measured for 10-90% of the full switch of the optic axis, i.e. twice the tilt angle. The selective reflection properties were measured using a UV-visible spectrometer and the pitch was measured using a wedge cell of angle 0.031°.

Figure 3.18(a) shows that a maximum tilt angle of 3.25° is achievable before dielectric coupling starts to cause degradation in the lying helix alignment. The response times shown in Figure 3.18(b) are very fast, ranging from 20 to 40μs.

From this data it is possible to calculate the flexo-elastic ratio and the average refractive index of the mixture. The results of these calculations are shown in Table 3.5.

Reduced Temperature, °C (Tc = 74°C)	Selective Reflection Wavelength, nm	Pitch, nm	$\bar{n}$	$\Delta\tan\phi/\Delta E$, μm V^{-1}	$\bar{e}/K$, C N^{-1} m^{-1}
-5	491	313	1.57	0.0212	0.43
-10	499	315	1.58	0.0227	0.46
-15	509	323	1.57	0.0227	0.45
-20	520	331	1.57	0.0243	0.47
-25	530	336	1.58	0.0229	0.43

Table 3.5 A comparison of the values at different reduced temperatures for the pitch, selective reflection and the calculated values for the average refractive index and the ratio of the effective flexoelectric coefficient to the average of the splay and bend elastic constants. The material studied was 3.91% BDH1281 in 7OCB.

Two observations can be made from these results. Firstly, the average refractive index is relatively constant (~1.58) and secondly, the flexo-elastic ratio is also relatively constant.

On comparing the three different mixtures, it can be seen that as a greater concentration of chiral dopant is incorporated (i.e. the pitch is shortened), the tilt angles and response times decrease in magnitude. This agrees with the theory of flexoelectro-optic switching[18] discussed in Chapter 2.

The tilt angle measurement accuracy is ±0.25° and, for smaller tilt angles this uncertainty can be significant. For the three 7OCB mixtures, the tilt angles measured are reasonably small, which leads to some inaccuracy in the value of the gradient of $\tan\phi$ against the applied electric field. Such inaccuracies would have a direct effect on the accuracy of the flexo-elastic ratios calculated, and may be partly responsible for the small fluctuations observed. From the results for all three mixtures, it would be suggested that the flexo-elastic ratio for 7OCB is approximately 0.45 C N^{-1} m^{-1}. This value agrees with results for 7OCB measured by the same technique, previously published.[23]

Values for the splay elastic constant are available in the literature for 7OCB.[24] Thus, if the assumption is made that $K_{11} \approx K_{33}$, it is possible to calculate an approximate value for the average of the splay and bend flexoelectric coefficient. The results are shown in Figure 3.19.

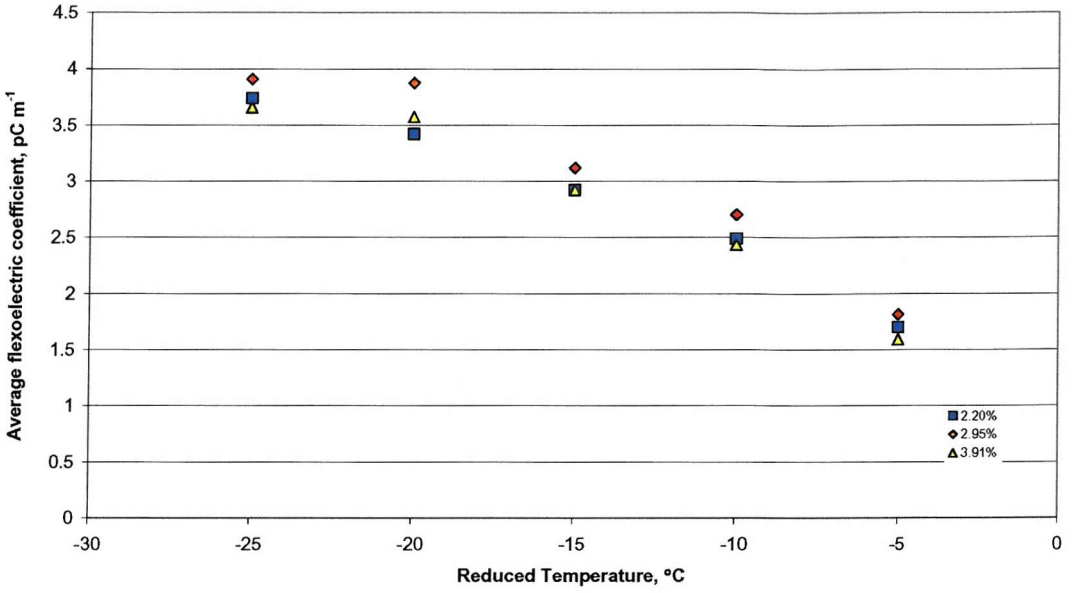

Figure 3.19 A comparison of the calculated values of $\bar{e}$ for the three mixtures of 7OCB and BDH1281.

The spread of the values of $\bar{e}$ for the three mixtures studied is believed to be a result of experimental inaccuracies, as previously discussed. Based on these observations, it is clear that varying the concentration of the chiral dopant has no measurable effect on $\bar{e}$.

In Chapter 2, a theoretical treatment for the flexoelectro-optic response time, τ was introduced. Recall Equation 2.38, which states:

$$\tau = \frac{\gamma}{K}\frac{P^2}{4\pi^2}, \tag{2.38}$$

where γ is the effective viscosity associated with the helix distortion. This equation can be re-arranged to give the ratio of the viscosity coefficient and the mean splay-bend elastic constant in terms of the response time and the pitch:

$$\frac{\gamma}{K} = \tau\frac{4\pi^2}{P^2}. \tag{3.11}$$

From the measurements made for the 7OCB mixtures, it is possible to calculate a value for the ratio of the effective viscosity to the mean of the splay and bend elastic constants. The results of these calculations are shown in Figure 3.20.

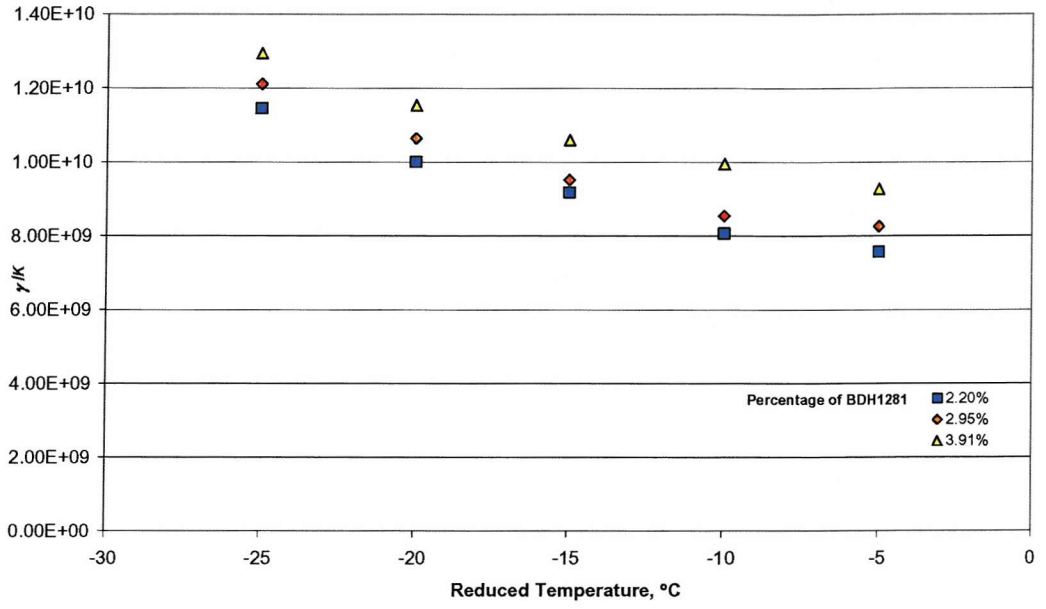

Figure 3.20 The calculated values of the ratio γ/K for the three mixtures of 7OCB doped with different concentrations of chiral dopant.

From Figure 3.20 it can be seen that the concentration of chiral dopant has a direct effect on the ratio γ/K. If it is assumed that at any given temperature K is invariant between the three mixtures, then it would seem that the viscosity associated with the helix distortion increases as the concentration of chiral additive is increased.

From this study, it can be seen that apart from its fast response times 7OCB doped with chiral additive is not an interesting candidate for the further study of flexoelectro-optic switching. Despite its high flexo-elastic ratio, the maximum achievable tilt angles are small and the mixtures undergo helix unwinding at small applied electric fields. The flexoelectro-optic properties of the chiral 7OCB mixtures are used as a reference for the materials studied in this work.

3.6.2 The effects of chiral dopant on some of the physical properties of 7OCB

The order parameters of pure 7OCB and of a mixture of 7OCB with the chiral additive BDH1305[20] (a dopant with lower twisting power than BDH1281) have been measured. The results are shown in Figure 3.21.

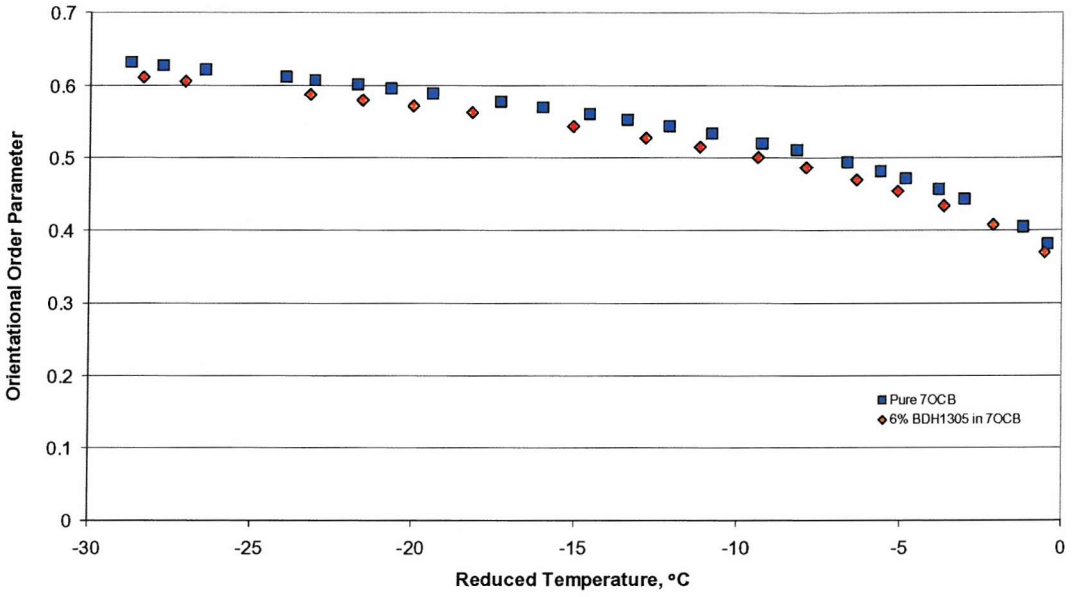

Figure 3.21 A comparison of the orientational order parameter as a function of temperature for pure 7OCB and when doped with a chiral additive. Data reproduced with permission of S. Morris.

Figure 3.21 shows that the orientational order parameter of 7OCB decreases by approximately 4% with the addition of a 6% (w/w) of the chiral additive BDH1305.

For the chiral mixtures it was possible to calculate the average refractive index from the pitch and selective reflection wavelength. The average refractive index of pure 7OCB has been measured directly by an alternative technique (using Abbé refractometry) and the results are reproduced here in Figure 3.22.

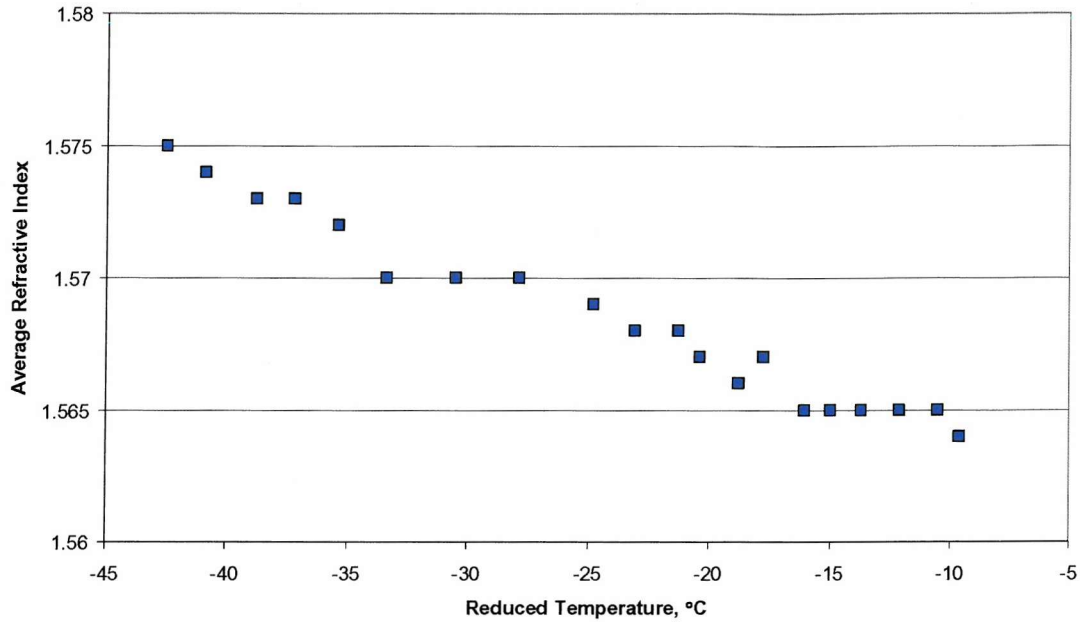

Figure 3.22 The average refractive index of pure 7OCB at 632.8nm. Data reproduced with permission of S. Morris.

The direct measurements of the average refractive index for pure 7OCB (~1.57) compare well with the indirectly measured values for 7OCB doped with chiral additive (1.57-1.59). From this, it is asserted that the average refractive index of the mixture is not significantly different from that of the pure host. It can be seen that the average refractive index measured in Figure 3.22 does not change by a great amount over a large temperature range; this is typical of a liquid crystal material.[25] These observations are important because they mean that the accuracy of pitch and selective reflection wavelengths can be compared as a function of temperature: an anomalously large or small value for the calculated refractive index would indicate that an erroneous measurement had been made. Also, in cases where the pitch cannot be measured directly, it can be estimated with a reasonable degree of accuracy using the average refractive index and the wavelength of selective reflection.

Full helix unwinding occurs at quite a low applied electric field for all three 7OCB mixtures, the unwinding field being lowest for the longer pitch mixture and highest for the shorter pitch mixture. The critical fields for each mixture are measured as a function of temperature, using the author's VEE program. The results of these measurements are shown in Figure 3.23.

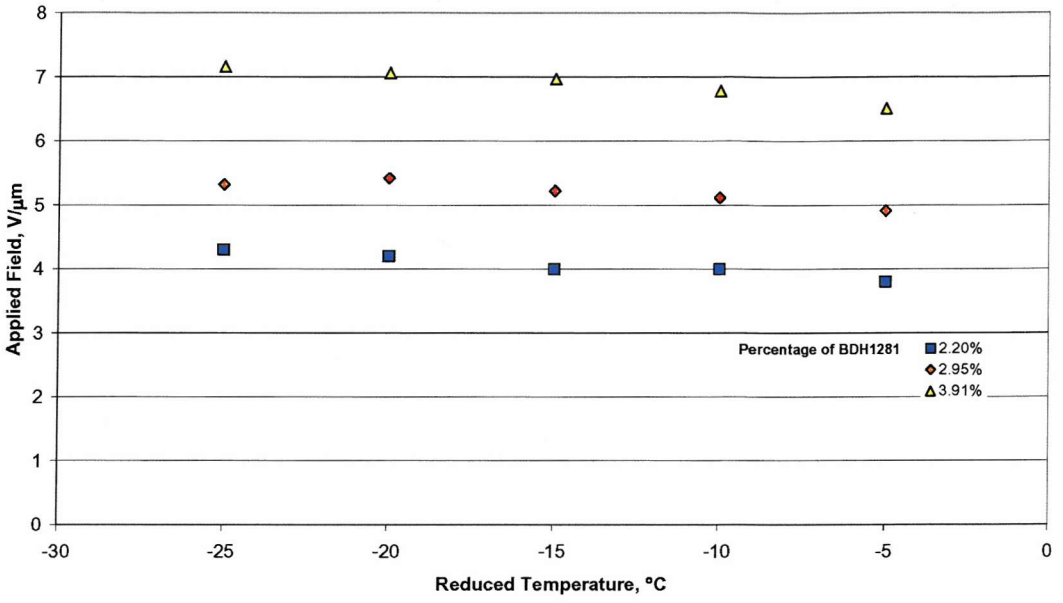

Figure 3.23 A comparison of the applied electric field at which full helix unwinding occurs for different percentages of BDH1281 in 7OCB, as a function of temperature. Data measured using a VEE program written by the author.

Equation 2.17 states that the field for total helix unwinding is given by:

$$E_{crit} = \frac{\pi^2}{P}\sqrt{\frac{K_{22}}{\varepsilon_0 \Delta\varepsilon}}, \qquad (2.17)$$

where P is the helical pitch, K_{22} is the twist elastic constant and $\Delta\varepsilon$ is the dielectric anisotropy of the chiral nematic material. The dielectric anisotropy of pure 7OCB has been measured. The results are shown in Figure 3.24.

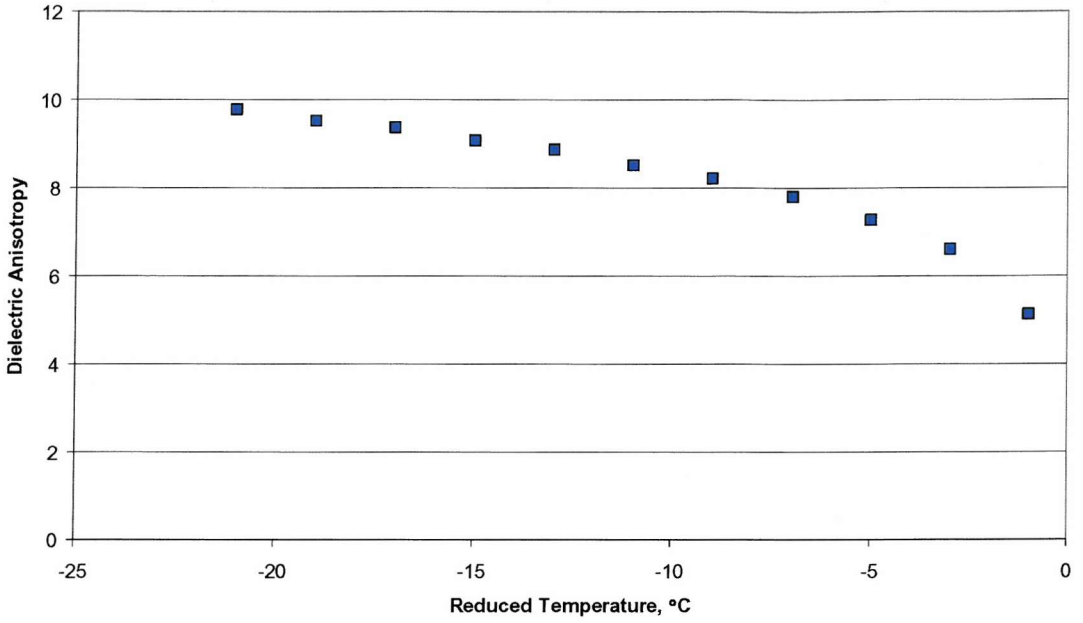

Figure 3.24 The dielectric anisotropy of pure 7OCB. Data reproduced with permission of S. Morris.

If it is assumed that, at any given temperature, the dielectric anisotropy is the same for each mixture, then any variation in the critical fields measured for the different mixtures (recalling Figure 3.23) can be assumed to be due to the changes in pitch and/or in K_{22}. To unwind a material with shorter pitch, a greater applied field is required than would be necessary to unwind the helical structure of a similar material with a longer pitch. Rearranging Equation 2.17 allows K_{22} to be calculated, if the values for the dielectric anisotropy, pitch and critical fields measured are used. The results of these calculations are shown in Figure 3.25. Published values of K_{22} for pure 7OCB are also shown as the "0%" data set.[24]

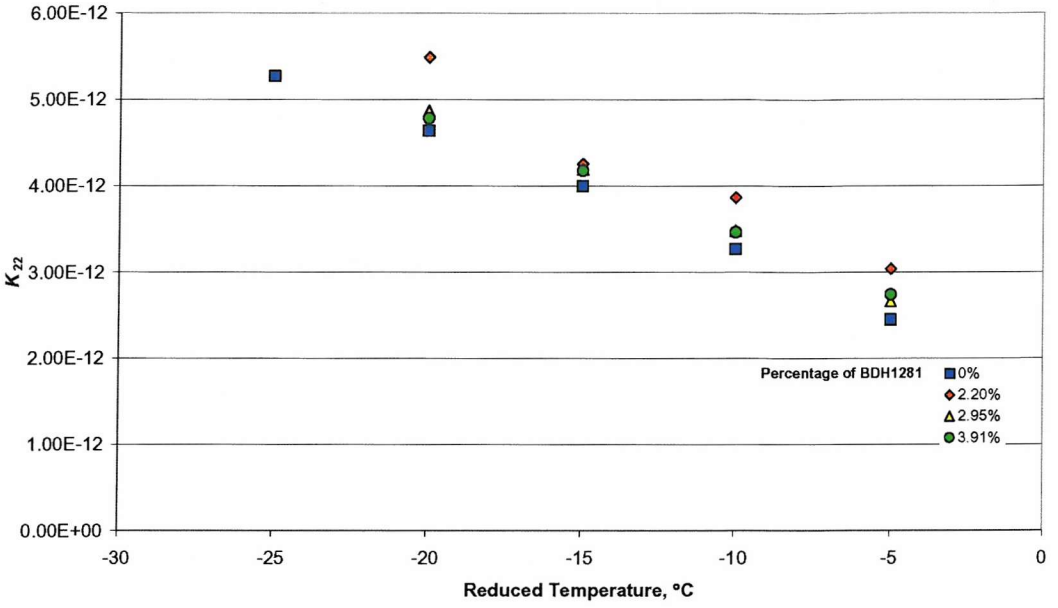

Figure 3.25 A comparison of the values for K_{22} for four mixtures of 7OCB doped with different concentrations of chiral dopant. The "0%" data set are derived from published literature (see text).

From Figure 3.25 it would seem that there is no measurable trend with concentration of chiral additive in the values of K_{22} measured for the chiral mixtures. The literature values of K_{22} for 7OCB are lower than those measured for the chiral mixtures. This difference is believed to be due to the inaccuracies associated with making an indirect measurement of K_{22} in the chiral mixtures.

In this section, it has been seen that some of the relevant physical properties of 7OCB, such as the twist elastic constant and the average refractive index, remain unchanged by the addition of chiral additive. However, the orientational order parameter was found to change with the introduction of chiral additive.

References

1 Olympus Optical Co. (UK) Ltd., Great Western Industrial Park, Southall, Middlesex, UK

2 Linkam Scientific Instruments, 8 Epsom Downs Metro Centre, Waterfield, Tadworth, Surrey, UK

3 Thurlby Thandar Instruments Ltd., Glebe Road, Huntingdon, Cambridgeshire, UK

4 Hewlett-Packard Ltd., Test and Measurement, Cain Road, Bracknell, Berkshire, UK

5 http://www.thorlabs.com

6 http://www.ibm.com

7 http://www.microsoft.com

8 Agilent Technologies UK Ltd., Test and Measurement, South Queensferry, West Lothian, UK

9 Mettler-Toledo Thornton Inc., Bedford, MA, USA

10 Perkin-Elmer Analytical Instruments, UK

11 http://www.jvc.co.uk

12 http://www.mediacybernetics.com

13 EEV Ltd., Waterhouse Lane, Chelmsford, Essex, UK

14 de Gennes, P. G., and Prost, J., The Physics of Liquid Crystals 2nd ed., Oxford Science publications, Oxford (1993)

15 Nara, Y., Kobayashi, S., and Miyaji, A., J. Appl. Phys. **49(7)** 4277 (1978)

16 Komitov, L., Lagerwall, S. T., Stebler, B., and Strigazzi, A., J. Appl. Phys. **76(6)** 3762 (1994)

17 Hauck, G., and Koswig, H. D., Chapter 5 in Selected Topics in Liquid Crystal Research Akademie-Verlag, Berlin (1990)

18 Patel, J. S., and Meyer, R. B., Phys. Rev. Lett., **58(15)** 1538 (1987)

19 Gray, G. W., J. Physique **36** C1-337 (1975)

20 Merck NB-C, Southampton, UK

21 Coles, H. J., Coles, M. J., Perkins, S., Musgrave, B., and Coates D., Bimesogenic Compounds and Flexoelectric Devices, EU Patent EP99119114 (1999)

22 Clark, N. A., and Lagerwall, S. T., Appl. Phys. Lett. **36** 899 (1980)

23 Musgrave, B., Coles M. J., Perkins, S., and Coles, H. J., Mol. Cryst. Liq. Cryst. **366** 2587 (2001)

24 Bancroft, M. S., Ph.D. Thesis, University of Manchester, UK (1989)

25 Private communication with Morris, S. M.

Chapter Four

4 A Direct Comparison of Two Different Methods for Measuring the Relative Flexoelectric Coefficients

4.1 Introduction

The majority of this work is concerned with the study of the flexoelectric properties of nematic materials. A valuable measure of a material's flexoelectric properties is the "flexo-elastic" ratio, $\bar{e}/K$, where $\bar{e}$ is the effective flexoelectric coefficient and K is the appropriate elastic constant. The greater the flexoelectric properties of the material, the greater the value measured for the flexo-elastic ratio.

In Chapter two, the process of flexoelectro-optic switching[1] in chiral nematics was discussed and it was shown in Chapter three that $\bar{e}/K$ could be derived from observations of this effect. However, a more commonly-used method for measuring $\bar{e}/K$ is to use hybrid aligned nematic (HAN) cells.[2] In this chapter the relative merits of both techniques will be studied and discussed.

4.2 Theory and experimental

The theory for flexoelectro-optic switching in chiral nematics was discussed previously in Chapter two, and the techniques for measuring the relevant properties were discussed in Chapter three. For convenience the key points are summarised in this section.

When making the measurements, the helix axis must be constrained to lie in a uniaxial planar geometry. Application of an external field between the walls of the cell causes the optical axis to rotate in the plane of the cell orthogonal to the applied field E and the amount of rotation ϕ is linearly proportional to E. From measurements of $\phi(E)$ and the pitch length we can determine $\bar{e}/K$ using

$$\frac{\bar{e}}{K} = \frac{\Delta \tan\phi}{\Delta E}\frac{2\pi}{P}, \qquad (3.10)$$

where the ratio $\Delta\tan\phi/\Delta E$ is the gradient of the linear graph of $\tan\phi$ versus E. The pitch measurements were performed by observing the Grandjean step texture in wedge cells and tilt measurements were carried out using commercially-made planar cells.

The HAN technique is applied for achiral nematics and uses a completely different geometry to that used for flexoelectro-optic switching. In a hybrid cell the opposing surfaces are treated with different alignment layers, one to induce planar alignment and the other to induce homeotropic alignment. This results in a splay-bend deformation of the director pattern through the cell and gives rise to flexoelectric polarisation. The application of an in-plane D.C. electric field will couple to this polarisation and cause a twist deformation to form (see Figure 4.1). This effect is the basis for measuring $\bar{e}/K$ in a hybrid aligned nematic. Due to the geometry of the system K represents the average of K_{11}, K_{22} and K_{33}; thus the flexo-elastic ratio is written as $\bar{e}/K_{av}$ for clarity.

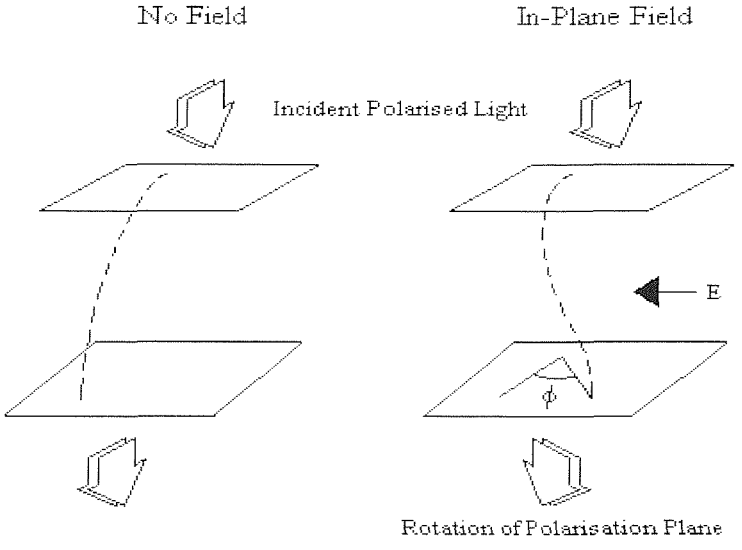

Figure 4.1 A schematic representation of a) a hybrid aligned nematic and b) a field induced twist in the hybrid alignment.

The formula for calculating the ratio $\bar{e}/K_{av}$ is derived from the standard equation for the macroscopic polarisation, taking the hybrid boundary conditions into account. The ratio $\bar{e}/K_{av}$ is given by[2]

$$\frac{e}{K_{av}} = \frac{\Delta \tan\phi}{\Delta V} \pi \frac{x}{d}, \qquad (4.1)$$

where ϕ is the angle of rotation of the polarisation plane, V is the applied voltage amplitude, x is the electrode gap and d the cell thickness. The ratio $\Delta\tan\phi/\Delta V$ is the gradient of the linear graph of the tangent of ϕ versus V.

Experimentally, the angle of rotation of the polarisation plane is measured using a polarising microscope. The cell is viewed between crossed polarisers and rotated until it is in extinction – the easy axis of the planar layer is aligned parallel to the transmission axis of one of the polarisers. When a field is applied in the plane of the glass cell an induced twist in the liquid crystal brings the cell out of extinction. The top polariser is then rotated until extinction is re-established and the difference in the new angle from the crossed polariser position is the angle of director twist within the cell. The angle measured is accurate to 0.5°.

4.3 Experimental results

In order to illustrate the differences between the data sets obtained using the two measurement techniques, the liquid crystal 5CB[3] was chosen for observation. The results obtained for 5CB (at a reduced temperature of –5°C) using the two techniques are shown below. 5CB is a nematic material with a clearing temperature of 32°C and was chosen because of its ready availability and because it has been measured previously.[4] The behaviour of 5CB in a hybrid cell was examined by observing the rotation of the plane of polarisation as a function of the applied D.C. voltage (see Figure 4.2). The electrode gap and thickness of the hybrid cell were 500μm and 18.1μm respectively.

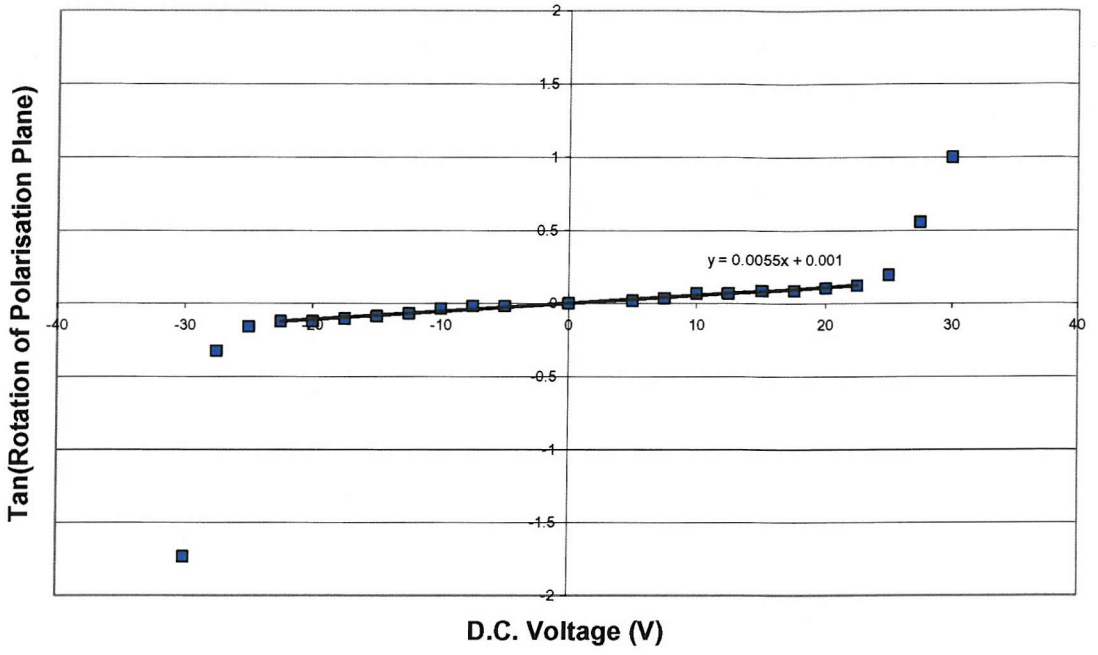

Figure 4.2 The tangent of the angle of rotation of the plane of polarisation versus the applied D.C. voltage for 5CB. Measurements were made in a hybrid cell at a reduced temperature of -5°C.

For the calculation of the ratio $\bar{e}/K_{av}$ only the linear part of the graph centred around zero voltage is of relevance. The resultant value for $\bar{e}/K_{av}$ was found to be 0.48 C N^{-1} m^{-1}. The regions for higher fields where the rotation rapidly approaches $\pi/2$ are attributed to the destabilising dielectric torque density, which forces the molecules to align parallel to the electric field[2]. The experimental uncertainty in the flexo-elastic ratio is calculated to be ± 0.05 C N^{-1} m^{-1}.

A value for $\bar{e}/K$ in 5CB was determined independently using the A.C. field driven flexoelectric electro-optic switching mechanism in the chiral nematic phase. To do this, a sample of 5CB was doped with a small amount of the chiral additive BDH1281. The pitch and tilt angles were measured to evaluate $\bar{e}/K$ at the same reduced temperature (-5°C). The pitch was found to be 391 nm, measured using a homemade wedge cell of angle 0.077°, and taken together with the gradient of the tangent of the tilt angle against applied field, this technique produces a value of $\bar{e}/K$ = 0.41 C N^{-1} m^{-1} for 5CB. This value is in reasonable agreement with the result obtained using the hybrid alignment method. The experimental uncertainty in the flexo-elastic ratio is calculated to be ± 0.02 C N^{-1} m^{-1}.

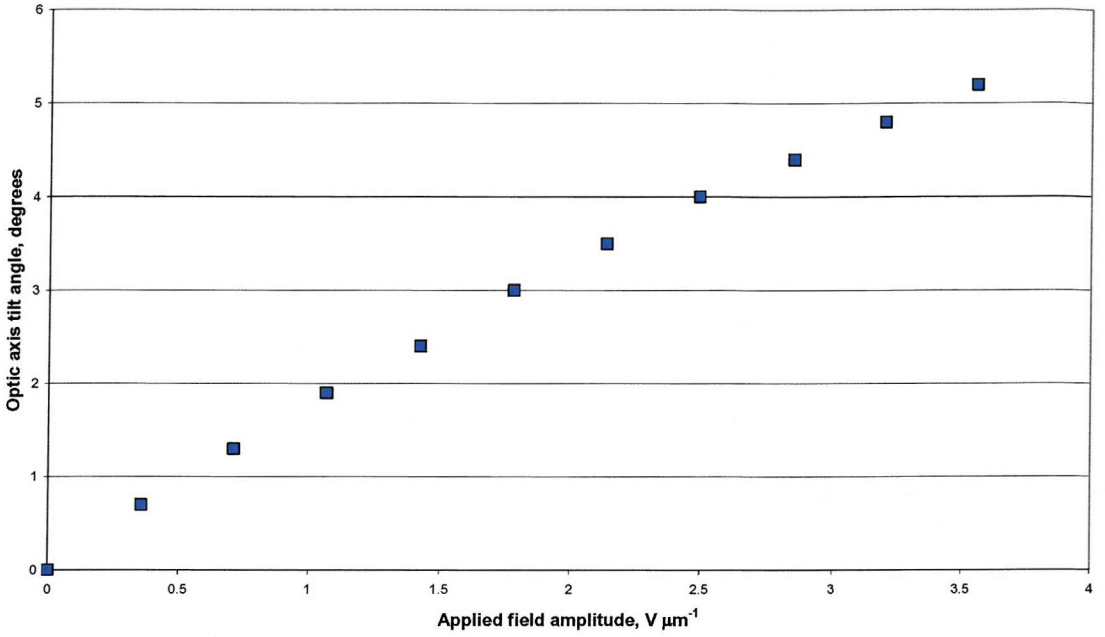

Figure 4.3 Graph of tilt angle versus applied electric field for 2.6% BDH1281 in 5CB. Measurements were made in a commercially-made planar cell at a reduced temperature of -5 °C.

One drawback to using 5CB is that its clearing temperature is only a few degrees above room temperature, making it difficult to measure the flexoelectric properties over a range of temperatures. To allow a range of temperatures to be measured, it was decided to use 7CB, which is similar to 5CB in structure but with a two extra carbon atoms in the alkyl chain. As a result of the molecular structure change 7CB has a clearing temperature of 44°C.

The rotation of the plane of polarisation as a function of the applied D.C. voltage for 7CB was studied in a homemade cell with hybrid alignment over a range of temperatures. The hybrid cell had an electrode gap of 500μm and a thickness of 19.5μm. Figure 4.4 shows the results at the reduced temperature of -6°C.

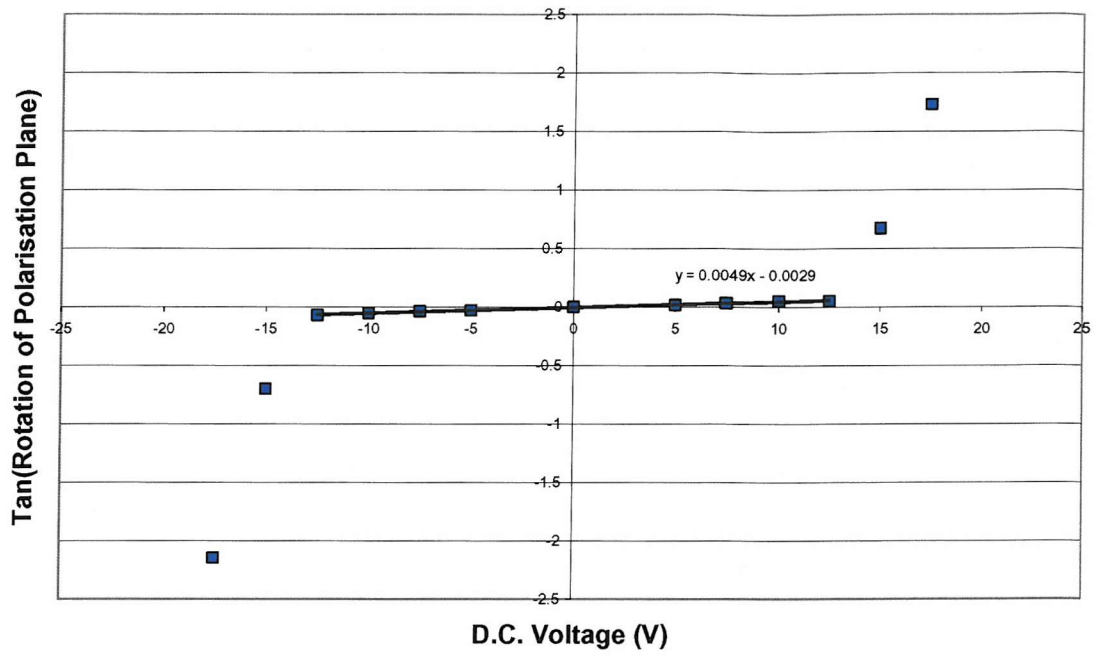

Figure 4.4 The tangent of the angle of rotation of the plane of polarisation versus the applied D.C. voltage for 7CB. Measurements were made in a hybrid cell at a reduced temperature of -6°C.

Flexoelectro-optic switching was also used to calculate the ratio $\bar{e}/K$. The naturally achiral 7CB was doped with the chiral additive BDH1281 to produce a chiral nematic phase. The tilt angles were measured using a commercially-made cell, while the pitch measurements were made using a homemade wedge cell of angle 0.077°. The tilt angle and pitch measurements are shown in Figure 4.5, below.

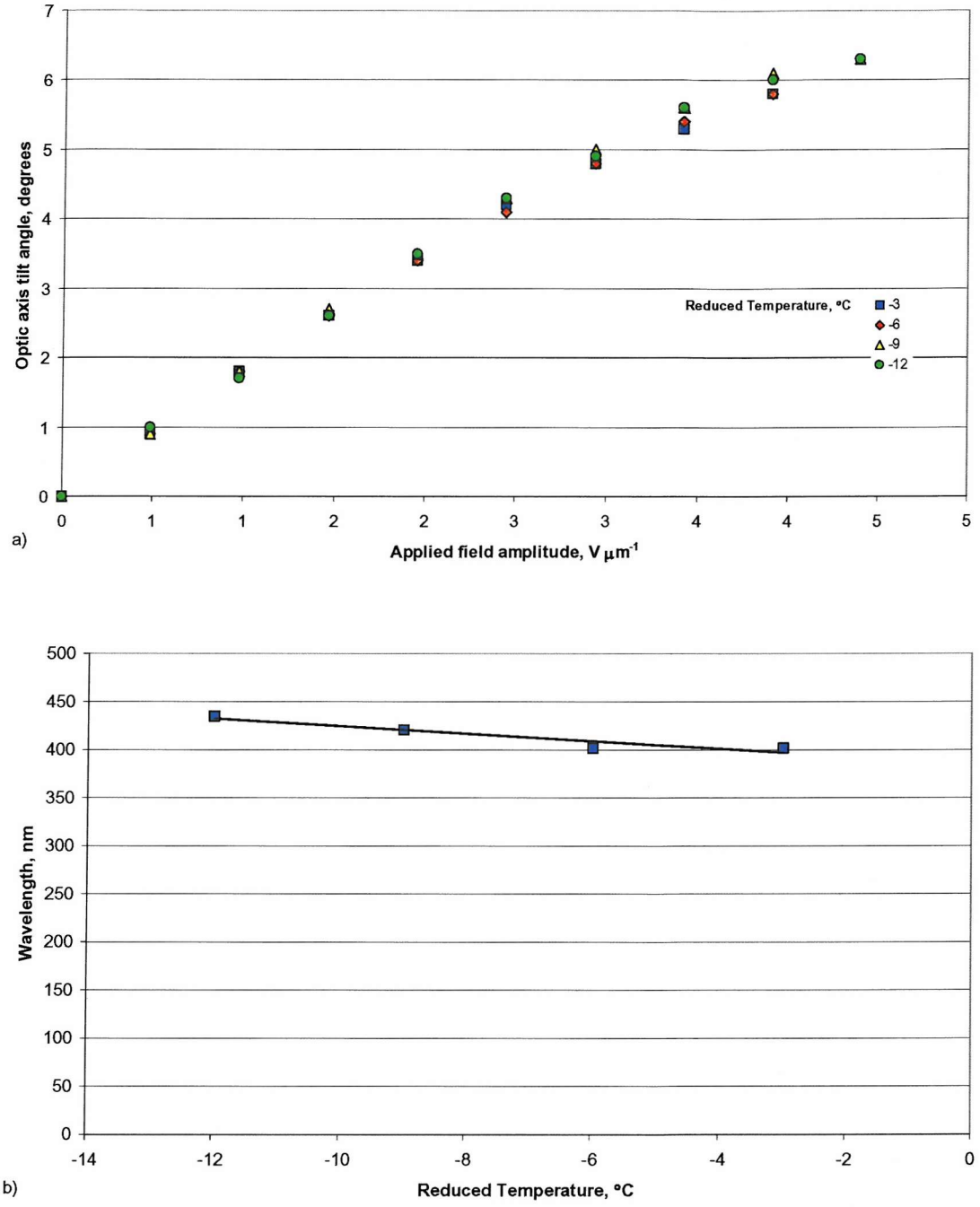

Figure 4.5 A comparison of a) the tilt angles, and b) the pitch for 2.6% BDH1281 in 7CB, across a range of reduced temperatures.

The flexo-elastic ratios were calculated for 7CB using both methods over a range of temperatures. A comparison of these data sets is shown in graphical form in Figure 4.6. It can be seen that the techniques produce similar results; the average difference between the data sets is 5%.

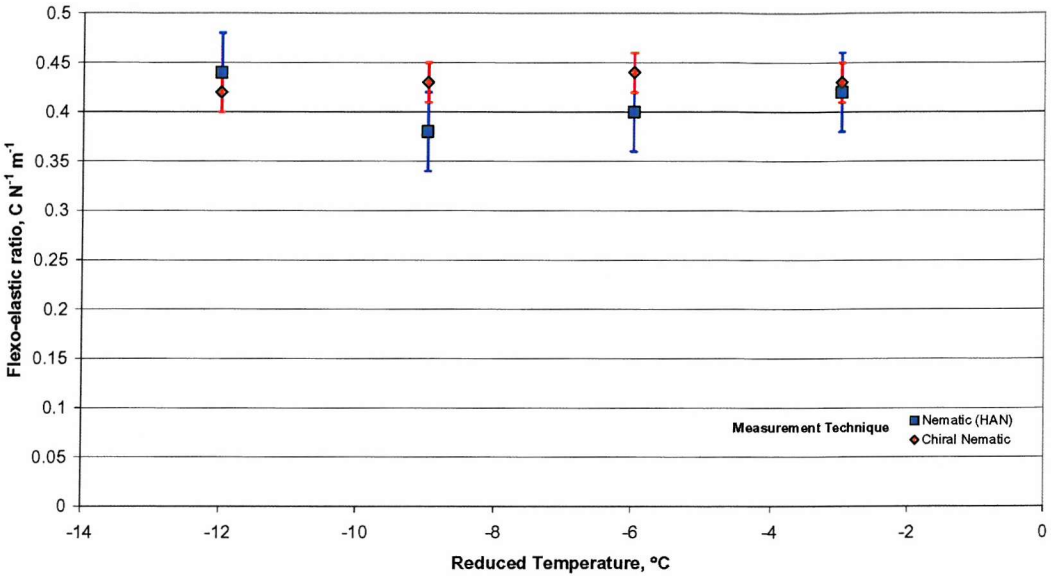

Figure 4.6 A comparison of values for flexo-elastic ratio using both the HAN technique and the flexoelectro-optic technique, across a range of reduced temperatures.

The results for 7CB, and previously 5CB, show that the flexo-elastic ratio can be accurately and successfully evaluated using either measurement technique. However, another purpose of this study was to test the limits of both techniques. The tests proposed were first to try measuring a material with a very small flexo-elastic ratio and secondly to test both techniques using a bimesogenic material, which has a very large flexo-elastic ratio.

For the low flexo-elastic ratio material, the Merck material ZLI3086, which is a nematic with a clearing temperature of 85°C, was chosen for examination. ZLI3086 is achiral, so as for the previous materials it was doped with a small percentage of the chiral additive BDH1281 to allow the flexoelectro-optic switching properties to be examined (Figure 4.7).

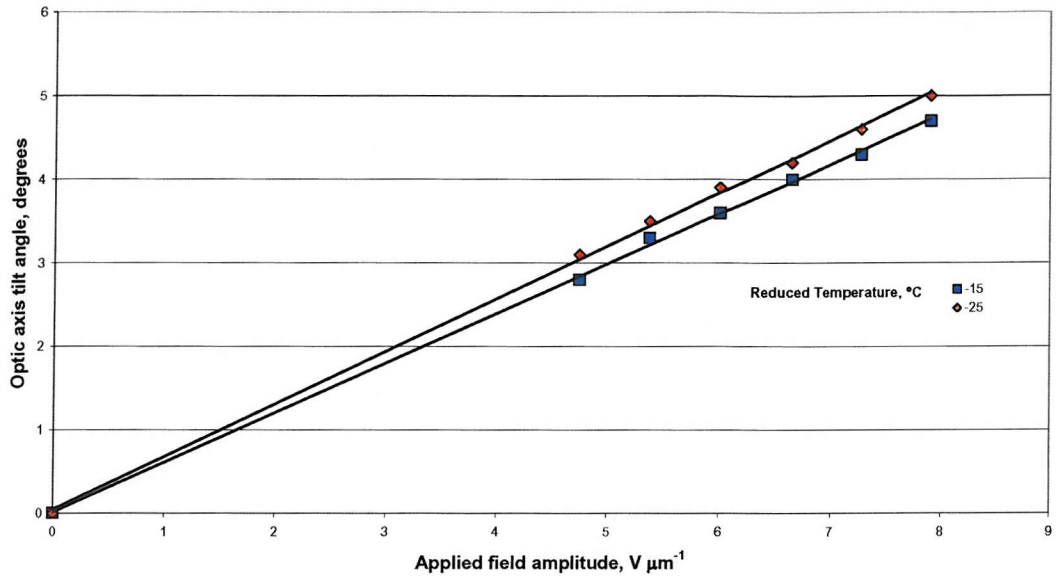

Figure 4.7 A comparison of the tilt angles for 3.1% BDH1281 in ZLI-3086 at a reduced temperature of -15°C and -25°C.

It was not possible for the doped ZLI-3086 to form distinct neat fringes when in a wedge cell, thus the pitch values had to be estimated to a certain extent. In this case the pitch was estimated to be 518nm and 509nm at the reduced temperatures of -15°C and -25°C respectively. From this data the flexo-elastic ratio was calculated to be 0.12 C N^{-1} m^{-1} and 0.14 C N^{-1} m^{-1} for the reduced temperatures of -15°C and -25°C respectively.

The doped ZLI-3086 mixture was placed in a HAN cell, where it adopted the correct alignment required for measuring the flexo-elastic ratio. It was found that the rotation of the plane of polarisation was very small, too small to measure accurately at low fields and for higher fields the dielectric effects dominates. From this it appeared that the ratio was too small to be measured using this method. The HAN cell method would appear to be limited in so much as it does not appear to work for materials with very low flexo-elastic ratios. In such cases, doping the low flexo-elastic ratio material with a chiral additive and applying the flexo-electric measurement technique is a viable alternative, producing a sensible value for the flexo-elastic ratio.

The bimesogenic material chosen for this work was a mixture of two symmetric achiral bimesogens[5] doped with the chiral additive BDH1281. This mixture comprised of the homologues with seven and eleven carbon atoms in their linking group. As similar

mixtures are discussed in great detail in Chapter 5 only the values for the flexo-elastic ratio are given here. The flexo-elastic ratio was found to be 0.98 C N^{-1} m^{-1} and 1.02 C N^{-1} m^{-1} at a reduced temperature of -5°C and -10°C respectively.

When the achiral form of the bimesogenic mixture was placed in a HAN cell, the mixture adopted planar alignment rather than the hybrid alignment required to measure the flexo-elastic ratio. Thus it would appear that it is not possible to use the HAN technique to measure the flexo-elastic ratio for the bimesogenic mixture. It was also found that this bimesogenic mixture would not adopt the homeotropic geometry when placed in a homeotropic cell. In such cases the flexoelectro-optic technique provides a simple method to measure the flexo-elastic ratio, when the HAN method cannot be applied.

In an attempt to force the bimesogenic mixture to adopt the necessary geometry to allow the HAN technique to be used it was decided to try doping the mixture with a material that did align well; in this case ZLI-3086 was used. Five different mixtures of the bimesogenic mixture and ZLI-3086 were made up containing approximately 5%, 10%, 20%, 40% and 60% ZLI-3086 by weight. It was found that only the ~60% ZLI-3086 mixture would adopt the correct geometry. This mixture is denoted 60/40 ZLI/bimeso. The flexo-elastic ratio, $\bar{e}/K_{av}$, was measured across a range of temperatures. The results of these measurements are shown in Figure 4.8, below.

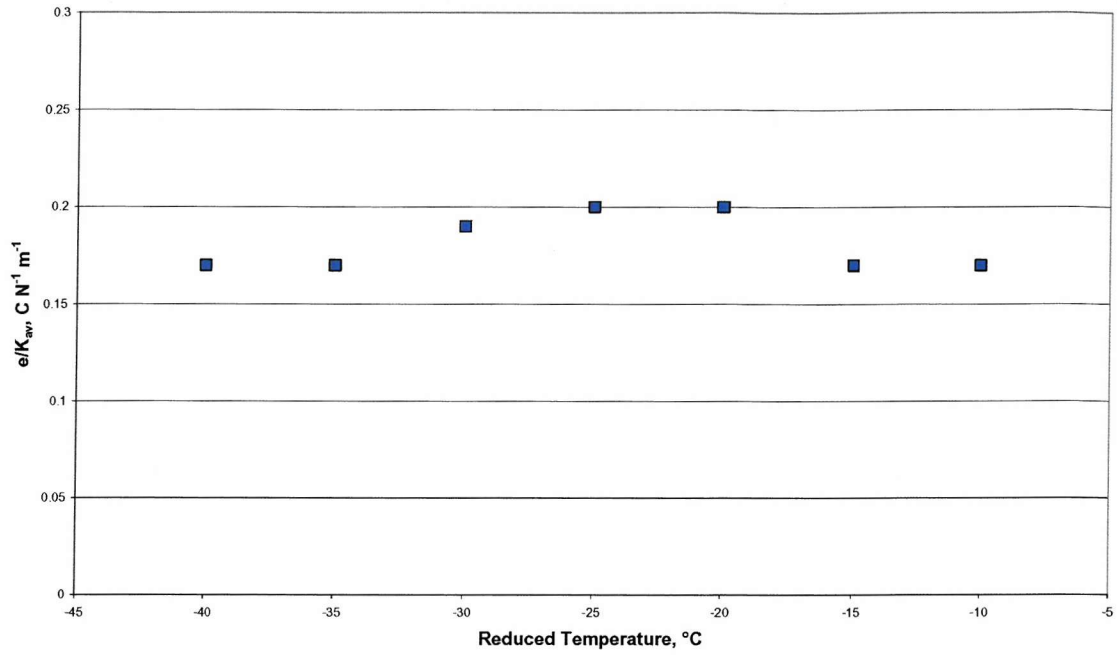

Figure 4.8 The flexo-elastic ratio for a 60/40 ZLI/bimeso for a range of reduced temperatures.

To examine the 60/40 ZLI/bimeso mixture using the flexoelectro-optic method it was necessary to dope the mixture with the chiral additive BDH1281. The tilt, pitch and resultant $\bar{e}/K$ values are shown in Figure 4.9 below.

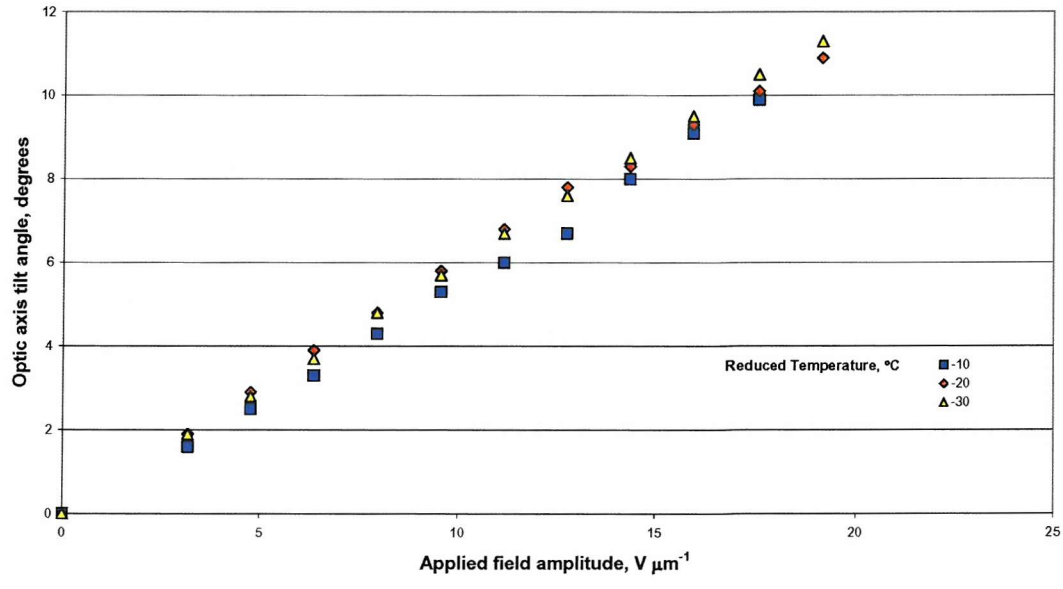

a)

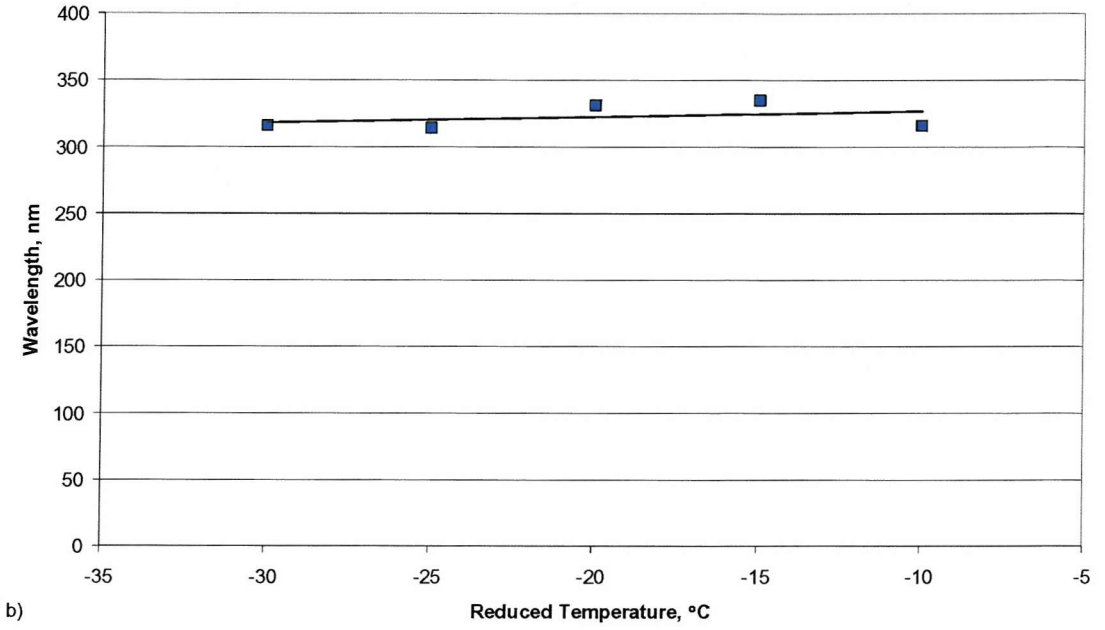

b)

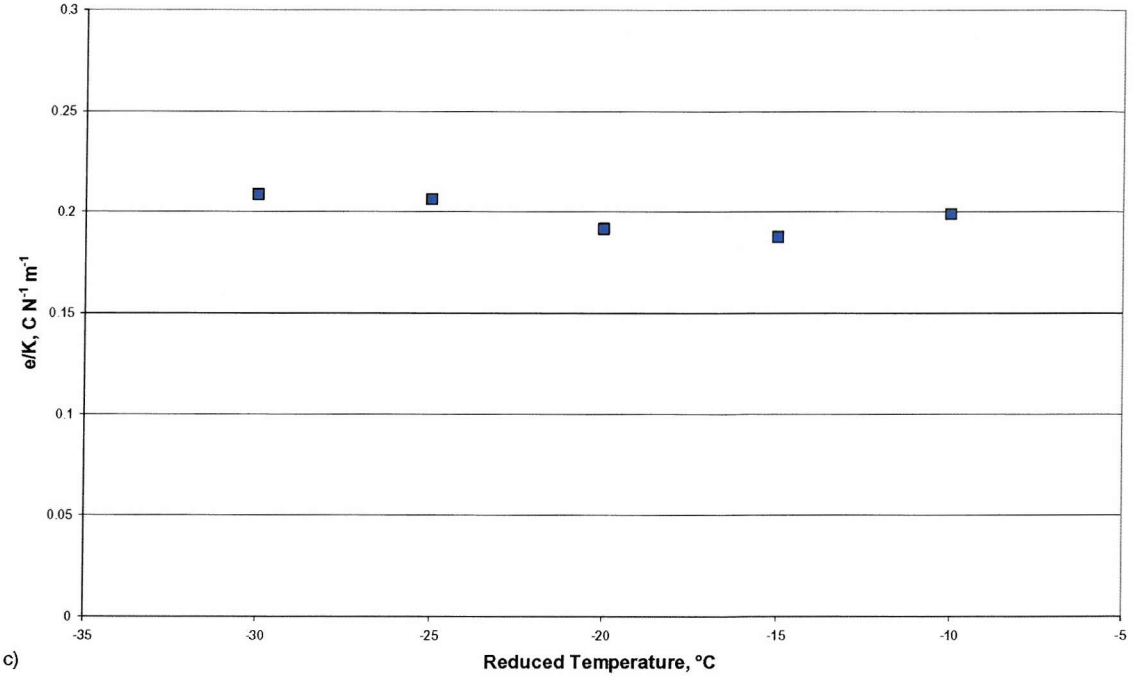

c)

Figure 4.9 The a) tilt, b) pitch and c) flexo-elastic ratio for 4.1% BDH1281 in the 60/40 ZLI/bimeso mixture.

Both methods produce similar results for the flexo-elastic ratio, in the region of 0.20 C N^{-1} m^{-1}. The pure bimesogen mixture produced a value for the flexo-elastic ratio of approximately 1.0 C N^{-1} m^{-1}, however when mixed with the ZLI-3086 to the extent that the new mixture would adopt the HAN geometry, the value for the flexo-elastic ratio was greatly reduced (by a factor of five). It was hoped that by doping the bimesogen with a

small amount of a mixture that does align correctly in a HAN cell, it would be possible for the mixture to adopt the HAN geometry, and the value measured for the flexo-elastic ratio using this method would give a reasonable estimate of the value for the pure bimesogen mixture. The percentage of mixture required to achieve the correct geometry was very large, this meant that it was impossible to estimate with any accuracy the value of the flexo-elastic ratio for the bimesogen using the HAN technique. An extrapolation to find the flexo-elastic ratio for the pure bimesogen mixture using the results for ZLI-3086 and the 60/40 ZLI/bimeso mixture was attempted, however it produced a value for the flexo-elastic ratio that was too small (by a factor of approximately three). This may suggest that when two materials are mixed the relationship between the flexo-elastic ratio and the percentages of the respective materials used is not linear.

4.4 Summary and discussion of results

The values measured for the flexo-elastic ratio using both methods for the different materials are summarised in Table 4.1. Literature values[6,7] for K and K_{av} are also included, so that values for $\bar{e}$ can be calculated.

				HAN		Flexoelectro-optic	
Material	T_{red}, °C	K, pN	K_{av}, pN	$\bar{e}/K_{av}$, C N^{-1} m^{-1}	$\bar{e}$, pC m^{-1}	$\bar{e}/K$, C N^{-1} m^{-1}	$\bar{e}$, pC m^{-1}
5CB	-5	5	4.8	0.48	2.3	0.41	2.1
7CB	-6	6	5.9	0.40	2.4	0.43	2.6
ZLI-3086	-15	-	-	-	-	0.12	-
Bimesogen mixture	-10	-	-	-	-	1.02	-
60/40 ZLI/bimeso	-20	-	-	0.20	-	0.19	-

Table 4.1 A summary of results obtained by both methods. K and K_{av} values obtained from literature.

It is clear from the data shown in Table 4.1 that the measurements made by the two methods are comparable, across a range of different nematic materials. It can also be seen that K and K_{av} are very similar, this means that $\bar{e}/K$ and $\bar{e}/K_{av}$ can be compared directly.

Comparing the ratios $\bar{e}/K$ (~0.4 – 0.5 C N^{-1} m^{-1}) and the flexoelectric coefficients $\bar{e}$ (~2.1 – 2.6 pC m^{-1}) obtained for the homologues 5CB and 7CB, it is seen that these materials

have similar flexoelectric coupling capability. The results for these two materials measured here are in agreement with published values.[4] The cyanobiphenyl homologues undergo stronger flexoelectric coupling than ZLI3086, which has a significantly lower $\bar{e}/K$ ratio (0.12 C N^{-1} m^{-1}) and was only measurable by using the flexoelectro-optic technique. Of the five materials reported here, the bimesogen mixture shows the largest $\bar{e}/K$ ratio at 1.02 C N^{-1} m^{-1} (measured only using the flexoelectro-optic technique). A mixture between the bimesogen (40% w/w) and the ZLI3086 material (60% w/w) was also examined and found to have a flexo-elastic ratio of approximately 0.20 C N^{-1} m^{-1}.

The results obtained illustrate some of the relative merits of the two techniques used. From Figure 4.6 it can be seen that the $\bar{e}/K_{av}$ data for 7CB measured using the HAN technique shows more scatter, owing to the difficulty involved with identifying the extinction position of the analyser. However, the HAN method is faster and yields a direct measure of $\bar{e}/K_{av}$. In contrast, the chiral nematic technique requires the separate measurement of the helical pitch of the phase, which may be an additional source of error.

It was not possible via the HAN technique to examine flexoelectric coupling in either the bimesogenic mixture or ZLI3086. The bimesogenic mixture could not be examined by this method because it would not adopt a splay-bend structure in the hybrid cell (it was not possible to find an alignment layer that would promote homeotropic orientation of the bimesogen). ZLI3086, on the other hand, did align appropriately in the hybrid cell but it was found that its flexoelectric response was too small to be measured accurately by this method. The chiral nematic electro-optic technique proved to be more effective and sensitive in that it allowed the $\bar{e}/K$ ratios to be evaluated for both these materials.

It has been shown that the techniques described measure the flexoelectric parameters comparably and that the addition of a small amount of chiral additive does not affect these parameters significantly in the case of the monomesogen materials. In Chapter 3 it was found for 7OCB that the variation of the concentration of chiral did not observably alter the flexo-elastic coefficient. In comparison with the HAN technique, we find that the chiral nematic electro-optic technique is the more sensitive method, useful when the flexoelectric coupling is weak, and that it is particularly valuable in cases where a material does not adopt hybrid alignment.

References

1 Patel, J. S., and Meyer, R. B., Phys. Rev. Lett., **58** 1538 (1987)

2 Dozov, I., Martinot-Lagarde, Ph., and Durand, G., J. Physique Lett. **43** pp. 365 (1982)

3 Merck NB-C, Southampton, UK

4 Maheswara Murthy, P. R., Raghunathan V. A., and N. V. Madhusudana, Liq. Cryst., **14** 483 (1993)

5 Coles, H. J., Coles, M. J., Perkins, S., Musgrave, B., and Coates, D., Bimesogenic Compounds and Flexoelectric Devices, EU Patent EP9119114 (1999)

6 Bradshaw, M. J., Raynes, E. P., Bunning, J. D., and Faber, T. E., J. Physique Lett., **46** 1513 (1985)

7 Sefton, M., Ph.D. thesis, University of Manchester (1985)

Chapter Five

5 Flexoelectro-optic Switching of Achiral Symmetric Bimesogens

5.1 Introduction

Chiral nematics with strong flexoelectric properties have been shown[1] to produce promising results in terms of large tilt angles and fast response times. One problem with exploiting this effect has been the need to minimise the effects of dielectric coupling, thus increasing the range of voltages over which flexoelectric coupling dominates the electro-optic switching mechanism. The obvious method for decreasing the effects of dielectric coupling is to reduce the dielectric anisotropy as much as possible while still maintaining a positive value. One approach to achieve this is to use bimesogens, where the two mesogenic groups have been substituted onto a spacer chain so that the dielectric anisotropies of the two mesogenic groups act to balance each other out, to a certain extent.[2] If the two mesogenic groups are the same, then it would be expected that the molecular dielectric anisotropy of the bimesogen would be very low, of course depending on the overall shape of the molecule.

The bimesogens used in this work have two oxy-fluorobiphenyl groups, as shown in Figure 5.1. The materials are denoted FfO-n-OfF, where n represents the number of carbon atoms in the spacer. The materials were initially synthesised by Steve Perkins[2] and remade by Andrew Blatch.

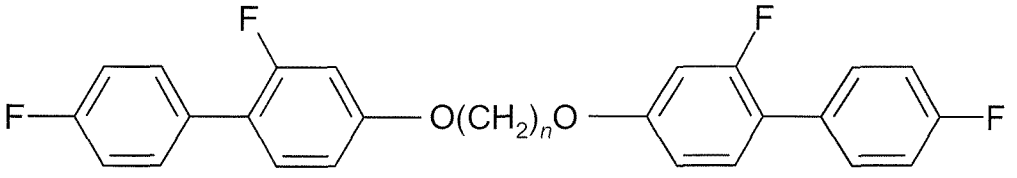

Figure 5.1 The generic structure of the bimesogens studied in this chapter. For simplicity the molecule is denoted FfO-n-OfF, where n represents the number of carbon atoms in the spacer.

It is expected that the resultant dielectric anisotropy of these molecules would be low. If the resultant dipole of one of the mesogenic groups is considered, it is suggested to point in the direction indicated in Figure 5.2, below.

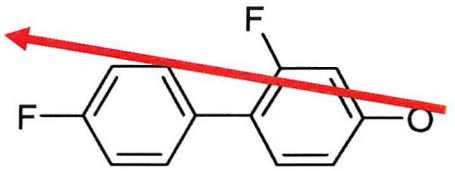

Figure 5.2 A suggestion for the molecular dipole direction of the mesogenic group.

By considering the whole bimesogen, the two "individual" dipoles would balance each other out to a certain degree, though not completely as they do not point in exactly opposite directions.

As well as having a low positive dielectric anisotropy, there are other properties that would be desirable in materials developed for the flexoelectro-optic effect. For instance, it is preferable that the materials have a broad nematic phase with no underlying smectic phases and a reasonably high birefringence. The presence of an underlying smectic phase tends to increase the dependence of the pitch of the chiral nematic phase on temperature, especially near the transition to the smectic phase.

5.2 The pure homologues

A range of homologues of different spacer lengths was produced for this work. The materials were initially examined using optical microscopy. The materials were placed on a glass slide and then covered with a glass coverslip. Table 5.1 lists the observations that were made.

Material	On Cooling (5°C/min)	On Heating
FfO - 4 - OfF	**I** -(133°C)-> **Crystal**	**Crystal** -(151°C)-> **I**
FfO - 6 - OfF	**I** -(107°C)-> **N** -(81°C)-> **Crystal**	**Crystal** -(127°C)-> **I**
FfO - 7 - OfF	**I** -(56°C)-> **N** -(33°C)-> **Crystal**	**Crystal** -(71°C)-> **I**
FfO - 9 - OfF	**I** -(58°C)-> **N** -(31°C)-> **Crystal**	**Crystal** -(64°C)-> **I**
FfO - 10 - OfF	**I** -(89°C)-> **N** -(85°C)-> **Crystal**	**Crystal** -(123°C)-> **I**
FfO - 11 - OfF	**I** -(65°C)-> **N** -(48°C)-> **Crystal**	**Crystal** -(61°C)-> **N** -(65°C)-> **I**
FfO - 12 - OfF	**I** -(94°C)-> **Crystal**	**Crystal** -(122°C)-> **I**

Table 5.1 The transition temperatures of the pure homologues measured via optical microscopy.

As these measurements show, not all of the materials have liquid crystal phases; the materials that do not were not studied further in this work. All the materials that exhibit a nematic phase, with the exception of FfO-11-OfF, are monotropic, that is to say they only exhibit a nematic phase on cooling from the isotropic phase. The texture that is typically observed is shown photographically in Figure 5.3. That the nematic phases are observed is a result of super-cooling; the materials will crystallise quickly if left in the nematic phase for any reasonable time. Only the FfO-11-OfF material shows a nematic phase on heating from the crystalline phase.

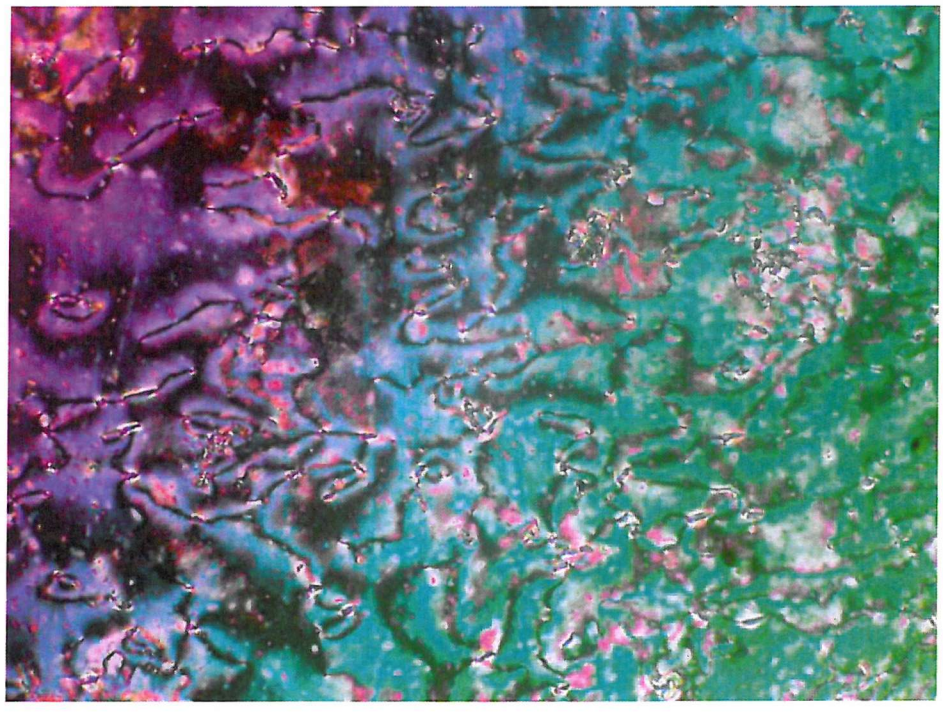

Figure 5.3 The nematic phase observed in FfO-11-OfF, taken between glass coverslips.

5.3 Inducing chirality to the homologues

The materials examined above are achiral, which means that in order to observe the flexoelectro-optic effect, chirality has to be introduced by using a chiral additive. It would be possible to form a chiral bimesogenic homologous series, using these mesogenic units, by adding a chiral centre to the spacer chain. This approach was not adopted for two reasons; firstly it was thought that the magnitude of the inherent chirality would be quite low due to the mesogens "shielding" the chiral centre, thus reducing the effect[3] and secondly the chirality of the phase would be fixed, whereas with a dopant it would be possible to vary the chirality of the mesophases by varying the amount of dopant used.

One method that can be used to induce chirality in the nematic phase is to add an inherently chiral liquid crystal to an achiral material. This approach would require a large percentage of dopant to be added to the bimesogens, to produce a suitable pitch for flexoelectro-optic switching - thus diluting the properties of the bimesogen. Instead, a highly chiral non-liquid crystalline additive known as BDH1281, produced by Merck,[4] was chosen for use as a dopant. When mixed with a nematic liquid crystal, this dopant induces a left-handed pitch. Only a small percentage (between 1-5%) of BDH1281 is required to make an achiral nematic sufficiently chiral to be used for flexoelectro-optic switching. This is advantageous because as such a small amount of dopant is used (other than inducing chirality) the effect on the host is small, e.g. the transition temperatures are relatively unchanged. For completeness the transition temperatures of BDH1281 were measured: the transition temperatures of this material are given below.

Crystal -(141°C)-> **Isotropic** (on heating)

There were, as expected, no liquid crystal phases observed.

5.4 Stabilising the nematic phase

For the purpose of this work it is preferable to have a stable nematic phase with a wide temperature range; a common way to achieve this is to use mixtures. It was decided that mixing two of the homologues together would be a good initial step and if this produced promising results then optimising the temperature range of the nematic phase would be the next step.

The first set of mixture studies were carried out by Marcus Coles[2] on a mixture of the FfO-7-OfF and FfO-9-OfF homologues, an initial contact preparation was prepared between the two materials and it was found to be promising with a relatively wide nematic phase. A number of mixtures of different percentages of the two homologues (all measurements were weight by weight) were then made and then their transition temperatures were examined using the DSC and optical microscopy. It was found that a combination of 20% FfO-7-OfF and 80% FfO-9-OfF produced the mixture with the lowest nematic phase to smectic phase transition.

A similar method was used by the author for mixtures between FfO-7-OfF and FfO-11-OfF, and FfO-9-OfF and FfO-11-OfF. The resultant mixtures and their transition temperatures are shown in Table 5.2. In both cases the DSC and the thermo-optic VEE program was used to find the transition temperatures.

Mixture composition (w/w)	Transition temperatures on cooling
20% FfO-7-OfF and 80% FfO-9-OfF	**I** -(57°C)-> **N** -(18°C)-> **SmX**
80% FfO-7-OfF and 20% FfO-11-OfF	**I** -(49°C)-> **N** -(13°C)-> **SmX**
89% FfO-9-OfF and 11% FfO-11-OfF	**I** -(56°C)-> **N** -(18°C)-> **SmX**

Table 5.2 The composition and transition temperatures of the mixtures chosen for initial flexoelectric studies. The transition temperatures were measured using the thermo-optic VEE program and the phases were identified using optical microscopy.

For simplicity the mixtures are denoted x%/y% FfO-n/m-OfF, where n and m represents the number of carbon atoms in the spacers of the two homologues and x and y represent the percentages by weight of FfO-n-OfF and FfO-m-OfF respectively. For example, the mixture of the FfO-7-OfF and FfO-9-OfF homologues described above would be known as 20%/80% FfO-7/9-OfF.

5.5 The nematic to smectic phase transition

Ideally, for the purpose of this work it would be preferable if the liquid crystal materials only have a nematic phase, with a wide temperature range. However, all the materials examined in this chapter exhibit a nematic to smectic phase transition somewhere between 10°C and 20°C on cooling. On cooling, the chiral nematic to smectic phase transition is typically characterised by a rapid increase in pitch as Figure 5.4 illustrates.

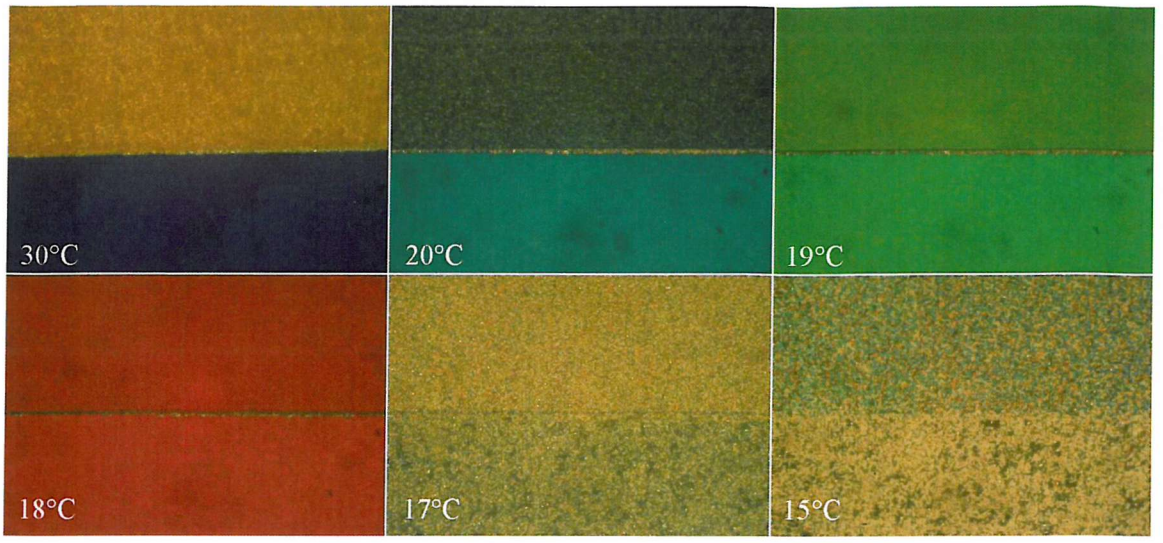

Figure 5.4 The effects of temperature change on 3.42% BDH1281 in 20%/80% FfO-7/9-OfF. The sample was contained in a commercially-made, planar electro-optic cell. The pictures are taken on the edge of the electrode area (top). An electric field was applied across the electrode area inducing flexoelectric alignment at 30°C and the field was maintained as the temperature was decreased. The phase transition occurs between 18°C and 17°C.

The mixture was aligned into the lying helix texture at 30°C, and the mixture was cooled with the aligning electric field still applied. It can be seen that for a few degrees above the phase transition at 19°C there is no longer any flexoelectric alignment. This loss of alignment may be indicative of a decrease in the dielectric anisotropy to zero or below. However, below the transition temperature there is indication that the applied field has an effect on the texture of the phase, see Figure 5.5 below. The phase appears different in the electrode region, where the field is applied, compared with the electrode free region.

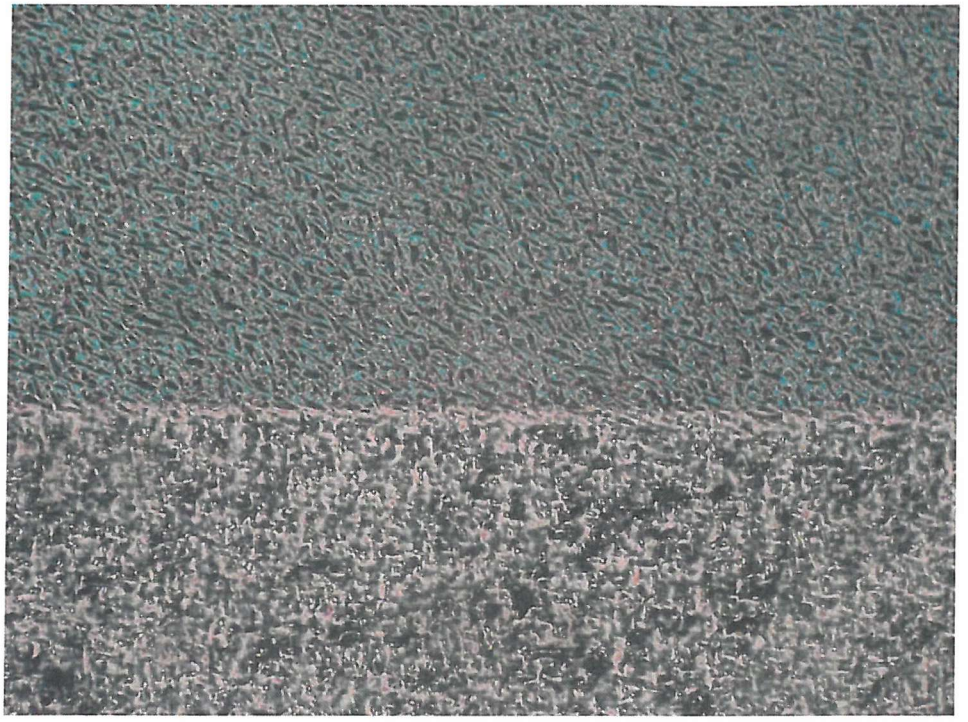

Figure 5.5 The smectic phase of 3.42% BDH1281 in 20%/80% FfO-7/9-OfF at a temperature of 10°C, an electric field is applied across the upper half of the material. The liquid crystal was contained in a commercially made planar cell.

Upon heating back into the chiral nematic phase under applied field, the flexoelectric alignment does not return; instead the focal conic chiral nematic texture is observed.

The author believes the phase to be chiral smectic A, however without additional proof, such as x-ray studies, the phase cannot be identified without ambiguity. For the purpose of this work it is important to know that there is a phase change, and that it affects the properties of the chiral nematic phase. The actual identity of the smectic phase is of less significance for the flexoelectro-optic effect other than pre-transitional phenomena.

5.6 The flexoelectric properties of the new mixtures

In the Section 5.4 it was shown that by mixing two different bimesogenic materials the nematic phase could be broadened significantly. This improvement led to the discovery of an underlying smectic phase. As discussed in Section 5.3, it is possible to induce chirality into an achiral phase by adding a chiral dopant. In this section the flexoelectro-optic properties of the doped mixtures will be examined.

5.6.1 Alignment for flexoelectro-optic switching

The most commonly used method to align a chiral nematic for the purpose of observing flexoelectro-optic switching is to shear the material in a glass cell under an applied field. With practice it is possible to achieve good uniform alignment by this method. The electric field used is higher than that required to induce the focal conic texture but lower than the field at which the dielectric coupling starts to become dominant (helix unwinding). Figure 5.6 shows an example of a lying helix texture formed by this method; this is a typical example of the alignment achievable.

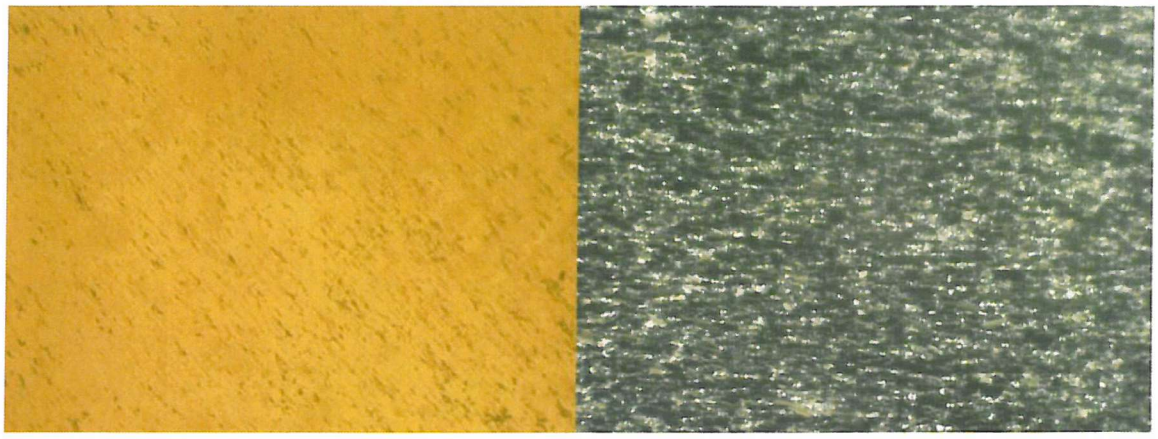

Figure 5.6 The texture observed for the uniformly lying helix geometry in a doped bimesogenic mixture. Both the bright and dark states are shown with no field applied.

The downfall of this alignment method is that the shearing process can take a number of attempts to get a satisfactory quality of alignment.

There are alternatives to the shearing method for achieving the uniformly lying helix geometry for these materials, two of which will be discussed here. The first method for achieving the necessary alignment was developed by Coles *et al.*[2]; this method uses a cell with hybrid alignment. The mixture is cooled very slowly (typically less than 1°C/minute) from the isotropic phase with an electric field applied across the cell, the field is similar to that used in the shearing method. This method can produce very good alignment.

The second method was discovered by the author during this work and uses a planar cell. The material is rapidly cooled (50°C/minute) from the isotropic phase with an electric field applied across the cell; the field in this method is greater than that of the previous two

UNIVERSITY OF BOURNEMOUTH LIBRARY

methods. The applied field is high enough so that the helix is on the verge of unwinding for a few degrees below the clearing point of the material. The material is cooled until dielectric coupling is no longer a factor. This produces alignment as good as the previous method and is generally quicker, although it tends not to work as well for materials which exhibit blue phases.

For the work in this chapter, the uniformly lying helix geometry is achieved using the second method described above or by shearing the cell.

5.6.2 Flexoelectro-optic switching in the doped bimesogenic mixtures

The three bimesogenic mixtures discussed in Section 5.4 were deemed to be promising materials for flexoelectro-optic switching as they have quite broad nematic phases. The three mixtures were doped with approximately the same amount of the chiral additive BDH1281 (~3.40%). The optical and electro-optical properties of the resulting chiral nematic phases are described below.

Mixture 1

The first sample studied was a mixture of 20% FfO-7-OfF and 80% FfO-9-OfF doped with 3.42% of BDH1281, where all percentages are measured by weight. For ease this mixture will be referred to as 3.42% BDH1281 in 20%/80% FfO-7/9-OfF. Initial visual observations, made between two coverslips, show that the material undergoes the transition from chiral nematic phase to the isotropic phase at 57°C, with no blue phases observed. Upon cooling from the isotropic phase at least one blue phase is observed before the formation of the chiral nematic phase. The transition was photographed and is shown in Figure 5.7.

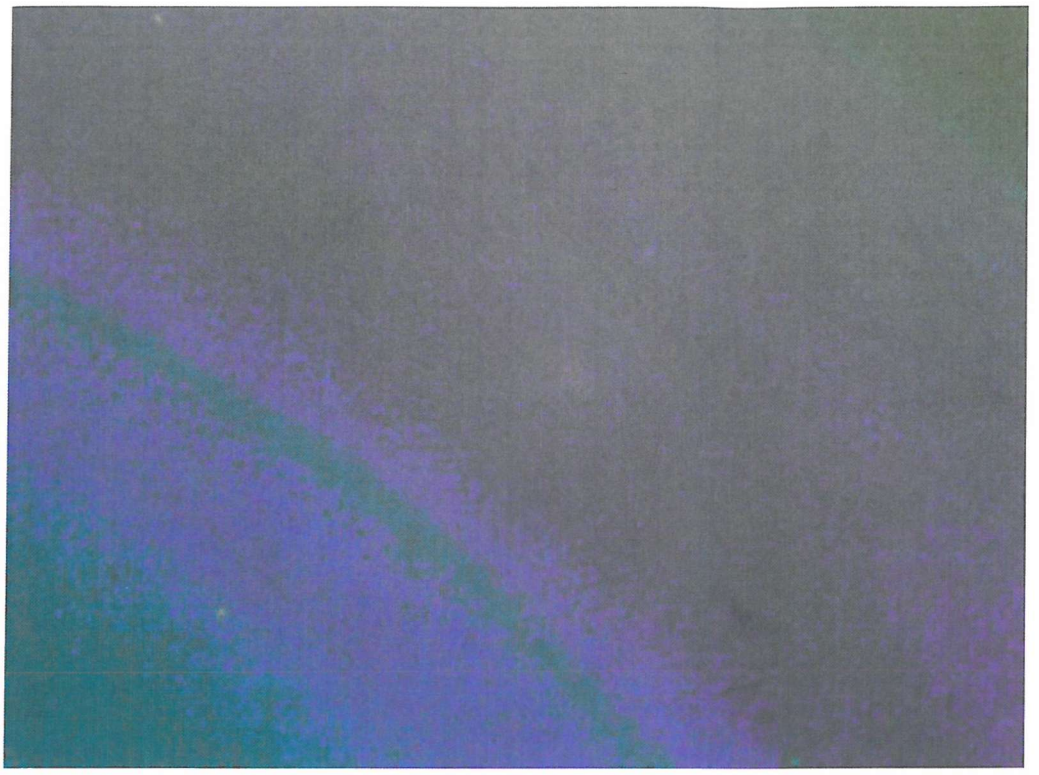

Figure 5.7 One or more blue phases observed in a mixture of 3.42% BDH1281 in 20%/80% FfO-7/9-OfF. The material was in a commercially-made planar cell.

The existence of a blue phase or phases indicates that the pitch of the material is less than 500 nm, as blue phases rarely occur in materials of pitches greater than 500nm.[5] Upon further cooling, the Grandjean chiral nematic texture is formed. Viewed with the cell between crossed polarisers, the Grandjean texture appears a mid- to dark blue. As the material cools towards room temperature, there is little change in the colour of the Grandjean texture; this implies that the pitch of the material remains relatively constant. Below 20-22°C the colour observed changes rapidly, with a colour shift towards the red end of the visible spectrum; this indicates that the pitch length is increasing rapidly. This process of rapid helix unwinding upon cooling in a chiral nematic is usually the pre-emptive indication of a phase change to a smectic phase; and at 18°C a phase change to a smectic phase is observed (as discussed previously in Section 5.5). The material was cooled down to -60°C and no further phase changes were observed. No crystallisation occurred, although upon reheating there was a small amount of crystal nucleation, which melted away as the temperature approached the isotropic phase transition.

The next stage was to examine the flexoelectro-optic properties of the material. To do this, the material was aligned into the lying helix geometry using the shearing method described previously. The flexoelectro-optic response of the material as a function of

applied field is shown in Figure 5.8. The measurements were made in a commercially-made cell, carrying planar alignment layers and a thickness of 5.83 μm.

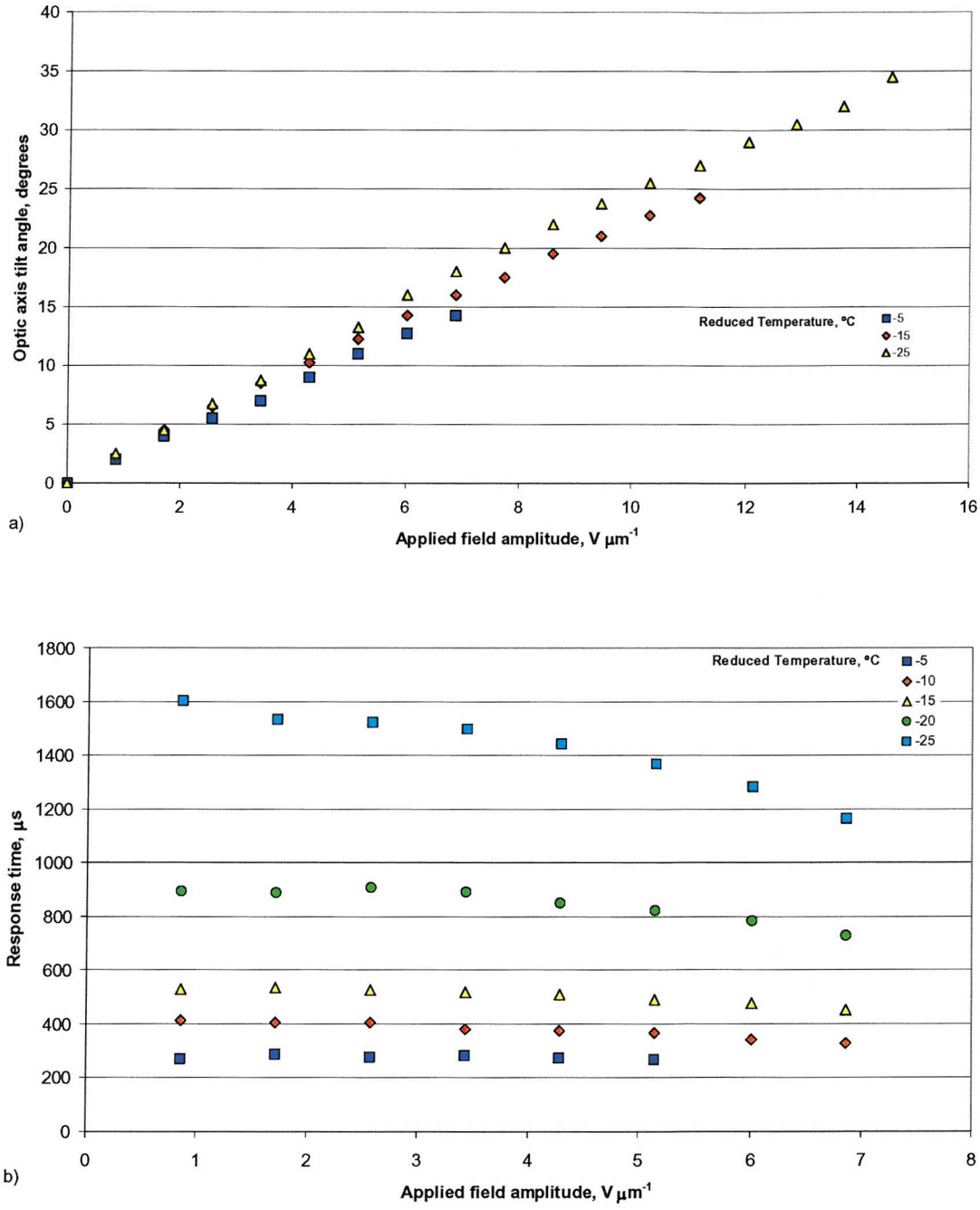

Figure 5.8 The flexoelectro-optic switching properties of a mixture of 3.42% BDH1281 in 20%/80% FfO-7/9-OfF (w/w). The graphs show, as a function of applied field amplitude, a) the induced tilt angles and b) the response times, both measured across a range of

reduced temperatures. The response times are measured for 10-90% of the full switch of the optic axis, i.e. twice the tilt angle.

With regard to the tilt measurements, it is noted that not all the sets of results are plotted, for reasons of clarity. There is at each reduced temperature a critical electric field where dielectric coupling starts to have a significant effect on the alignment. This is usually observable under a microscope as the onset of degradation in the uniformity of the lying helix texture. Although it is possible to observe flexoelectro-optic switching above this voltage, the accuracy of the measurement decreases, so for this work very few measurements are made past this point. The voltage at which the degradation in alignment starts increases as the temperature is reduced; this may be due to the increase in the elastic constants of the material, i.e. the material starts to resist dielectric coupling and a greater voltage is required before the degradation in the lying helix alignment is observed. Recall Equation 2.17 for the field required for total unwinding of the helix:[6]

$$E_{crit} = \frac{\pi^2}{P}\sqrt{\frac{K_{22}}{\varepsilon_0 \Delta\varepsilon}}. \qquad (2.17)$$

Although only partial unwinding is being discussed here, it is not unreasonable to suggest that partial unwinding depends on the same factors as total unwinding. The field for total unwinding was observed to increase as temperature was decreased in Chapter 3 for 7OCB doped with chiral additive. With the current mixture (and all the mixtures studied in this chapter) it has not been possible to completely unwind the helix, this is believed to be due to the bimesogenic mixture having a very low dielectric anisotropy.[7]

From Figure 5.8 it can be seen that the tilt angles initially vary linearly as a function of applied field, and this is true for all temperatures in the chiral nematic phase. At applied fields approaching the onset of alignment degradation it is observed that the tilt angles vary in a less linear fashion, this due to dielectric coupling becoming a more significant factor. With this material it is possible to achieve tilt angles of above 45°, that it to say a full switch of 90°, at room temperature. For the same applied electric field at different temperatures the tilt angles are quite different. Some theories suggested to explain this observation are discussed later in this chapter.

The response times of the mixture increase as the temperature decreases. This is to be expected since the theory of flexoelectric coupling predicts that the response time is proportional to the effective viscosity associated with helix distortion, which has an inverse

dependence on temperature. The response times also decrease as the field applied is increased. This is typical behaviour (in varying degrees) for materials in which flexoelectro-optic switching has been examined.[1,8] This effect is less pronounced at higher temperatures, which indicates that the theoretical approximation[9] that response time is independent of field holds reasonably well at low effective viscosities. The response times measured are comparable to those of a surface stabilised ferroelectric device.[10]

There are two further measurements that can be made, which are not electro-optic in nature but are important to this work; these are pitch and selective reflection measurements. The selective reflection measurements can be made using the same cell as the flexoelectro-optic response. However, the measurement of the pitch requires a wedge cell of known angle. The results of these measurements on the 3.42% BDH1281 in 20%/80% FfO-7/9-OfF mixture are shown in Figure 5.9.

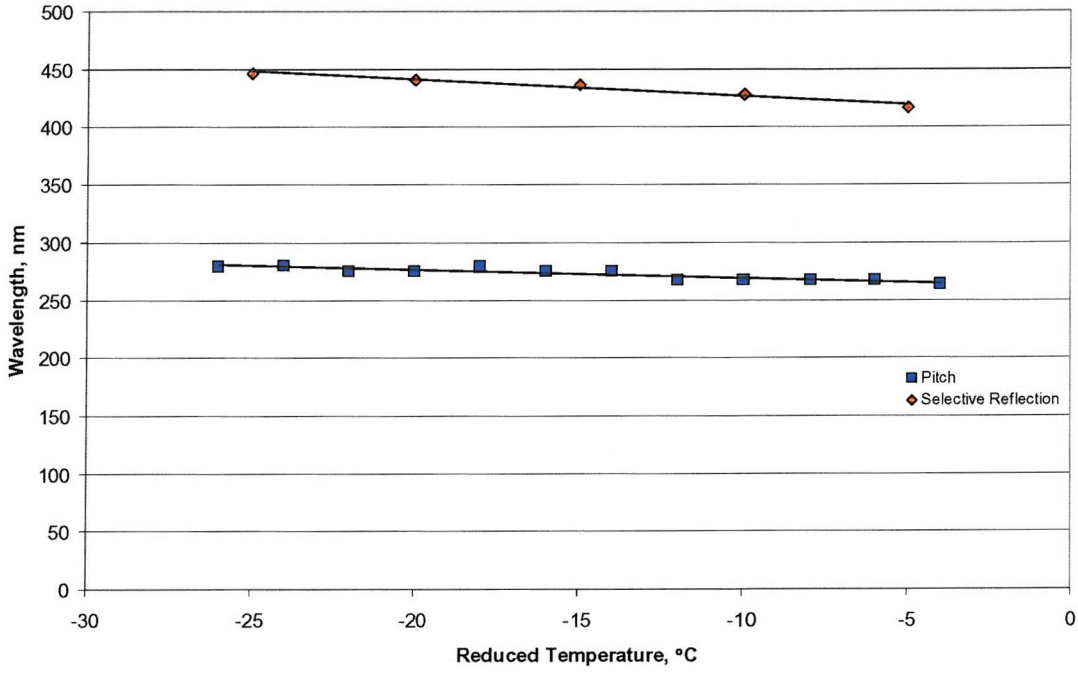

Figure 5.9 The selective reflection and pitch properties of a mixture of 3.42% BDH1281 in 20%/80% FfO-7/9-OfF (w/w). Trend-lines were added to guide the eye. The selective reflection wavelength properties were measured using a UV-visible spectrometer and the pitch was measured using a wedge cell of angle 0.035°.

It can be seen from the results given in Figure 5.9 that the pitch and the wavelength of selective reflection do not vary a great deal on cooling from the isotropic to approximately

room temperature. Recall from Chapter 2, the following relationship between pitch and the selective reflection

$$\lambda_0 = \bar{n}P, \qquad (2.5)$$

where $\bar{n}$ is the average refractive index of the director planes. This implies that if the pitch increases in a rapid non-linear fashion below room temperature, so too does the wavelength of the selectively reflected light. Table 5.3 shows a comparison of the measured values of pitch and selective reflection and hence a calculated value for the average refractive index.

Reduced Temperature, °C (T_c = 57°C)	Pitch, nm	Selective reflection wavelength, nm	$\bar{n}$
-5	265	416.5	1.57
-10	269	428	1.59
-15	273	436.5	1.60
-20	276	440.5	1.60
-25	280	446.5	1.59

Table 5.3 A comparison of the values at different reduced temperatures for the pitch, selective reflection and the calculated values for the average refractive index. The mixture studied was 3.42% BDH1281 in 20%/80% FfO-7/9-OfF (w/w).

From Table 5.3, it can be seen that the average refractive index is relatively constant (~1.6) across the range of temperatures measured. Typically, as seen for 7OCB, the average refractive index increases slowly as the temperature is reduced, as a result of the order parameter increasing. However, this increase is small and would not be noticeable in the values calculated from the pitch and selective reflection wavelength. However, this calculation of the average refractive index using the pitch and selectively reflected wavelength allow the accuracy of the pitch and selective reflection measurements to be judged for a certain temperature by comparing the value of the average refractive index with that at different temperatures. For biphenyl based liquid crystals the average refractive index is typically between 1.55 and 1.62.[11,12]

The pitch and flexoelectro-optic tilt measurements give the necessary data to calculate the ratio of the effective flexoelectric coefficient and the average of the splay and bend elastic constants, $\bar{e}/K$. Recall from Chapter 3 the following equation

$$\frac{\bar{e}}{K} = \frac{\tan\phi}{\Delta E}\frac{2\pi}{P}, \tag{3.10}$$

where $\tan\phi/\Delta E$ can be represented by the gradient of the tangent of ϕ against applied electric field. The flexoelectric properties of this material are shown in Table 5.4. It should be noted in this work that $\tan\phi/\Delta E$ is always derived from the linear region of the tilt angle versus applied field plot, this minimises any effects due to dielectric coupling and the small angle approximation used to derive Equation 3.10.

Reduced Temperature, °C (T_c = 57°C)	$\Delta\tan\phi/\Delta E$, μm V^{-1}	Pitch, nm	$\bar{e}/K$, C N^{-1} m^{-1}
-5	0.0273	265	0.86
-10	0.0299	269	0.89
-15	0.0314	273	0.93
-20	0.0330	276	0.99
-25	0.0345	280	1.02

Table 5.4 A comparison of the values at different reduced temperatures for the ratio of $\bar{e}/K$. The material studied was 3.42% BDH1281 in 20/80 FfO-7/9-OfF.

Table 5.4 shows that $\bar{e}/K$ increases as the material is cooled. This behaviour will be discussed in further detail later.

Mixture 2

The next sample studied was a mixture of 80% FfO-7-OfF and 20% FfO-11-OfF doped with 3.36% of BDH1281, where all percentages are given by weight. Visual observations show that the material undergoes the transition from the chiral nematic phase to isotropic phase at 49°C. At least one blue phase was observed upon cooling from the isotropic phase to chiral nematic phase. Approaching 13°C on cooling, there is a rapid change in colour of

the material due to a rapid change in pitch, and at 13°C the phase changes from the chiral nematic phase to a smectic phase. This is very similar to the behaviour of mixture 1.

The flexoelectro-optic properties of mixture two, in the uniformly lying helix texture, were measured as a function of applied field. The texture was formed by shearing the mixture in a commercial planar glass cell under an applied field. The cell thickness in this case was 5.73 μm. The results of the flexoelectro-optic measurements are shown in Figure 5.10.

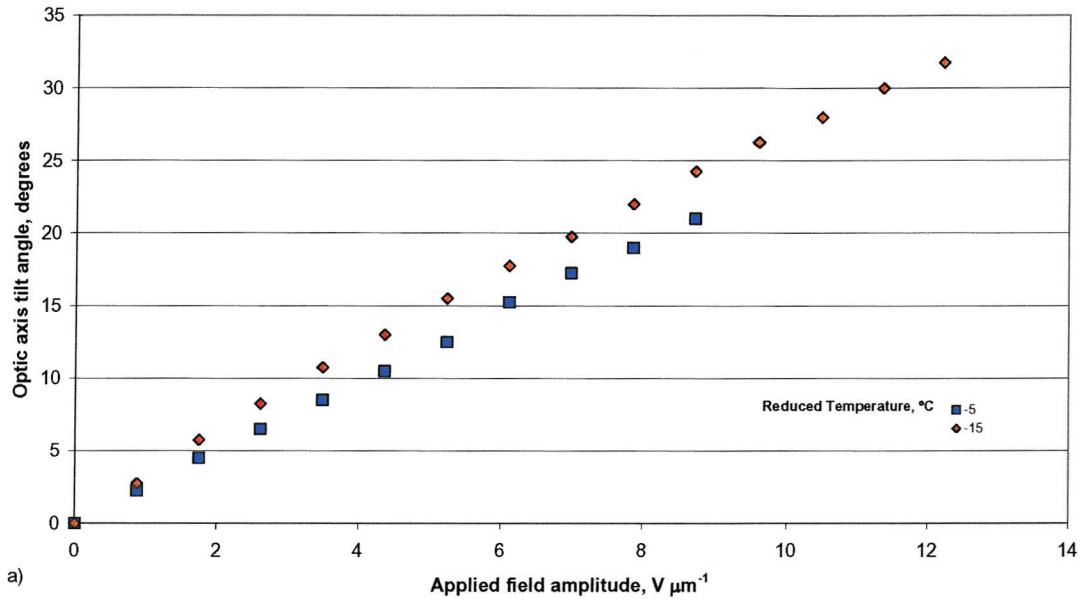

a)

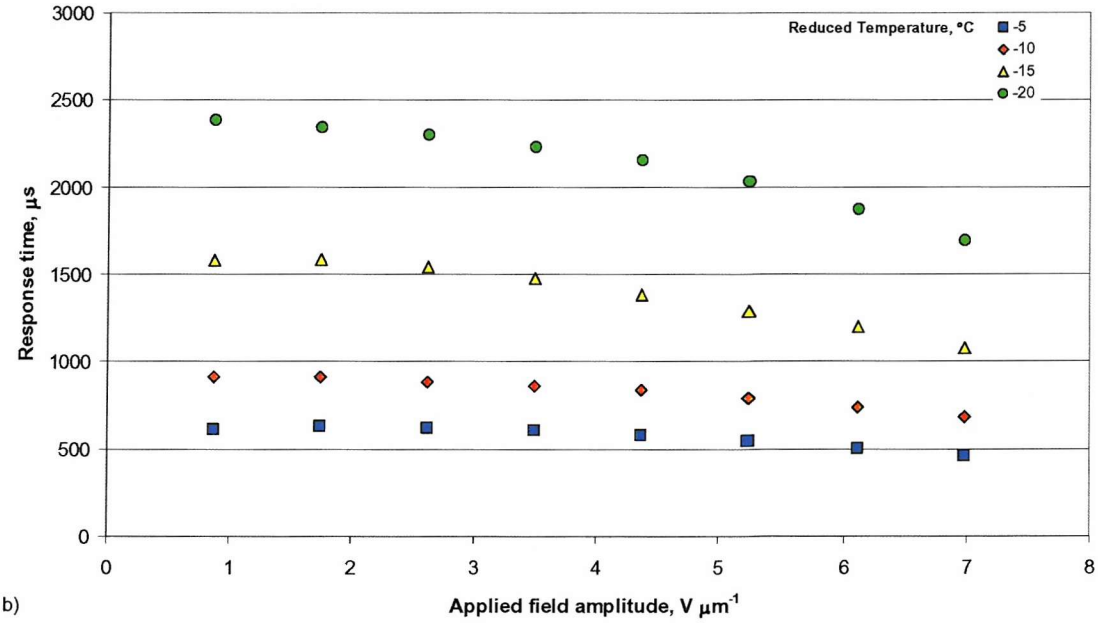

b)

Figure 5.10 The flexoelectro-optic switching properties of a mixture of 3.36% BDH1281 in 80%/20% FfO-7/11-OfF (w/w). The graphs show, as a function of applied field amplitude, a) the induced tilt angles and b) the response times, both measured across a range of reduced temperatures. The response times are measured for 10-90% of the full switch of the optic axis, i.e. twice the tilt angle.

As expected from theory, the tilt angles vary linearly with applied field and, as was observed for the first mixture, the tilt angles at the same applied field increase as the temperature is reduced.

The response times behave in a similar manner to that observed for the first mixture, being almost independent of field amplitude at higher temperatures, in agreement with the theory.

The selective reflection wavelength and pitch were also measured; the results are shown in Figure 5.11.

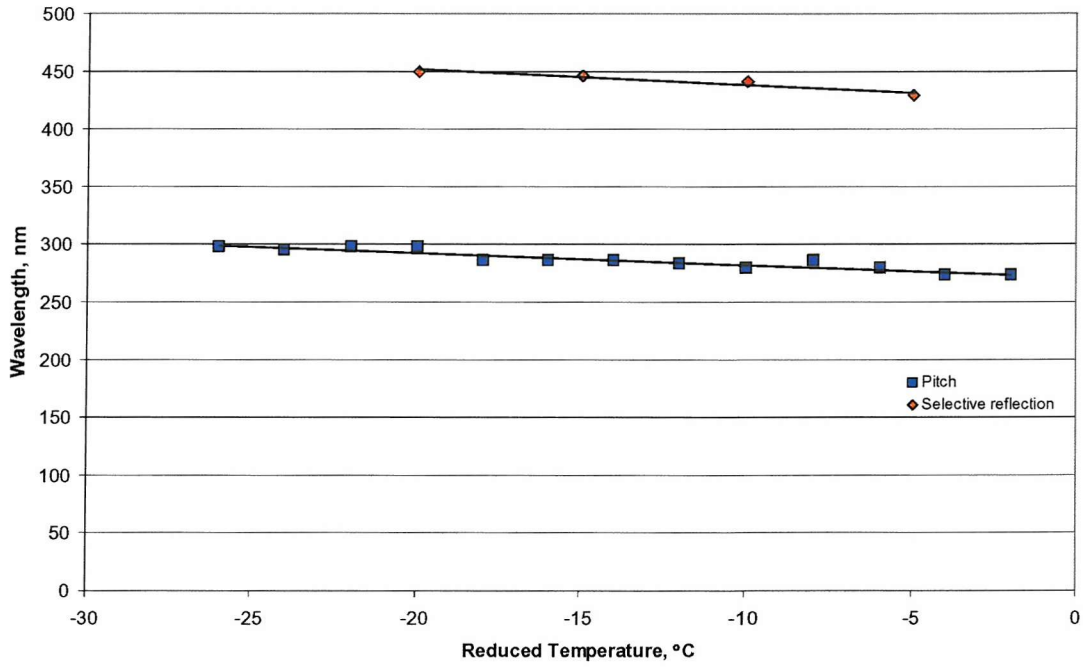

Figure 5.11 The selective reflection and pitch properties of a mixture of 3.36% BDH1281 in 80%/20% FfO-7/11-OfF (w/w). Trend-lines were added to guide the eye. The selective reflection wavelength properties were measured using a UV-visible spectrometer and the pitch was measured using a wedge cell of angle 0.029°.

Figure 5.11 shows that the pitch and selective reflection wavelength increase slightly as the temperature is reduced to room temperature.

As was seen previously, the pitch and selective reflection wavelength are related to each other by the average refractive index. The measured values of the pitch and selective reflection wavelengths are shown in Table 5.5 below, together with the calculated value for the average refractive index.

Reduced Temperature, °C (T_c = 49°C)	Pitch, nm	Selective reflection wavelength, nm	$\bar{n}$
-5	276	429	1.55
-10	282	441	1.56
-15	287	446	1.55
-20	293	450	1.54

Table 5.5 A comparison of the values at different reduced temperatures for the pitch, selective reflection and the calculated values for the average refractive index. The material studied was 3.36% BDH1281 in 80/20 FfO-7/11-OfF.

Table 5.5 shows that the average refractive index is relatively constant (~1.55) as was the case for the first mixture, the values however are a little lower. If it was a case of the pitch measurement being slightly inaccurate, this would have only a small effect on the ratio $\bar{e}/K$ (less than 3%).

The next step is to calculate $\bar{e}/K$ from the tilt and pitch values measured. The results are shown in Table 5.6.

Reduced Temperature, °C (T_c = 49°C)	$\Delta\tan\phi/\Delta E$, μm V^{-1}	Pitch, nm	$\bar{e}/K$, C N^{-1} m^{-1}
-5	0.0440	276	1.00
-10	0.0468	282	1.04
-15	0.0504	287	1.10
-20	0.0537	293	1.15

Table 5.6 A comparison of the values at different reduced temperatures for the ratio of $\bar{e}/K$. The material studied was 3.36% BDH1281 in 80/20 FfO-7/11-OfF.

As for the first mixture the flexo-elastic ratio shows the same trend of increasing as the temperature is reduced.

Mixture 3

The final sample studied was a mixture of 89% FfO-9-OfF and 11% FfO-11-OfF doped with 3.40% of BDH1281, where all percentages are given by weight. Optical microscopy observations show that the mixture has a clearing temperature from the chiral nematic phase to the isotropic phase of 56°C. On cooling from the isotropic phase at least one blue phase is observed before the chiral nematic phase is observed. Approaching 18°C on cooling, there is a rapid change in colour of the material due to a rapid change in pitch, and at 18°C the phase changes from the chiral nematic phase to a smectic phase.

Once again, flexoelectro-optic measurements as a function of applied field were made with the material in the uniformly lying helix geometry. The results are given in Figure 5.12. The glass cell used was a 6.40μm commercially made cell with planar alignment layers.

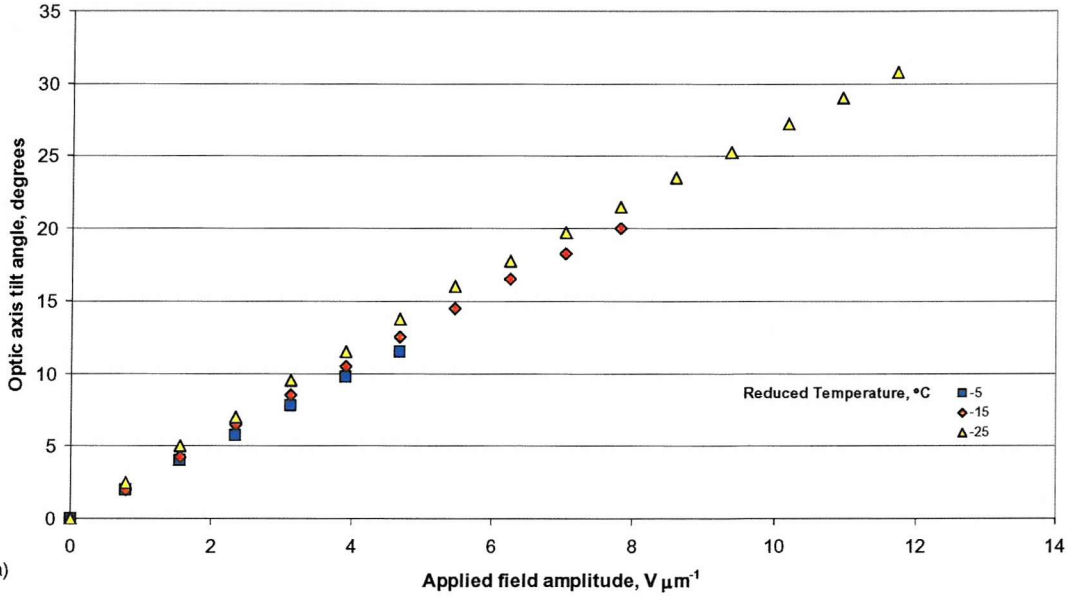

a)

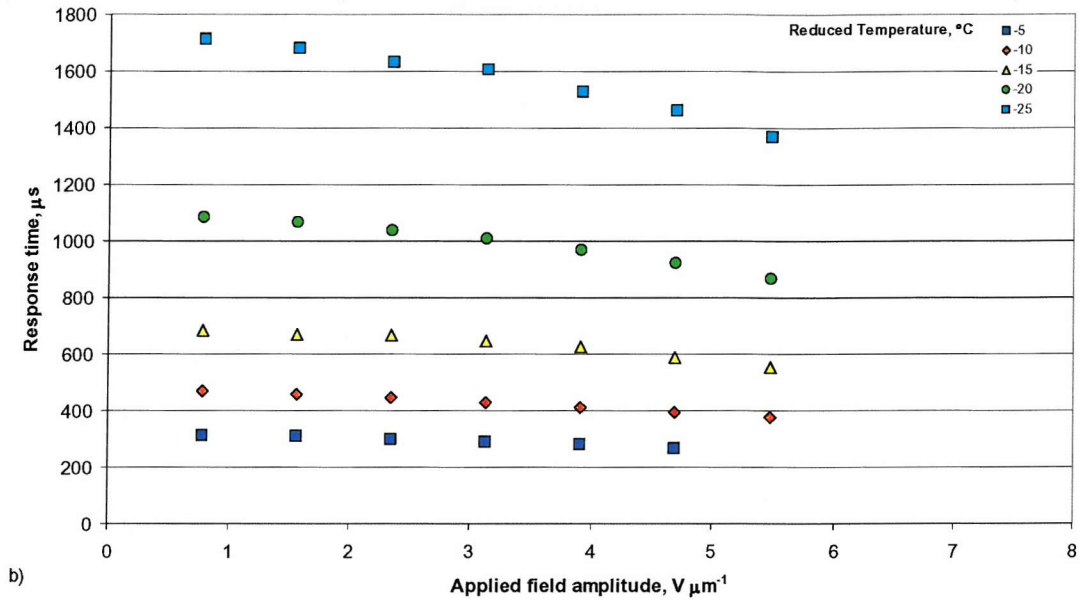

b)

Figure 5.12 The flexoelectro-optic switching properties of a mixture of 3.40% BDH1281 in 89%/11% FfO-9/11-OfF (w/w). The graphs show, as a function of applied field amplitude, a) the induced tilt angles and b) the response times, both measured across a range of reduced temperatures. The response times are measured for 10-90% of the full switch of the optic axis, i.e. twice the tilt angle.

As with the previous two mixtures, the tilt angles vary linearly with field and for a constant field the tilt angles increase as the temperature is reduced.

The response times behave in a similar manner to that observed for the previous mixtures, being almost independent of field amplitude at higher temperatures, in agreement with the theory.

The selective reflection wavelength and pitch were also measured; the results are shown in Figure 5.13.

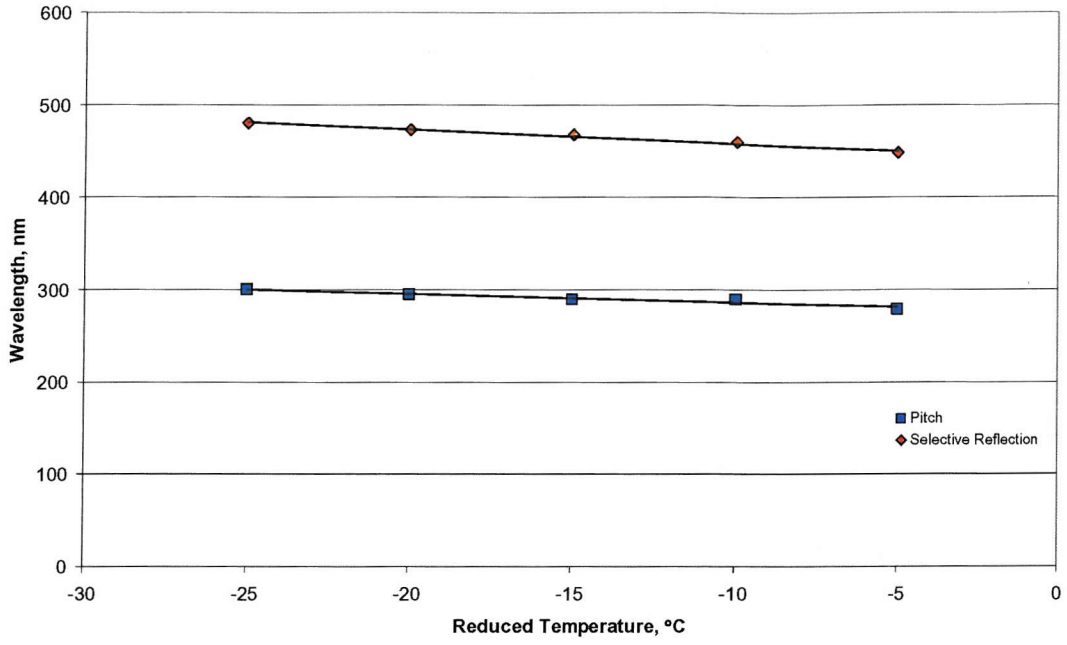

Figure 5.13 The selective reflection and pitch properties of a mixture of 3.40% BDH1281 in 89%/11% FfO-7/11-OfF (w/w). Trend-lines were added to guide the eye. The selective reflection wavelength properties were measured using a UV-visible spectrometer and the pitch was measured using a wedge cell of angle 0.025°.

As before, the pitch and selective reflection wavelength were used to calculate the average refractive index. The results are shown in Table 5.7.

Reduced Temperature, °C (T_c = 56°C)	Pitch, nm	Selective reflection wavelength, nm	$\bar{n}$
-5	279	448	1.61
-10	290	460	1.59
-15	290	468	1.61
-20	295	473	1.60
-25	300	481	1.60

Table 5.7 A comparison of the values at different reduced temperatures for the pitch, selective reflection and the calculated values for the average refractive index. The material studied was 3.40% BDH1281 in 89/11 FfO-9/11-OfF.

As for the previous two mixtures the average refractive index is relatively constant (~1.60).

Finally, the pitch and tilt measurements are used to calculate $\bar{e}/K$, the results of which are shown in Table 5.8.

Reduced Temperature, °C (T_c = 56°C)	$\Delta\tan\phi/\Delta E$, μm V^{-1}	Pitch, nm	$\bar{e}/K$, C N^{-1} m^{-1}
-5	0.0434	279	0.98
-10	0.0454	290	0.98
-15	0.0474	290	1.03
-20	0.0492	295	1.05
-25	0.0513	300	1.07

Table 5.8 A comparison of the values at different reduced temperatures for the ratio of $\bar{e}/K$. The material studied was 3.40% BDH1281 in 89/11 FfO-9/11-OfF.

Once again, it can be seen that $\bar{e}/K$ increases as the temperature is reduced.

Directly comparing these three materials reveals a number of key similarities and differences which will be discussed here.

The materials are similar in that they all exhibit the following phase progression

I -> BP -> N* -> SmX*.

However, the transition temperatures are all quite different. It was considered important to have a similar pitch for all three materials and this was achieved by using a similar amount of chiral dopant for each material. The pitches of the three mixtures differed by no more than 10% at the same reduced temperatures. The pitches for the three materials are compared in Figure 5.14.

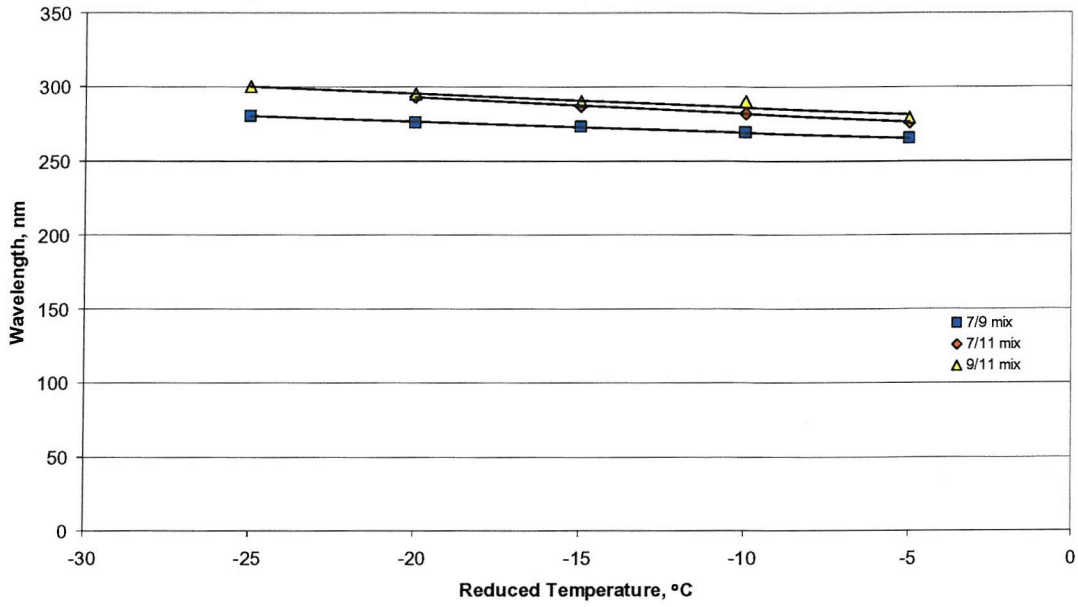

Figure 5.14 A comparison of the pitch for the three different materials studied in this section. Trend-lines were added to guide the eye.

The flexoelectro-optic switching properties of the three materials are compared directly in Figure 5.15.

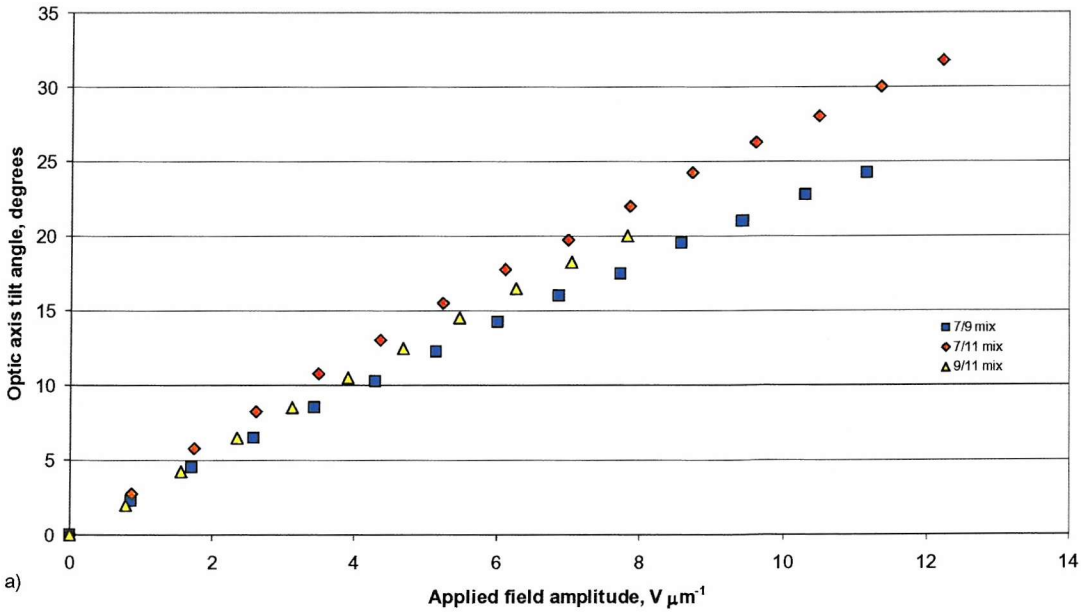

a)

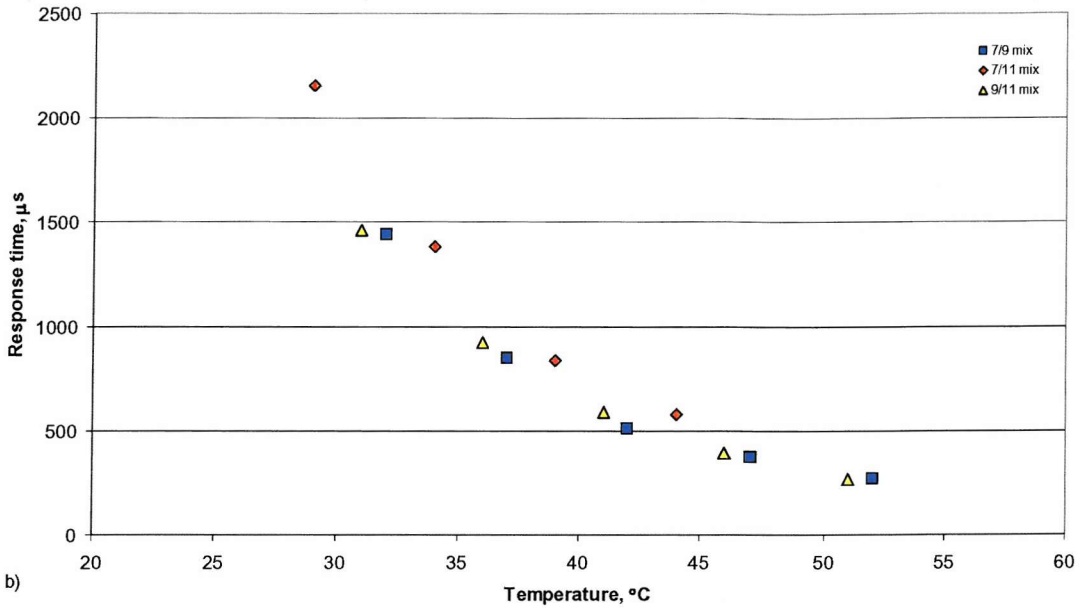

Figure 5.15 A comparison of a) the tilt angles, at a reduced temperature of -15°C, and b) the response times at a similar applied field for the three materials studied in this section.

From Figure 5.15a) it can be seen that the gradient of the tilt angle as a function of applied field is different for the three materials, being largest for the FfO-7/11-OfF mixture and smallest for the FfO-7/9-OfF mixture. While the FfO-7/9-OfF mixture had the shortest pitch of the three mixtures, the difference is not significant enough on its own to account for the differences in the gradient of tilt angle against applied field. It may be that the difference in the gradients occurs because different nematic host materials are used in the mixtures.

The response times are compared at absolute temperatures, as response time is a function of viscosity which itself is a function of absolute temperature. The response times of the three different mixtures are reasonably similar, with the FfO-7/11-OfF mixture having a slower response than the other two mixtures. Recall Equation 3.11 which gives:

$$\frac{\gamma}{K} = \tau \frac{4\pi^2}{P^2}. \qquad (3.11)$$

Using Equation 3.11, values for the ratio of the viscosity coefficient and the mean splay-bend elastic constant were calculated. The results are shown in Table 5.9.

	γ/K, kg m^{-1} s^{-1} N^{-1}		
Mixture	T = 44°C	T = 46°C	T = 47°C
20/80 FfO-7/9-OfF	-	-	2.3 x 10^{11}
80/20 FfO-7/11-OfF	3.2 x 10^{11}	-	-
89/11 FfO-9/11-OfF	-	2.2 x 10^{11}	-

Table 5.9 A comparison of the ratio of the viscosity coefficient and the mean splay-bend elastic constant.

From Table 5.9 it can be seen that the ratio of the viscosity coefficient and mean splay-bend elastic constant is similar for the FfO-7/9-OfF and FfO-9/11-OfF mixtures, but higher for the FfO-7/11-OfF mixture. There is some discrepancy as the measurements were made at different temperatures; however, the results do indicate that the slower response times for the FfO-7/11-OfF mixture are due to the higher ratio.

From studying the three mixtures, it has been seen that $\bar{e}/K$ increases in value as the temperature is reduced in all cases. The work of Maheswara Murthy *et al*[13] suggests that $\bar{e}$ is a function of the order parameter squared, i.e. $[S(T)]^2$, but the theoretical work of Osipov[14] suggests there may be linear dependence on the order parameter, i.e. S(T), when the flexibility of the molecules are taken in to account for long alkoxy chain materials (this has been seen experimentally for 8OCB[15]). K is also believed to be a function of the order parameter squared to the first approximation. If both $\bar{e}$ and K are dependent on the order parameter squared, it would be expected that that the ratio would remain relativity constant with temperature and this has been observed for a number of materials.[13,15] This work shows that the flexo-elastic ratio in fact decreases with temperature for the materials studied: this would imply that $\bar{e}$ and K depend on the order parameter in different ways. The behaviour of K as a function of temperature is well documented for monomesogens[11,16,17] and it is rare that K deviates greatly from being dependent on the order parameter squared (to the first approximation). However, Dilisi *et al.*[18] have shown for an achiral symmetric bimesogen, based on the monomer 4.4'-dipentyloxyphenylbenzoate, that K_{33} can deviate significantly from theory. As a result it would seem probable that K is the source of the temperature dependence of the flexo-elastic ratio. However, anomalous behaviour in $\bar{e}$ cannot be dismissed without further study. (Attempts were made to measure the elastic constants using a dynamic light scattering experiment. However, it was not possible to get the symmetric fluorobiphenyl

bimesogens to adopt the homeotropic geometry necessary to complete these measurements.)

5.7 The effects of varying the amount of chiral dopant

By adding a chiral dopant to an achiral bimesogenic nematic host, chirality can be induced in the system. One of the advantages of using a chiral dopant is that it allows the pitch of the chiral nematic phase to be controlled, thus allowing the properties of the host to be compared, where the only significant difference is in the respective pitches. In this section the effects of pitch in a flexoelectro-optic system were studied, by varying the amount of chiral dopant added to the bimesogenic materials.

20% / 80% FfO-7/9-OfF

The first host material used was the mixture of FfO-7-OfF and FfO-9-OfF as discussed previously in Section 5.4. Two new mixtures were made up for this section to complement the mixture studied in Section 5.5, one containing a lower amount of chiral additive and the other containing a greater amount. The first mixture was made with only 1.99% of the chiral additive BDH1281 (by weight) and the second mixture was made with 3.93% chiral additive. Optical microscopy indicated that the new mixtures exhibited a chiral nematic phase similar to the mixture described in Section 5.5. The difference between the mixtures was in the reflected colours of the Grandjean chiral nematic texture. The reflected wavelength was longer or shorter, depending on whether there was a lesser or greater concentration of chiral additive. This is of no surprise as the addition of a greater amount of dopant would decrease the pitch of the material, such that the reflected colour observed would be blue-shifted. It was also noted that the longer pitch material did not appear to exhibit a blue phase; this indicates a pitch approaching 500nm.[5]

As in Section 5.5, the relevant measurements for calculating the ratio of the effective flexoelectric coefficient and the average of the splay and bend elastic constants were performed. The first mixture to be studied was the 1.99% BDH1281 mixture. The results of the electro-optic, selective reflection and pitch measurements are shown in Figure 5.16.

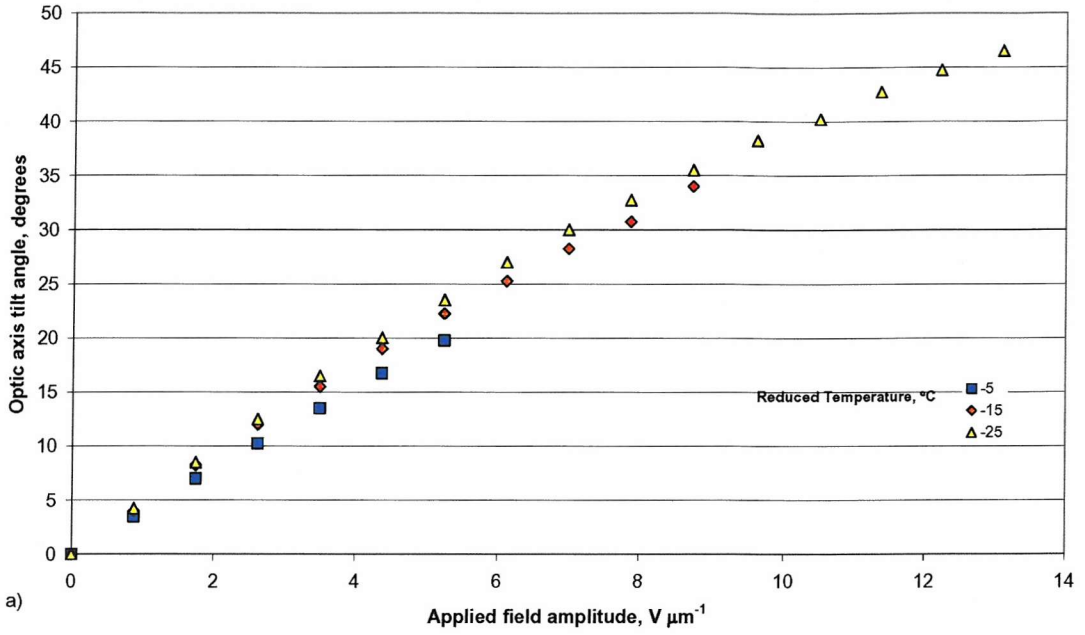
Optic axis tilt angle, degrees
Applied field amplitude, V µm-1
Reduced Temperature, °C
-5
-15
-25

a)

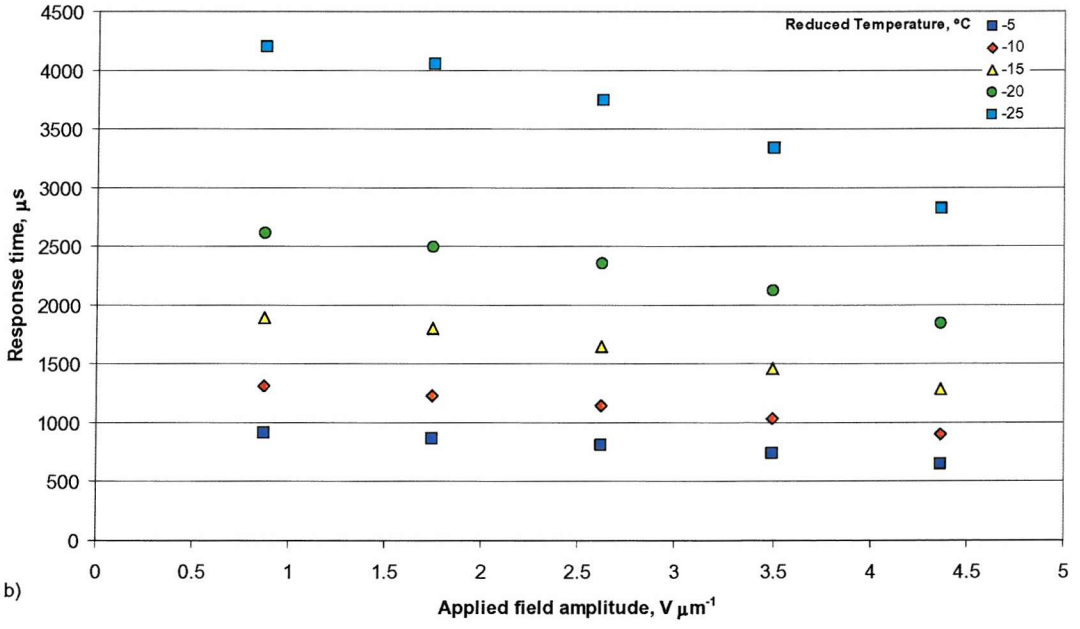
Response time, µs
Applied field amplitude, V µm-1
Reduced Temperature, °C
-5
-10
-15
-20
-25

b)

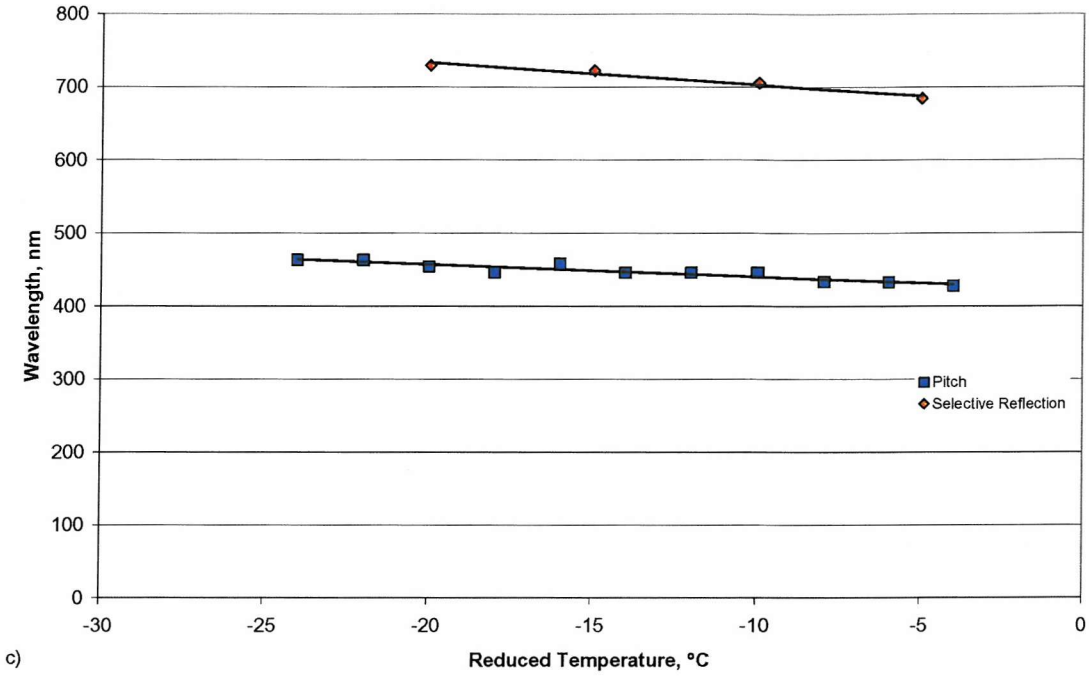

Figure 5.16 The optical and electro-optical properties of a mixture of 1.99% BDH1281 in 20%/80% FfO-7/9-OfF (w/w). The graphs show a) the induced tilt angles, b) the response times and c) selective reflection wavelength and pitch, all measured across a range of reduced temperatures. The response times are measured for 10-90% of the full switch of the optic axis, i.e. twice the tilt angle. The selective reflection properties were measured using a UV-visible spectrometer and the pitch was measured using a wedge cell of angle 0.049°. Trend-lines were added to guide the eye.

The average refractive index and the flexo-elastic ratio have been calculated and the results are shown in Table 5.10.

Reduced Temperature, °C (T_c = 57°C)	$\Delta\tan\phi/\Delta E$, μm V^{-1}	Pitch, nm	Selective reflection Wavelength, nm	$\bar{n}$	$\bar{e}/K$, C N^{-1} m^{-1}
-5	0.0685	432	685	1.59	0.99
-10	0.0745	440	706	1.60	1.06
-15	0.0767	449	723	1.61	1.07
-20	0.0793	457	730	1.60	1.09
-25	0.0827	465	749	1.61	1.12

Table 5.10 The values at different reduced temperatures for the pitch, selective reflection and the calculated values for the average refractive index and the ratio of the effective

flexoelectric coefficient to the average of the splay and bend elastic constants. The material studied was 1.99% BDH1281 in 20%/80% FfO-7/9-OfF.

For the mixture containing 3.42% BDH1281 in the same host, it can be seen that the average refractive index appears to be constant with no discernable variation with temperature. Again, as with the previous mixtures studied in Chapter 5, there is a clear trend in the value of the ratio $\bar{e}/K$; once again it increases as the temperature is reduced.

A second mixture with a higher concentration of dopant was also studied; the mixture contained 3.93% of dopant (w/w). The results of the electro-optic and selective reflection measurements are shown in Figure 5.17. It was difficult to obtain an accurate pitch measurement for this sample, thus the pitch was estimated from the selective reflection using Equation 2.5, using a value of 1.60 for the average refractive index.

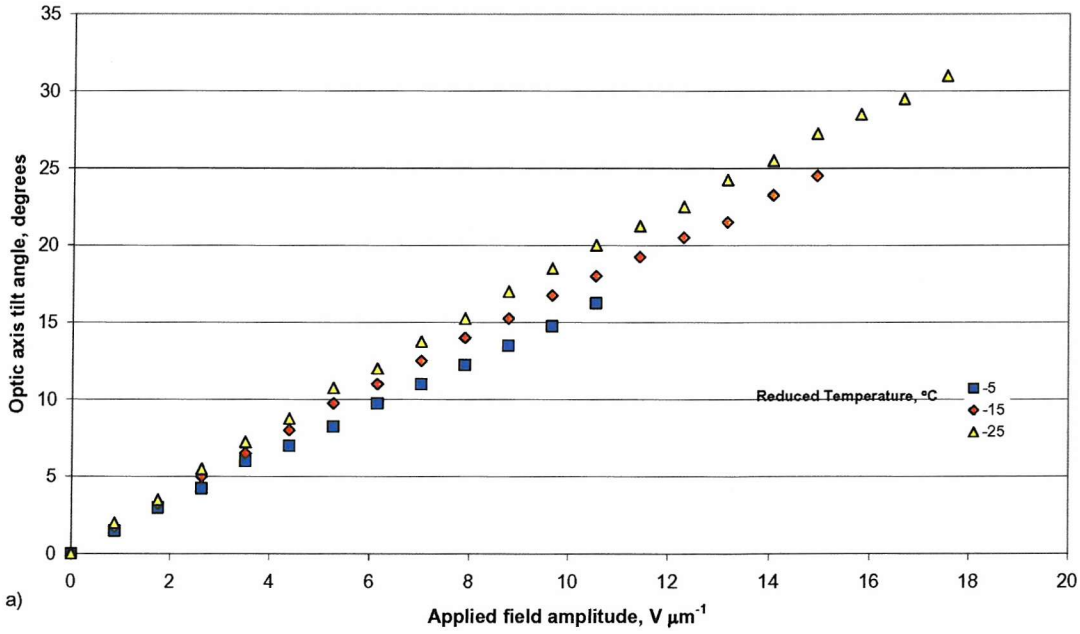

a)

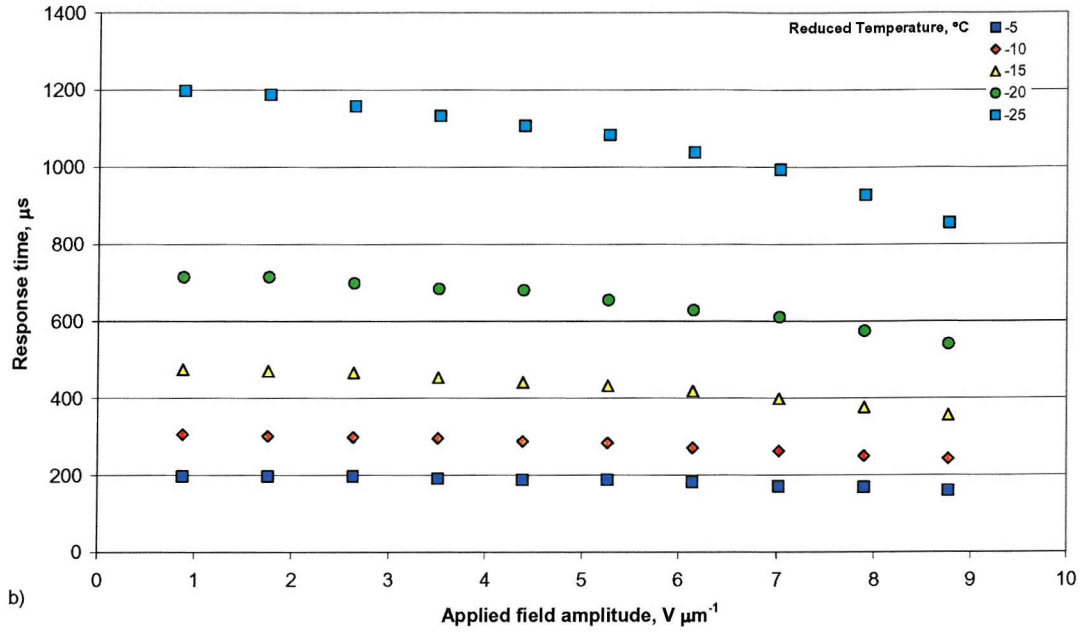

b)

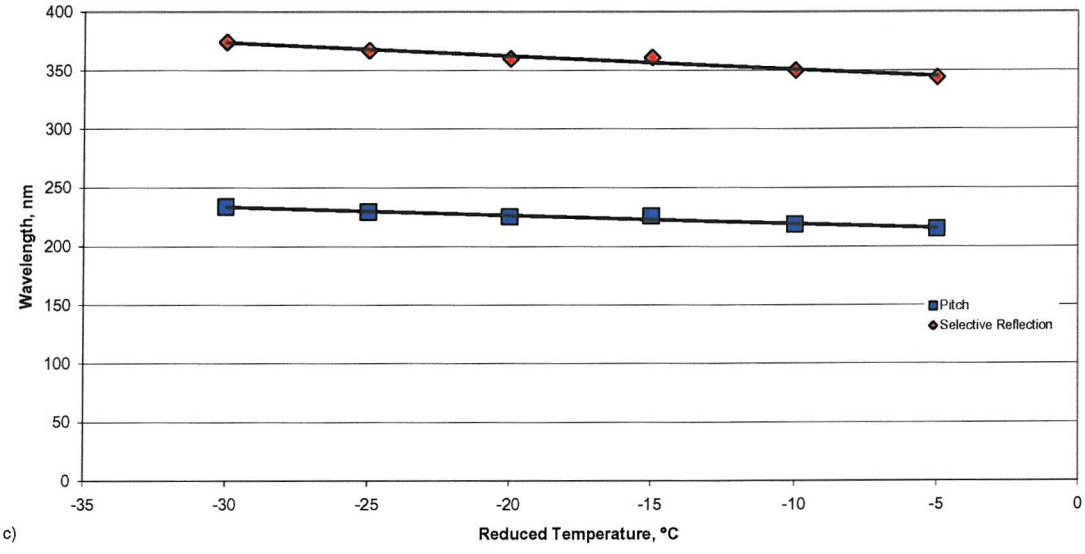

c)

Figure 5.17 The optical and electro-optical properties of a mixture of 3.93% BDH1281 in 20%/80% FfO-7/9-OfF (all percentages are measured by weight). The graphs show a) the induced tilt angles, b) the response times and c) selective reflection wavelength and pitch, all measured across a range of reduced temperatures. The response times are measured for 10-90% of the full switch of the optic axis, i.e. twice the tilt. The selective reflection properties were measured using a UV-visible spectrometer, and the pitch was estimated from these results. Trend-lines were added to guide the eye.

From the data it is possible to calculate the flexo-elastic ratio, using the calculated value for the pitch, the results of which are shown in Table 5.11.

Reduced Temperature, °C (T_c = 57°C)	$\Delta\tan\phi/\Delta E$, μm V^{-1}	Selective reflection wavelength, nm	Pitch (calculated), nm	$\bar{e}/K$, C N^{-1} m^{-1}
-5	0.0273	344	215	0.80
-10	0.0299	350	219	0.86
-15	0.0314	361	226	0.87
-20	0.0330	360	225	0.92
-25	0.0345	367	229	0.95

Table 5.11 A comparison of the values at different reduced temperatures for the selective reflection and the calculated values for the pitch and the ratio of the effective flexoelectric coefficient to the average of the splay and bend elastic constants. The material studied was 3.93% BDH1281 in 20%/80% FfO-7/9-OfF.

Once again, there is an increase in $\bar{e}/K$ as the temperature is reduced.

The tilt angles of all three materials are compared directly at two different temperatures in Figure 5.18 below.

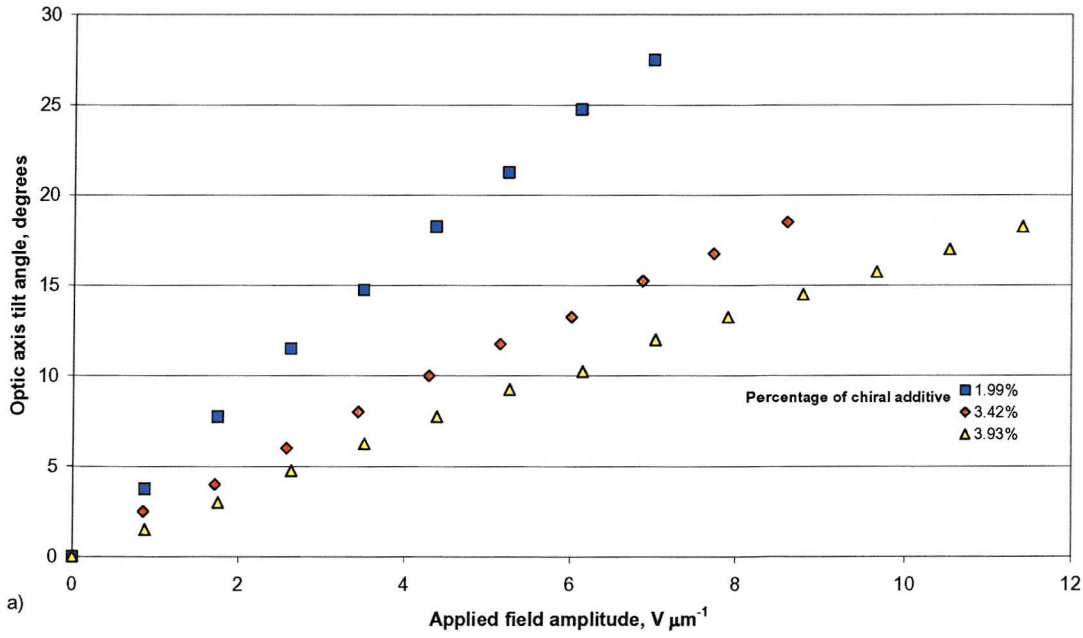

a)

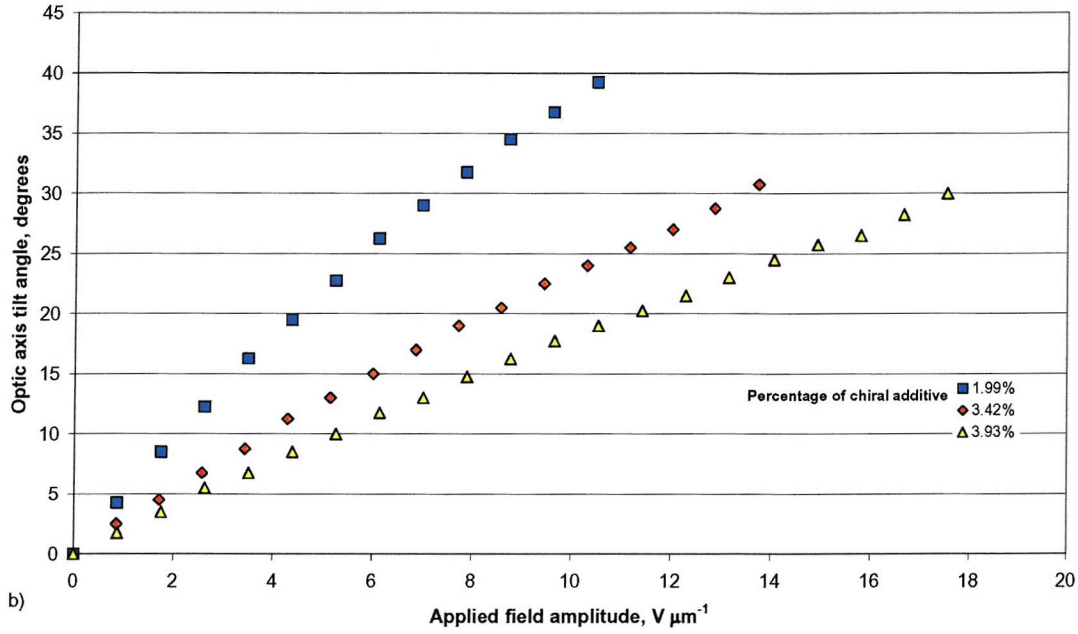

b)

Figure 5.18 A comparison of the tilt angles at two different reduced temperatures, a) -10°C and b) -20°C, for 20%/80% FfO-7/9-OfF doped with differing amounts of the chiral additive BDH1281.

From Figure 5.18, it can be seen that the tilt angles for the original 3.42% additive mixture, for the same temperature and applied field, are less than those of the 1.99% additive mixture but are higher than those of the 3.93% mixture. However the maximum applied field at which tilt angles can be measured (before the effects of dielectric coupling start becoming significant as the lying helix texture is disrupted) is lowest for the 1.99% mixture and highest for the 3.93% mixture. The theoretical treatment of the total unwinding process (see Equation 2.17) suggests that with a greater concentration of dopant, the total unwinding field would be greater because the pitch would be shorter. It would not seem unreasonable to suggest that the field required for partial unwinding would depend on the same factors.

From the comparison of the tilt angles, it is clear that the amount of dopant - and hence the pitch - has a major effect on the tilt angles and the size of the applied field for which the dielectric coupling becomes significant. By increasing the pitch, the maximum achievable tilt angle is decreased, and perhaps more importantly the tilt per unit field is decreased.

Similarly, it is possible to compare the response times of the three different mixtures at different temperatures, as shown in Figure 5.19 for two temperatures.

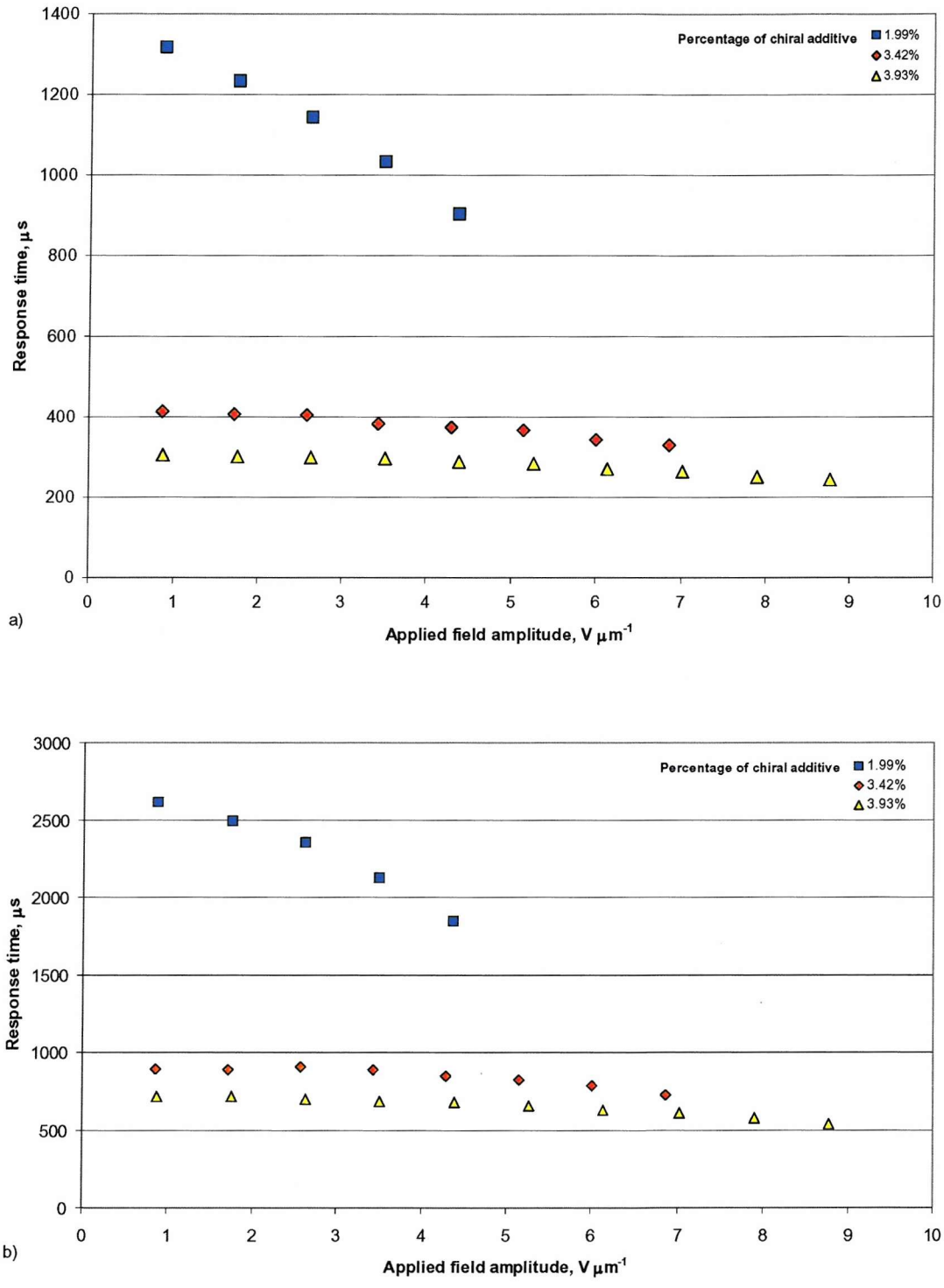

Figure 5.19 A comparison of the response times at two different reduced temperatures, a) -10°C and b) -20°C, for 20%/80% FfO-7/9-OfF doped with differing amounts of the chiral additive BDH1281.

The response times clearly show a dependence on the amount of chiral additive in the mixture, with the response of the 1.99% mixture being the slowest and the response of the 3.93% mixture being the fastest.

As essentially the only parameter that is changing between the mixtures is the amount of chiral additive it expected that the respective pitches would behave in a similar manner as a function of temperature; this was found to be the case, as Figure 5.20 shows.

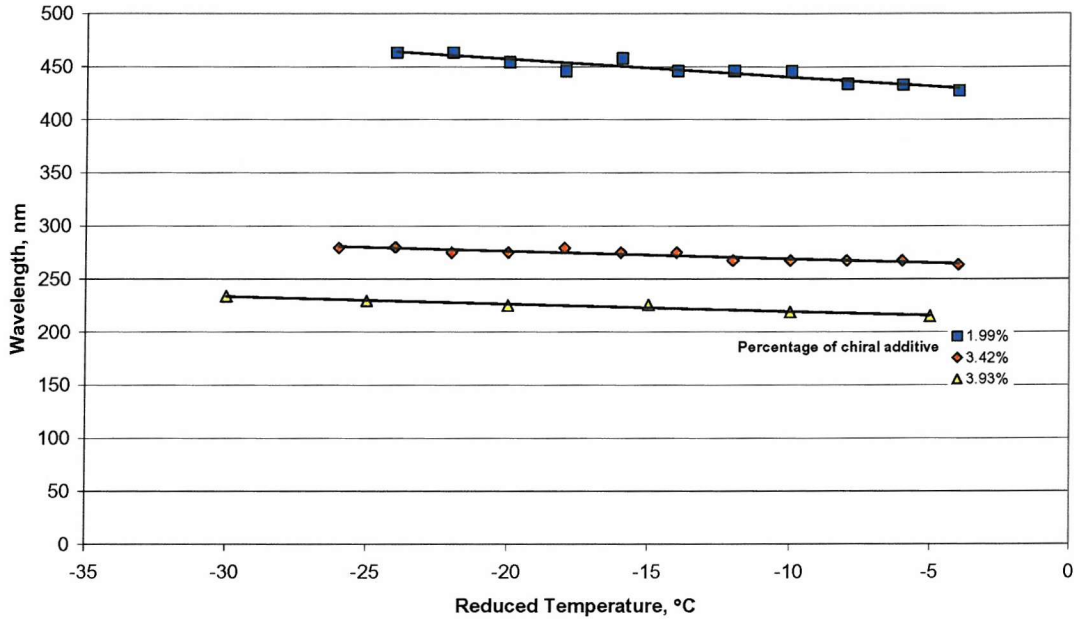

Figure 5.20 A comparison of the pitch values of the same host material with differing concentrations of the chiral dopant BDH1281. For the 3.93% mixture the pitch was calculated using the selective reflected wavelength. Trend-lines were added to guide the eye.

If the ratio of the different pitches for the three mixtures is compared to the ratio of their response times, it is found that the ratio of the response times is approximately equal to the square of the ratio of the pitches, in agreement with theory (Equation 2.38). Similarly, the ratio of the tilt angles is comparable to the ratio of the pitches for the three mixtures (Equation 2.32).

Another point to consider is the magnitude of the flexo-elastic ratio for the different mixtures, as shown in Figure 5.21 and Table 5.12, below.

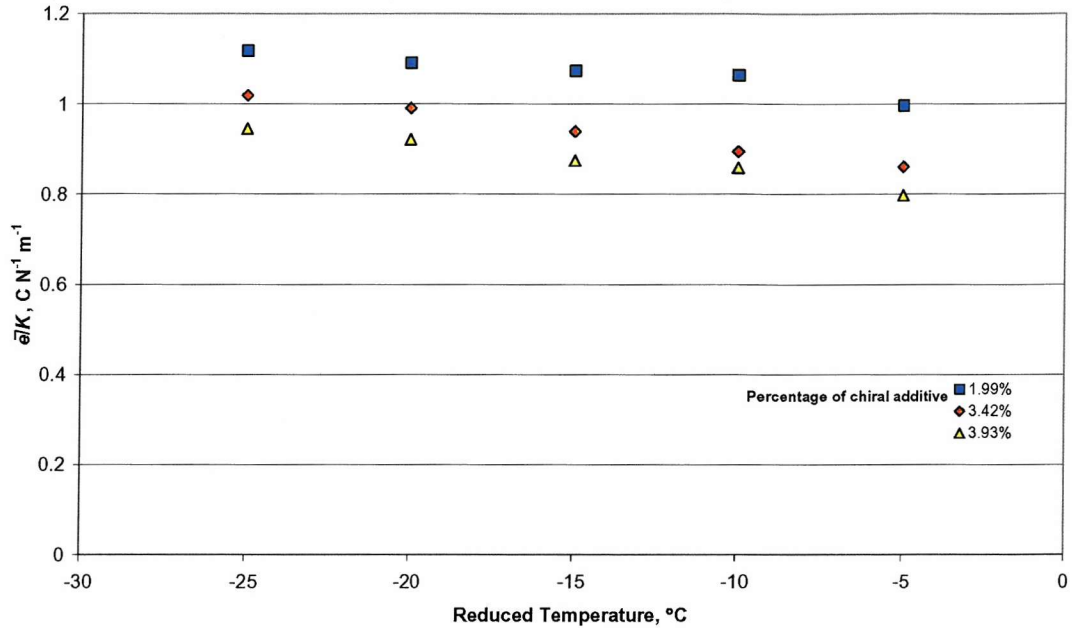

Figure 5.21 A comparison of $\bar{e}/K$ for three different concentrations of BDH1281 in 20%/80% FfO-7/9-OfF.

Percent of chiral additive	$\Delta\tan\phi/\Delta E$, μm V^{-1}	Pitch, nm	$\bar{e}/K$, C N^{-1} m^{-1}
1.99%	0.0765	440	1.06
3.42%	0.0383	269	0.89
3.93%	0.0299	219*	0.86

Table 5.12 A comparison of the ratio of $\bar{e}/K$ for three different concentrations of the chiral additive BDH1281 in 20%/80% FfO-7/9-OfF at a reduced temperature of -10°C.

* - calculated using the selective reflection wavelength.

In Table 5.12, the ratio of $\bar{e}/K$ is compared for the three mixtures with different percentages of chiral additive and it can be seen that the flexo-elastic ratio is greatest for the material with the lowest amount of chiral dopant, and hence the longest pitch. This is an unexpected result, if the assumption is made that only the pitch of the mixture is changed by the addition of chiral dopant. However, in Chapter 3 it was observed that for 7OCB doped with 6% BDH1305[4] (w/w) the order parameter decreased by approximately 4%, compared with pure 7OCB. It cannot be assumed for the bimesogenic mixtures that the order parameter would change by a similar amount because a number of factors are different, such as the use of a different chiral additive. However, it is reasonable to assume

that the order parameter is altered when the chiral dopant in incorporated into the system. Earlier in this chapter, it was seen that there is uncertainty in the relationships of $\bar{e}$ and K to the order parameter for a bimesogenic mixture. It is conceivable that a difference in the order parameter, due to a variation in the concentration of chiral additive, could change the flexo-elastic ratio significantly, depending on how $\bar{e}$ and K individually relate to the order parameter.

To confirm all the observations made above a mixture of FfO-9/11-OfF with a lower concentration of chiral additive than that described in Section 5.6.2 was studied. This new mixture studied is 2.00% BDH1281 in 89%/11% FfO-9/11-OfF and the results are shown in Figure 5.22.

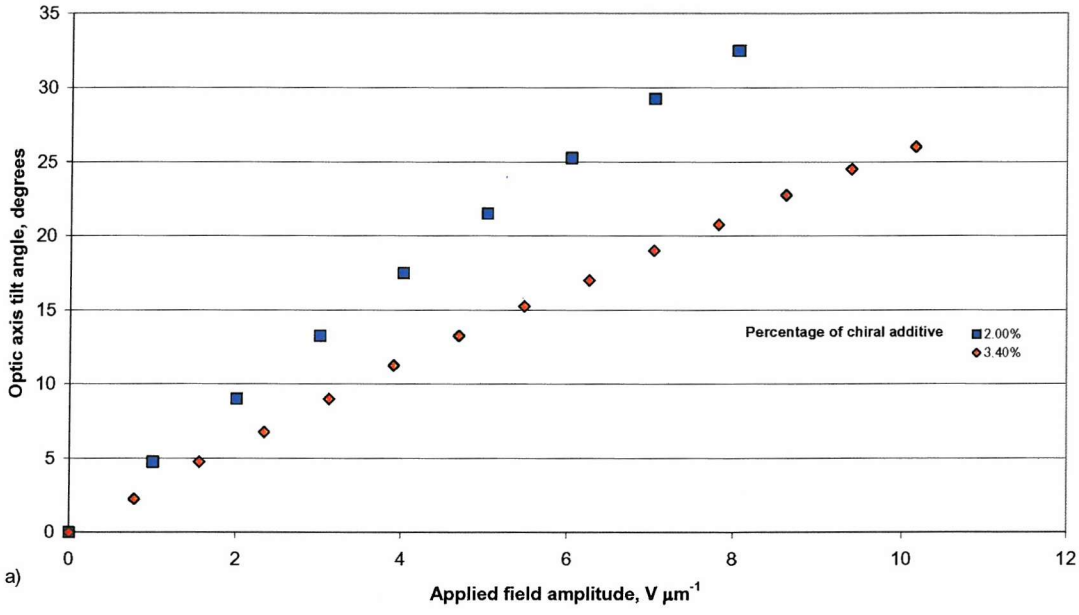

a)

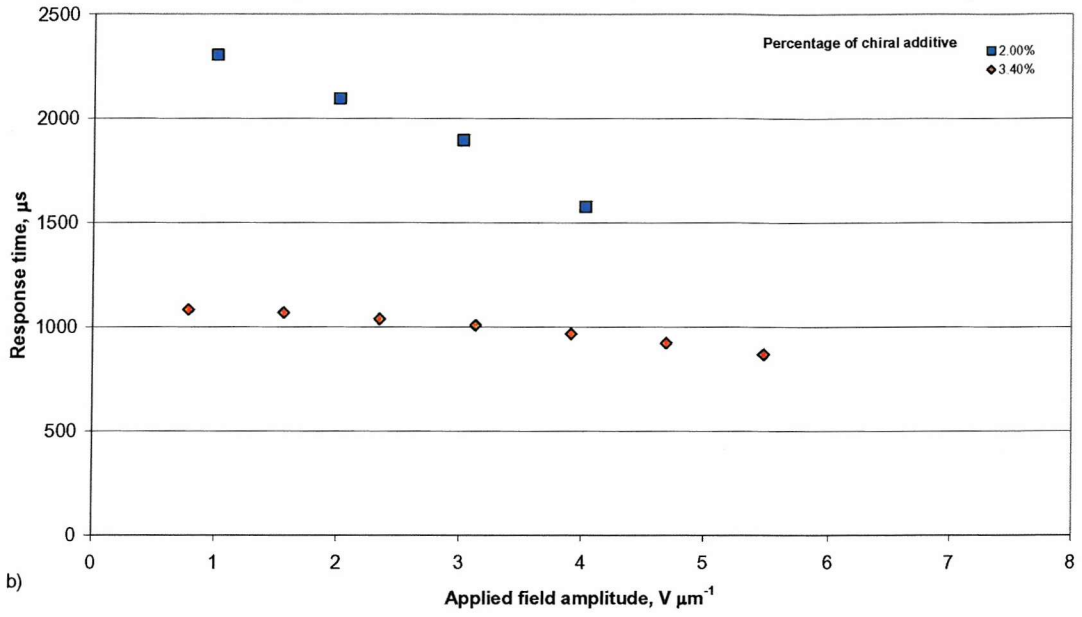

b)

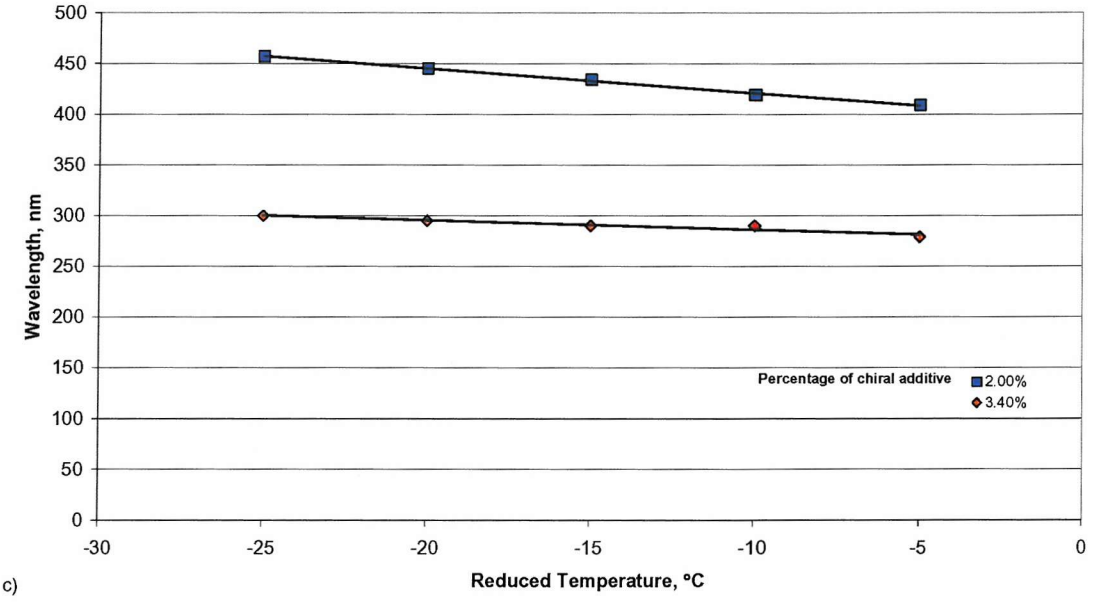

c)

Figure 5.22 A comparison of the optical and electro-optical properties of 2.00% BDH1281 in 89%/11% FfO-9/11-OfF and 3.40% BDH1281 in 89%/11% FfO-9/11-OfF. The data shown are a) the tilt angles, b) the response times and c) the pitches. The tilt angles and response times were measured at a reduced temperature of -20°C. Trend-lines were added to guide the eye.

From Figure 5.22, it can be seen that, in agreement with both theory and the observations on the FfO-7/9-OfF mixtures, the tilt angles per unit field are higher for the material with less chiral dopant, and this material also has slower response times.

The flexo-elastic ratios for the two different mixtures are compared in Table 5.13.

Reduced Temperature, °C (T_c = 56°C)	2.00% BDH1281 Mixture			3.40% BDH1281 Mixture		
	$\Delta\tan\phi/\Delta E$, μm V^{-1}	Pitch, nm	$\bar{e}/K$, C N^{-1} m^{-1}	$\Delta\tan\phi/\Delta E$, μm V^{-1}	Pitch, nm	$\bar{e}/K$, C N^{-1} m^{-1}
-5	0.0656	409	1.01	0.0434	279	0.98
-10	0.0713	419	1.07	0.0454	290	0.98
-15	0.0756	434	1.10	0.0474	290	1.03
-20	0.0791	445	1.12	0.0492	295	1.05
-25	0.0821	457	1.13	0.0513	300	1.08

Table 5.13 A comparison of the ratio of $\bar{e}/K$ for two different concentrations of the chiral additive BDH1281 in 89%/11% FfO-9/11-OfF.

From Table 5.13, it can be seen that, as has been previously observed for other mixtures in this chapter, for the 2.00% mixture the flexo-elastic ratio increases as its temperature is reduced. Again, it appears that the flexo-elastic ratio is higher for the mixture with the lower percentage of the chiral dopant.

Both the FfO-7/9-OfF and FfO-9/11-OfF mixtures show similar behaviour, as their pitches are varied by changing the added chiral dopant concentrations.

5.8 Conclusions

The aim of the work presented in this chapter was to examine the flexoelectro-optic properties of the symmetric fluorobiphenyl bimesogens. By using bimesogens it is possible to combine a high dipole moment with a low dielectric anisotropy, which is fundamental for a material to exhibit good flexoelectric properties. It was hoped that these new bimesogens would display room temperature flexoelectro-optic switching.

A series of homologues were synthesised, most of which were found to be monotropic. However, on cooling it was possible for some of the materials to super-cool in the nematic phase to a temperature close to near room temperature. Mixtures between the three most promising homologues were prepared, to see if the temperature ranges of the materials could be improved, and the preliminary results were promising. However, the new mixtures exhibited an underlying smectic phase, which is disadvantageous. By making a

series of two-component mixtures between the homologues, it was possible to optimise the mixtures such that the nematic to smectic phase transition occurred at the lowest possible temperature. The composition of the three mixtures (w/w) and their transition temperatures on cooling are:

1) 20% FfO-7-FfO and 80% FfO-9-OfF

I -(57°C)-> **N** -(18°C)-> **SmX**

2) 80% FfO-7-FfO and 20% FfO-11-OfF

I -(49°C)-> **N** -(13°C)-> **SmX**

2) 89% FfO-7-FfO and 11% FfO-11-OfF

I -(56°C)-> **N** -(18°C)-> **SmX**

Unfortunately, all three mixtures were monotropic or only exhibited a small nematic range on heating. The smectic phase was tentatively identified as the smectic A phase. The precise nature of the smectic phase is unimportant; it is only of consequence that there is a phase change.

To examine the flexoelectro-optic effect, chirality was introduced into the nematic phase by use of a chiral additive. The additive BDH1281 was chosen for its high twisting power. The three mixtures discussed above were all doped with approximately 3.40% (w/w) BDH1281. All three of the chiral mixtures exhibited a blue Grandjean chiral nematic texture and, on cooling from the isotropic phase, blue phases were observed. The presence of blue phases indicated that the respective pitches of the mixtures were shorter than 500nm.[5]

The mixtures were forced to adopt the uniformly lying helix geometry for the flexoelectro-optic properties to be studied. The flexoelectro-optic properties of all three of the mixtures were studied and tilt angles greater than 30° were observed in each case. The response times of the mixtures ranged from 300μs to 2.4ms, depending on the temperature. The pitch was measured for the three mixtures and it was found to be similar for all, ranging from approximately 270nm to 300nm for the temperatures studied. The tilt angles and pitch were used to calculate the flexo-elastic ratio for the mixtures and the values were found to range between 0.86-1.15 C N^{-1} m^{-1}. In comparison to the flexoelectric properties of the chiral doped 7OCB mixtures studied in Chapter 3, it can be seen that the flexo-

elastic ratio of the bimesogens is approximately double that of 7OCB mixtures (0.45 C N^{-1} m^{-1}). Likewise the tilt angles per unit field for the bimesogens are double those of 7OCB mixture. In contrast, the response times of the 7OCB mixtures (typically 20-120μs) are much faster than the bimesogenic mixtures (300-2400μs). By comparing the ratio of the viscosity coefficient to the mean splay-bend elastic constant of the bimesogenic mixtures (~$2.6x10^{11}$ kg m^{-1} s^{-1} N^{-1}) with the 7OCB mixture (~$1x10^{10}$ kg m^{-1} s^{-1} N^{-1}), it can be seen that this ratio is approximately an order of magnitude greater for the bimesogenic mixtures. This would account for the significant difference in response times between the monomesogenic and the bimesogenic mixtures.

The maximum available electric field (~20 V/μm) was not large enough to fully unwind the helix of any of the bimesogenic mixtures. This is significantly higher than the field required to fully unwind the chiral doped 7OCB mixture of a similar pitch (< 8 V/μm). From Equation 2.17, this observation implies that the ratio of the twist elastic constant and the dielectric anisotropy is greater for the bimesogenic materials. Measurements of the dielectric properties of a different chiral bimesogenic mixture made from the FfO-7-OfF and FfO-11-OfF homologues have been made.[7] A value of ~1 for the dielectric anisotropy of this mixture was reported.

The behaviour of the flexo-elastic ratio as a function of temperature does not appear to be explained fully by the simple theory that was developed to describe flexoelectro-optic switching. It is hypothesised that the behaviour of K as a function of temperature deviates from the predicted response, however, unexpected behaviour in $\bar{e}$ cannot be dismissed. To take this work forward, it would be useful to measure the elastic constants for these bimesogenic mixtures, in order to determine whether this hypothesis is correct.

The effects of varying the concentration of chiral dopant in the mixtures were studied. By using more or less chiral dopant, the induced helical pitch is shorter or longer, respectively. From flexoelectro-optic theory, it is expected that if the pitch of a material is lengthened, then the tilt angles (per unit field) and response times would increase. It was assumed that the only significant change in physical properties caused by varying the concentration of the chiral dopant would be a change in the pitch length.

Three mixtures based on the 20%/80% FfO-7/9-OfF mixture were characterised. These mixtures contained 1.99%, 3.42% and 3.93% (w/w) of the chiral dopant BDH1281. From preliminary observations, it was seen that the selective reflection wavelengths of the three

mixtures increased as the concentration of chiral additive was decreased. This indicates that the pitch of the materials lengthened. It was also observed that the longer pitch material did not exhibit a blue phase between the chiral nematic phase and the isotropic phase.

The flexoelectro-optic switching properties of these mixtures were studied and compared. It was found that:

- the tilt angles per unit field were highest for the mixture with the least chiral dopant, and lowest for the mixture with the most. This agrees with theory,[9] which states that tilt angle per unit field is directly proportional to pitch;
- the applied field for which the effects of dielectric coupling start to become significant is higher for shorter pitch. This agrees with theory, if the assumption is made that the factors that determine this field are the same as those for calculating the total helix unwinding applied field;
- the response times are slowest for the mixture with the lowest concentration of dopant and fastest for the mixture with the highest dopant concentration. This too agrees with theory of flexoelectro-optic switching,[9] which states that the response time is proportional to the square of the pitch.

For the three mixtures, the ratios of the response times were found to be comparable to the square of ratios of the pitch lengths. Likewise, the ratios of the tilt angles were directly proportional to the ratio of the pitch lengths.

It was observed that the flexo-elastic ratio increased as the sample temperature was reduced and, as explained above, this deviation from the behaviour predicted by theory is believed to result from the way K and $\overline{e}$ individually depend on the order parameter.

The flexo-elastic ratio decreases as the concentration of the chiral additive is increased: this is an unexpected result. In Chapter 3, it was observed that for 7OCB there was no visible trend in the flexo-elastic ratio as the concentration of chiral dopant was varied. For 7OCB, either the amount of chiral dopant does not affect the flexo-elastic ratio, or the change in the ratio is so small it is masked by experimental uncertainty. Using 7OCB, it was observed that the order parameter changes with the addition of chiral dopant. A change in the order parameter of the bimesogenic mixtures, due to the addition of chiral

dopant, could cause a change in the flexo-elastic ratio. This would explain the observed decrease in the flexo-elastic ratio as the concentration of the chiral additive is increased.

For confirmation, the experiment was repeated for mixtures of the FfO-9-OfF and FfO-11-OfF homologues. The results showed the same trends observed above.

References

1 Rudquist, P., Buivydas, M., Komitov, L., and Lagerwall, S. T., J. Appl. Phys. **76(12)** 7778 (1994)

2 Coles, H. J., Coles, M. J., Perkins, S., Musgrave, B., and Coates D., Bimesogenic Compounds and Flexoelectric Devices, EU Patent EP99119114 (1999)

3 Private correspondence with Blatch, A. E.

4 Merck NB-C, Southampton, UK

5 Stegemeyer, H., Blümel, T., Hiltrop, K., Onusseit, H., and Porsch, F., Liq. Cryst. **1(1)** 3 (1986)

6 de Gennes, P. G., Solid-State Commun., **6** 163 (1968)

7 Schott, C., Perkins, S., and Coles, H. J., Mol. Cryst. Liq. Cryst. **366** 2567 (2001)

8 Musgrave, B., Coles M. J., Perkins, S., and Coles, H. J., Mol. Cryst. Liq. Cryst. **366** 2587 (2001)

9 Patel, J. S., and Meyer, R. B., Phys. Rev. Lett., **58(15)** 1538 (1987)

10 Clark, N. A., and Lagerwall, S. T., Appl. Phys. Lett. **36** 899 (1980)

11 Bancroft, M. S., Ph.D. Thesis, University of Manchester, UK (1989)

12 Morris, S. M., Thesis in preparation

13 Maheswara Murthy, P. R., Raghunathan, V. A., and Madhusudana, N. V., Liq. Cryst. **14(2)** 483 (1993)

14 Osipov, M. A., J. Physique Lett., **45** L-823 (1984)

15 Dozov, I., Martinot-Lagarde, Ph., Durand, G., J. Physique Lett. **44** L-817 (1983)

16 Karat, P. P., and Madhusudana, N. V., Mol. Cryst. Liq. Cryst. **40** 239 (1977)

17 Bradshaw, M. J., Raynes, E. P., Bunning, J. D., and Faber, T. E., J. Physique Lett., **46** 1513 (1985)

18 Dilisi, G. A., Terentjev, E. M., Griffin, A. C., and Rosenblatt, C., J. Phys. II **3(5)** 597 (1993)

Chapter Six

6 Flexoelectro-optic Switching of Achiral Non-symmetric Bimesogens

6.1 Introduction

It has been seen in Chapter 5 that the symmetric bimesogens when doped with a high twisting power chiral additive have strong flexoelectro-optic properties. However, a major problem with the materials used is that the pure homologues have either no mesophases or have mesophases that occur over a small temperature range. The solution to this problem was to use eutectic mixtures of two of the homologues; this produced broad temperature range nematic phases. It was decided that it would be of value to study a series of bimesogenic homologues that have inherent broad nematic phases. This would allow a greater insight into the effects of molecular shape on flexoelectric properties.

In previous work,[1] a bimesogen made up of two oxy-cyanobiphenyl groups was examined. This material, when doped with chiral additive was seen to have a lower flexo-elastic ratio than the mixtures studied in Chapter 5; however it had a nematic phase over 30°C wide (albeit with the transition from the nematic phase to the isotropic phase occurring at 201°C). Ideally, the flexoelectric properties of a new homologous series of bimesogens would be as good as those of the oxy-fluorobiphenyl bimesogens studied in Chapter 5 and the new materials would have a nematic phase temperature range comparable to that of the oxy-cyanobiphenyl bimesogen. For this reason, it was decided that a combination of the two materials might produce good results, i.e. maintaining the high flexoelectric properties of the oxy-fluorobiphenyl mixtures but having the nematic phase range of the oxy-cyanobiphenyl bimesogen.

Consequently, the bimesogens synthesised for in this work are based on the structure shown in Figure 6.1. The materials are denoted as FfO-n-OCB, where n represents the number of carbon atoms in the spacer. These novel materials were synthesised by Andrew Blatch.

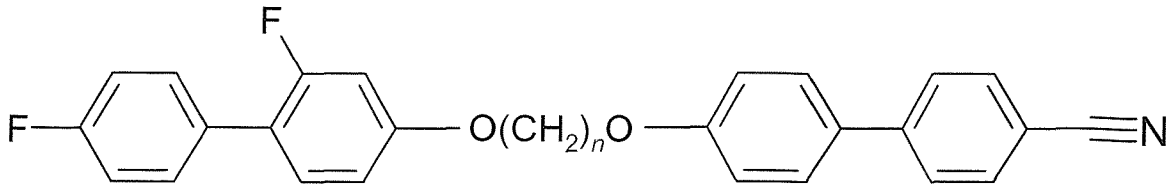

Figure 6.1 The generic structure of the bimesogens studied in this chapter. For simplicity, the series is denoted FfO-n-OCB, where n represents the number of carbon atoms in the spacer.

It would be expected that the dielectric anisotropy of these molecules would not be as low as the materials studied in Chapter 5, as the "individual" dipoles of the two groups will be of differing magnitudes. Any increase in the dielectric anisotropy of a material affects the materials flexoelectro-optic properties since the fields for total helix unwinding are reduced. The dipole moment for an oxy-cyanobiphenyl group is greater than that for an oxy-fluorobiphenyl group, thus it is hypothesised that the flexo-elastic ratio would be greater than for the symmetric oxy-fluorobiphenyl bimesogens.[2]

6.2 The pure homologues

A range of homologues of different spacer lengths was produced for this work. The materials were initially examined using optical microscopy. The materials were placed on a glass slide and then covered with a glass slip. Table 6.1 lists the observations that were made.

Material	On Cooling (5°/min)	On Heating
FfO - 5 - OCB	**I** -(111°C)-> **N** -(45°C)-> **Crystal**	**Crystal** -(100°C)-> **N** -(111°C)-> **I**
FfO - 6 - OCB	**I** -(166°C)-> **N** -(80°C)-> **Crystal**	**Crystal** -(137°C)-> **N** -(166°C)-> **I**
FfO - 7 - OCB	**I** -(116°C)-> **N** -(45°C)-> **Crystal**	**Crystal** -(97°C)-> **N** -(116°C)-> **I**
FfO - 8 - OCB	**I** -(147°C)-> **N** -(93°C)-> **Crystal**	**Crystal** -(123°C)-> **N** -(147°C)-> **I**
FfO - 9 - OCB	**I** -(114°C)-> **N** -(60°C)-> **Crystal**	**Crystal** -(75°C)-> **N** -(115°C)-> **I**
FfO - 10 - OCB	**I** -(134°C)-> **N** -(104°C)-> **Crystal**	**Crystal** -(112°C)-> **N** -(134°C)-> **I**
FfO - 11 - OCB	**I** -(113°C)-> **N** -(55°C) -> **SmX** -(54°C)-> **Crystal**	**Crystal** -(80°C)-> **N** -(113°C)-> **I**
FfO - 12 - OCB	**I** -(123°C)-> **N** -(90°C)-> **Crystal**	**Crystal** -(121°C)-> **N** -(123°C)-> **I**

Table 6.1 Initial microscopy observations of transition temperatures for pure homologues.

From these initial measurements it can be seen that all the materials have a nematic phase on both heating and cooling. The FfO-11-OCB was unique in that it was the only material for which a smectic phase was observed when super-cooled. With the exception of FfO-12-OCB all the materials had a nematic phase of greater than 10°C wide on heating, with the FfO-9-OCB material having the largest nematic phase at 40°C wide. The transition temperatures on heating show a distinct odd-even effect in terms of the number of carbon atoms in the spacer, this is shown graphically in Figure 6.2. The odd-even effect in terms of transition temperatures is a common occurrence in liquid crystals, and is purely a result of shape anisotropy,[3] and it is found to be more pronounced in bimesogenic homologous series than in monomeric series.[4]

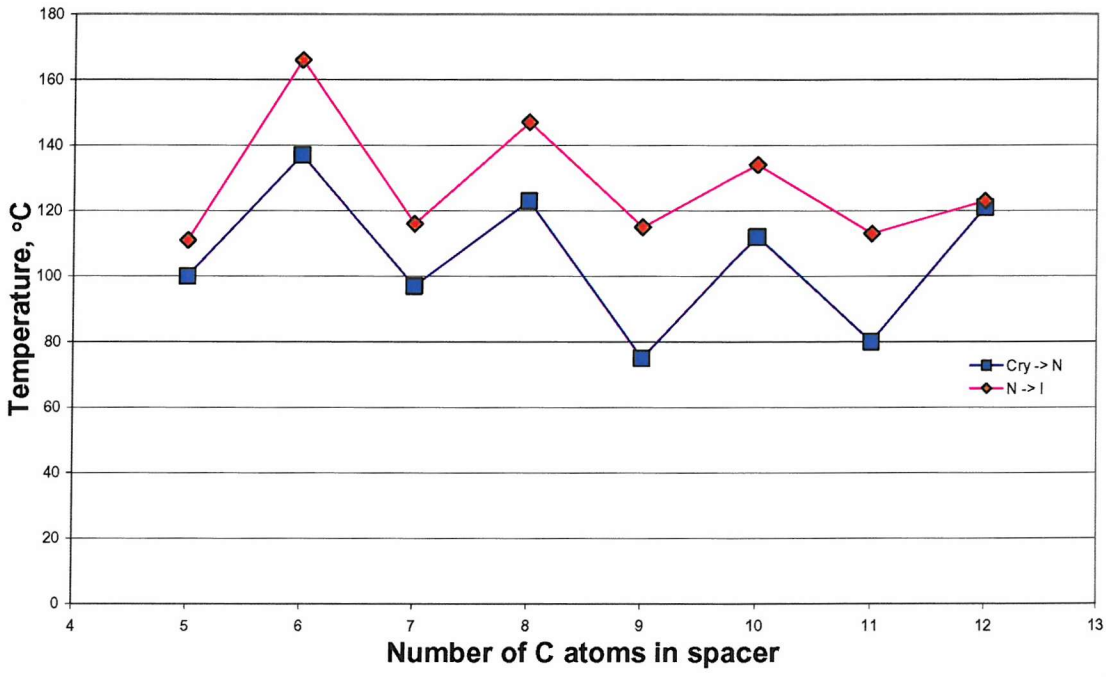

Figure 6.2 A comparison of the transition temperatures upon heating against the number of carbon atoms in the spacer.

For more accurate confirmation of these results, the materials were also examined using the differential scanning calorimeter. The results are tabulated below.

Material	Transition Temperatures on Heating
FfO - 5 - OCB	**Crystal** -(93°C)-> **N** -(106°C)-> **I**
FfO - 6 - OCB	**Crystal** -(143°C)-> **N** -(158°C)-> **I**
FfO - 7 - OCB	**Crystal** -(97°C)-> **N** -(114°C)-> **I**
FfO - 8 - OCB	**Crystal** -(121°C)-> **N** -(144°C)-> **I**
FfO - 9 - OCB	**Crystal** -(73°C)-> **N** -(112°C)-> **I**
FfO - 10 - OCB	**Crystal** -(110°C)-> **N** -(130°C)-> **I**
FfO - 11 - OCB	**Crystal** -(76°C)-> **N** -(113°C)-> **I**
FfO - 12 - OCB	**Crystal** -(116°C)-> **N** -(122°C)-> **I**

Table 6.2 The transition temperatures on heating measured using the differential scanning calorimeter (DSC).

The values for the transition temperatures measured using the differential scanning calorimeter confirm the odd-even effect observed using optical microscopy.

6.3 Inducing chirality to the mesophases

The new non-symmetric bimesogenic materials examined above are achiral, which means chirality has to be introduced in to the system. As with the oxy-fluorobiphenyl bimesogenic materials examined in Chapter 5, the materials were mixed with a chiral additive. By varying the amount of dopant the effects of varying the chirality of the mixture can to be studied.

Rather than use a chiral nematic as an additive the chiral additive known as BDH1281,[5] as introduced previously, was used. Only a small percentage (< 5%) of BDH1281 is required to make an achiral nematic sufficiently chiral to be used for flexoelectro-optic switching, this is advantageous because as such a small amount of dopant is used (other than inducing chirality) the effects on the host is small, i.e. the transition temperatures are almost unchanged.

6.4 The chiral properties of the doped homologues

As discussed in Section 6.3, it is possible to induce chirality into an achiral phase by adding a chiral dopant. In this section the flexoelectro-optic properties of the doped homologues will be examined.

6.4.1 Alignment for flexoelectro-optic switching

The most common method for aligning a chiral nematic for the purpose of measuring/observing flexoelectro-optic switching, i.e. adopting the uniformly lying helix geometry, is to shear the material in a glass cell under an applied field. With practise it is possible to achieve good uniform alignment by this method. This method works for all the doped bimesogenic mixtures discussed in this chapter, though less well for the materials with an even number of carbon atoms in the spacer. This method can be inconvenient because the material has to be physically sheared.

In this work a number of alternative methods for aligning the materials were used which do not require shearing, one of which was discovered during the course of this work.

The first of these alternative methods only worked on materials with sufficient chirality to exhibit blue phases, which had been previously reported for monomesogenic materials.[6] This method works by cooling the material in a glass cell (in this case a commercially made cell) from the isotropic phase into blue phase I (also denoted as BP I), which is the phase directly above the chiral nematic phase. Once the material is in blue phase I, by applying a sufficient electric field across the material it is forced into the chiral nematic phase. If it is done correctly the material will adopt the uniformly lying helix geometry required for flexoelectro-optic switching. The alignment can be very good, significantly better than that achievable by the shearing method and the helix lies parallel to the alignment layers of the cell. Figure 6.3 shows an example of the quality of alignment achievable by this method.

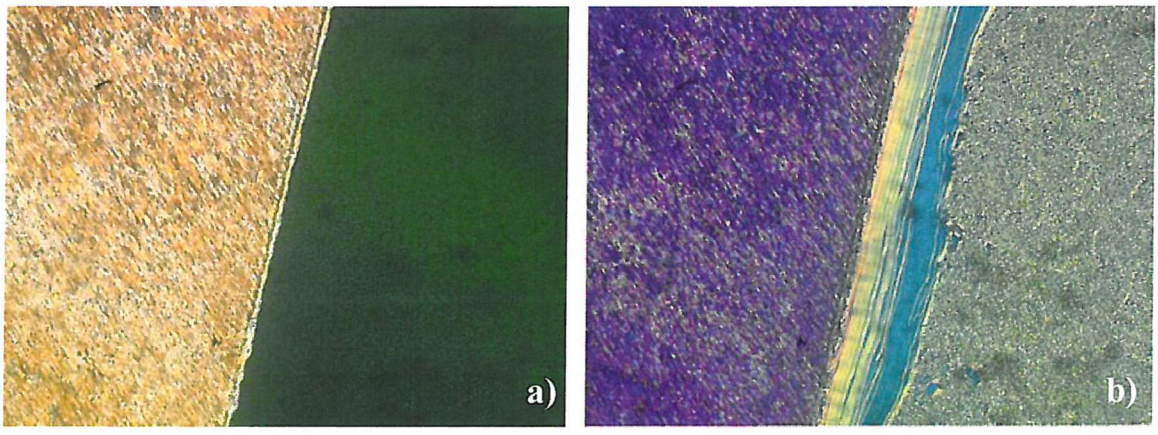

Figure 6.3 a) Uniformly lying helix geometry achieved by applying an electric field in BP I at 104°C and b) subsequently after cooling to 90°C. The electrode area is on the left-hand side of both photomicrographs.

Another method for achieving the correct geometry for flexoelectro-optic studies was discovered during this work,[7] which appears to work for the majority of materials used in this chapter (rather than just the materials that exhibit blue phases). This method is referred to as the "field ramping method." This technique works best at temperature a few degrees below the chiral nematic to isotropic phase transition. A sufficient electric field is applied across the cell to force the material to adopt a homeotropic alignment and then the field is reduced incrementally until the lying helix alignment is achieved. This method produces the best alignment of the methods discussed and is the quickest and easiest to implement. The typical alignment quality achievable is shown in Figure 6.4.

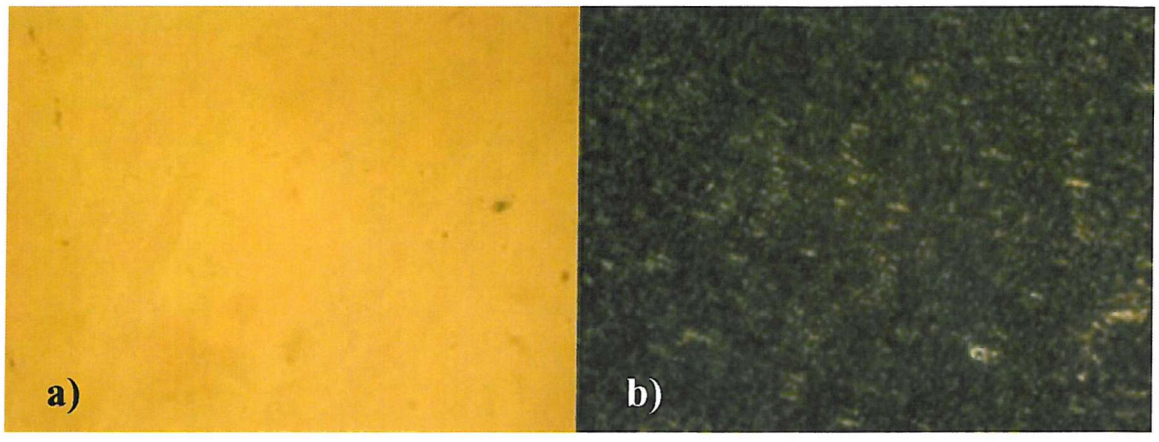

Figure 6.4 The uniformly lying helix alignment achieved by the "field ramping method" for 3.40% BDH1281in FfO-7-OCB when a) the helix is aligned at 45° to the polarisers with no field applied and b) the helix is aligned parallel to one of the polarisers.

The hybrid cell technique discussed in Chapter 5 also works for the materials studied in this chapter. However the "field ramping method" is preferred as it requires only standard planar cells rather than the less common hybrid cells and is quicker to implement as it does not require slow cooling from the isotropic phase.

6.4.2 A comparison of the flexoelectro-optic properties of the extreme homologues

The whole series of homologues were doped with a similar amount of the chiral additive BDH1281 (~3.50% w/w). The first two mixtures studied were the homologues at the extremities of the series, i.e. FfO-5-OCB and FfO-12-OCB.

3.50% BDH1281 in FfO-5-OCB

The first mixture studied was FfO-5-OCB doped with 3.50% BDH1281. Initial visual observations of the mixture in a commercial cell were made; the mixture was seen to exhibit a transition from the chiral nematic phase to the isotropic phase at 110°C. On cooling the mixture was seen to exhibit blue phases I and II and the foggy phase between the isotropic phase and the chiral nematic phase. It was possible to super-cool the chiral nematic phase down to less than 50°C (at a rate of 5°C per minute) before crystallisation occurred.

The flexoelectro-optic switching properties of the mixture were studied. The uniformly lying helix geometry was obtained using the field ramping method, discussed in Section 6.4.1. The tilt angles and response times measured are shown in Figure 6.5, along with the pitch and selective reflection wavelengths.

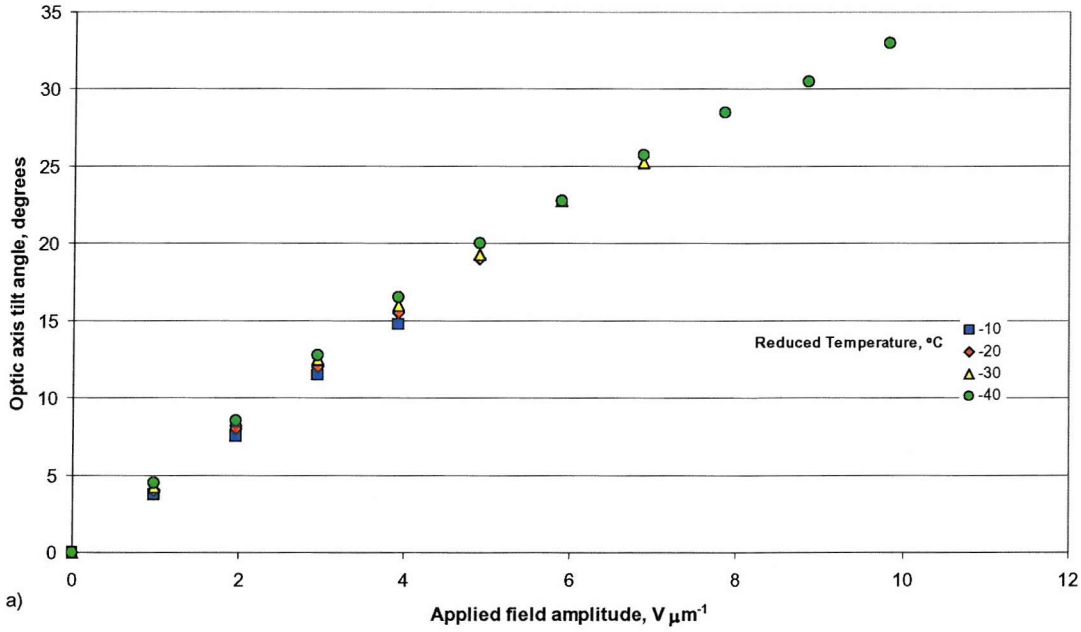

a)

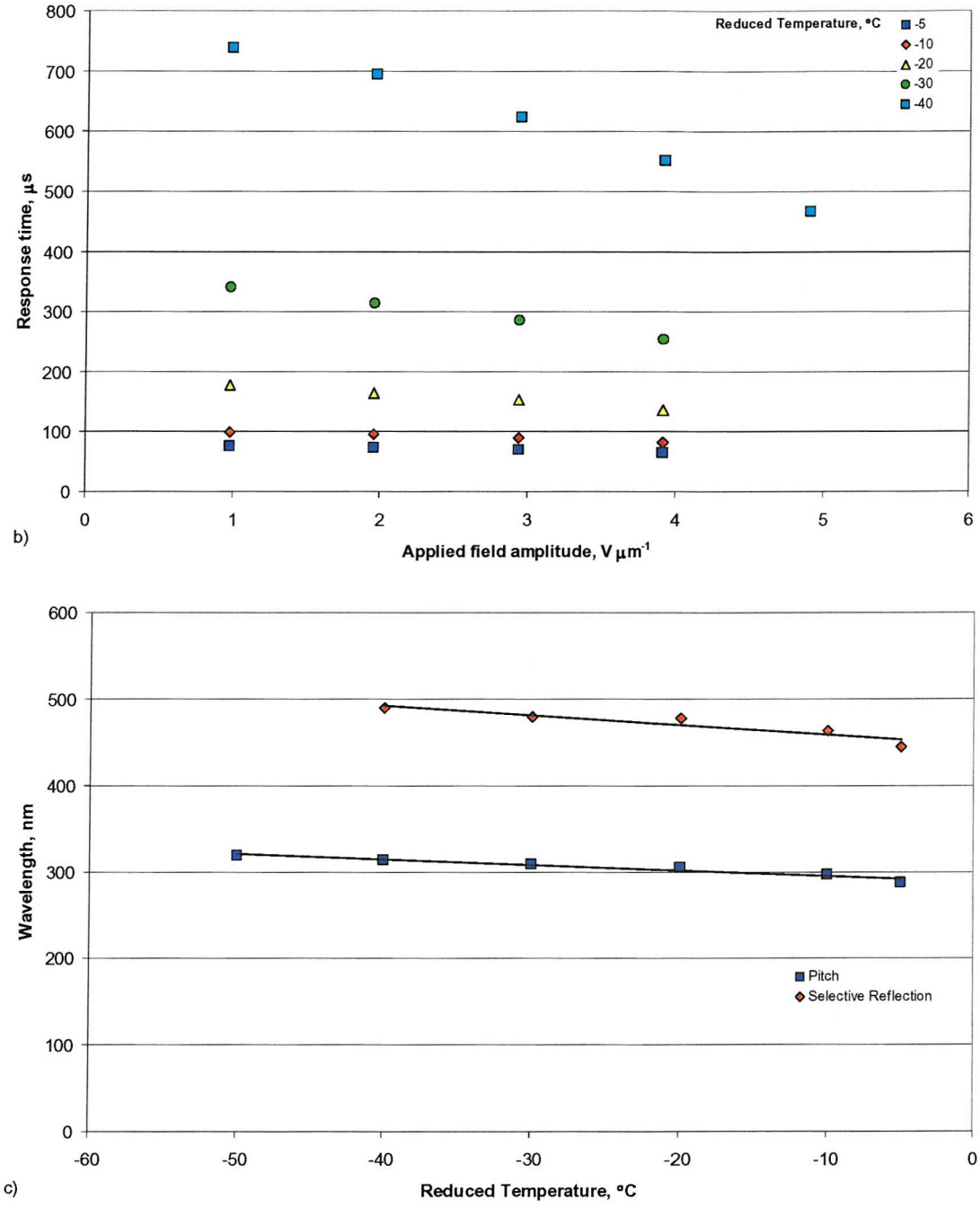

Figure 6.5 The relevant properties of a mixture of 3.50% BDH1281 in FfO-5-OCB (w/w). The graphs show a) the induced tilt angles, b) the response times and c) the selective reflection wavelength and pitch. All measurements were across a range of reduced temperatures. The response times are measured for 10-90% of the full switch of the optic axis, i.e. twice the tilt. The selective reflection properties were measured using a UV-visible spectrometer and the pitch was measured using a wedge cell of angle 0.031°. Trend-lines were added to guide the eye.

Firstly, it can be seen that the gradient of tilt angle against field is quite high and at lower temperatures very high tilt angles are achievable. The tilt angles were measured as a function of increasing applied field until the uniformly lying helix texture was seen to be disrupted by dielectric coupling dominating over flexoelectric coupling. The applied field at which this disruption occurs can be seen to increase as the temperature is decreased.

The response times are fast, especially near the clearing temperature; this is to be expected as the clearing temperature is quite high (111°C) and thus the viscosity is very low.

From the data in Figure 6.5 it is possible to calculate using Equation 3.9 the flexoelectro-optic ratio, $\bar{e}/K$, and using Equation 2.5 the average refractive can also be calculated, the results for both are shown in Table 6.3.

Reduced Temperature, °C (T_c = 111°C)	$\Delta\tan\phi/\Delta E$, μm V^{-1}	Pitch, nm	Selective reflection wavelength, nm	$\bar{n}$	$\bar{e}/K$, C N^{-1} m^{-1}
-5	0.0635	288	445	1.54	1.39
-10	0.0678	297	464	1.56	1.43
-20	0.0704	305	478	1.57	1.45
-30	0.0716	309	480	1.55	1.46
-40	0.0744	314	490	1.56	1.49

Table 6.3 A comparison of the values at different reduced temperatures for the pitch, selective reflection and the calculated values for the average refractive index and the ratio of the effective flexoelectric coefficient and the average of the splay and bend elastic constants. The mixture studied was 3.50% BDH1281 in FfO-5-OCB.

The value calculated for the ratio $\bar{e}/K$ was found to be large, significantly larger than for the materials studied in Chapter 5, in agreement with the hypothesis previously stated in Section 6.1. The flexo-elastic ratio appears to increase as the temperature is reduced, as was seen in Chapter 5.

The average refractive index was found to be approximately 1.56, which is again a reasonable value for a liquid crystal material.

3.48% BDH1281 in FfO-12-OCB

The second mixture studied was from the opposite end of the homologous series from FfO-5-OCB, namely FfO-12-OCB, which for the purpose of this work was doped with 3.48% BDH1281 (w/w). Initial visual observations of the mixture in a commercial cell were made; the mixture was seen to exhibit a transition from the chiral nematic phase to the isotropic phase at 124°C. On cooling, the mixture was seen to exhibit no blue phases between the isotropic phase and the chiral nematic phase. It was possible to super-cool the chiral nematic phase down to less than 105°C (at a rate of 5°C per minute) before crystallisation occurred. It was interesting to note that the Grandjean texture appeared red/grey rather than the deep blue of the FfO-5-OCB mixture, this indicates (along with the absence of any blue phases) that despite containing approximately the same amount of chiral dopant that the FfO-12-OCB mixture has a significantly lower pitch.

The flexoelectro-optic switching properties of the mixture were studied. To obtain the required uniformly lying helix geometry, the field ramping method, discussed in Section 6.4.1 was used. Reasonable alignment was achieved though not as good as achieved for the FfO-5-OCB mixture. The tilt angles and response times measured are shown in Figure 6.6, along with the pitch and selective reflection wavelengths.

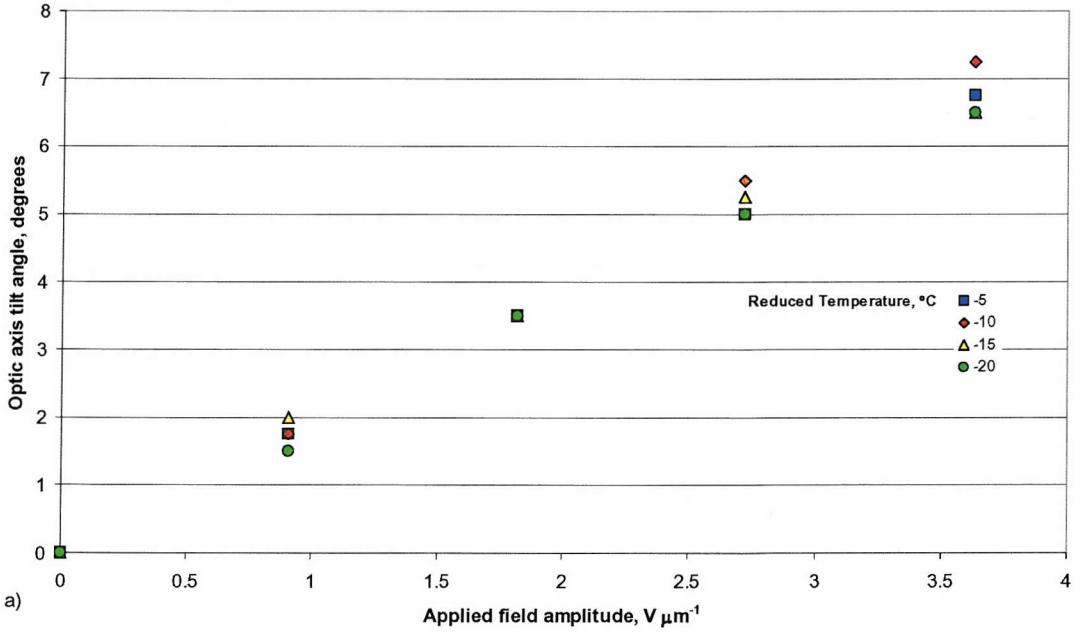

a)

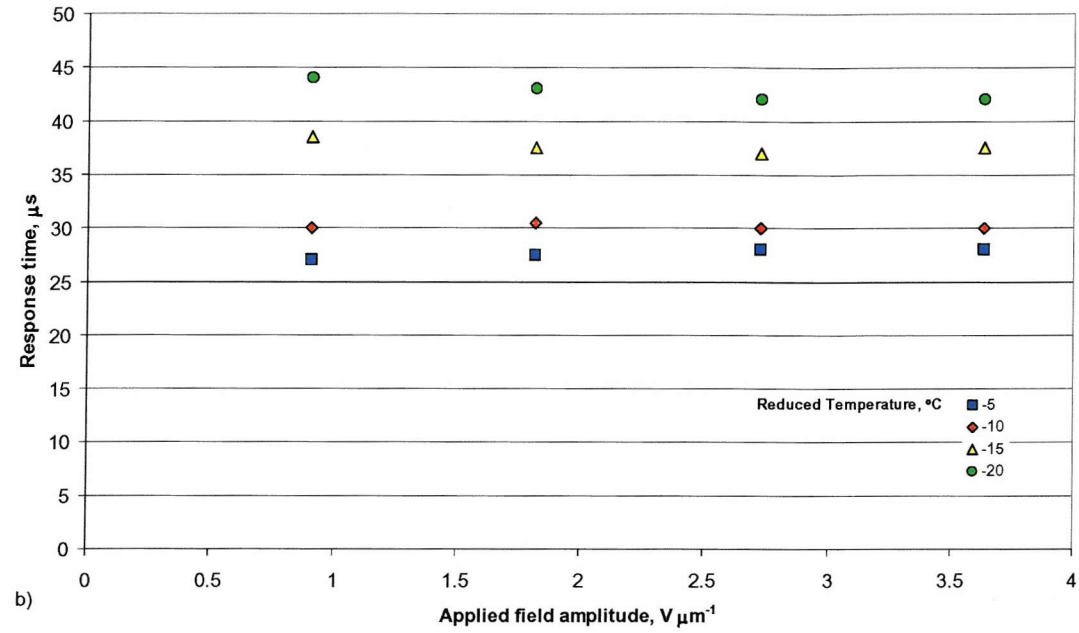

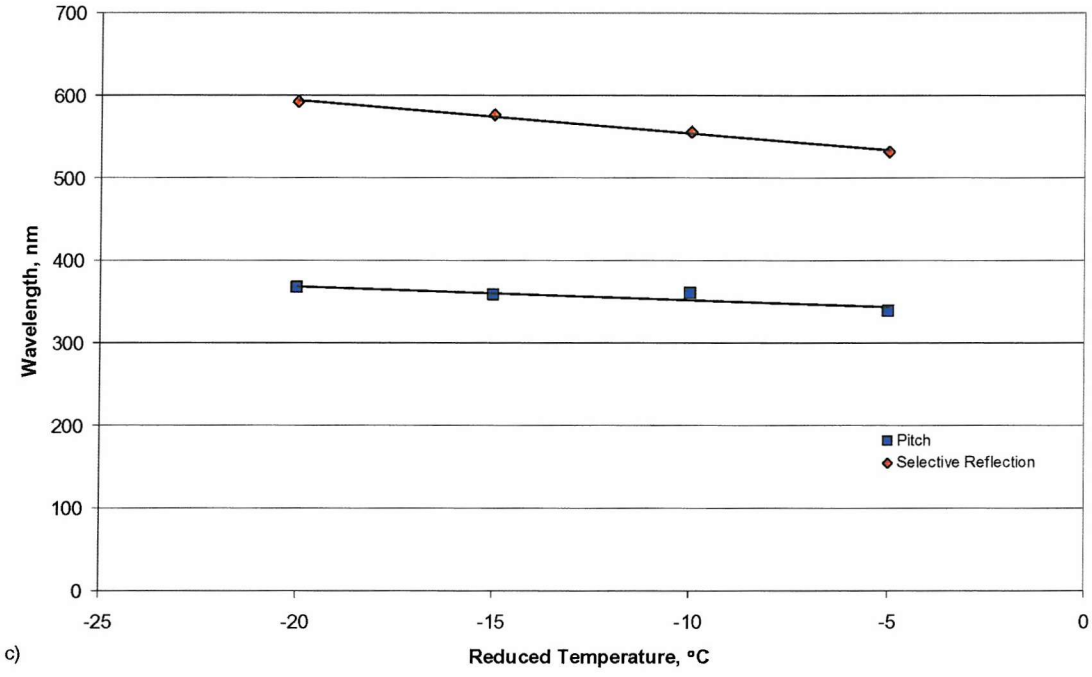

Figure 6.6 The relevant properties of a mixture of 3.48% BDH1281 in FfO-12-OCB (w/w). The graphs show a) the induced tilt angles, b) the response times and c) the selective reflection wavelength and pitch. All measurements were taken across a range of reduced temperatures. The response times are measured for 10-90% of the full switch of the optic axis, i.e. twice the tilt. The selective reflection properties were measured using a UV-visible spectrometer and the pitch was measured using a wedge cell of angle 0.035°. Trend-lines were added to guide the eye.

The gradient of tilt angle against applied field is smaller than that of the FfO-5-OCB mixture, combined with the fact that the chiral nematic phase range is relatively small means that the maximum achievable tilt angles are much smaller.

The response times of the mixture are very fast, faster than those of the FfO-5-OCB mixture. This is probably a result of lower viscosity and/or larger elastic constants.

As was suspected from the lack of any blue phases and the colour of the Grandjean texture viewed between crossed polarisers, the pitch was found to be significantly longer (~19%) than for the FfO-5-OCB mixture, this implies that K_{22} is higher for this mixture as it is more difficult to induce twist. The data in Figure 6.6 was used to calculate the ratio $\bar{e}/K$ and the average refractive index and the results are shown in Table 6.4.

Reduced Temperature, °C (T_c = 124°C)	$\Delta\tan\phi/\Delta E$, μm V^{-1}	Pitch, nm	Selective reflection wavelength, nm	$\bar{n}$	$\bar{e}/K$, C N^{-1} m^{-1}
-5	0.0324	339	532	1.57	0.60
-10	0.0353	360	555	1.54	0.64
-15	0.0314	358	576	1.61	0.55
-20	0.0319	367	592	1.61	0.55

Table 6.4 A comparison of the values at different reduced temperatures for the pitch, selective reflection and the calculated values for the average refractive index and the ratio of the effective flexoelectric coefficient and the average of the splay and bend elastic constants. The mixture studied was 3.48% BDH1281 in FfO-12-OCB.

The values calculated for the ratio $\bar{e}/K$ were found to be lower by approximately a factor of two than those calculated for the FfO-5-OCB mixture.

The average refractive index was found to be approximately 1.58, which is a reasonable value for a liquid crystal material and is similar to that of the FfO-5-OCB mixture.

It was difficult to obtain the appropriate Grandjean alignment to measure the pitch for these two mixtures, in particular for the FfO-12-OCB mixture. As a result it was decided to estimate the pitch of the subsequent mixtures from the selective reflection using Equation 2.5 and a value of 1.57 for the average refractive index.

6.4.3 A comparison of the flexoelectro-optic properties of three neighbouring homologues

It was considered useful to compare the flexoelectro-optic properties of three neighbouring homologues, namely FfO-9-OCB, FfO-10-OCB and FfO-11-OCB. All three homologues were doped with the chiral additive BDH1281 to allow the flexoelectro-optic switching properties to be studied.

3.75% BDH1281 in FfO-9-OCB

The first mixture studied was FfO-9-OCB doped with 3.75% BDH1281 (w/w). Initial visual observations of the mixture in a commercial cell were made; the mixture was seen to exhibit a transition from the chiral nematic phase to the isotropic phase at 114°C. On cooling the mixture was seen to exhibit blue phases between the isotropic phase and the chiral nematic phase. It was possible to super-cool the mixture down to less than 60°C (at a rate of 5°C per minute) before crystallisation occurred. There appeared to be a smectic phase below the chiral nematic phase; however crystallisation occurred too quickly for this phase to be examined in any detail.

The flexoelectro-optic switching properties of the mixture were studied. The uniformly lying helix geometry was obtained using the field ramping method, discussed in Section 6.4.1. The tilt angles and response times measured are shown in Figure 6.7, along with the selective reflection wavelengths and the values calculated for the pitch.

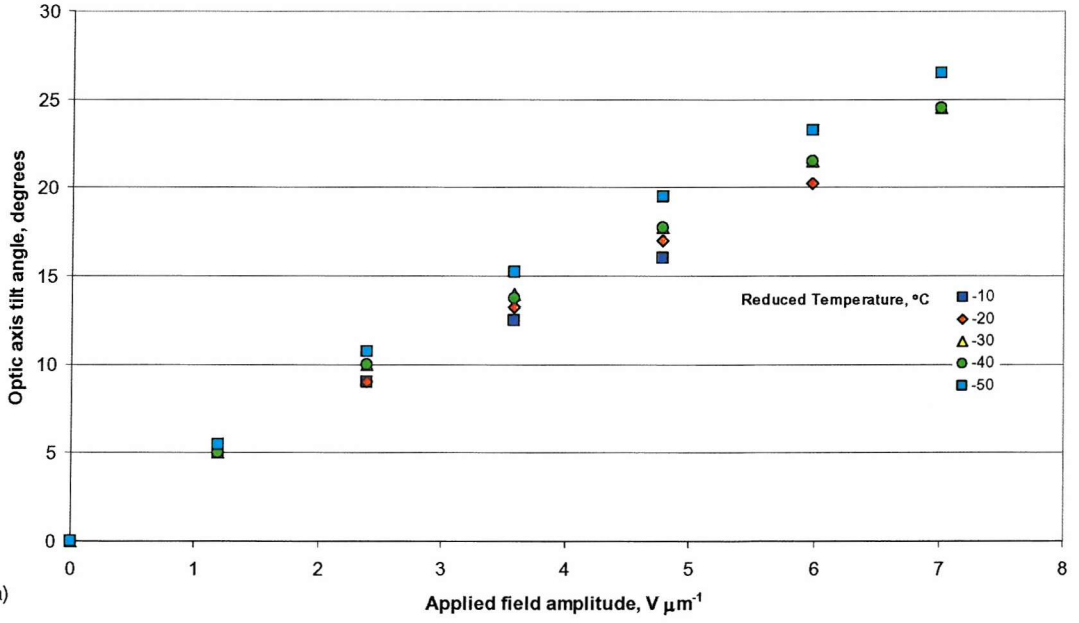

a)

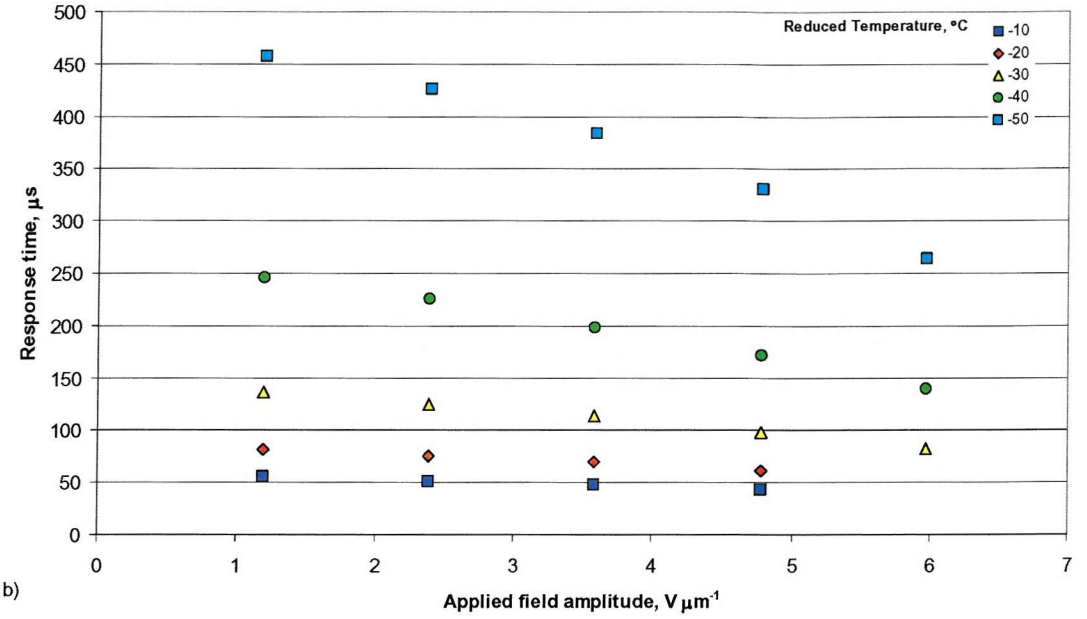

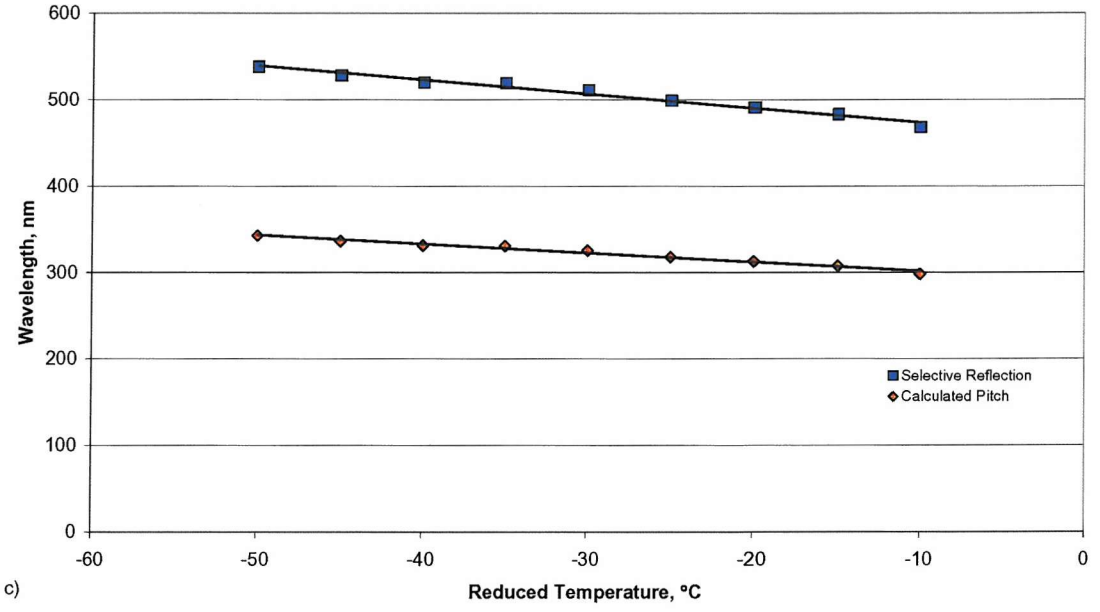

Figure 6.7 The relevant properties of a mixture of 3.75% BDH1281 in FfO-9-OCB (w/w). The graphs show a) the induced tilt angles, b) the response times, and c) the selective reflection wavelength and calculated pitch. All measurements were taken across a range of reduced temperatures. The response times are measured for 10-90% of the full switch of the optic axis, i.e. twice the tilt. The selective reflection properties were measured using a UV-visible spectrometer and the pitch was calculated from this using a value of 1.57 for the average refractive index. Trend-lines were added to guide the eye.

The results show that the gradient of tilt angle against applied field is high and large tilt angles are achievable. The response times are fast, ranging from ~50 to ~500 microseconds, which is comparable to those achievable for ferroelectric devices.

The results in Figure 6.7 are used to calculate the ratio $\bar{e}/K$, the results of which are shown in Table 6.5.

Reduced Temperature, °C (T_c = 114°C)	$\Delta\tan\phi/\Delta E$, μm V^{-1}	Selective reflection wavelength, nm	Pitch (calculated), nm	$\bar{e}/K$, C N^{-1} m^{-1}
-10	0.0569	468	298	1.20
-20	0.0617	491	313	1.24
-30	0.0656	511	326	1.26
-40	0.0668	520	331	1.27
-50	0.0696	538	343	1.28

Table 6.5 A comparison of the values at different reduced temperatures for the selective reflection and the calculated values for the pitch and the ratio of the effective flexoelectric coefficient and the average of the splay and bend elastic constants. The mixture studied was 3.75% BDH1281 in FfO-9-OCB.

It can be seen from Table 6.5 that the ratios of $\bar{e}/K$ are high and there may be some evidence of an increase in the ratio as the temperature is reduced.

3.48% BDH1281 in FfO-10-OCB

The second mixture studied was FfO-10-OCB which for the purpose of this work was doped with 3.48% BDH1281, where all percentages were measured by weight. Initial visual observations of the mixture in a commercial cell were made; the mixture was seen to exhibit a transition from the chiral nematic phase to the isotropic phase at 134°C. On cooling the mixture was seen to exhibit no blue phases between the isotropic phase and the chiral nematic phase. It was possible to super-cool the chiral nematic phase down to less than 110°C (at a rate of 5°C per minute) before crystallisation occurred. It was noted that the Grandjean texture appeared red/grey, similar to what was observed for the FfO-12-OCB mixture studied in the previous section, indicating a longer pitch.

The flexoelectro-optic switching properties of the mixture were studied. The uniformly lying helix geometry was obtained using the field ramping method. Reasonable alignment was achieved though it was not as good as that achieved for the FfO-9-OCB

mixture. The tilt angles and response times measured are shown in Figure 6.8, along with the pitch and selective reflection wavelengths.

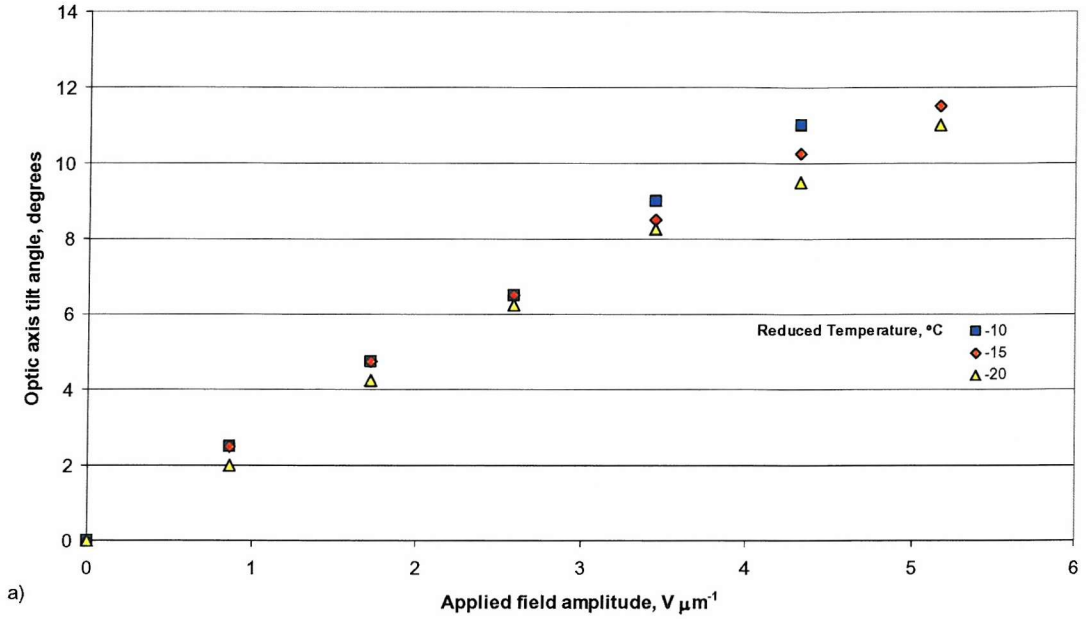

a)

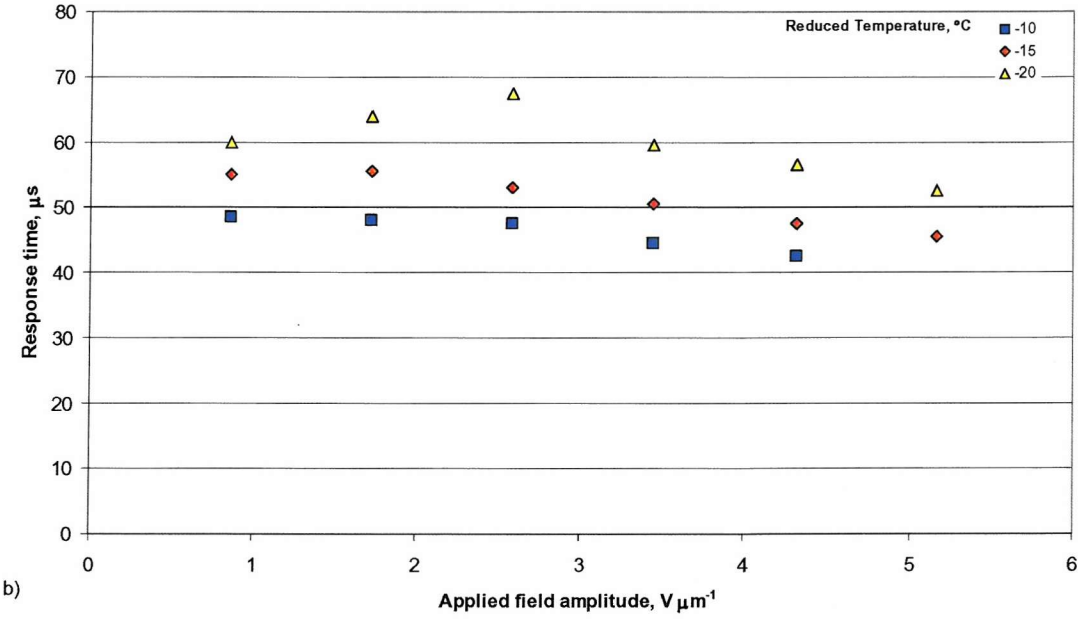

b)

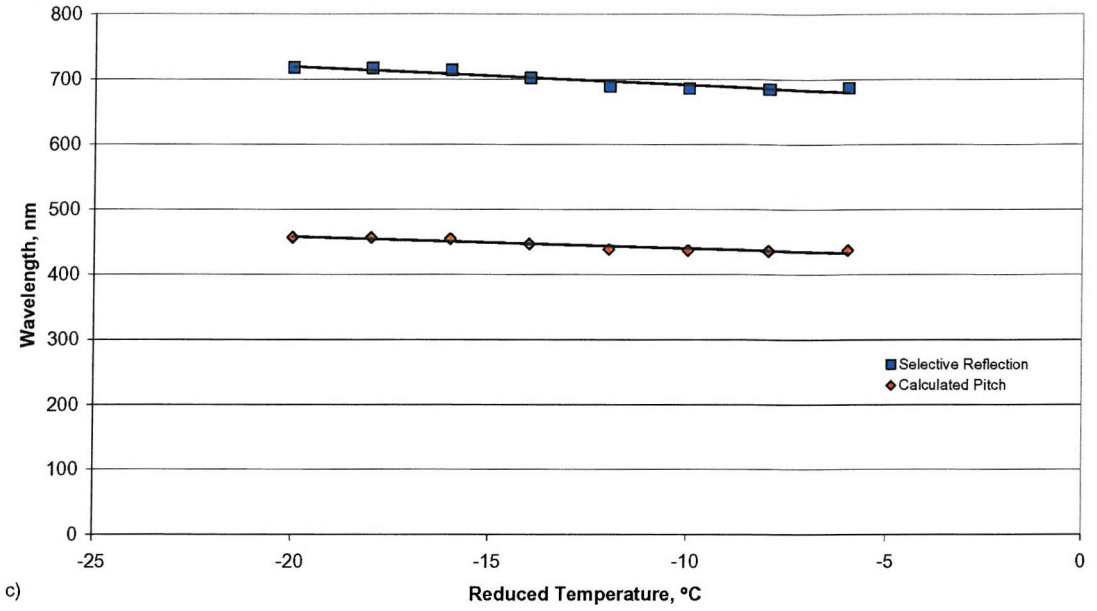

Figure 6.8 The relevant properties of a mixture of 3.48% BDH1281 in FfO-10-OCB (w/w). The graphs show a) the induced tilt angles, b) the response times and c) selective reflection wavelength and calculated pitch, all measured across a range of reduced temperatures. The response times are measured for 10-90% of the full switch of the optic axis, i.e. twice the tilt. The selective reflection properties were measured using a UV-visible spectrometer and the pitch was calculated from this using a value of 1.57 for the average refractive index. Trend-lines were added to guide the eye.

From Figure 6.8 it can be seen that the maximum tilt angles are in the region of ~12°, which are significantly smaller than for the FfO-9-OCB mixture. The gradients of tilt angle against applied field are also smaller than those of the FfO-9-OCB mixture. The response times shown in Figure 6.8 are very fast; this may be a result of the high clearing temperature, and hence low viscosity, and larger elastic constants.

The data in Figure 6.8 are used to calculate the flexo-elastic ratio $\bar{e}/K$ and the results are shown in Table 6.6.

Reduced Temperature, °C (T_c = 134°C)	$\Delta\tan\phi/\Delta E$, μm V^{-1}	Selective reflection wavelength, nm	Pitch (calculated), nm	$\bar{e}/K$, C N^{-1} m^{-1}
-10	0.0447	686	437	0.64
-15	0.0395	708	451	0.55
-20	0.0381	718	457	0.52

Table 6.6 A comparison of the values at different reduced temperatures for the selective reflection and the calculated values for the pitch and the ratio of the effective flexoelectric coefficient and the average of the splay and bend elastic constants. The mixture studied was 3.48% BDH1281 in FfO-10-OCB.

From Table 6.6 it can be seen that the ratio $\bar{e}/K$ is much lower for this mixture compared to that calculated for the FfO-9-OCB mixture.

3.48% BDH1281 in FfO-11-OCB

The next mixture studied was FfO-11-OCB doped with 3.48% BDH1281, where all percentages were measured by weight. Initial visual observations of the mixture in a commercial cell were made; the mixture was seen to exhibit a transition from the chiral nematic phase to the isotropic phase at 113°C. On cooling the mixture was seen to exhibit blue phases between the isotropic phase and the chiral nematic phase. It was possible to super-cool the mixture down to less than 55°C (at a rate of 5°C per minute) before crystallisation occurred. There is a smectic phase below the chiral nematic phase at 54°C; however crystallisation occurs too quickly for this phase to be examined in any great detail.

The flexoelectro-optic switching properties of the mixture were studied. The uniformly lying helix geometry was obtained using the field ramping method. The tilt angles and response times measured are shown in Figure 6.9, along with the selective reflection wavelengths and the values calculated for the pitch.

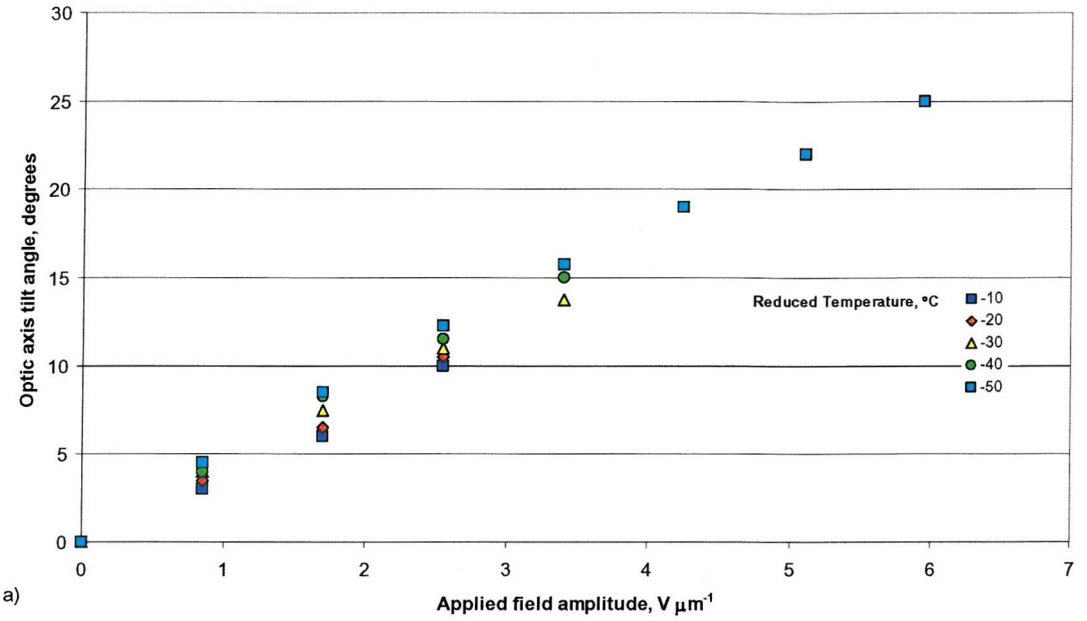
Optic axis tilt angle, degrees
Applied field amplitude, V µm-1
Reduced Temperature, °C
-10
-20
-30
-40
-50

a)

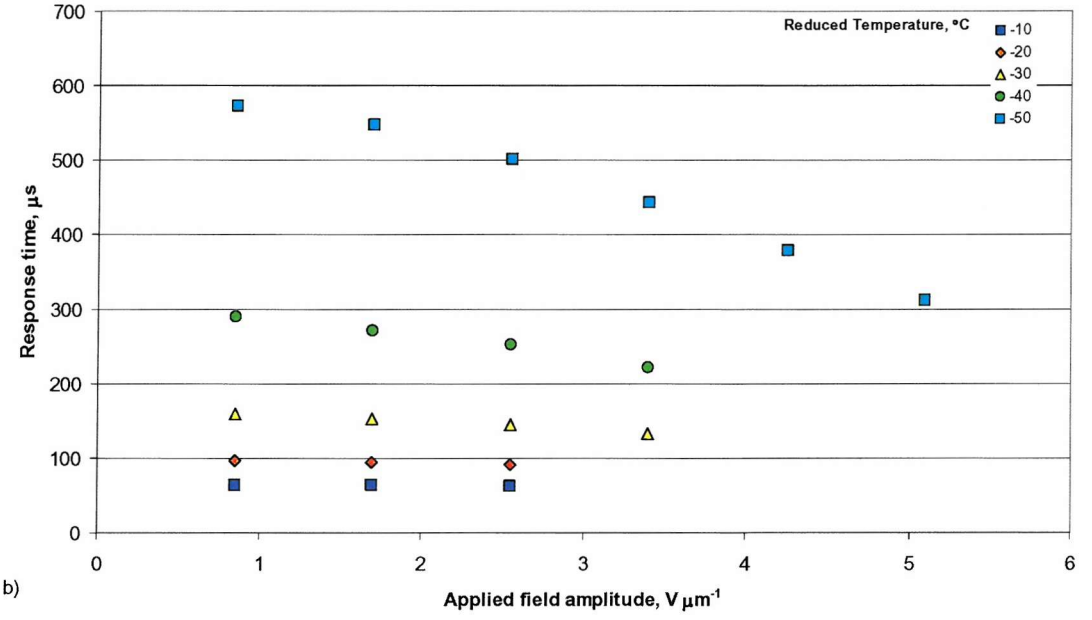
Response time, µs
Applied field amplitude, V µm-1
Reduced Temperature, °C
-10
-20
-30
-40
-50

b)

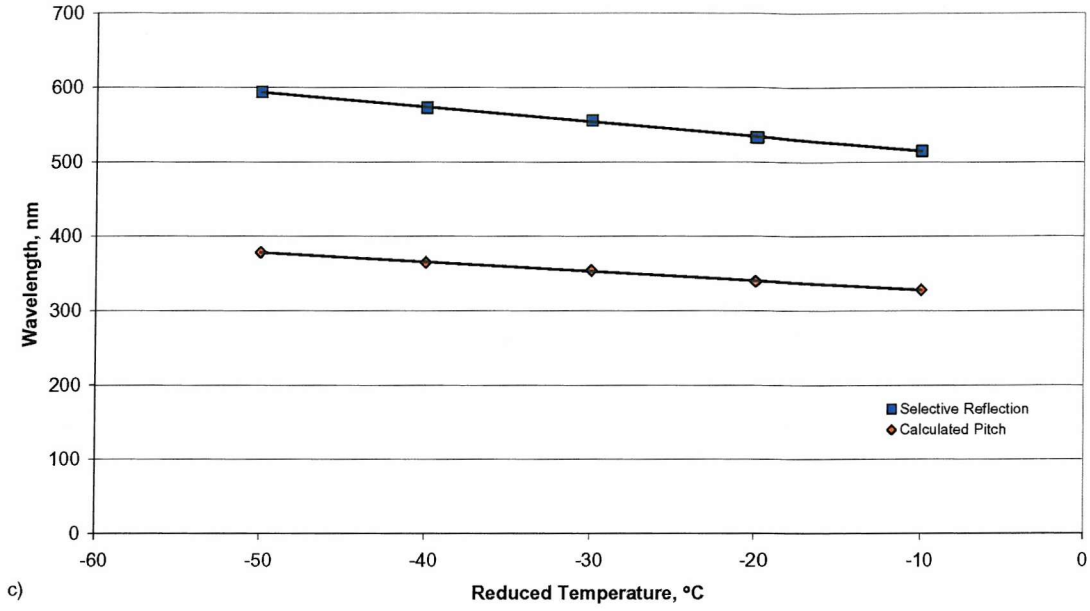

Figure 6.9 The relevant properties of a mixture of 3.48% BDH1281 in FfO-11-OCB (w/w). The graphs show a) the induced tilt angles, b) the response times and c) selective reflection wavelength and calculated pitch, all measured across a range of reduced temperatures. The response times are measured for 10-90% of the full switch of the optic axis, i.e. twice the tilt. The selective reflection properties were measured using a UV-visible spectrometer and the pitch was calculated from this using a value of 1.57 for the average refractive index. Trend-lines were added to guide the eye.

From Figure 6.9 it can be that tilt angles in the region of 25° are achievable with reasonably small applied fields. The response times range from less than 100 microseconds up to 600 microseconds across the temperature range studied.

The data in Figure 6.9 is used to calculate the flexo-elastic ratio $\bar{e}/K$ and the results are shown in Table 6.7.

Reduced Temperature, °C (T_c = 114°C)	$\Delta\tan\phi/\Delta E$, μm V^{-1}	Selective reflection wavelength, nm	Pitch (calculated), nm	$\bar{e}/K$, C N^{-1} m^{-1}
-10	0.0685	515	328	1.31
-20	0.0717	533	340	1.33
-30	0.0760	556	354	1.35
-40	0.0789	573	365	1.36
-50	0.0828	594	378	1.38

Table 6.7 A comparison of the values at different reduced temperatures for the selective reflection and the calculated values for the pitch and the ratio of the effective flexoelectric coefficient and the average of the splay and bend elastic constants. The mixture studied was 3.48% BDH1281 in FfO-11-OCB.

Comparing the properties of the three mixtures studied in this section and the properties of the two homologues studied in Section 6.4.2, it can be seen that the flexo-elastic ratio is much higher (approximately doubled) for the materials with an odd number of carbon atoms in the spacer when compared with those with an even number. The pitches are also shorter for the "odd" mixtures despite roughly the same amount of chiral additive being used for the "even" mixtures. These results are discussed further, below.

The properties of the remaining homologues in the series are summarised in the next section.

6.4.4 A summary of the remaining homologues

In this section the flexoelectric behaviour of the remaining homologues is studied. The remaining homologues are FfO-6-OCB, FfO-7-OCB and FfO-8-OCB; the homologues were doped with 3.41%, 3.40% and 3.22% of the chiral additive BDH1281 respectively. From the results for the mixtures studied in the previous two sections it would be expected that the seven carbon atom spacer material would have a greater flexo-elastic ratio than the other two. The tilt angles, response times and pitches of all three mixtures are summarised in Figure 6.10.

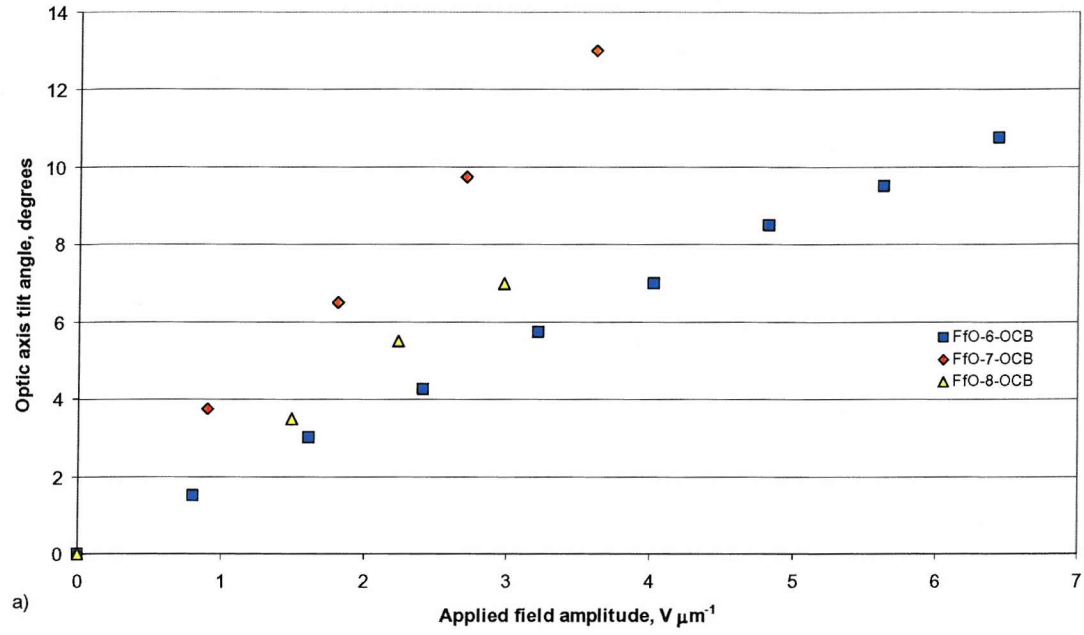
Optic axis tilt angle, degrees
Applied field amplitude, V μm-1
FfO-6-OCB
FfO-7-OCB
FfO-8-OCB

a)

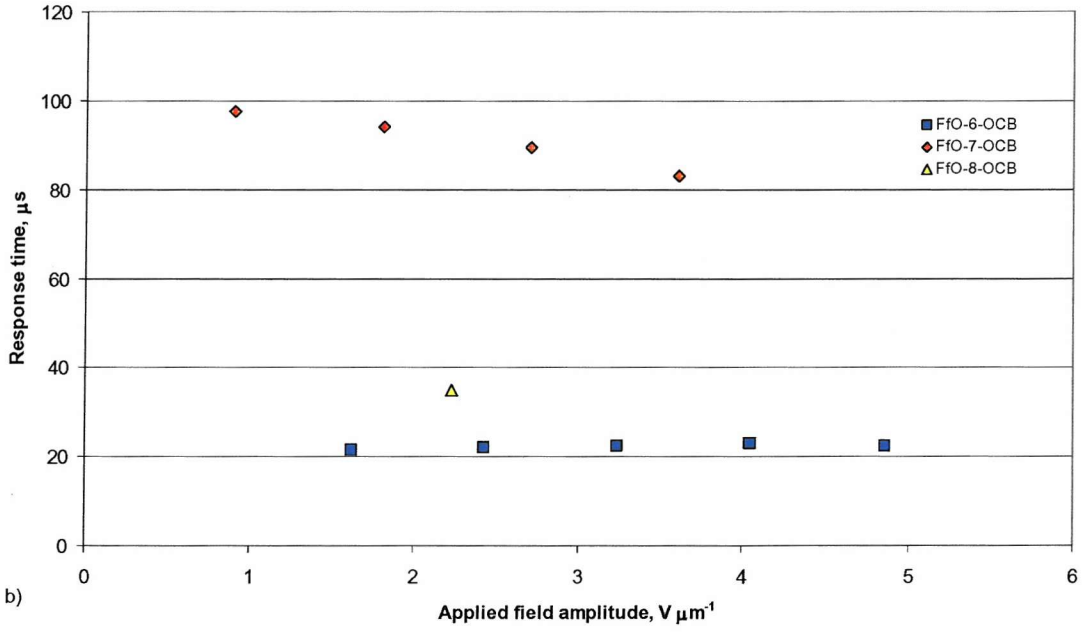
Response time, μs
Applied field amplitude, V μm-1
FfO-6-OCB
FfO-7-OCB
FfO-8-OCB

b)

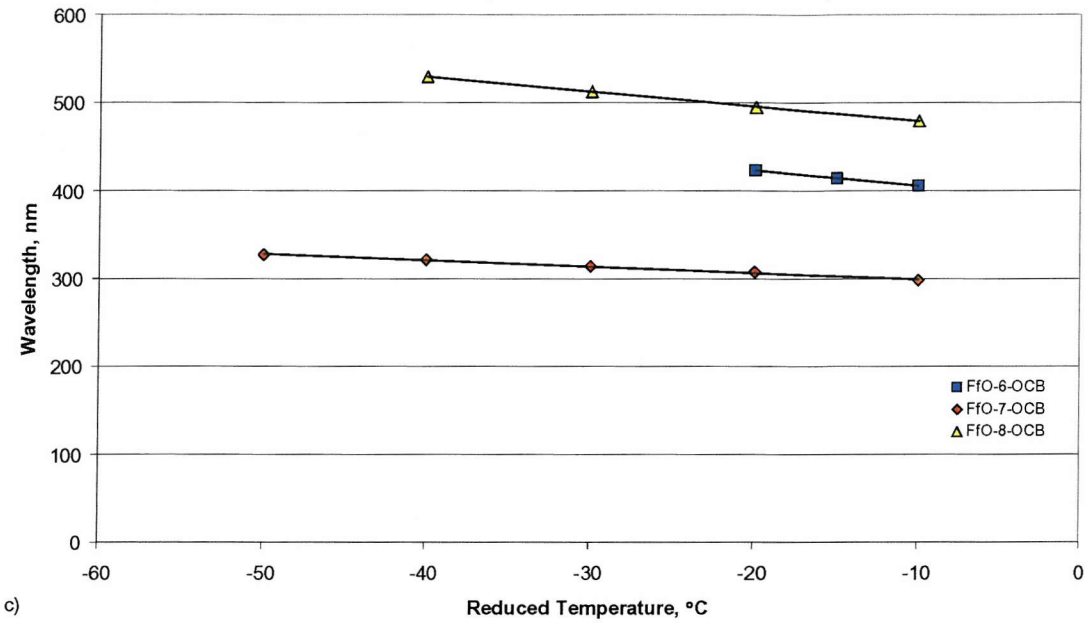

Figure 6.10 A summary of a) the tilt angles, b) the response times and c) the pitches of the three different homologues. The tilt angles and response times were measured at a reduced temperature of -20°. The response times are measured for 10-90% of the full switch of the optic axis, i.e. twice the tilt. The pitch was calculated from the selective reflection wavelength using a value of 1.57 for the average refractive index. Trend-lines were added to guide the eye.

From Figure 6.10 it can be seen that, in comparison with the FfO-6-OCB and FfO-8-OCB mixtures, the tilt angles are largest for the FfO-7-OCB mixture and its response times are slower (though less than 100μs). These observations are in agreement with previous results. The mixture containing the material with the odd number of carbon atoms in the spacer also had a smaller pitch than the mixtures containing materials with an even number of carbon atoms in the spacer, as was seen for the homologues studied previously. The maximum measured tilt angle for the FfO-7-OCB mixture exceeded 40° when super-cooled to its lowest temperature, compared to less than 15° and 10° for FfO-6-OCB and FfO-8-OCB respectively

There is quite a marked difference between the pitches of the FfO-6-OCB and FfO-8-OCB mixtures, this can be attributed in part to the fact that the FfO-8-OCB material was mixed with less chiral additive (3.22% to 3.41%). Flexoelectro-optic theory suggests that a longer pitch material shows a larger tilt angle per unit field and a longer response time than a shorter pitch material. This theory was confirmed by the results given in Chapter 5. This

effect is also observed in Figure 6.10 when the data is compared for the two mixtures with an even number of carbon atoms in their spacers.

From the tilt angles per unit field and the pitch values measured it was possible to calculate the flexo-elastic ratios, $\bar{e}/K$, for the three mixtures. The results of which are shown in Table 6.8 to 6.10.

Reduced Temperature, °C (T_c = 166°C)	$\Delta\tan\phi/\Delta E$, μm V^{-1}	Selective reflection wavelength, nm	Pitch (calculated), nm	$\bar{e}/K$, C N^{-1} m^{-1}
-10	0.0327	636	405	0.51
-15	0.0316	649	413	0.48
-20	0.0296	664	423	0.44

Table 6.8 A comparison of the values at different reduced temperatures for the selective reflection and the calculated values for the pitch and the ratio of the effective flexoelectric coefficient and the average of the splay and bend elastic constants. The mixture studied was 3.22% BDH1281 in FfO-6-OCB.

Reduced Temperature, °C (T_c = 116°C)	$\Delta\tan\phi/\Delta E$, μm V^{-1}	Selective reflection wavelength, nm	Pitch (calculated), nm	$\bar{e}/K$, C N^{-1} m^{-1}
-10	0.0616	469	298	1.30
-20	0.0631	483	307	1.29
-30	0.0656	494	314	1.31
-40	0.0705	504	321	1.38
-50	0.0730	514	327	1.40

Table 6.9 A comparison of the values at different reduced temperatures for the selective reflection and the calculated values for the pitch and the ratio of the effective flexoelectric coefficient and the average of the splay and bend elastic constants. The mixture studied was 3.40% BDH1281 in FfO-7-OCB.

Reduced Temperature, °C (T_c = 147°C)	$\Delta\tan\phi/\Delta E$, μm V^{-1}	Selective reflection wavelength, nm	Pitch (calculated), nm	$\bar{e}/K$, C N^{-1} m^{-1}
-10	0.0394	752	479	0.52
-20	0.0418	777	495	0.53
-30	0.0418	803	512	0.51
-40	0.0376	830	529	0.45

Table 6.10 A comparison of the values at different reduced temperatures for the selective reflection and the calculated values for the pitch and the ratio of the effective flexoelectric coefficient and the average of the splay and bend elastic constants. The mixture studied was 3.40% BDH1281 in FfO-8-OCB.

As in the previous two sections an odd-even effect is observed in the flexo-elastic ratio. All the homologues studied in this chapter have their flexo-elastic ratios and pitches compared in Figure 6.11.

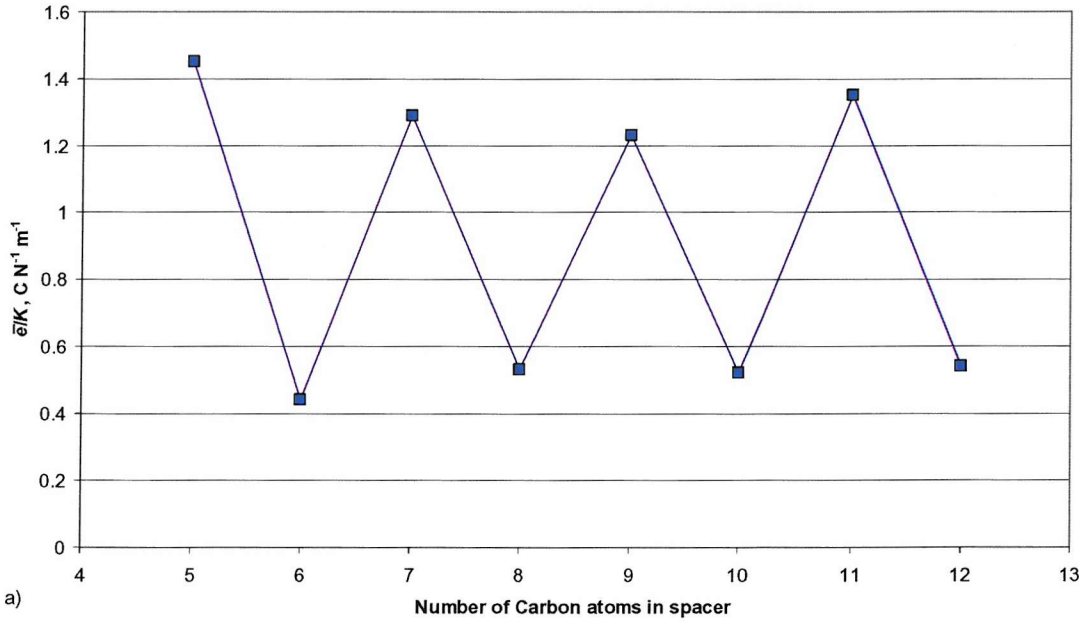

a)

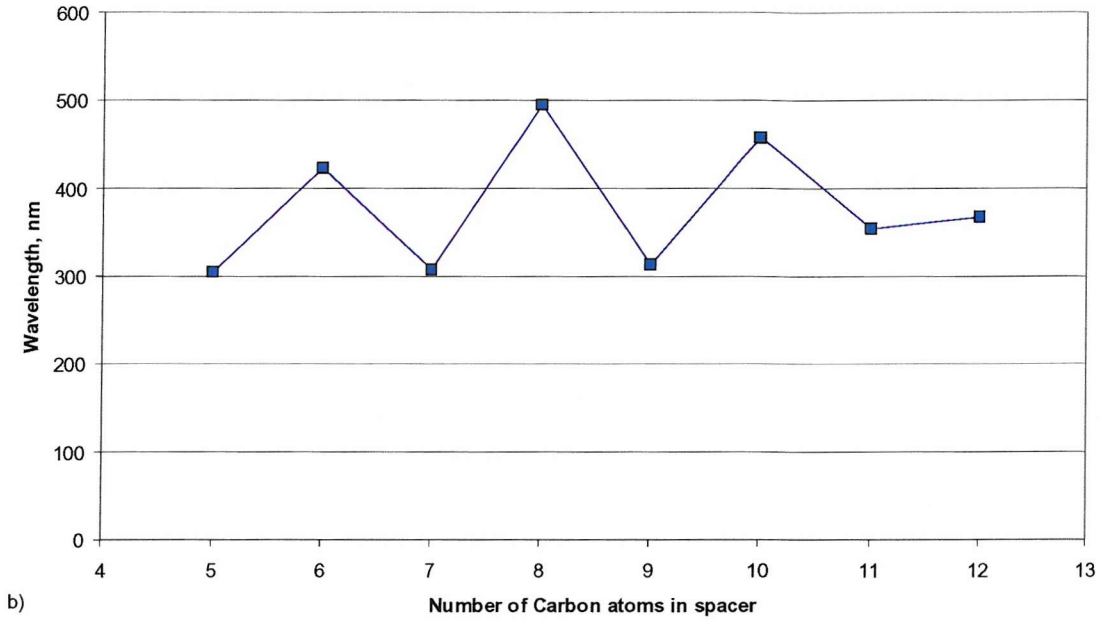

b)

Figure 6.11 A comparison of a) the flexo-elastic ratio and b) the pitch of the homologues of FfO-n-OCB at a reduced temperature of -20°C, where n ranges from 5 to 12. All the homologues were doped with approximately 3.50% BDH1281 (w/w).

It is clear from Figure 6.11(a) that there exists a significant odd-even effect in the flexo-elastic ratio for bimesogenic homologues. Dilisi *et al.*[8] propose that for symmetric bimesogens it would be expected that the elastic constants, K_{11}, K_{22} and K_{33}, would be significantly higher for molecules with an even number of carbon atoms in the spacer group. This was proven for two different achiral bimesogens based upon the monomer 4.4'-dipentyloxyphenylbenzoate, one molecule with an even number of carbon atoms in the spacer and one with an odd number. The results show that compared with values measured for the material with an odd number of carbon atoms in the spacer, the elastic constants are approximately double for the material with an even number of carbon atoms in the spacer. If the magnitude of the odd-even effect in elastic constants is similar for all bimesogens then this would explain the majority of the difference in the flexo-elastic ratios between neighbouring homologues of the non-symmetric molecules studied in this chapter. Figure 6.11(b) shows an odd-even effect in the pitch of the mixtures studied (although it is noted that there is a slight variation in the amount of chiral additive present in each case) and, as the induced pitch is proportional to the K_{22} elastic constant of the host, this would suggest strongly that there is a significant difference in the twist elastic constant between

neighbouring homologues. The physical properties of the non-symmetric materials are discussed further in the next section.

6.5 The physical properties of the non-symmetric homologues

6.5.1 Dielectric properties

The dielectric properties of the non-symmetric bimesogens were measured using the method outlined by Meyerhofer.[9] The measurements were performed using a Wayne-Kerr Electronics[10] capacitance bridge. The dielectric anisotropies of some of the homologues are shown in Figure 6.12.

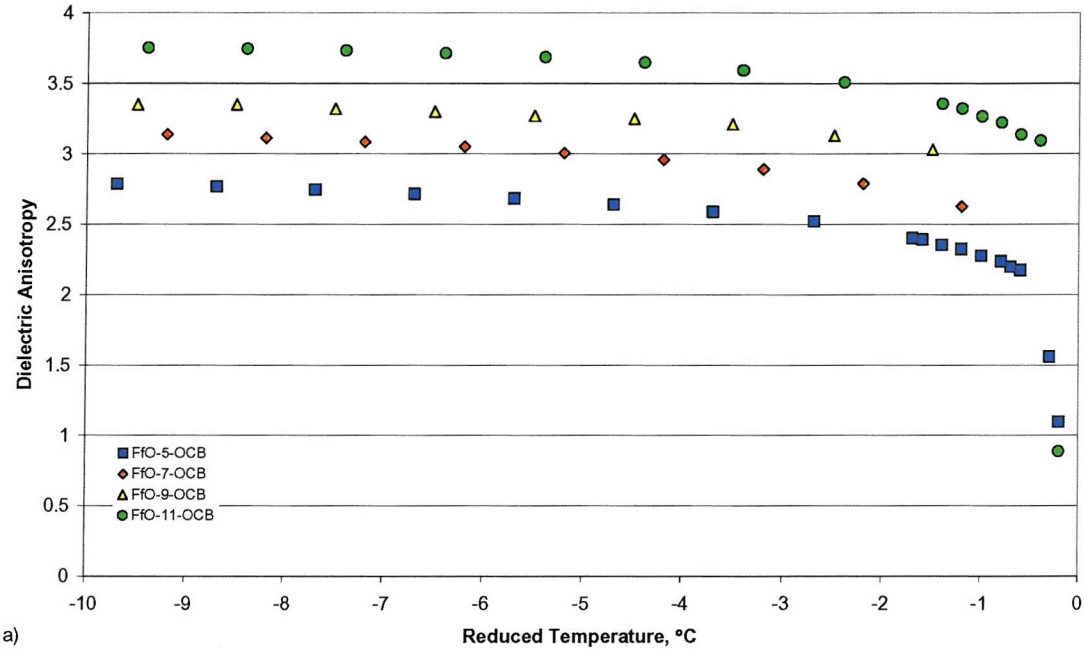

a)

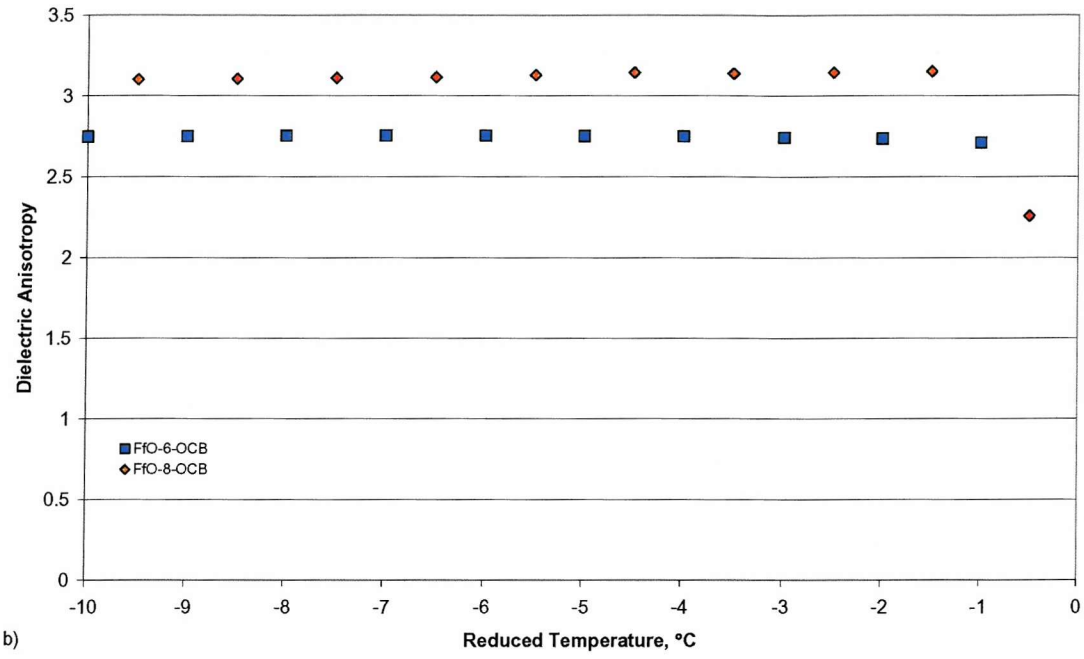

Figure 6.12 The dielectric anisotropies of a) the "odd" and b) the "even" homologues from the series FfO-n-OCB.

From Figure 6.12, it can be seen that the dielectric anisotropies lie in the range 2.5 to 3.8. This agrees with the earlier hypothesis that using a non-symmetric bimesogenic molecular template would increase the dielectric anisotropy when compared to a symmetric bimesogenic mixture, as discussed in Section 5.6.2.

6.5.2 The splay elastic constant

Measurements of the splay elastic constant, K_{11}, were performed (using a method described by Khoo and Wu[11]) on the pure achiral non-symmetric homologues. The variation in the splay elastic constant as a function of temperature for two of the homologues is shown in Figure 6.13.

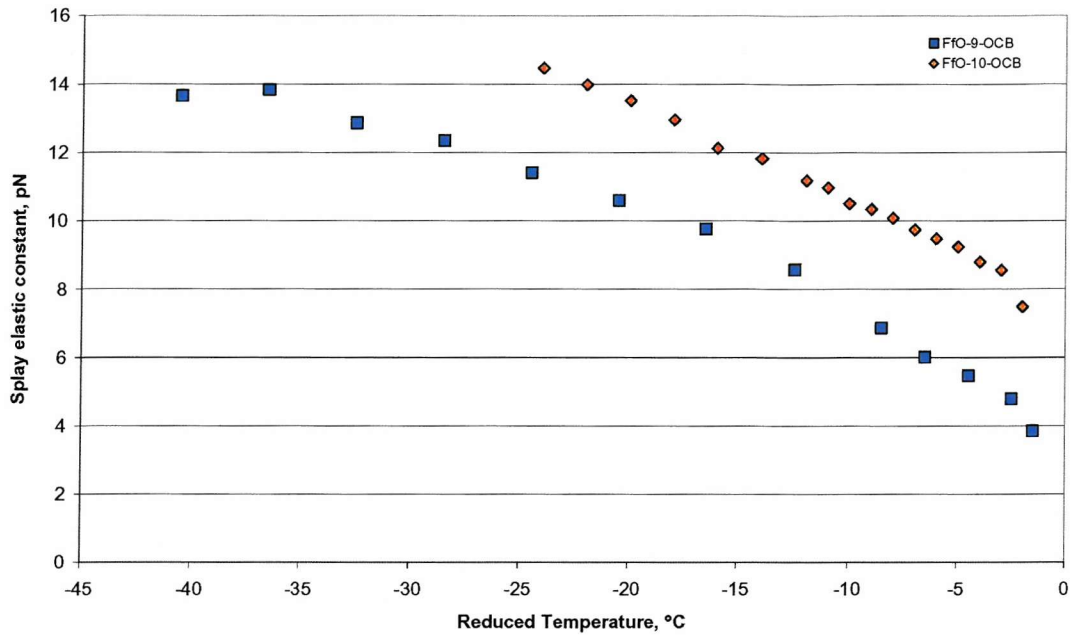

Figure 6.13 The splay elastic constant measured, as a function of temperature, for the homologues FfO-9-OCB and FfO-10-OCB.

From Figure 6.13 it can be seen that for the FfO-9-OCB homologue the splay elastic constant shows a dependence on temperature that varies with the square of the order parameter, as expected from theory. The splay elastic constant of the FfO-10-OCB homologue is higher than that of the FfO-9-OCB homologue by approximately 25-30%.

The splay elastic constant was measured for most of the remaining homologues; the results are tabulated in Table 6.11.

FfO-n-OCB	Splay Elastic Constant, pN	
	$T_{red} = -5$	$T_{red} = -10$
5	5.1	6.4
6	9.4	10.9
7	5.8	7.4
8	10.8	12.6
9	6	7.9
10	9.2	10.5
11	7.5	-

Table 6.11 The splay elastic constants for the homologues of FfO-n-OCB, measured at reduced temperatures of -5°C and -10°C.

Table 6.11 shows that there is a clear difference in the splay elastic constants of the "odd" and "even" homologues. The splay elastic constants are higher for the homologues with an even number of carbon atoms in their spacer groups.

6.5.3 The twist elastic constant

The twist elastic constant, K_{22}, was calculated for the homologues FfO-9-OCB and FfO-10-OCB using the critical field for helix unwinding. The results are shown in Figure 6.14.

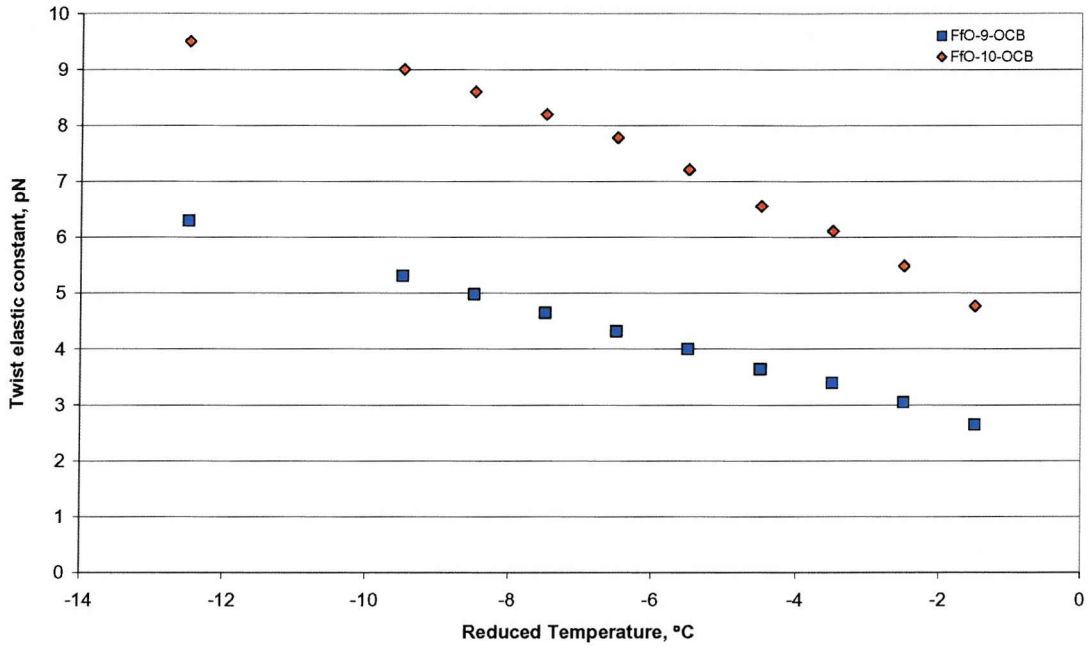

Figure 6.14 The twist elastic constants calculated for the homologues FfO-9-OCB and FfO-10-OCB.

From Figure 6.14 it can be seen that the twist elastic constant is significantly higher for the material with an even number of carbon atoms in the spacer group. It was previously hypothesised that the difference in the pitches measured for all the homologues, despite roughly the same concentration of chiral dopant being used, was due to the "even" mixtures having a larger twist elastic constant; the results shown in Figure 6.14 confirm that this hypothesis was correct.

The "odd-even" variation in the splay and twist elastic constants observed agree with the observations made by Dilisi *et al.*[8] Unfortunately to date, it has not been possible to obtain bend elastic constant values for the non-symmetric bimesogens.

6.6 The effect of the amount of chiral dopant on flexoelectro-optic properties

It has been repeatedly observed throughout this work that the amount of chiral additive used in a mixture has a direct result upon the pitch of the mixture. In Chapter 5 it was also observed that on using less chiral dopant it was possible to observe an enhancement of the flexo-elastic properties of the mixture. In this section the effects of the varying the amount of chiral dopant are studied for one of the non-symmetric bimesogens, in this case FfO-9-OCB, to see if a similar effect is observed as for the symmetric bimesogens. The results of the flexoelectro-optic measurements and the selective reflection wavelengths measured are shown in Figure 6.15.

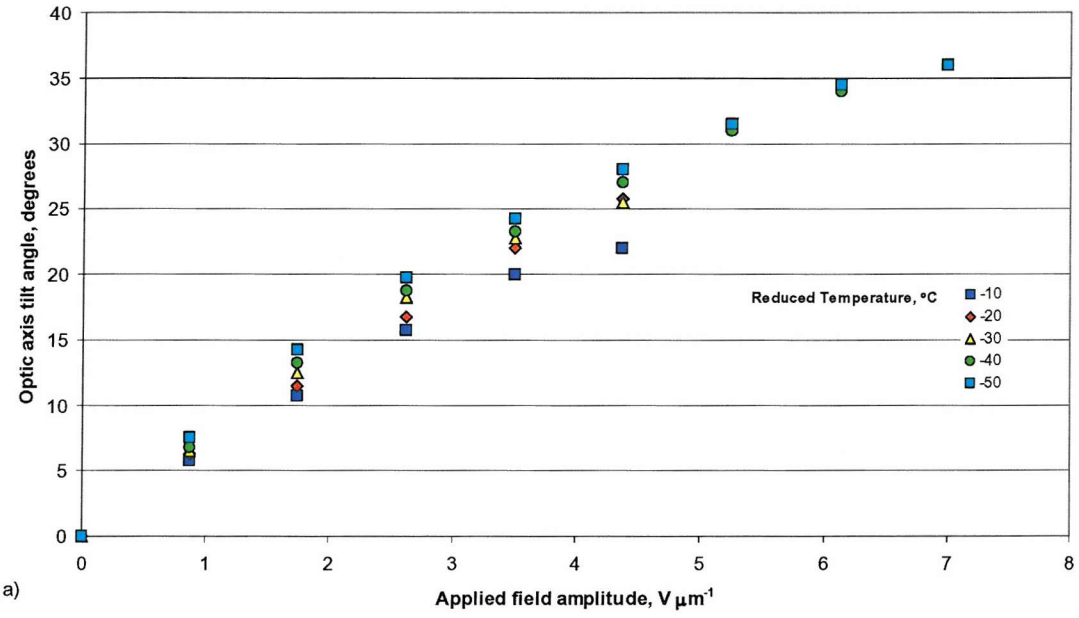

a)

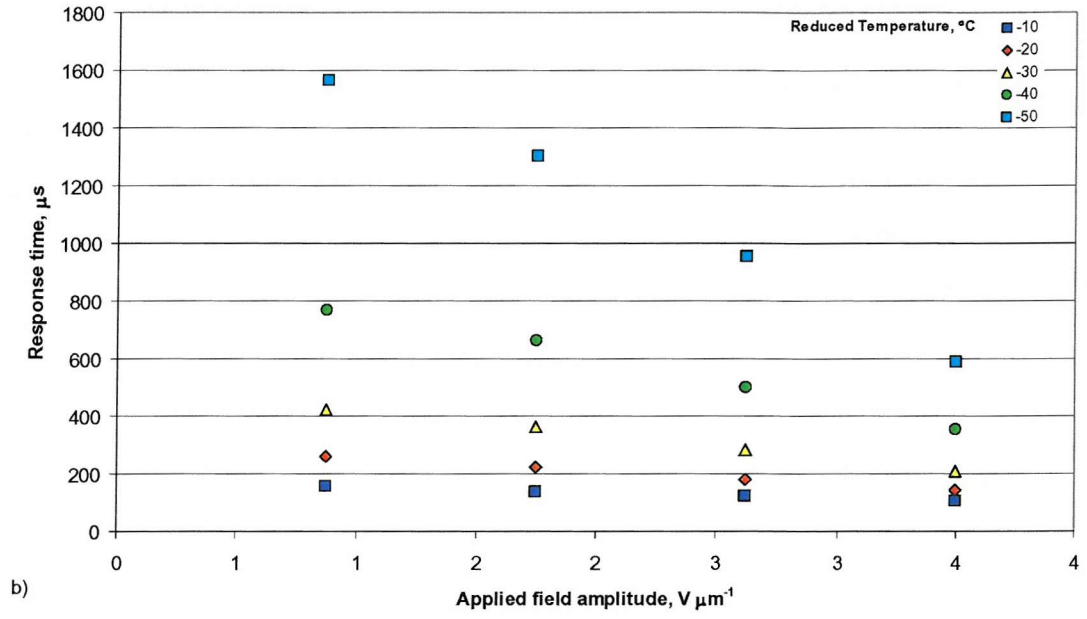

b)

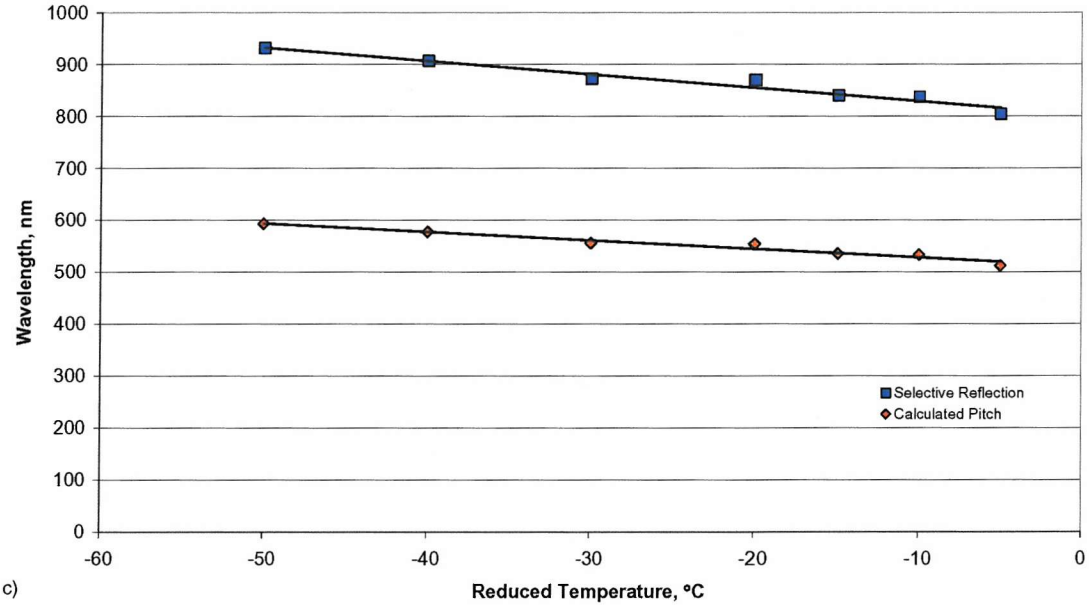

c)

Figure 6.15 The relevant properties of a mixture of 1.91% BDH1281 in FfO-9-OCB (w/w). The graphs show a) the induced tilt angles, b) the response times and c) selective reflection wavelength and calculated pitch, all measured across a range of reduced temperatures. The response times are measured for 10-90% of the full switch of the optic axis, i.e. twice the tilt. The selective reflection properties were measured using a UV-visible spectrometer and the pitch was calculated from this using a value of 1.57 for the average refractive index. Trend-lines were added to guide the eye.

In comparison to the results measured for the 3.75% BDH1281 in FfO-9-OCB previously, it can be seen that firstly that the tilt angles are much larger (~60%) and the response times are significantly longer (2-2.5 times longer) for the 1.91% BDH1281 mixture. These observations agree with both theory and previous observations in Chapter 5, in that a lengthening of the pitch results in bigger tilt angles per unit field and longer response times.

Using the data from Figure 6.15 it is possible to calculate the flexo-elastic ratio, $\bar{e}/K$, as a function of temperature. The results are shown in Table 6.12.

Reduced Temperature, °C (T_c = 114°C)	$\Delta\tan\phi/\Delta E$, μm V^{-1}	Selective reflection wavelength, nm	Pitch (calculated), nm	$\bar{e}/K$, C N^{-1} m^{-1}
-10	0.107	838	533	1.26
-20	0.1143	870	554	1.30
-30	0.1206	873	556	1.36
-40	0.1236	907	578	1.34
-50	0.1291	932	593	1.37

Table 6.12 A comparison of the values at different reduced temperatures for the selective reflection and the calculated values for the pitch and the ratio of the effective flexoelectric coefficient and the average of the splay and bend elastic constants. The mixture studied was 1.91% BDH1281 in FfO-9-OCB.

From Table 6.12 and referring back to Table 6.5 it can be seen that the flexo-elastic ratio is slightly higher (~6%) for the mixture with less chiral dopant; this agrees with the observations made in Chapter 5.

It is hypothesised that the increase in the flexo-elastic ratio is due to $\bar{e}$ and K having different dependences on the order parameter. Thus, if the concentration of chiral additive alters the order parameter then the flexo-elastic ratio would change as a function of concentration.

6.7 The effects of creating a chiral mixture composed of two non-symmetric bimesogens

In Chapter 5 mixtures of symmetric bimesogens were studied, mixtures of two of the bimesogens were used to increase the temperature range of the nematic phase. In this section the effects of varying the percentages of two non-symmetric bimesogens are studied for two reasons, firstly to see if the temperature range of the chiral nematic phase could be improved and secondly to see if the flexo-elastic ratio could be increased. The non-symmetric bimesogens FfO-5-OCB and FfO-7-OCB were arbitrarily chosen to be the constituents of the mixtures; it was decided to use materials with an odd number of carbon atoms in their spacer group as they have been seen to have a wider chiral nematic phase and higher flexo-elastic ratios. Four mixtures were made containing different percentages of the two bimesogenic materials. The mixtures are denoted a/b FfO-x/y-OCB indicating that the mixture contains a% of the material FfO-x-OCB and b% of the FfO-y-OCB. The four mixtures were each doped with approximately 3.50% of the chiral additive BDH1281. The four mixtures were each studied optically using a polarising microscope. All the mixtures show a chiral nematic phase with an underlying smectic phase on cooling, and the transition temperatures are shown in Table 6.13.

Percentages (w/w)	On Cooling (5°/min)	On Heating
19 / 81 FfO-5/7-OCB	**I** -(113°C)-> **BP** –(109°C)-> **N*** -(47°C)-> **SmX***	**Crystal** -(81°C)-> **N*** -(112°C)-> **BP** –(113°C)->**I**
40 / 60 FfO-5/7-OCB	**I** -(112°C)-> **BP** –(109°C)-> **N*** -(46°C)-> **SmX***	**Crystal** -(78°C)-> **N*** -(111°C) -> **BP** –(112°C)->**I**
60 / 40 FfO-5/7-OCB	**I** -(110°C)-> **BP** –(105°C)-> **N*** -(43°C)-> **SmX***	**Crystal** -(75°C)-> **N*** -(109°C) -> **BP** –(110°C)->**I**
78 / 22 FfO-5/7-OCB	**I** -(108°C)-> **BP** –(105°C)-> **N*** -(40°C)-> **SmX***	**Crystal** -(71°C)-> **N*** -(105°C) -> **BP** –(108°C)->**I**

Table 6.13 Initial microscopy observations of transition temperatures for different percentage mixtures of two non-symmetric bimesogens. All mixtures were doped with approximately 3.50% BDH1281. BP represents one or more blue phases.

All four mixtures show one or more blue phases on heating and cooling. This was expected, because it has previously been seen that when a non-symmetric material with an

odd number of methyl groups is mixed with more than 3% BDH1281 (w/w) blue phases appear.

Of the four mixtures studied it would appear that the 78%/22% mixture was closest to a eutectic composition as it had the lowest crystal to chiral nematic phase transition temperature and it also had the lowest temperature for the chiral nematic phase to smectic phase transition.

The smectic phase observed for these mixtures appears to be the chiral version of the smectic phase observed for the pure FfO-11-OCB material. A few degrees above the smectic phase transition temperature, the pitch of the chiral nematic phase changes rapidly, as was observed in Chapter 5 for the symmetric mixtures. It was possible by shearing to get the mixtures in the smectic phase to adopt a homeotropic alignment, and this is generally indicative of the presence of a Smectic A phase (or its chiral version). It was also possible to get the mixtures to adopt the homeotropic alignment by applying a sufficient electric field, as shown in Figure 6.16.

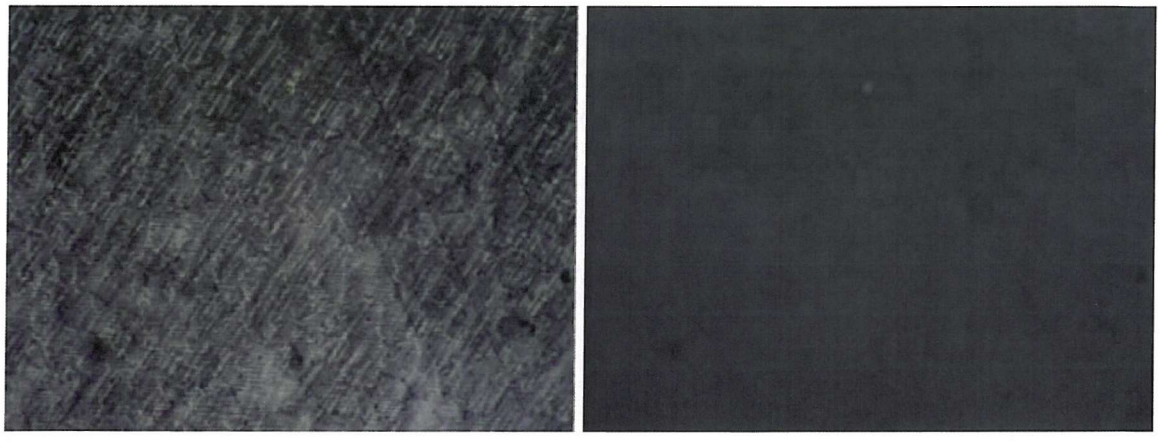

Figure 6.16 The smectic X phase with a) no electric field applied and b) with electric field applied.

The author believes that the observed smectic phase is the same as that observed in Chapter 5, namely the chiral smectic A phase. The observations made in this chapter would seem to indicate belief that this phase is chiral smectic A, however the author would still require further confirmation, from x-ray analysis for example, before stating without doubt the nature of the phase.

6.7.1 Flexoelectro-optic measurements of the four mixtures

The flexoelectro-optic properties and selective reflection wavelengths of the four mixtures of different percentages of FfO-5-OCB and FfO-7-OCB were measured.

3.57% BDH1281 in 19/81 FfO-5/7-OCB

The mixture was aligned in the uniformly lying helix geometry using the field ramping method discussed in Section 6.4.1. Both the flexoelectro-optic and selective reflection wavelength measurements were made in the same commercially made planar cell. The data measured is summarised in Figure 6.17.

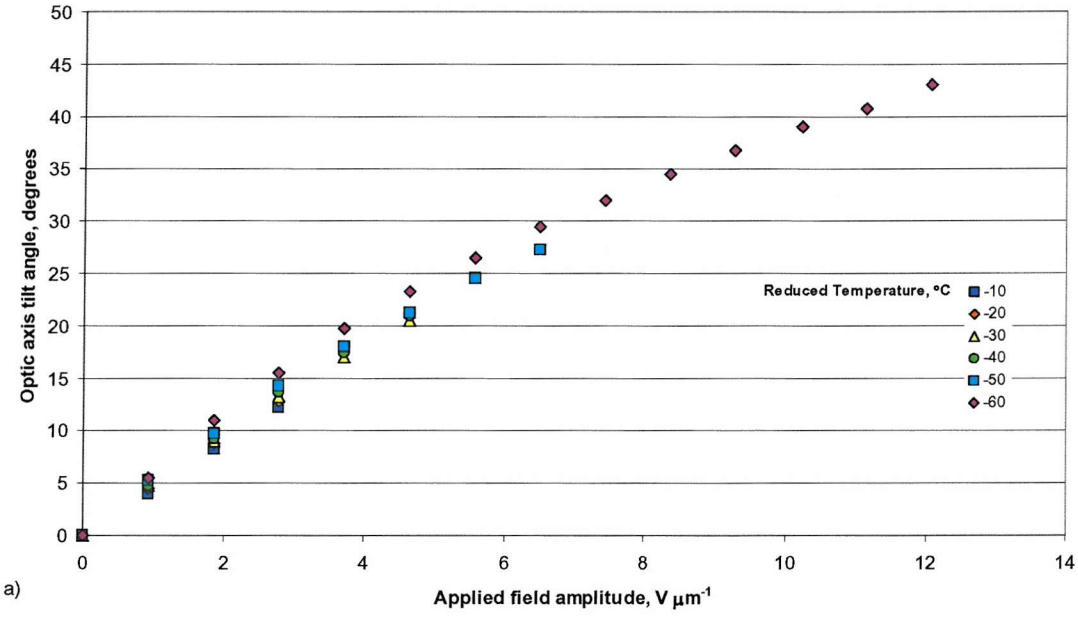

a)

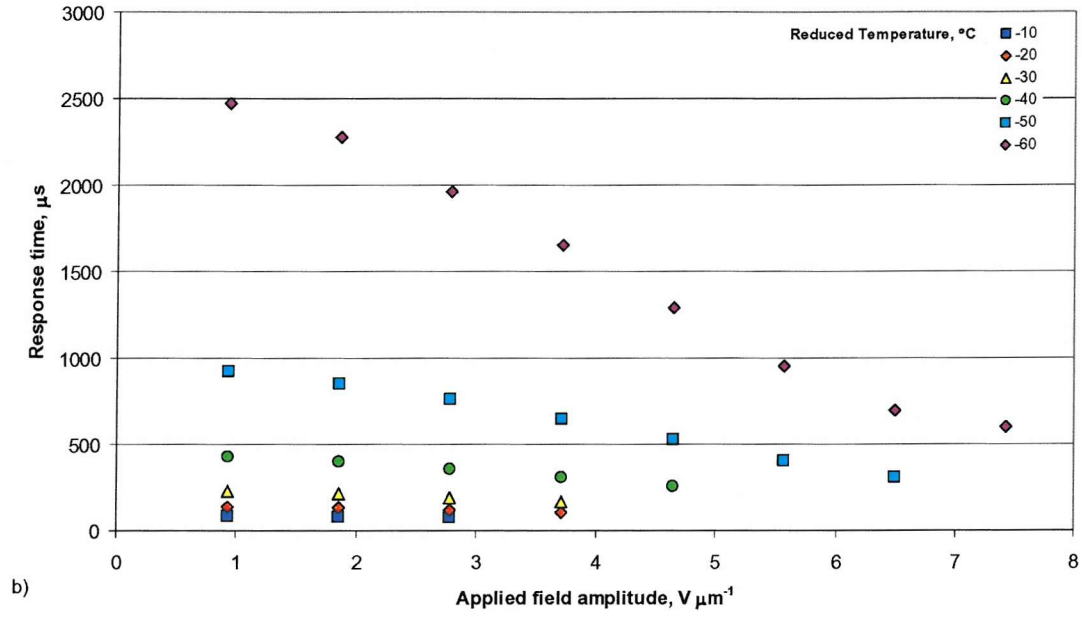

b)

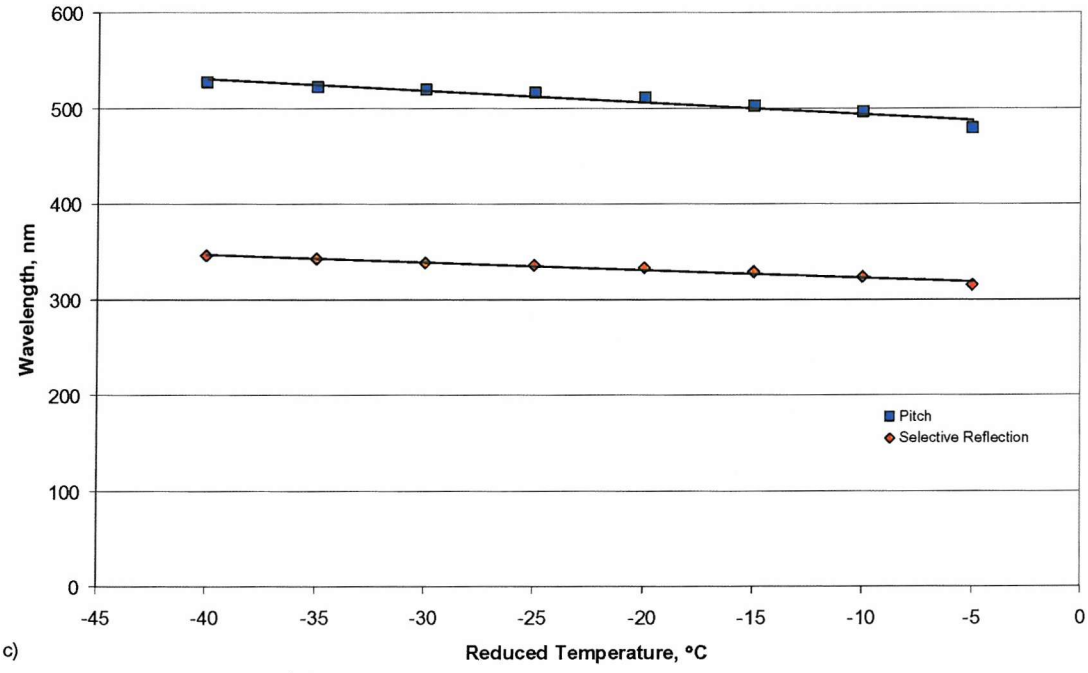

c)

Figure 6.17 The relevant properties of a mixture of 3.57% BDH1281 in 19%/81% FfO-5/7-OCB (w/w). The graphs show a) the induced tilt angles, b) the response times and c) selective reflection wavelength and calculated pitch. All measurements were performed across a range of reduced temperatures. The response times are measured for 10-90% of the full switch of the optic axis, i.e. twice the tilt. The selective reflection properties were measured using a UV-visible spectrometer and the pitch was calculated from this using a value of 1.57 for the average refractive index. Trend-lines were added to guide the eye.

From Figure 6.17 it can be that tilt angles in the region of 40-45° are achievable. The response times range from less than 100 microseconds up to 2.5 milliseconds across the temperature range studied.

The data in Figure 6.17 was used to calculate the flexo-elastic ratio $\bar{e}/K$ and the results are shown in Table 6.14.

Reduced Temperature, °C (T_c = 113°C)	$\Delta\tan\phi/\Delta E$, μm V^{-1}	Selective reflection wavelength, nm	Pitch (calculated), nm	$\bar{e}/K$, C N^{-1} m^{-1}
-5	0.0715	495	315	1.43
-10	0.0783	516	324	1.52
-20	0.0813	523	333	1.53
-30	0.0825	531	338	1.53
-40	0.0854	543	346	1.55

Table 6.14 A comparison of the values at different reduced temperatures for the selective reflection and the calculated values for the pitch and the ratio of the effective flexoelectric coefficient and the average of the splay and bend elastic constants. The mixture studied was 3.57% BDH1281 in 19%/81% FfO-5/7-OCB.

3.48% BDH1281 in 40/60 FfO-5/7-OCB

The mixture was aligned in the uniformly lying helix geometry using the field ramping method discussed in Section 6.4.1. Both the flexoelectro-optic and selective reflection wavelength measurements were made in the same commercially made planar cell. The data measured is summarised in Figure 6.18.

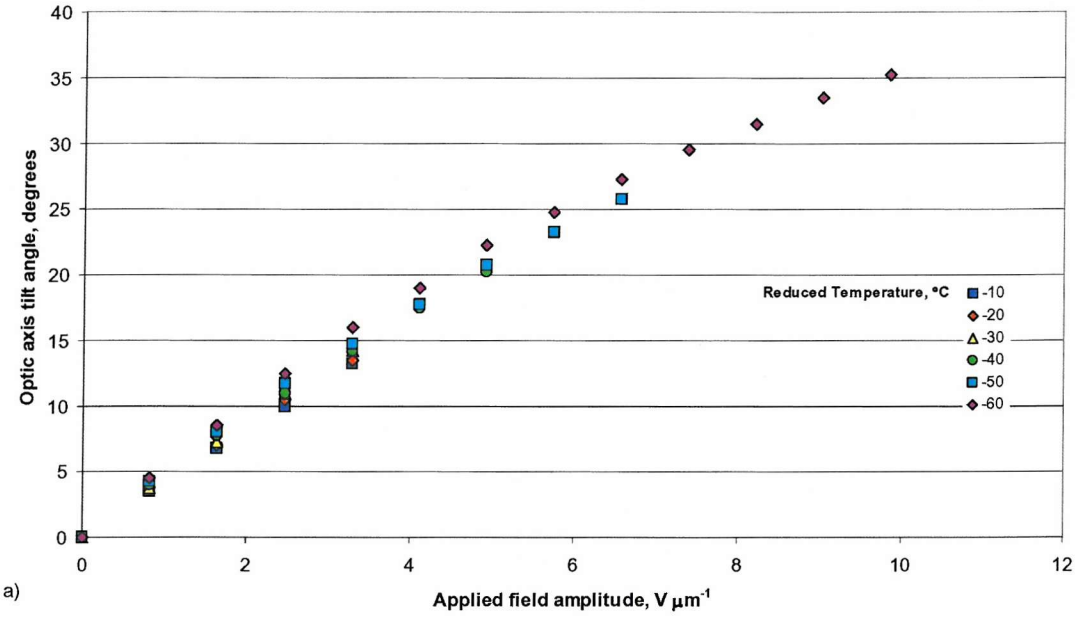
Optic axis tilt angle, degrees
Applied field amplitude, V µm-1
Reduced Temperature, °C
-10
-20
-30
-40
-50
-60
0
5
10
15
20
25
30
35
40
0
2
4
6
8
10
12

a)

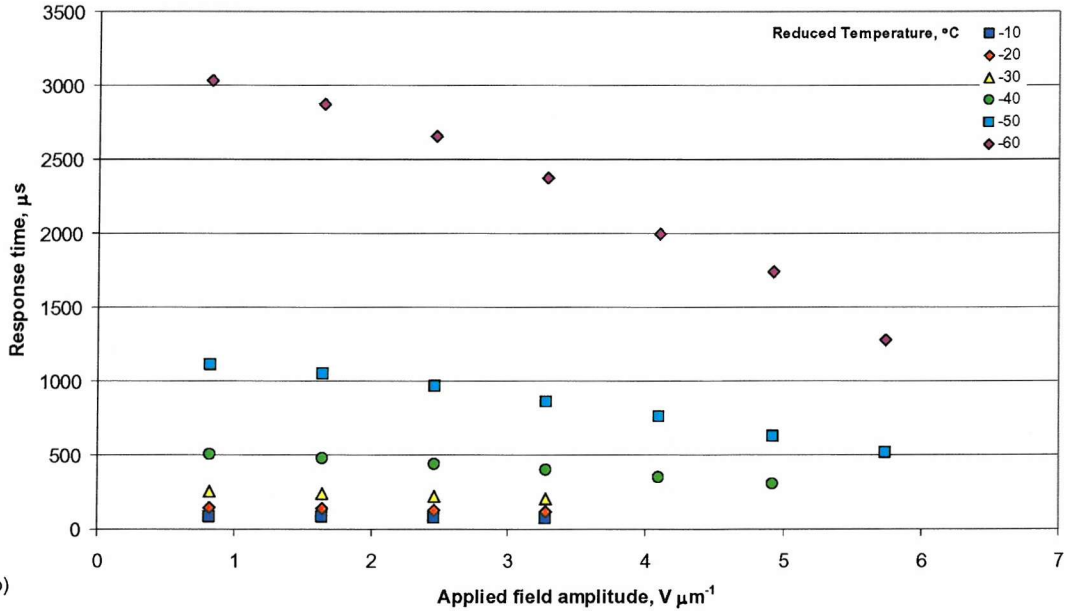
Response time, µs
Applied field amplitude, V µm-1
Reduced Temperature, °C
-10
-20
-30
-40
-50
-60
0
500
1000
1500
2000
2500
3000
3500
0
1
2
3
4
5
6
7

b)

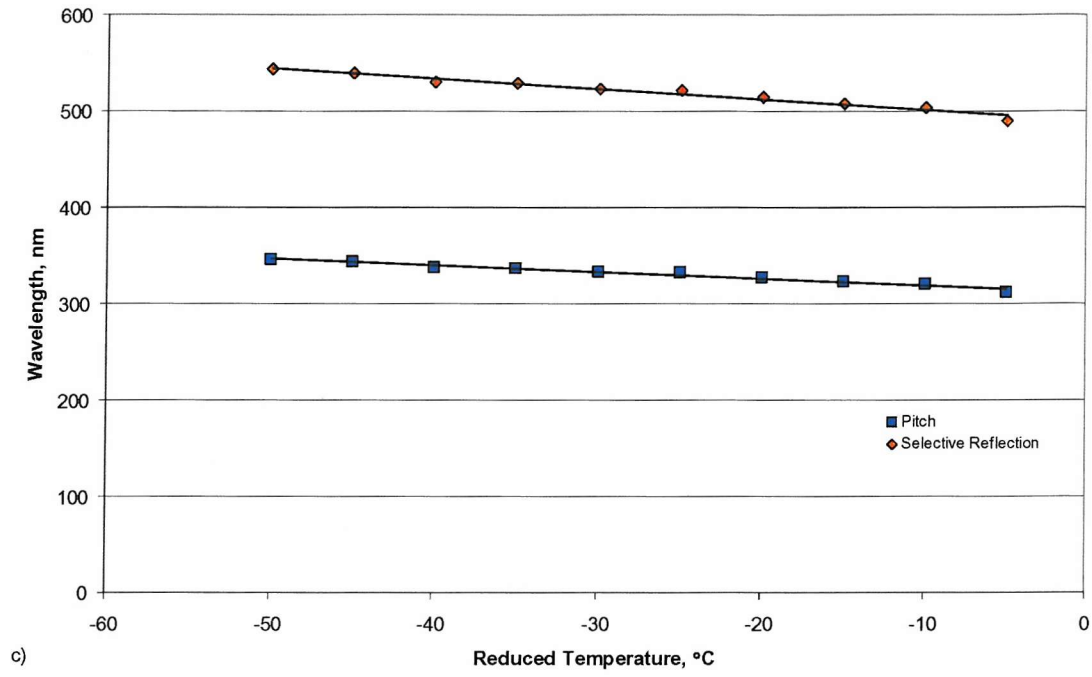

c)

Figure 6.18 The relevant properties of a mixture of 3.48% BDH1281 in 40%/60% FfO-5/7-OCB (w/w). The graphs show a) the induced tilt angles, b) the response times and c) selective reflection wavelength and calculated pitch. All measurements were taken across a range of reduced temperatures. The response times are measured for 10-90% of the full switch of the optic axis, i.e. twice the tilt. The selective reflection properties were measured using a UV-visible spectrometer and the pitch was calculated from this using a value of 1.57 for the average refractive index. Trend-lines were added to guide the eye.

From Figure 6.18 it can be that tilt angles in the region of 35° are achievable. The response times range from less than 100 microseconds up to approximately 3 milliseconds across the temperature range studied.

The data in Figure 6.18 was used to calculate the flexo-elastic ratio $\bar{e}/K$ and the results are shown in Table 6.15.

Reduced Temperature, °C (T_c = 112°C)	$\Delta\tan\phi/\Delta E$, μm V^{-1}	Selective reflection wavelength, nm	Pitch (calculated), nm	$\bar{e}/K$, C N^{-1} m^{-1}
-5	0.0659	490	312	1.33
-10	0.0715	503	320	1.40
-20	0.0732	515	328	1.40
-30	0.0777	523	333	1.47
-40	0.0772	530	338	1.44
-50	0.0805	544	347	1.46

Table 6.15 A comparison of the values at different reduced temperatures for the selective reflection and the calculated values for the pitch and the ratio of the effective flexoelectric coefficient and the average of the splay and bend elastic constants. The mixture studied was 3.48% BDH1281 in 40%/60% FfO-5/7-OCB.

3.51% BDH1281 in 60/40 FfO-5/7-OCB

The mixture was aligned in the uniformly lying helix geometry initially using the field ramping method discussed in Section 6.4.1. However it was found that better alignment was achievable by applying an electric field while the mixture was in blue phase I. Both the flexoelectro-optic and selective reflection wavelength measurements were made in the same commercially made planar cell. The data measured is summarised in Figure 6.19.

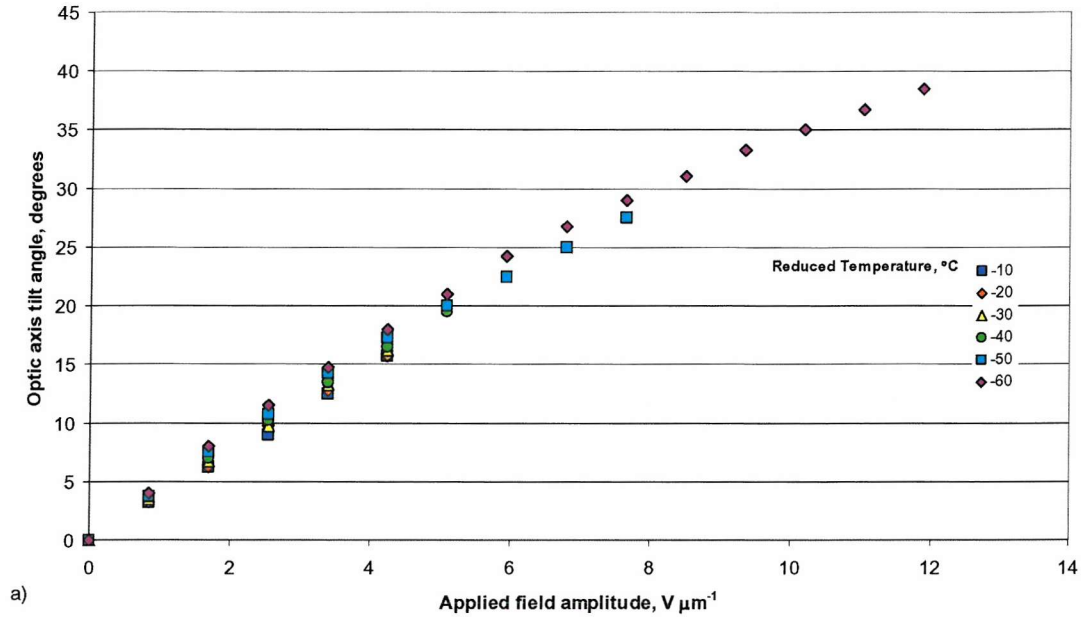
Optic axis tilt angle, degrees
Applied field amplitude, V µm-1
Reduced Temperature, °C
-10
-20
-30
-40
-50
-60
0
5
10
15
20
25
30
35
40
45
0
2
4
6
8
10
12
14

a)

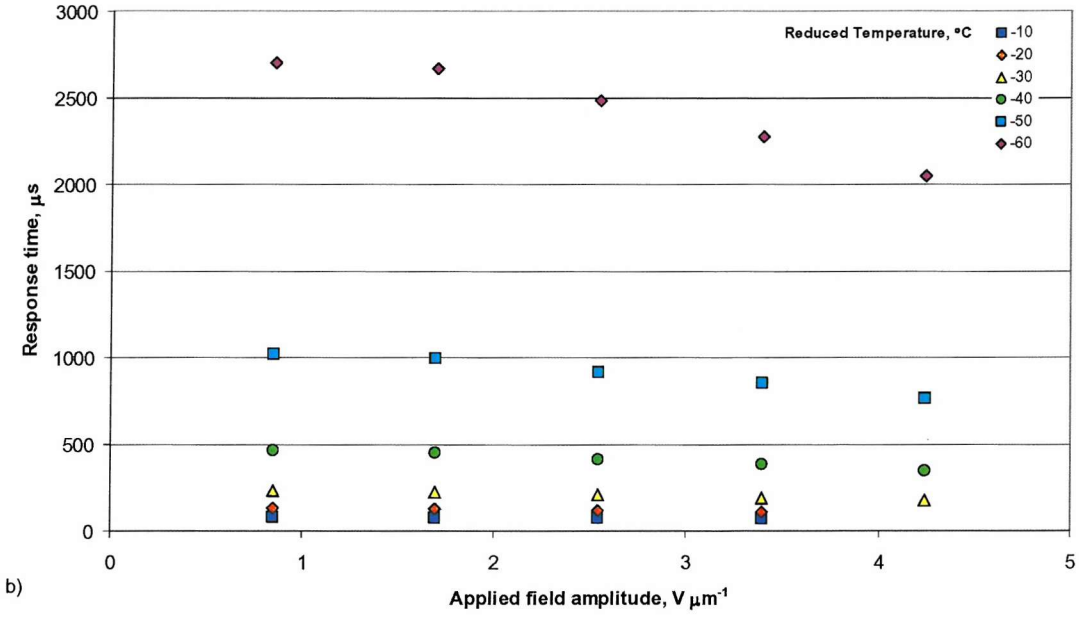
Response time, µs
Applied field amplitude, V µm-1
Reduced Temperature, °C
-10
-20
-30
-40
-50
-60
0
500
1000
1500
2000
2500
3000
0
1
2
3
4
5

b)

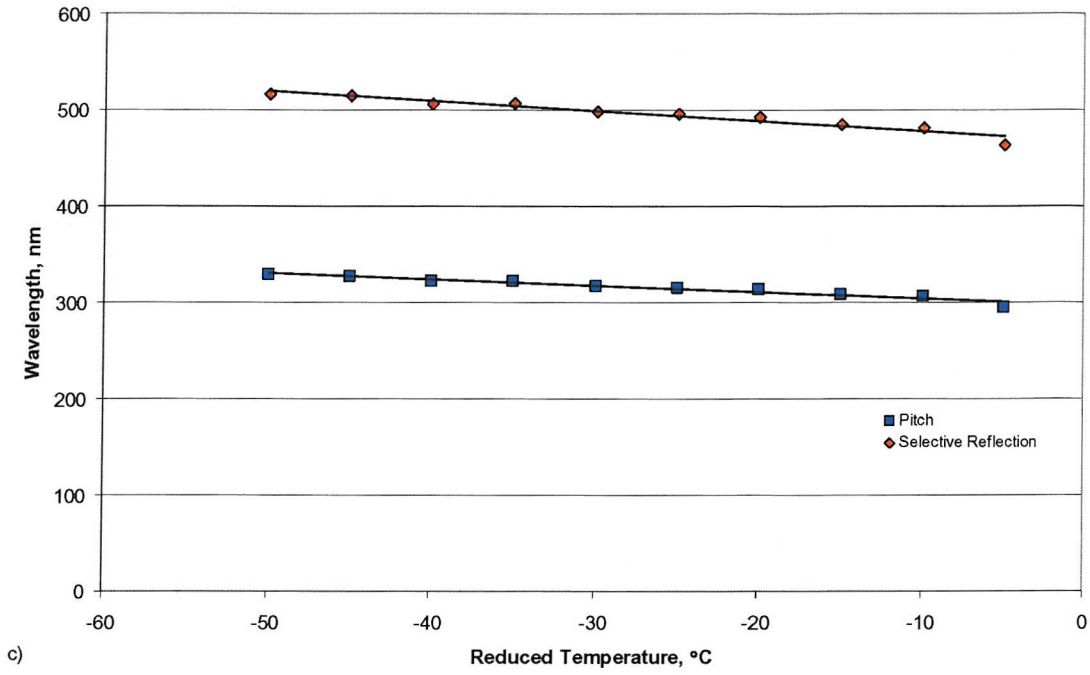

Figure 6.19 The relevant properties of a mixture of 3.51% BDH1281 in 60%/40% FfO-5/7-OCB (w/w). The graphs show a) the induced tilt angles, b) the response times and c) selective reflection wavelength and calculated pitch. All measurements were taken across a range of reduced temperatures. The response times are measured for 10-90% of the full switch of the optic axis, i.e. twice the tilt. The selective reflection properties were measured using a UV-visible spectrometer and the pitch was calculated from this using a value of 1.57 for the average refractive index. Trend-lines were added to guide the eye.

From Figure 6.19 it can be seen that tilt angles up to 40° are achievable. The response times range from less than 100 microseconds up to over 2.5 milliseconds across the temperature range studied.

The data in Figure 6.19 was used to calculate the flexo-elastic ratio $\bar{e}/K$ and the results are shown in Table 6.16.

Reduced Temperature, °C (T_c = 110°C)	$\Delta\tan\phi/\Delta E$, μm V^{-1}	Selective reflection wavelength, nm	Pitch (calculated), nm	$\bar{e}/K$, C N^{-1} m^{-1}
-5	0.0616	463	295	1.31
-10	0.0643	482	307	1.32
-20	0.0668	492	313	1.34
-30	0.0676	499	318	1.34
-40	0.0692	506	322	1.35
-50	0.0718	516	329	1.37

Table 6.16 A comparison of the values at different reduced temperatures for the selective reflection and the calculated values for the pitch and the ratio of the effective flexoelectric coefficient and the average of the splay and bend elastic constants. The mixture studied was 3.51% BDH1281 in 60%/40% FfO-5/7-OCB.

3.45% BDH1281 in 78/22 FfO-5/7-OCB

The mixture was aligned in the uniformly lying helix geometry initially using the field ramping method discussed in Section 6.4.1. However, as for the previous mixture, it was found that better alignment was achievable by applying an electric field while the mixture was in blue phase I. Both the flexoelectro-optic and selective reflection wavelength measurements were made in the same commercially made planar cell. The data measured is summarised in Figure 6.20.

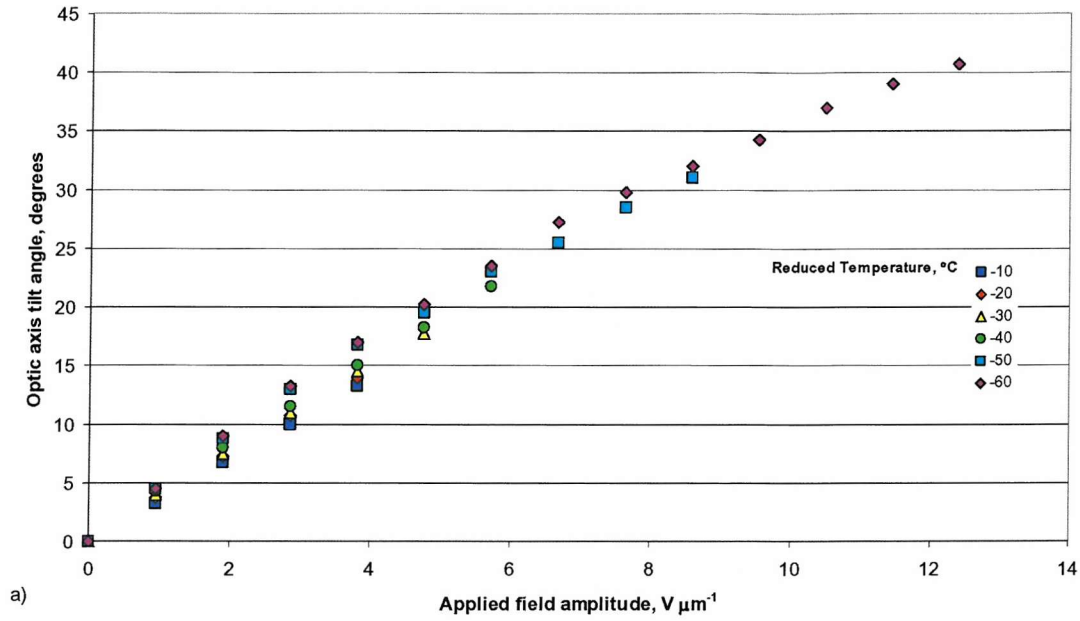
Optic axis tilt angle, degrees
Applied field amplitude, V μm-1
Reduced Temperature, °C
-10
-20
-30
-40
-50
-60

a)

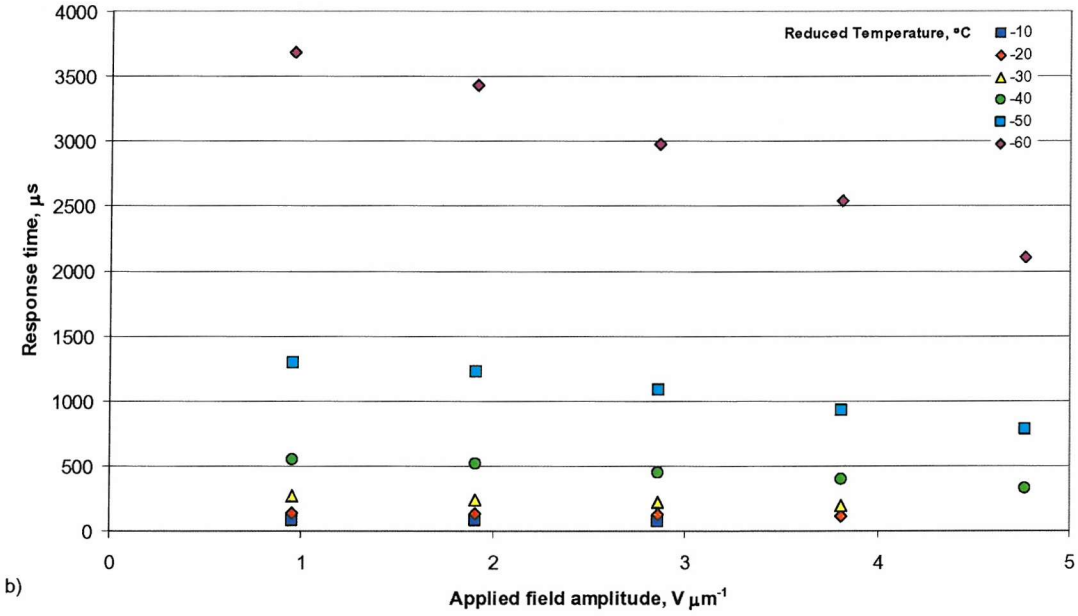
Response time, μs
Applied field amplitude, V μm-1
Reduced Temperature, °C
-10
-20
-30
-40
-50
-60

b)

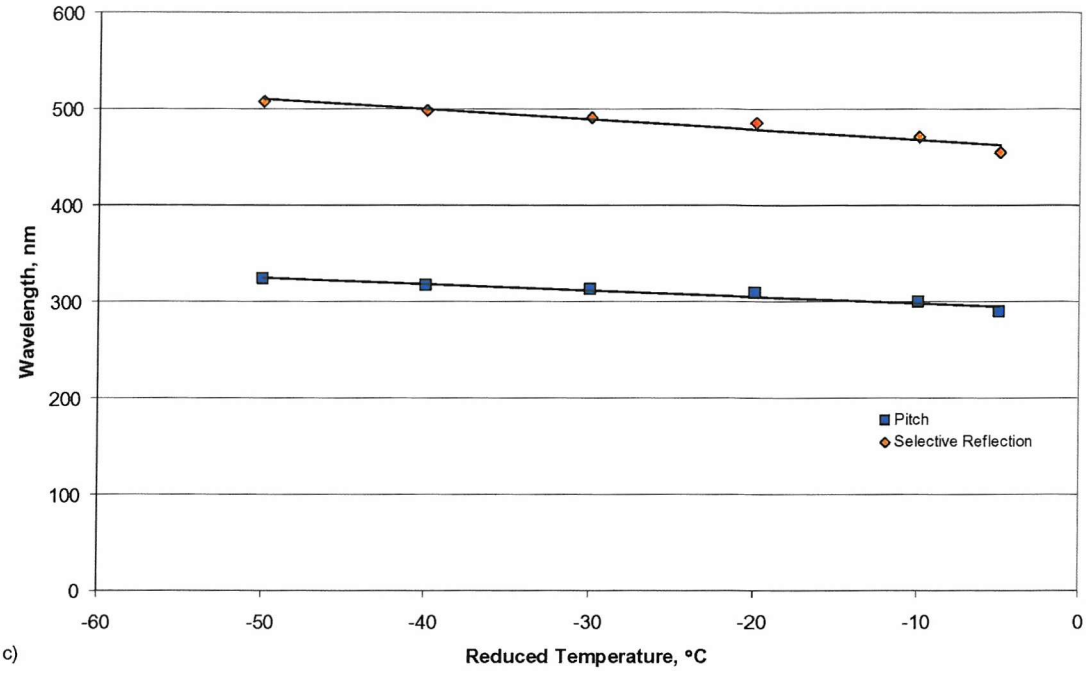

Figure 6.20 The relevant properties of a mixture of 3.45% BDH1281 in 78%/22% FfO-5/7-OCB (w/w). The graphs show a) the induced tilt angles, b) the response times and c) selective reflection wavelength and calculated pitch. All measurements were taken across a range of reduced temperatures. The response times are measured for 10-90% of the full switch of the optic axis, i.e. twice the tilt. The selective reflection properties were measured using a UV-visible spectrometer and the pitch was calculated from this using a value of 1.57 for the average refractive index. Trend-lines were added to guide the eye.

From Figure 6.20 it can be seen that tilt angles over 40° are achievable. The response times range from less than 100 microseconds up to over 3.5 milliseconds across the temperature range studied.

The data in Figure 6.20 was used to calculate the flexo-elastic ratio $\bar{e}/K$ and the results are shown in Table 6.17.

Reduced Temperature, °C (T_c = 109°C)	$\Delta\tan\phi/\Delta E$, μm V^{-1}	Selective reflection wavelength, nm	Pitch (calculated), nm	$\bar{e}/K$, C N^{-1} m^{-1}
-5	0.0583	455	290	1.26
-10	0.0620	471	300	1.30
-20	0.0654	486	309	1.33
-30	0.0669	491	312	1.35
-40	0.0688	498	317	1.36
-50	0.0705	508	324	1.37

Table 6.17 A comparison of the values at different reduced temperatures for the selective reflection and the calculated values for the pitch and the ratio of the effective flexoelectric coefficient and the average of the splay and bend elastic constants. The mixture studied was 3.51% BDH1281 in 60%/40% FfO-5/7-OCB.

As Figure 6.21 shows, there is a small difference in pitch for the four mixtures at the same temperature. The maximum deviation from the average of the pitches is approximately 5%. It is felt that this small variation in pitch would have very little effect on the flexo-elastic ratio measured for the mixtures.

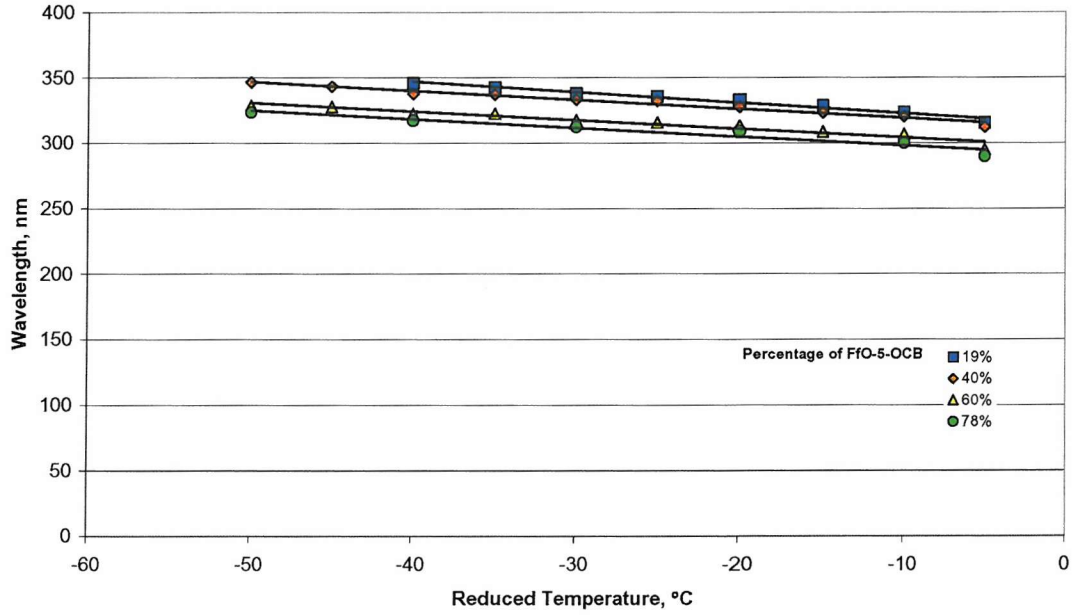

Figure 6.21 A comparison of pitches as a function of reduced temperature for the four different ratio mixtures of the bimesogens FfO-5-OCB and FfO-7-OCB. The mixtures have all been doped with approximately 3.5% BDH1281. The pitches were calculated from the selective reflection wavelengths using a value of 1.57 for the average refractive index. Trend-lines were added to guide the eye.

A direct comparison of the tilt angle against applied electric field is shown in Figure 6.22.

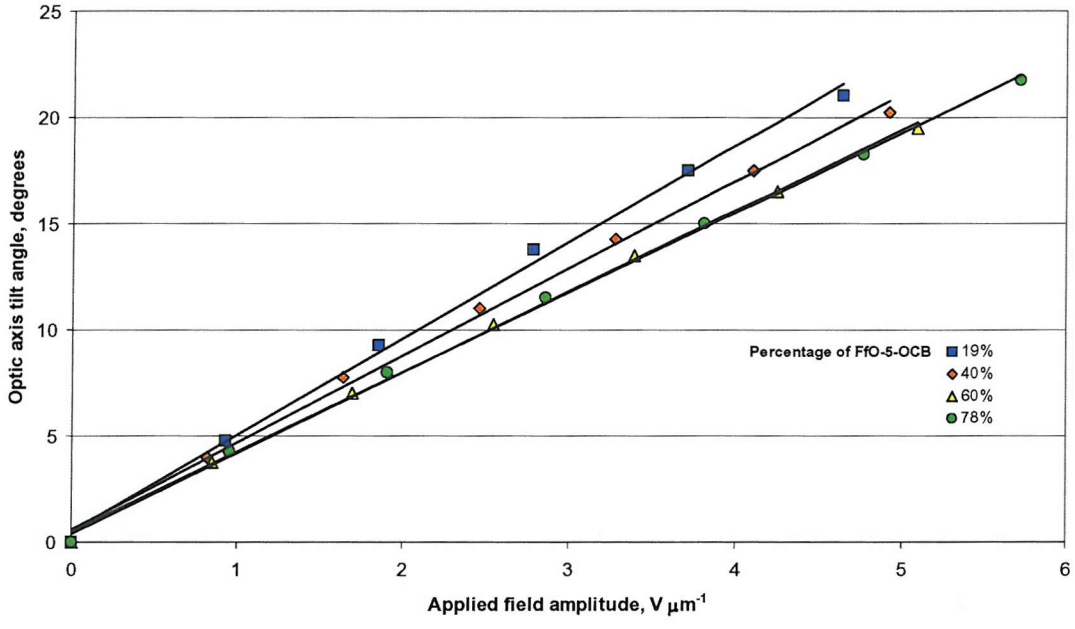

Figure 6.22 A comparison of tilt angle against applied electric field at a reduced temperature of -40°C for the four different ratio mixtures of the bimesogens FfO-5-OCB and FfO-7-OCB. The mixtures have all been doped with approximately 3.5% BDH1281.

From Figure 6.22 it is clear that the tilt angle achieved per unit applied field decreases as more of the FfO-5-OCB bimesogen is added. This observation combined with the fact that the pitches are similar for all four mixtures means that the flexo-elastic ratio decreases with an increase in the concentration of FfO-5-OCB. Table 6.18 summaries the typical flexo-elastic ratios measured for the four mixtures, and it is seen that the value of $\bar{e}/K$ falls as the concentration of FfO-5-OCB is increased.

Percentage of FfO-5-OCB	$\Delta\tan\phi/\Delta E$, $\mu m\ V^{-1}$	Selective reflection wavelength, nm	Pitch (calculated), nm	$\bar{e}/K$, $C\ N^{-1}\ m^{-1}$
19	0.0854	543	346	1.55
40	0.0772	530	338	1.44
60	0.0692	506	322	1.35
78	0.0688	498	317	1.36

Table 6.18 A comparison of the flexoelectric properties of the four different ratio mixtures of the bimesogens FfO-5-OCB and FfO-7-OCB.

From the results it can be seen that when two mixtures are mixed in a series of differing ratios it is found that the trend in the flexo-elastic ratio is discontinuous. However there seems to be no obvious relationship between the ratio of the two bimesogens and the flexo-elastic ratio, for example in this case the eutectic point was found to have a low value for the flexo-elastic ratio.

6.8 Conclusions

The aim of the work presented in this chapter was to examine the flexoelectro-optic properties of a homologous series of non-symmetric bimesogens. It was seen in Chapter 5 that the symmetric oxy-fluorobiphenyl bimesogens have good flexoelectric properties. However, the pure homologues show either no mesophases or mesophases that occur over a small temperature range. It was hypothesised that a new series of bimesogens combining an oxy-fluorobiphenyl mesogenic unit with an oxy-cyanobiphenyl unit would have mesophases with a greater temperature range. Additionally, it was hoped that because the oxy-cyanobiphenyl unit has a greater dipole moment than the oxy-cyanobiphenyl unit the flexoelectric properties of the new bimesogens would be higher. It was also expected that these new bimesogens would have a larger dielectric anisotropy than the symmetric bimesogens studied in Chapter 5, due to the mismatch between the dipoles of the two different mesogenic units.

A homologous series of the new non-symmetric bimesogens was synthesised and it was found that all the new materials were enantiotropic and exhibited a nematic phase. The temperature range of the nematic phase ranged from 2°C (for FfO-12-OCB) to 40°C (for

FfO-9-OCB). An odd-even effect was observed for the nematic to isotropic phase transition temperature, with the molecules with an even number of carbon atoms in the spacer group having a higher transition temperature.

To examine the flexoelectro-optic effect, chirality was introduced into the nematic phase by use of a chiral additive. The additive BDH1281 was chosen for its high twisting power. All the new non-symmetric bimesogens materials were doped with approximately 3.50% (w/w) BDH1281. The new chiral mixtures containing the bimesogenic material with an odd number of carbon atoms in the spacer group exhibited blue-reflecting Grandjean chiral nematic textures; however in general, for the "even" bimesogenic materials the Grandjean texture is more red. It was inferred that this difference in the reflection colour of the Grandjean texture indicated a difference in the pitch of the materials.

The flexoelectro-optic properties of all the chiral mixtures were studied in the uniform lying helix geometry. For the mixtures based on the bimesogens with an odd number of carbon atoms in the spacer group, it was found that the flexo-elastic ratio ranged from ~1.2 - 1.5 C N^{-1} m^{-1}. Tilt angles greater than 25° were measured for all the mixtures and the response times ranged from 50-800μs, depending on sample temperature. The helical pitch of the "odd" mixtures was measured to be approximately 300nm increasing to approximately 350nm as the temperature was reduced.

For the mixtures based on the bimesogens with an even number of carbon atoms in the spacer group it was found that the flexo-elastic ratio ranged from ~0.45 - 0.55 C N^{-1} m^{-1}. The maximum tilt angles measured ranged from 7° to 12° and the response times measured were less than 100μs. With the exception of the FfO-12-OCB mixture, the pitch of the "even" mixtures ranged from approximately 400-500nm, this confirms the inferences drawn from the colour of the Grandjean texture.

It was originally hypothesised that the non-symmetric bimesogens would have greater flexoelectric properties than the symmetric bimesogens studied in Chapter 5. This was found to be true in the case of the bimesogenic materials with an odd number of carbon atoms in the spacer group. However, for the "even" materials it was found that the flexo-elastic ratio was low, comparable to the 7OCB mixtures studied in Chapter 3. The experimental and theoretical work of Dilisi *et al.*[8] suggested that the elastic constants (K_{11}, K_{22} and K_{33}) would be significantly higher for the "even" bimesogenic materials, if this is the case then this would help explain the differences observed in the flexo-elastic ratio. Both the splay and twist elastic constants were measured for a selection of the non-symmetric bimesogens. It was found in both cases that the elastic constants were

significantly higher for the materials with an even number of carbon atoms in the spacer group. The difference in the twist elastic constant would explain the odd-even effect in the measured pitches. If the approximation is made that $K_{11} \approx K_{33}$ then it is possible to estimate values for $\bar{e}$. It was estimated for the "odd" materials that $\bar{e}$ is in the region of 9-10 pC m^{-1}, while for the "even" materials $\bar{e}$ was found to range from 6-7 pC m^{-1}. It the assumption that $K_{11} \approx K_{33}$ is valid then it would appear that $\bar{e}$ shows an odd-even effect. However, the experimental work of Dilisi *et al.*[8] showed that the behaviour of the bend elastic constant can be unpredictable.

In Chapter 5, it was observed that the flexo-elastic ratio of the symmetric bimesogens increased as the temperature was reduced. A similar observation was made for the non-symmetric bimesogens with an odd number of carbon atoms in the spacer group. It was hypothesised in Chapter 5 that the behaviour of K deviates from the predicted response deviates from the $S^2(T)$ dependence predicted by theory but unexpected behaviour in $\bar{e}$ cannot be ruled out. From Figure 6.13 it can be seen that the splay elastic constant appears to decrease with increasing temperature as the square of the order parameter. Thus it must be concluded that either the bend elastic constant or $\bar{e}$, which are also predicted to vary as $S^2(T)$, have an additional dependence on temperature.

It has been observed that when the concentration of chiral additive in a host material is varied, the pitch and flexoelectro-optic properties of the mixture also change. Unsurprisingly, it was found that the pitch length was shorter if a greater concentration of chiral additive was used. The tilt angles, response times and flexo-elastic ratio were all found to be lower for the mixture containing the greater concentration of chiral additive. The behaviour of the tilt angles and response times agrees with flexoelectro-optic theory; however, the decrease in the flexo-elastic ratio does not. It is hypothesised that the reason for this unusual behaviour is the same as given in Chapter 5, namely, $\bar{e}$ and K depend on the order parameter in different ways. Thus, if the concentration of chiral additive changes the order parameter (as seen in Chapter 3 for 7OCB) then the ratio of $\bar{e}$ and K would change.

In Chapter 5 it was seen that by making mixtures between two members of the symmetric bimesogenic homologous series, the temperature range of the nematic phase could be increased. As a result, mixtures between two of the non-symmetric bimesogenic materials were made, to see if the nematic temperature range could be increased. The two

homologues chosen were FfO-5-OCB and FfO-7-OCB; four different ratio mixtures were made. It was found for all four mixtures that the nematic range was significantly higher than that of either of the base homologues. The mixtures all super-cooled into a smectic phase, which is believed to be the smectic A* phase. The flexoelectro-optic properties of the four mixtures were examined. It was found that the flexo-elastic ratio as a function of concentration of FfO-5-OCB showed a discontinuous relationship. The 19%/81% FfO-5/7-OCB mixture showed the highest flexo-elastic ratio (1.55 C N^{-1} m^{-1}) of all the materials studied in this chapter. This suggests that the use of mixtures between different homologues, as well as increasing the temperature range of the mesophases over those of the base homologues, can also increase the flexo-elastic ratio over that of the pure host components.

References

1 Musgrave, B., Coles M. J., Perkins, S., and Coles, H. J., Mol. Cryst. Liq. Cryst. **366** 2587 (2001)

2 Meyer, R. B., Phys. Rev. Lett., **22(18)** 918 (1969)

3 Vorlander, D., Z. Phys. Chem., **126** 449 (1927)

4 Emsley, J. W., Luckhurst, G. R., and Shilstone, G. N., Mol. Cryst. Liq. Cryst. **53** 1023 (1984)

5 Merck NB-C, Southampton, UK

6 Coles, H. J., Musgrave B., Coles, M. J., Willmott, J., J. Mater. Chem. **11(11)** 2709 (2001)

7 Coles, H. J., Coles, M. J., Clarke, M. J., Blatch, A. E., and Ionescu, D., Liquid Crystal Medium and Liquid Crystal Display, EU Patent No. 02022328.5 (2002)

8 Dilisi, G. A., Terentjev, E. M., Griffin, A. C., and Rosenblatt, C., J. Phys. II **3(5)** 597 (1993)

9 Meyerhofer, D., J. Appl. Phys. **46(12)** 5084 (1975)

10 http://www.wayne-kerr.co.uk

11 Khoo, I. C., and Wu, S. T., The Optics and Nonlinear Optics of Liquid Crystals, World Scientific Publishing (1993)

Chapter Seven

7 The Effects of the Addition of Ester Groups to the Symmetric Bimesogens

7.1 Introduction

It was seen in Chapter five that when doped with a chiral additive the achiral symmetric bimesogens have strong flexoelectro-optic properties. It was theorised that the addition of ester linking groups to these molecules may increase the flexo-elastic ratio, $\bar{e}/K$. The reason for this hypothesis is that it would be expected that the inclusion of the unsaturated ester linkage would increase the dipole moment of the "individual" mesogens, compared with those of the molecules studied in Chapter five, thus resulting in greater flexoelectro-optic properties.[1] A predicted consequence of the addition of the ester groups was that the liquid crystallinity of the materials would be decreased as the molecules would deviate from the model of an "ideal" liquid crystal molecule, which is that of a long rod.[2] It was hoped that the benefit of a large increase in the flexo-elastic ratio could be reaped if a mixture between different homologues could be found which would increase the temperature ranges of the liquid crystal phases.

The bimesogens used in this work are based on the structure shown in Figure 7.1. The materials are denoted FfE-n-EfF, where n represents the number of carbon atoms in the spacer. These materials were synthesised by Andrew Blatch.

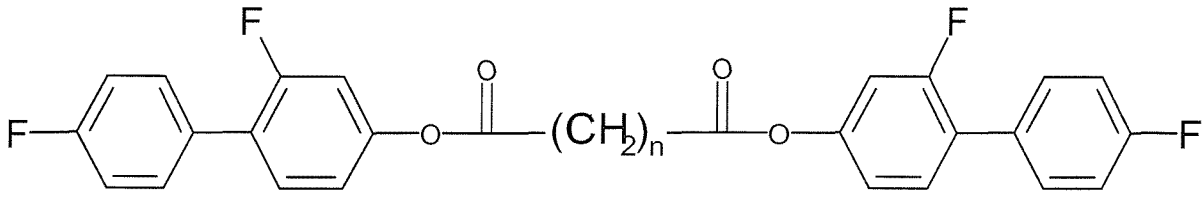

Figure 7.1 The generic structure of the bimesogens studied in this chapter, for simplicity denoted FfE-n-EfF, where n represents the number of carbon atoms in the spacer.

It would be expected that the dielectric anisotropy of these molecules would be similar to that of the materials studied in Chapter 5, since the "individual" dipoles of the two mesogenic groups would balance each other out to a certain degree.

7.2 The pure homologues

A range of homologues of different spacer lengths was produced for this work. The materials were initially examined using optical microscopy. The materials were placed on a glass slide and then covered with a glass slip. Table 7.1 lists the observations that were made.

Material	On Cooling (5°/min)	On Heating
FfE - 9 - EfF	**I** -(68°C)-> **N** -(53°C)-> **Crystal**	**Crystal** -(93°C)-> **I**
FfE - 10 - EfF	**I** -(86°C)-> **N** -(84°C)-> **Crystal**	**Crystal** -(106°C)-> **I**
FfE - 11 - EfF	**I** -(68°C)-> **N** -(65°C)-> **Crystal**	**Crystal** -(96°C)-> **I**
FfE - 12 - EfF	**I** -(93°C)-> **Crystal**	**Crystal** -(107°C)-> **I**
FfE - 14 - EfF	**I** -(99°C)-> **Crystal**	**Crystal** -(108°C)-> **I**

Table 7.1 Initial microscopy observations of transition temperatures for pure homologues.

From these initial measurements it can be seen that only some of the materials exhibit a liquid crystal phase, with only the FfE-9-EfF material having a liquid crystal phase temperature range greater than a few degrees. All of the homologues are monotropic only exhibiting a liquid crystalline phase on cooling. There is evidence of an odd-even effect in the clearing temperature of the materials, which was expected given the behaviour of the homologues series discussed previously in this work.

As the FfE-9-EfF and FfE-11-EfF materials both show a liquid crystal phase on cooling, and these materials have lower transition temperatures than the other homologues, the most promising course of action was to make mixtures between these two homologues.

As the homologues are naturally achiral, chirality was introduced to the system using the chiral additive BDH1281.[3] Only a small percentage (< 5%) of BDH1281 is required to make an achiral nematic sufficiently chiral to be used for flexoelectro-optic switching. A new mixture between 51% FfE-9-EfF and 49% FfE-11-EfF was doped with 3.48% BDH1281 (where all percentages are measured by weight), was studied between coverslips using an optical microscope.

The transition temperatures were (on cooling at 5°C/minute):

Isotropic -(65°C)-> **N*** -(43°C)-> **Crystal.**

On heating, the material showed no liquid crystal phases before melting into the isotropic phase. The Grandjean texture of the chiral nematic phase was dark blue, which suggests a pitch of significantly less than 400nm however no blue phases were detected, though this does not mean they were not present! Both the achiral and chiral materials would crystallise if left in the liquid crystal phase for any length of time (typically anymore than fifteen minutes).

7.3 The flexoelectro-optic properties of the doped homologues

As discussed in Section 7.2, it is possible to induce chirality into an achiral phase by adding a chiral dopant. In this section the flexoelectro-optic properties of the doped mixture of the FfE-9-EfF and FfE-11-EfF homologues is examined.

The material described in Section 7.2 (denoted 3.48% BDH1281 in 51/49 FfE-9/11-EfF for simplicity) was placed in a commercially made planar glass cell of thickness 5.63 μm. To measure the flexoelectro-optic properties of the material it was necessary for it to adopt the uniformly lying helix geometry, this was achieved by cooling the mixture rapidly from the isotropic phase under an applied electric field. This method produced reasonable alignment. It also was possible to achieve an acceptable level of alignment by shearing the cell in the chiral nematic phase with an applied field. With the material in the uniformly lying helix geometry it was possible to measure its flexoelectro-optic switching properties. The selective reflection wavelength and pitches were also measured and the results are shown together with the switching properties in Figure 7.2.

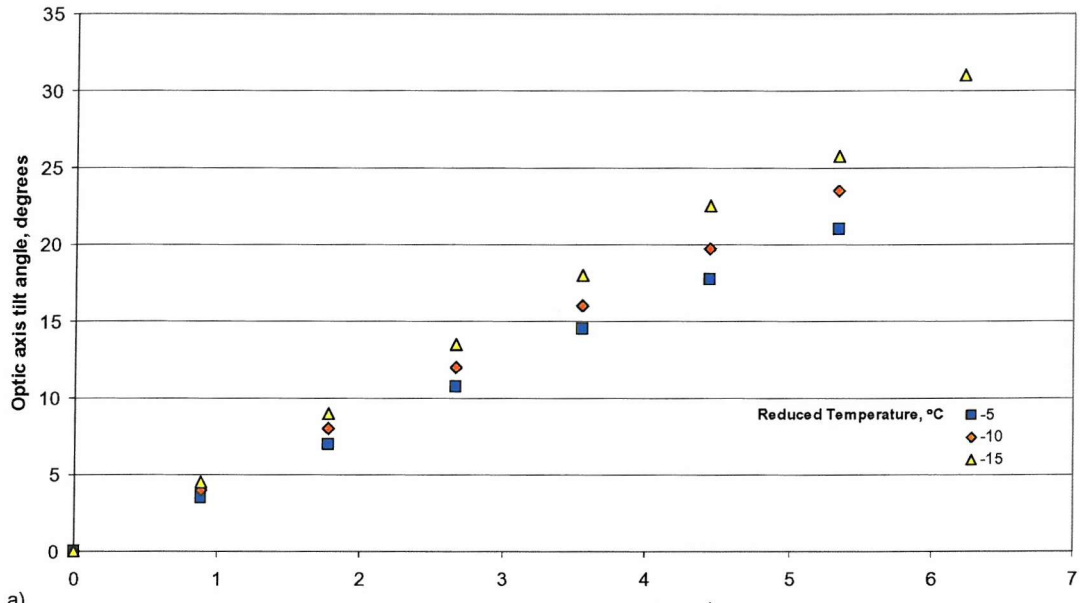
Optic axis tilt angle, degrees
Applied field amplitude, V µm-1
Reduced Temperature, °C
-5
-10
-15

a)

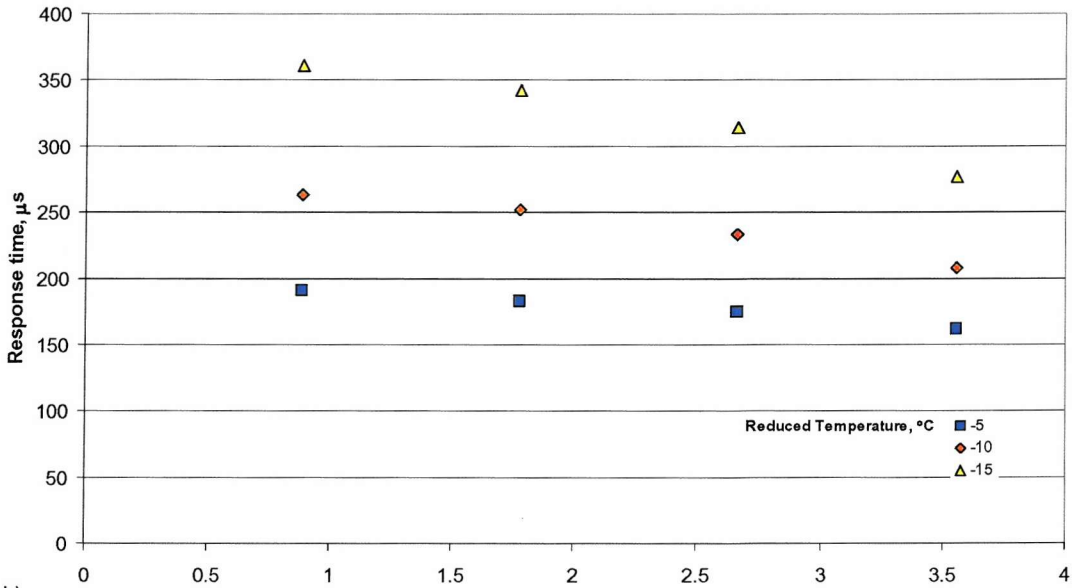
Response time, µs
Applied field amplitude, V µm-1
Reduced Temperature, °C
-5
-10
-15

b)

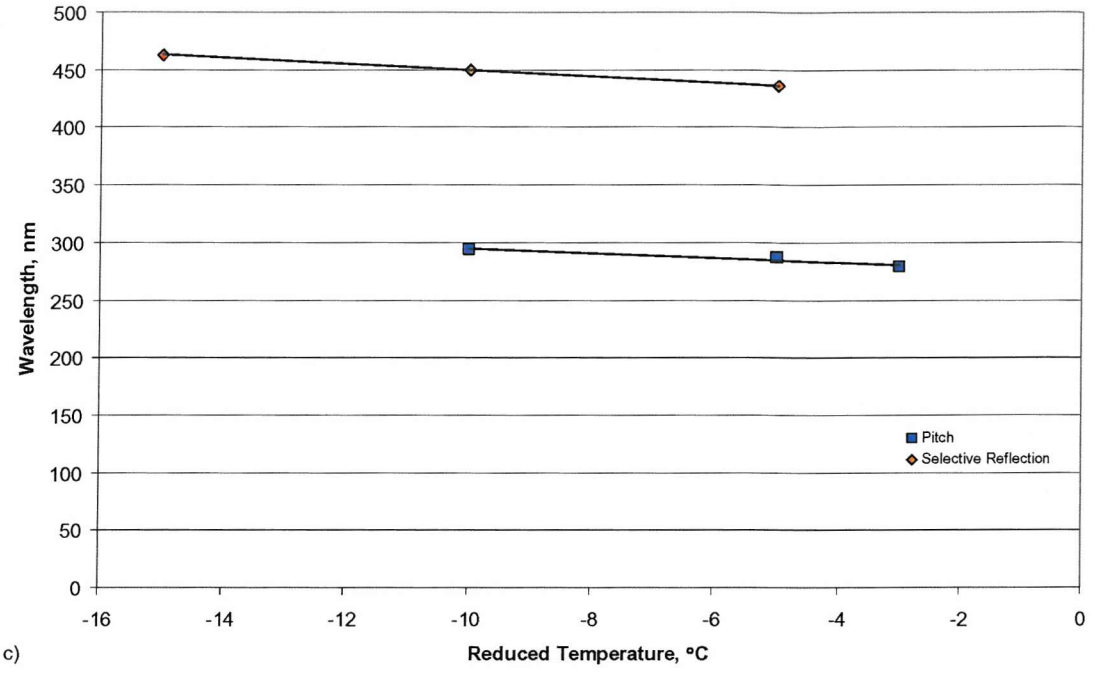

Figure 7.2 The properties of a mixture of 3.48% BDH1281 in 51/49 FfE-9/11-EfF (w/w). The graphs show a) the induced tilt angles, b) the response times and c) selective reflection wavelength and pitch, all measured across a range of reduced temperatures. The response times are measured for 10-90% of the full switch of the optic axis, i.e. twice the tilt. The selective reflection properties were measured using a UV-visible spectrometer and the pitch was measured using a wedge cell of angle 0.027°. Trend-lines were added to guide the eye.

The results in Figure 7.2 were used to calculate the flexo-elastic ratio and average refractive index, the calculations are summarised in Table 7.2.

Reduced Temperature, °C (T_c = 65°C)	$\Delta\tan\phi/\Delta E$, μm V^{-1}	Pitch, nm	Selective reflection wavelength, nm	$\bar{n}$	$\bar{e}/K$, C N^{-1} m^{-1}
-5	0.0726	287	436	1.52	1.59
-10	0.0816	294	450	1.53	1.74
-15	0.0949	-	463	-	-

Table 7.2 A comparison of the values at different reduced temperatures for the pitch, selective reflection wavelength and the calculated values for the average refractive index

and the ratio of the effective flexoelectric coefficient and the average of the splay and bend elastic constants. The material studied was 3.48% BDH1281 in 51/49 FfE-9/11-EfF.

The values for the flexo-elastic ratio are the highest measured in this work so far, which justifies the decision to study this material. The average refractive index seems slightly lower than expected; this is probably a consequence of the conditions in which the selective reflection and pitch were measured.

The pitch and selective reflection wavelength measurements for each temperature were made in relatively quick succession because the material would crystallise if left too long, and as a result the material may not have reached thermal equilibrium when the measurement was taken, leading to larger uncertainties in the pitch and selective reflection measurements.

The tilt angles per unit field for this mixture are very high, over twice that of the bimesogenic mixtures studied in Chapter 5 and of which these base homologues are a modification. The tilt angles measured above are compared directly to the 3.42% in 20/80 FfO-7/9-OfF mixture which was studied in Chapter 5 in Figure 7.3. The pitches of the two materials are reasonably similar with the "ester" material having a longer pitch by approximately ten percent, which should not have a strong effect on the difference in tilt angles.

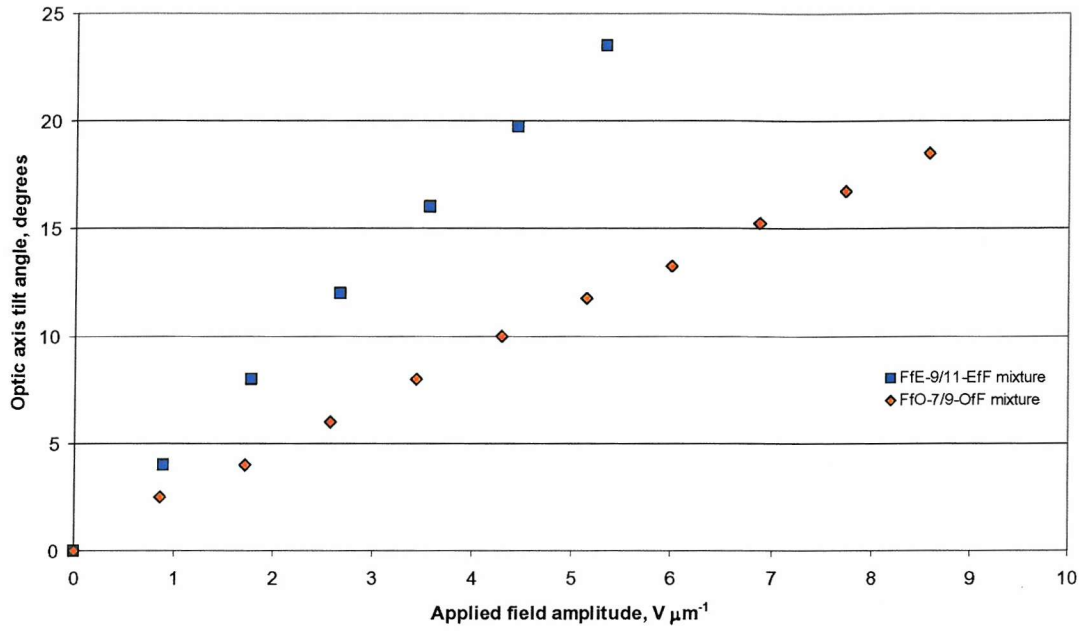

Figure 7.3 A direct comparison of the tilt angles as a function of applied electric field of 3.48% BDH1281 in 51/49 FfE-9/11-EfF and 3.42% in 20/80 FfO-7/9-OfF. Both sets of measurements were made at a reduced temperature of -10°C.

From Figure 7.3 it can be seen that the tilt angles for the FfE-9/11-EfF material are approximately twice that of the FfO-7/9-OfF material which is a very significant result. The response times are very different when compared at the same reduced temperature (the FfO-7/9-OfF material is approximately 50% slower). However when compared at similar absolute temperatures the response times are comparable.

In this section it has been seen that the new ester-linked symmetric bimesogenic materials can produce a high flexo-elastic ratio. However the liquid crystal phase is monotropic. The next progression in this work was to try mixing these high $\bar{e}/K$ materials with materials with a greater liquid crystal phase range and stability.

7.4 Mixing the symmetric ester materials with the non-symmetric materials

7.4.1 The effects of varying the concentrations of the materials

In the previous section it was seen that the symmetric ester materials have a high flexo-elastic ratio but low liquid crystallinity, as a result it was decided to try mixing these materials with the non-symmetric bimesogens studied in Chapter six.

As a test of the suitability of mixing these two materials, a beginning was made by studying a mixture of fifty percent of a symmetric ester material and fifty percent of a non-symmetric material (w/w). The symmetric ester material chosen was the mixture described in Section 7.3 and the non-symmetric material chosen was the 19/81 FfO-5/7-OCB from Chapter six. This particular material was chosen as it had the highest flexo-elastic ratio of all the non-symmetric materials studied.

3.45% BDH1281 in 50% [49/51 FfE-9/11-EfF] + 50% [19/81 FfO-5/7-OCB]

The material was studied using optical microscopy and was found to exhibit the following phase sequences:

Isotropic –(85°C)-> **Blue Phases** –(80°C)-> **N*** –(33°C)-> **SmX*** (On cooling)

SmX* –(34°C)-> **N*** –(84°C)-> **Blue Phases** –(85°C)-> **Isotropic** (On heating)

There were at least two and maybe a third blue phase observed on cooling from the isotropic phase. There was a rapid change in the colour of the Grandjean texture observed below 40°C; this is a result of the pitch lengthening before the transition from the chiral nematic phase to the smectic phase. The smectic phase appeared to be similar to those observed for the non-symmetric materials described in Section 6.7, and it is believed to smectic A*. This material tends to crystallise if left for too long at lower temperatures, once crystallised it was found that it melts in to the chiral nematic phase at 68°C on heating.

It was possible to achieve very good lying helix alignment for measuring the flexoelectro-optic properties using the field ramping material described in Section 6.4.1 (despite the material not quite adopting the homeotropic alignment when the maximum available electric field was applied). The flexoelectro-optic switching properties of the mixture were measured, along with the selective reflection wavelength and pitch, which were measured with the material aligned in the Grandjean texture. The results are shown in Figure 7.4.

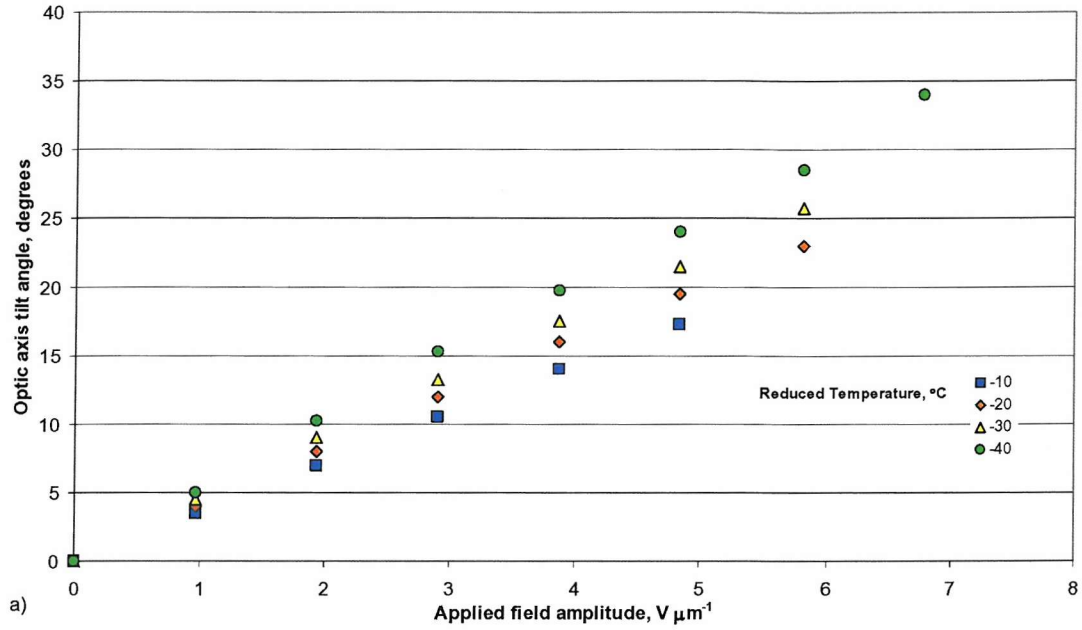
Optic axis tilt angle, degrees
Applied field amplitude, V µm-1
Reduced Temperature, °C
-10
-20
-30
-40

a)

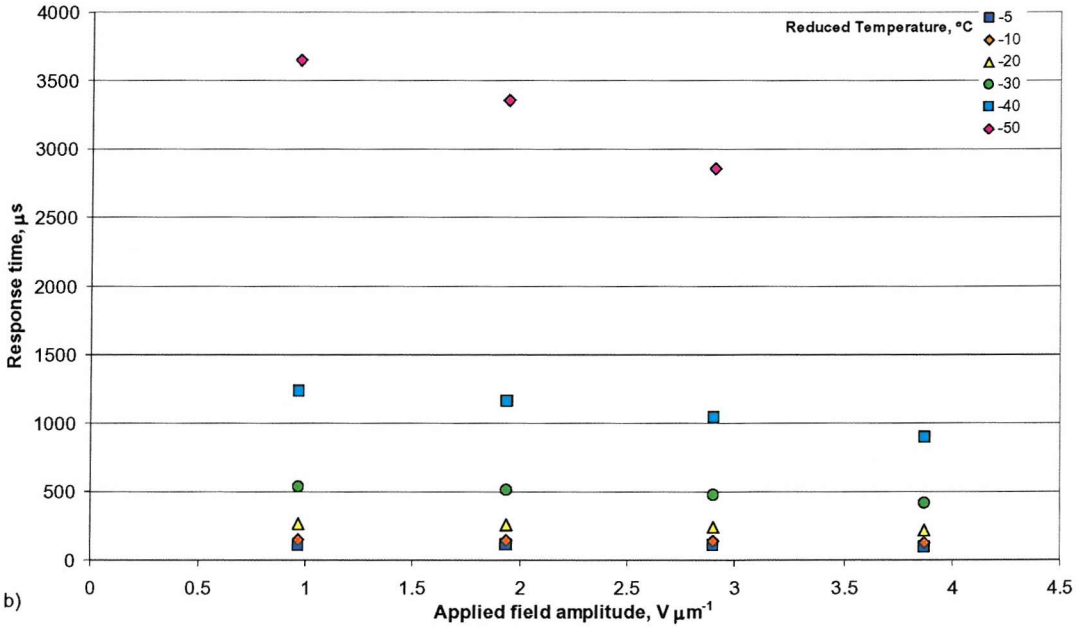
Response time, µs
Applied field amplitude, V µm-1
Reduced Temperature, °C
-5
-10
-20
-30
-40
-50

b)

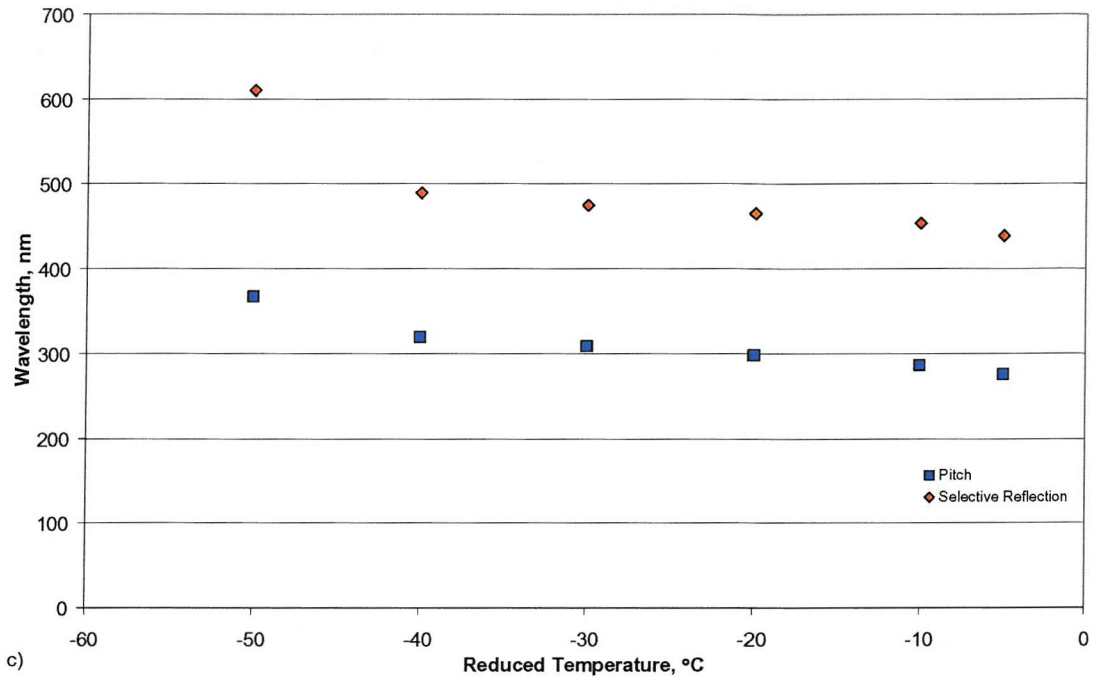

Figure 7.4 The properties of a mixture of 3.45% BDH1281 in 50% [49/51 FfE-9/11-EfF] + 50% [19/81 FfO-5/7-OCB] (w/w). The graphs show a) the induced tilt angles, b) the response times and c) selective reflection wavelength and pitch, all measured across a range of reduced temperatures. The response times are measured for 10-90% of the full switch of the optic axis, i.e. twice the tilt. The selective reflection properties were measured using a UV-visible spectrometer and the pitch was measured using a wedge cell of angle 0.030°.

Figure 7.4(a) shows that large tilt angles are achievable with this new mixture and (c) shows the rapid change in pitch as the smectic phase is approached. From the results in Figure 7.4 it was possible to calculate the flexo-elastic ratio and the average refractive index. The results are shown in Table 7.3.

Reduced Temperature, °C (T_c = 85°C)	$\Delta\tan\phi/\Delta E$, μm V^{-1}	Pitch, nm	Selective reflection wavelength, nm	$\bar{n}$	$\bar{e}/K$, C N^{-1} m^{-1}
-5	0.0582	276	440	1.59	1.33
-10	0.0644	286	454	1.59	1.42
-20	0.0737	298	466	1.56	1.55
-30	0.0825	309	476	1.54	1.68
-40	0.0932	319	490	1.54	1.84
-50	0.1141	367	611	1.66	1.95

Table 7.3 A comparison of the values at different reduced temperatures for the pitch, selective reflection wavelength and the calculated values for the average refractive index and the ratio of the effective flexoelectric coefficient and the average of the splay and bend elastic constants. The material studied was 3.45% BDH1281 in 50% [49/51 FfE-9/11-EfF] + 50% [19/81 FfO-5/7-OCB].

From Table 7.3 it can be seen that a very large value for the flexo-elastic ratio was achieved and that it varies strongly with temperature, much more significantly that observed in previous chapters. The average refractive index seems to be reasonably stable with sensible values bar the final value which appears to be an anomalous measurement. This anomalous result is believed to be a result of the coarseness of the Mettler[4] temperature controller used to measure the selective reflection wavelength. In the temperature region slightly above the smectic phase transition the gradient of pitch against temperature is very steep and as a result any inaccuracy in the temperature control has a larger effect than in a temperature range where the pitch is relatively constant.

If the gradient of the tangent of ϕ as a function of applied field is compared for this mixture with that of the pure symmetric ester mixture studied in Section 7.3, it can be seen that it is higher for the pure symmetric ester mixture by approximately 25%. This would suggest that the addition of the non-symmetric material dilutes the flexoelectric properties of the symmetric ester material.

At a reduced temperature of -50°C, i.e. slightly above the smectic phase transition, interesting results were measured for the tilt angles, the results of which are shown in Figure 7.5.

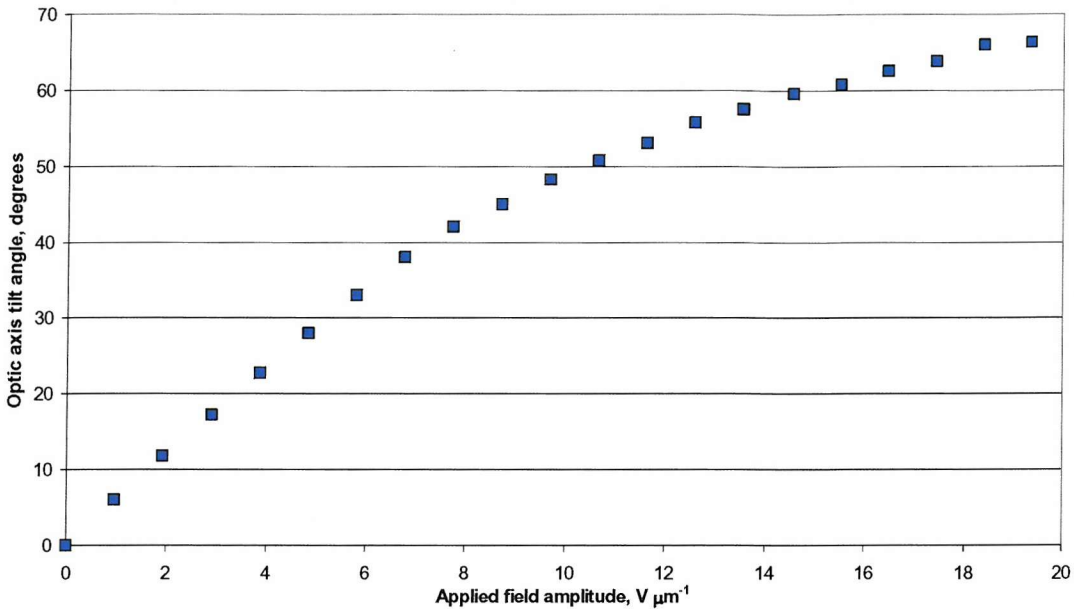

Figure 7.5 The tilt angles measured using for the material 3.45% BDH1281 in 50% [49/51 FfE-9/11-EfF] + 50% [19/81 FfO-5/7-OCB] at a reduced temperature of -50°C.

The alignment of the lying helix starts to degrade when the applied field exceeds approximately 7 V/μm (corresponding to a tilt angle of 38°), however a dark and light state is still observable and this remains the case up to nearly 20 V/μm, where the alignment is severely disrupted by dielectric coupling. The maximum tilt angle measured was approximately 66° and this was confirmed by using the rotating analyser[5] technique for measuring the tilt angle. Further measurements were limited by the available equipment for generating an applied electric field available in the laboratory; 20 V/μm was the maximum field safely achievable. The high tilt angles are a result of the long helical pitch at this reduced temperature, so close to the smectic phase transition (recall that tilt angle per applied field is inversely proportional to the pitch). Of course such high tilt angles are only possible if flexoelectro-optic switching can occur at these high applied fields and for this to happen the critical field for helix unwinding must be high.

In previous chapters it was seen that in mixtures between two materials, it was possible for the flexo-elastic ratio to vary depending on the relative concentrations of the two components in the mixture. For completeness, two further mixtures were made, containing different percentages of the symmetric ester materials and the non-symmetric materials. The flexoelectro-optic properties of these two materials were studied.

3.47% BDH1281 in 28% [50/50 FfE-9/11-EfF] + 72% [20/80 FfO-5/7-OCB]

This material was studied using optical microscopy and was found to exhibit the following phase sequences:

Isotropic –(96°C)-> **Blue Phases** –(92°C)-> **N*** –(38°C)-> **SmX*** (On cooling)

SmX* –(38°C)-> **N*** –(95°C)-> **Blue Phases** –(96°C)-> **Isotropic** (On heating)

As for the previous mixture, at least two blue phases were observed, as well as the rapid pitch change on cooling the mixture towards the smectic phase transition.

It was possible to achieve very good alignment for measuring the flexoelectro-optic properties using the field ramping material (despite the material not quite adopting the homeotropic alignment when the maximum available electric field was applied). With the uniformly lying helix geometry adopted the flexoelectro-optic switching properties were measured, and the selective reflection wavelength and pitch were measured with the mixture in the Grandjean texture. All the results are shown in Figure 7.6.

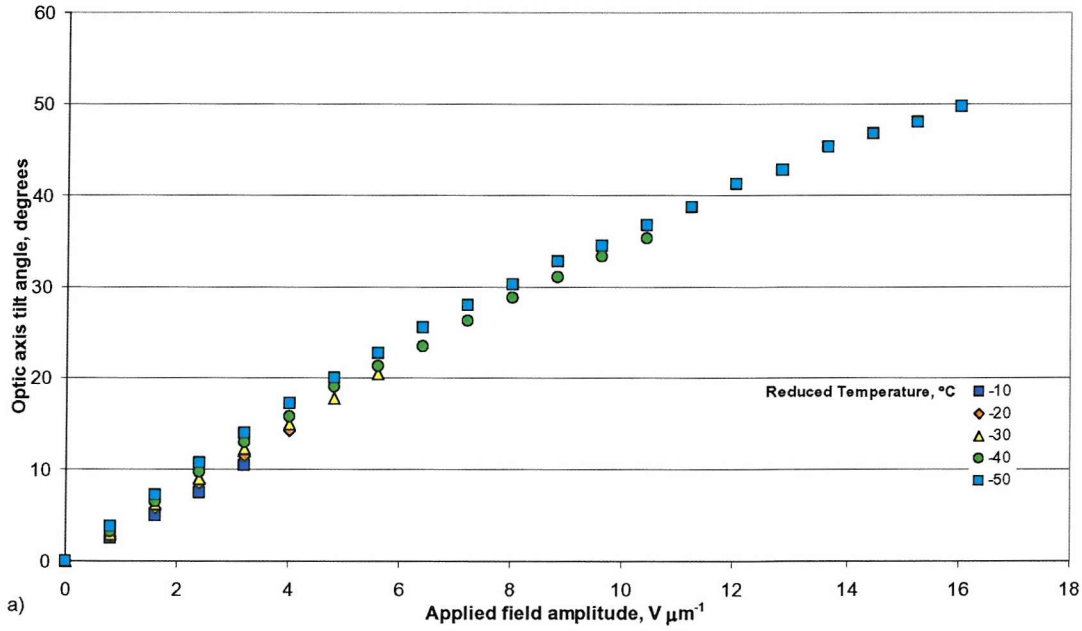

a)

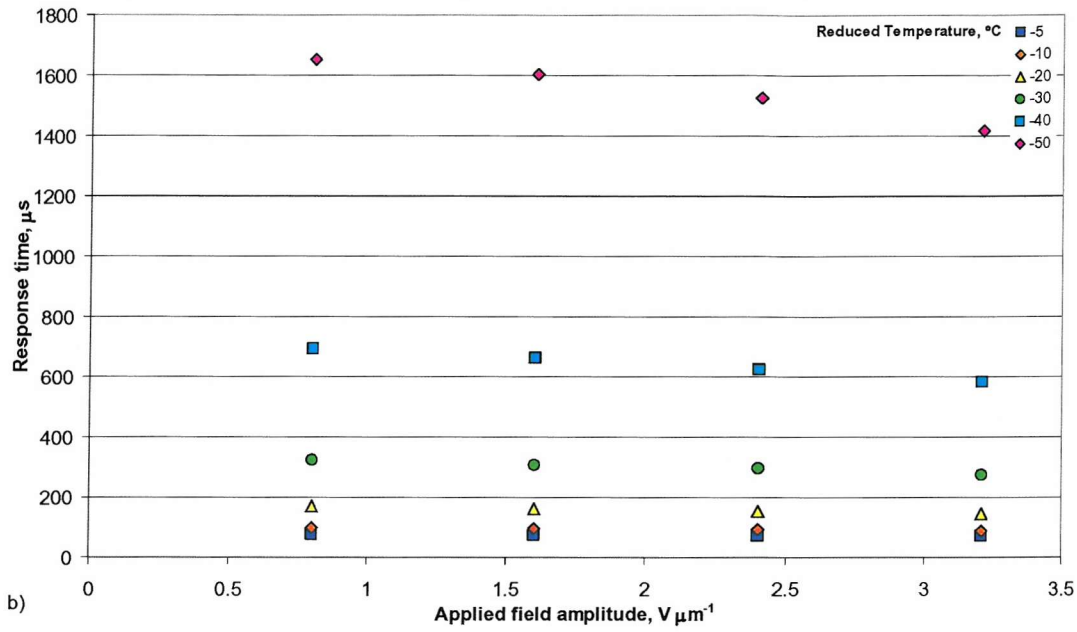

b)

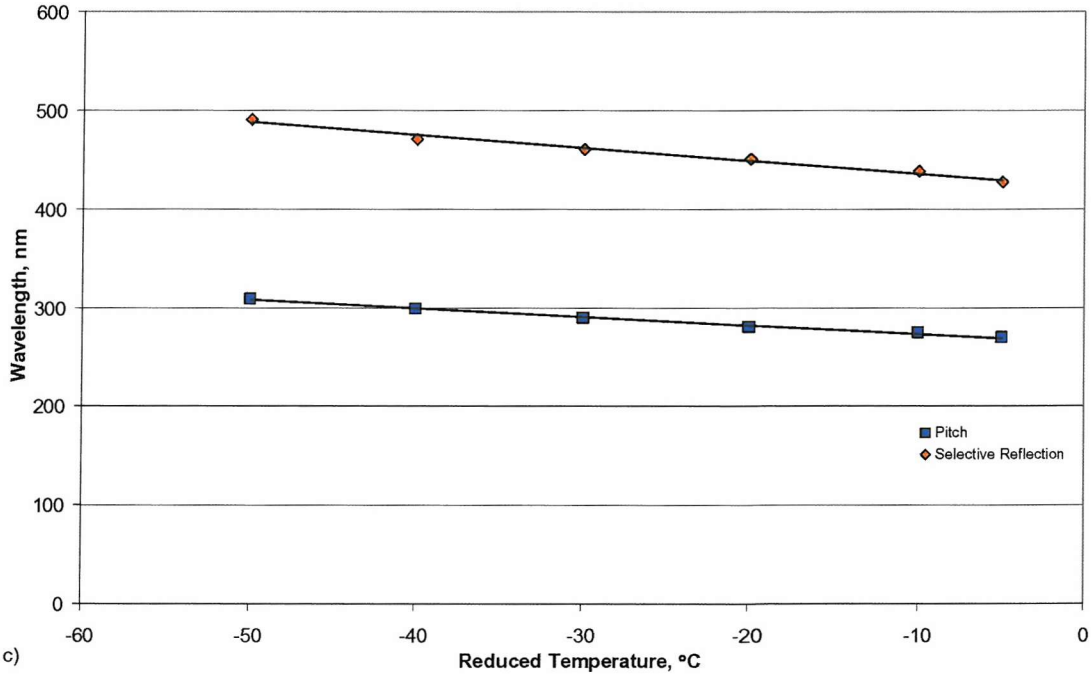

c)

Figure 7.6 The properties of a mixture of 3.47% BDH1281 in 28% [50/50 FfE-9/11-EfF] + 72% [20/80 FfO-5/7-OCB] (w/w). The graphs show a) the induced tilt angles, b) the response times and c) selective reflection wavelength and pitch, all measured across a range of reduced temperatures. The response times are measured for 10-90% of the full switch of the optic axis, i.e. twice the tilt. The selective reflection properties were measured using a UV-visible spectrometer and the pitch was measured using a wedge cell of angle 0.017°. Trend-lines were added to guide the eye.

From the results in Figure 7.6 it was possible to calculate the flexo-elastic ratio and the average refractive index, which are shown in Table 7.4.

Reduced Temperature, °C (T_c = 96°C)	$\Delta\tan\phi/\Delta E$, μm V^{-1}	Pitch, nm	Selective reflection wavelength, nm	$\bar{n}$	$\bar{e}/K$, C N^{-1} m^{-1}
-5	0.0556	269	427	1.59	1.30
-10	0.0572	274	439	1.60	1.31
-20	0.0636	280	451	1.61	1.43
-30	0.0667	289	461	1.60	1.45
-40	0.0713	299	471	1.58	1.50
-50	0.0759	309	491	1.59	1.54

Table 7.4 A comparison of the values at different reduced temperatures for the pitch, selective reflection wavelength and the calculated values for the average refractive index and the ratio of the effective flexoelectric coefficient and the average of the splay and bend elastic constants. The material studied was 3.47% BDH1281 in 28% [50/50 FfE-9/11-EfF] + 72% [20/80 FfO-5/7-OCB].

Table 7.4 shows that for this material the flexo-elastic ratio is reasonably high, it is on a par with that of the non-symmetric mixture used as part of this material. The values for the flexo-elastic ratio are approximately 28% less than that of the pure non-symmetric ester material in Section 7.3 indicating a dilution of the flexoelectric properties.

3.44% BDH1281 in 74% [50/50 FfE-9/11-EfF] + 26% [19/81 FfO-5/7-OCB]

This material was studied using optical microscopy and was found to exhibit the following phase sequences:

Isotropic –(74°C)-> **Blue Phases** –(72°C)-> **N*** –(30°C)-> **SmX*** (On cooling)

SmX* –(31°C)-> **N*** –(72°C)-> **Blue Phases** –(74°C)-> **Isotropic** (On heating)

This material tends to crystallise if left for too long at lower temperatures, once crystallised it was found that it melts in to the chiral nematic phase at 64°C on heating. As for the

previous mixture, at least two blue phases were observed as well as the rapid pitch change approaching the smectic phase transition.

As with the previous two materials it was possible to achieve very good alignment for measuring the flexoelectro-optic properties by using the field ramping material (despite the material not quite adopting the homeotropic alignment when the maximum available electric field was applied). The selective reflection and pitches were measured with the material in the Grandjean texture. The results for all are shown in Figure 7.7.

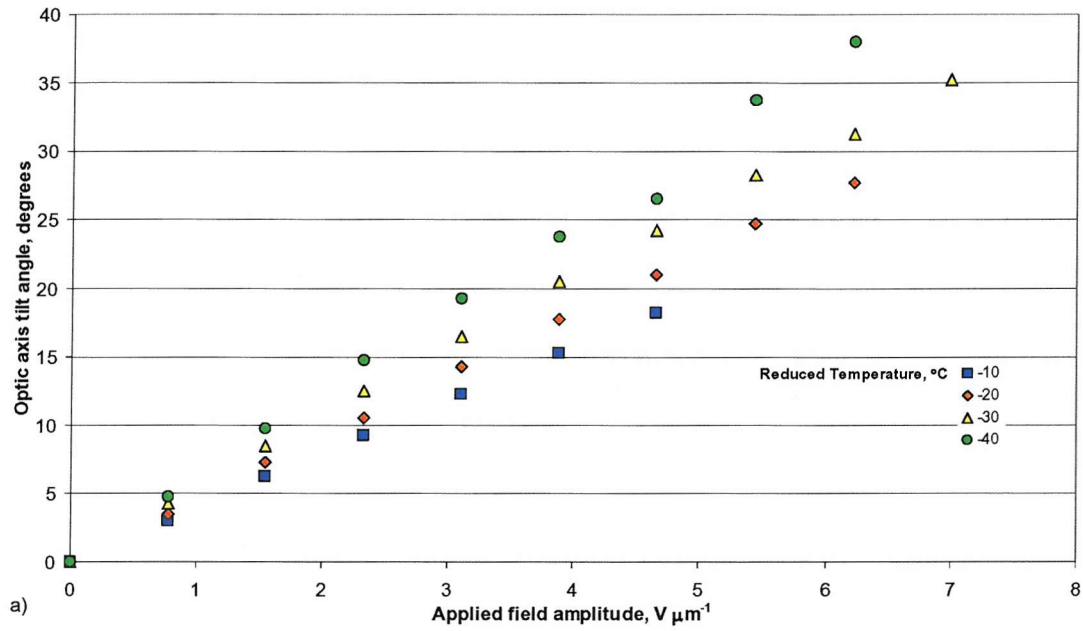

a)

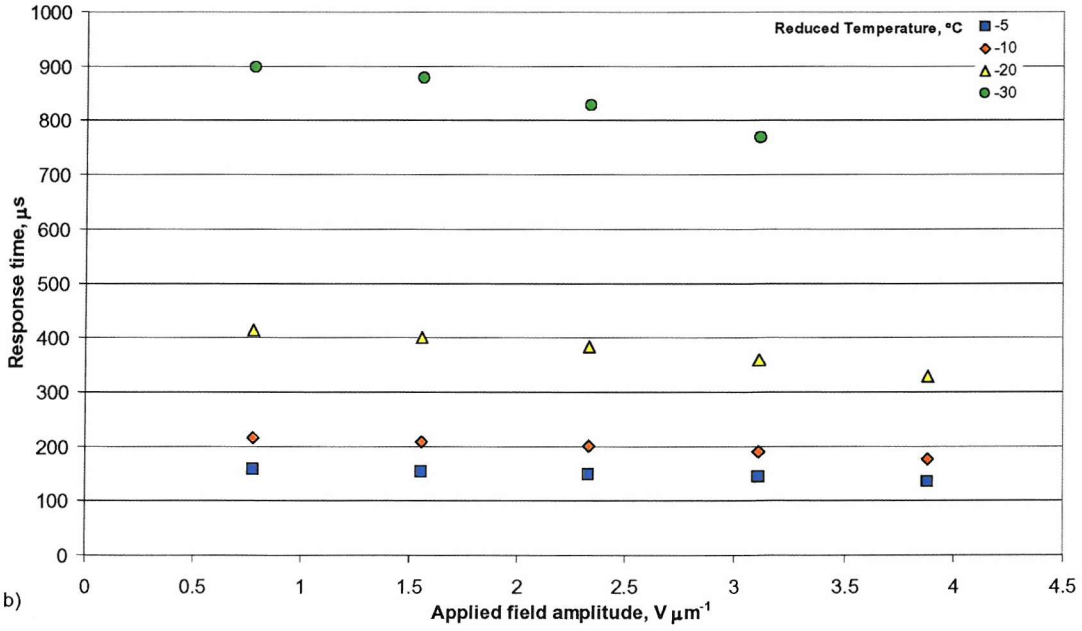

b)

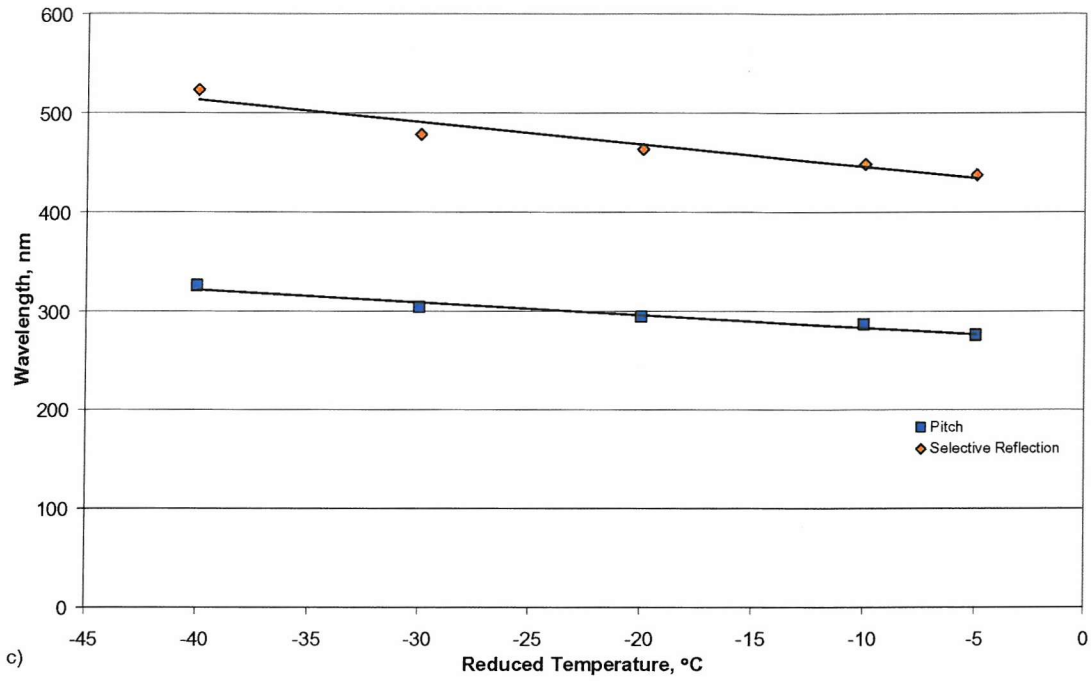

c)

Figure 7.7 The properties of a mixture of 3.44% BDH1281 in 74% [50/50 FfE-9/11-EfF] + 26% [19/81 FfO-5/7-OCB] (w/w). The graphs show a) the induced tilt angles, b) the response times and c) selective reflection wavelength and pitch, all measured across a range of reduced temperatures. The response times are measured for 10-90% of the full switch of the optic axis, i.e. twice the tilt. The selective reflection properties were measured using a UV-visible spectrometer and the pitch was measured using a wedge cell of angle 0.030°. Trend-lines were added to guide the eye.

When measuring the tilt angles at a reduced temperature of -40°C the material would crystallise quickly, hence a full set of measurements up to the onset of dielectric coupling was were impossible to complete. Likewise the pitch and selective reflection measurements at -40°C were taken quickly as a result of rapid crystallisation. From the results in Figure 7.7 it was possible to calculate the flexo-elastic ratio and the average refractive index. The results are shown in Table 7.5.

Reduced Temperature, °C (T_c = 74°C)	$\Delta\tan\phi/\Delta E$, μm V^{-1}	Pitch, nm	Selective reflection wavelength, nm	$\bar{n}$	$\bar{e}/K$, C N^{-1} m^{-1}
-5	0.0617	275	437	1.59	1.41
-10	0.0707	286	449	1.57	1.55
-20	0.0848	294	463	1.58	1.81
-30	0.0999	303	479	1.58	2.07
-40	0.1137	325	524	1.61	2.20

Table 7.5 A comparison of the values at different reduced temperatures for the pitch, selective reflection wavelength and the calculated values for the average refractive index and the ratio of the effective flexoelectric coefficient and the average of the splay and bend elastic constants. The material studied was 3.44% BDH1281 in 74% [50/50 FfE-9/11-EfF] + 26% [19/81 FfO-5/7-OCB].

From Table 7.5 it can be seen that the flexo-elastic ratio and the tilt per unit field are approaching that of the pure symmetric ester material studied in Section 7.3; this is understandable as this material is made up of a large percentage of the pure symmetric ester material.

The tilt angles for the three materials studied in this section are compared at the same reduced temperature in Figure 7.8.

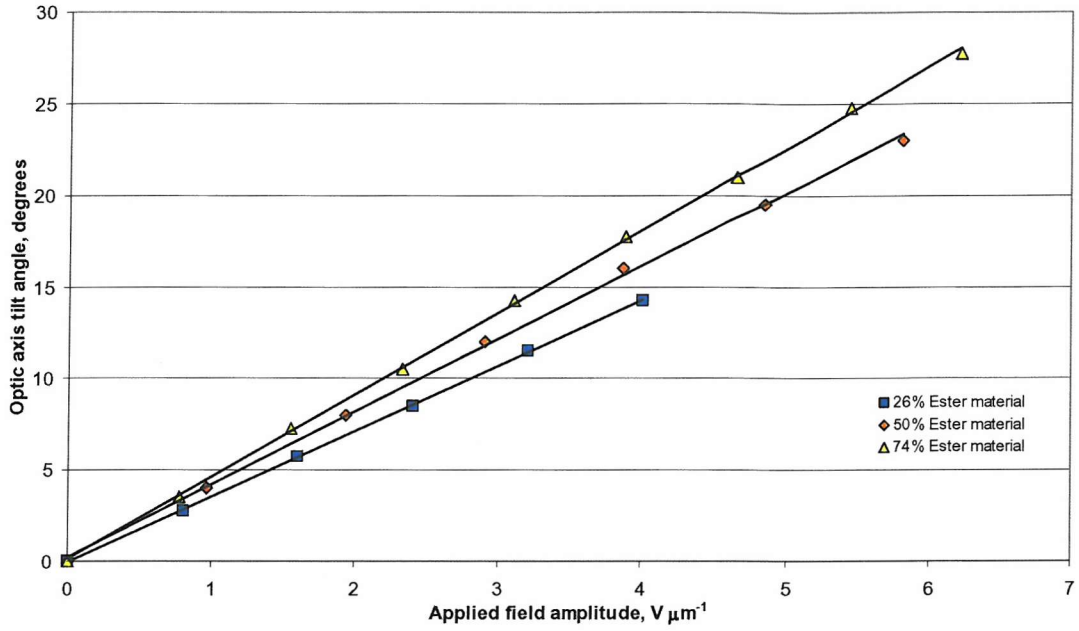

Figure 7.8 A comparison of the tilt angles of the three materials at a reduced temperature of -20°C.

It can clearly be seen from Figure 7.8 that the magnitude of the tilt angle for a given applied field is dependent on the concentration of the pure non-symmetric ester mixture present in the material. It is also apparent that the applied field at which dielectric coupling starts to disrupt the alignment is greater when a larger percentage of the ester mixture is present; this is due to the symmetric ester materials having a lower dielectric anisotropy than the non-symmetric material. Thus, the greater percentages of the symmetric esters homologues present in the mixture, the lower the dielectric anisotropy of the mixture.

The flexo-elastic ratio of all three materials at a number of reduced temperatures is compared in Figure 7.9.

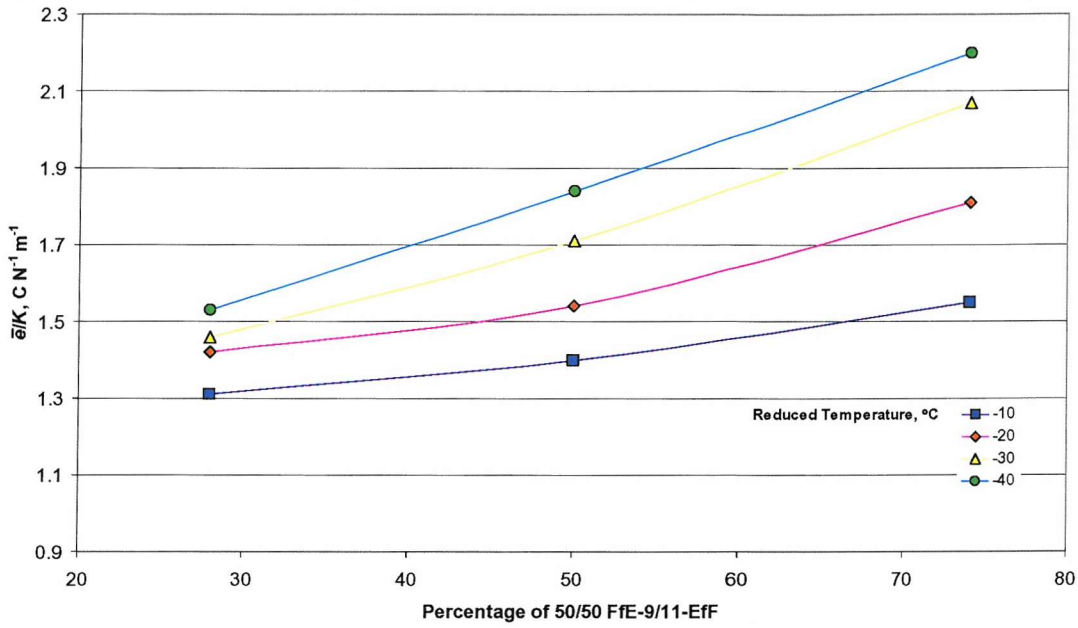

Figure 7.9 A comparison of the flexo-elastic ratio for the three materials studied in this section, at a number of reduced temperatures. Trend-lines were added to guide the eye.

Figure 7.9 graphically shows what was clear from Tables 7.3, 7.4 and 7.5, namely that the flexo-elastic ratio increases with the concentration of symmetric ester materials present. In Section 7.3 it was observed that the liquid crystallinity of the pure ester mixture was quite low, resulting in the mixture crystallising rapidly in the chiral nematic phase. It has been seen that, by mixing the esters with a suitable amount of a liquid crystal material of higher liquid crystallinity, it is possible to produce a stable material with a wide chiral nematic phase. This means that it may be possible to create a material with good flexoelectric properties and favourable phase ranges by selecting a suitable liquid crystal material to mix with the symmetric ester materials.

7.4.2 The effect on the flexoelectric properties of varying the concentration of chiral dopant

In Chapters 5 and 6 it was seen that when the chiral dopant BDH1281 was mixed with a liquid crystal material, the flexo-elastic ratio of the mixture decreases as the quantity of chiral dopant is increased. This is interesting because a material with a higher flexo-elastic ratio exhibits a greater tilt angle per unit applied field. In Section 7.4.1 it was seen that the material 3.45% BDH1281 in 50% [49/51 FfE-9/11-EfF] + 50% [19/81 FfO-5/7-OCB] could produce tilt angles of approximately 66° (measured using the maximum available

applied field). It was hoped that, by doping the same host material with less chiral additive it would be possible to obtain a larger maximum tilt angle. To test this, a mixture was made containing 1.46% BDH1281 in 52% [47/53 FfE-9/11-EfF] + 48% [20/80 FfO-5/7-OCB]. The mixture was found to have the following phase sequences:

Isotropic –(85°C)-> **N*** –(33°C)-> **SmX*** (On cooling)

SmX* –(33°C)-> **N*** –(85°C)-> **Isotropic** (On heating)

The material was found to align well using the field ramping technique. After the uniform lying helix alignment was achieved, the flexoelectro-optic switching properties were measured. Pitch measurements were also made, and all the results are shown in Figure 7.10.

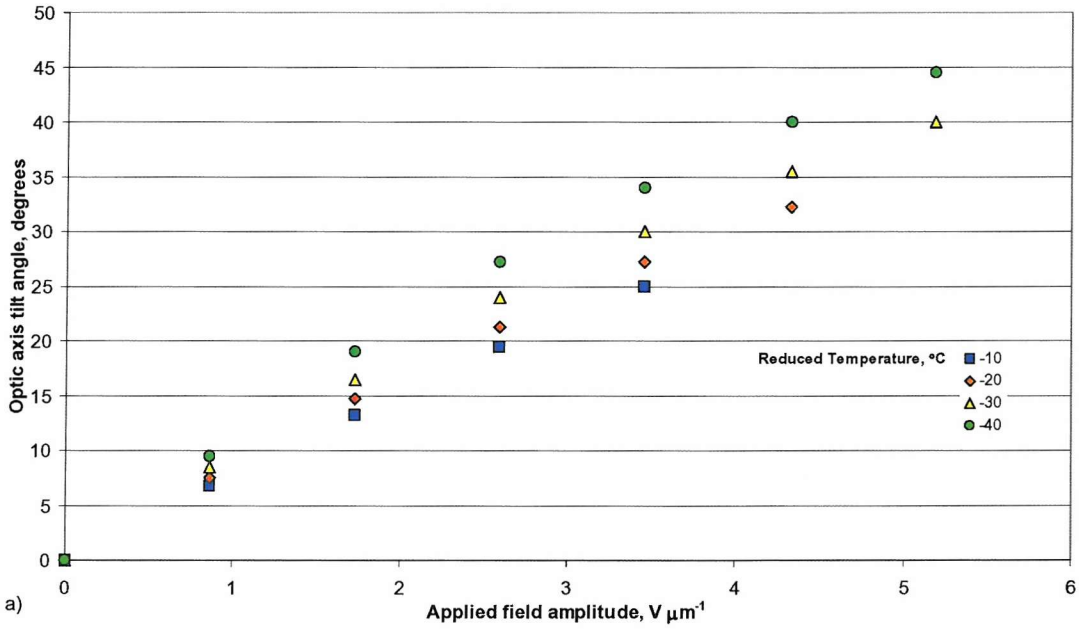

a)

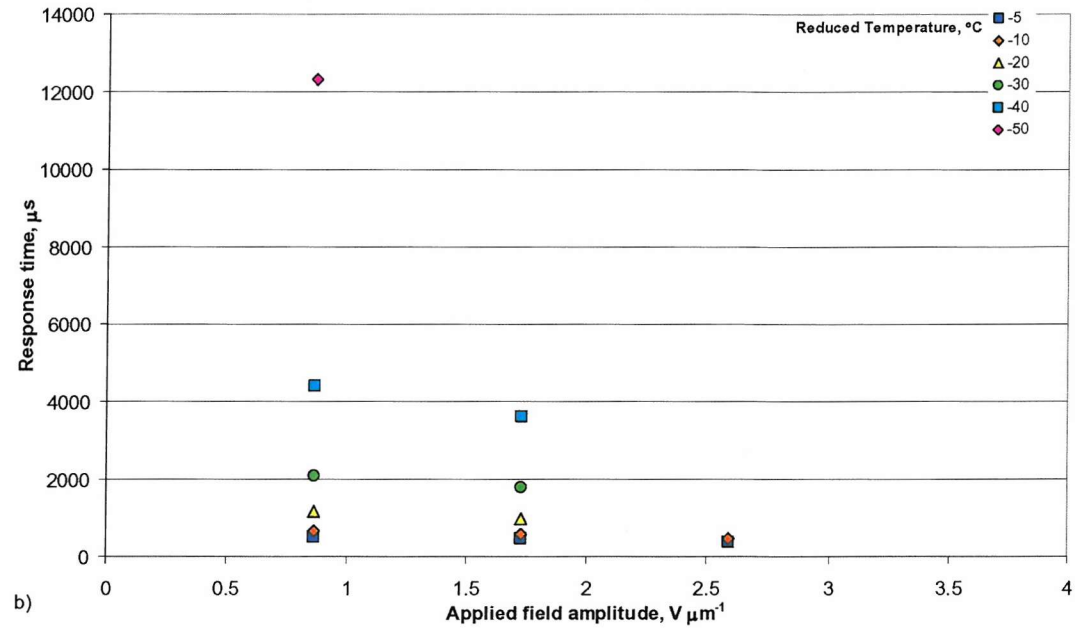

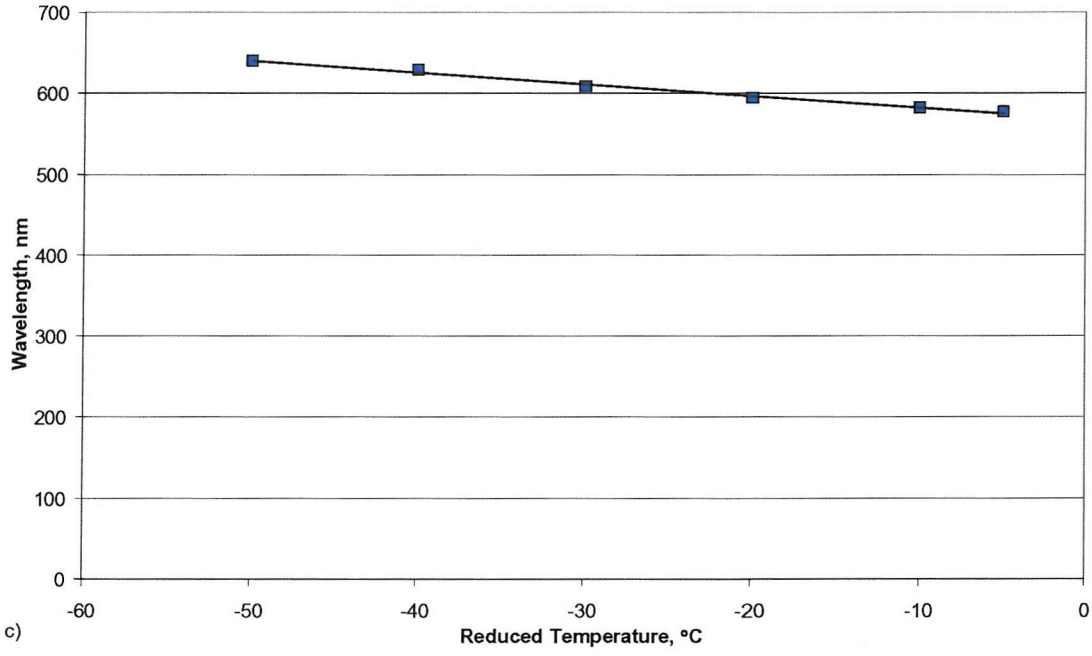

Figure 7.10 The properties of a mixture of 1.46% BDH1281 in 52% [47/53 FfE-9/11-EfF] + 48% [20/80 FfO-5/7-OCB] (w/w). The graphs show a) the induced tilt angles, b) the response times and c) pitch, all measured across a range of reduced temperatures. The response times are measured for 10-90% of the full switch of the optic axis, i.e. twice the tilt. The pitch was measured using a wedge cell of angle 0.032°. Trend-line added to guide the eye.

Figure 7.10 shows firstly that the tilt angles per unit applied field are very high and secondly the response times are relatively long. No selective reflection wavelength measurements were made as the reflected wavelengths were outside the range of the UV-visible spectrometer. In Section 7.4.1 it was seen that at a reduced temperature of -50°C the 3.45% BDH1281 in 50% [49/51 FfE-9/11-EfF] + 50% [19/81 FfO-5/7-OCB] material produced tilt angles of approximately 66°. Figure 7.11 shows the tilt angles produced under the same conditions for the new material with less chiral dopant. The tilt angles shown in Figure 7.11 were measured using two methods, firstly by optical microscopy and secondly using the rotating analyser method.[5]

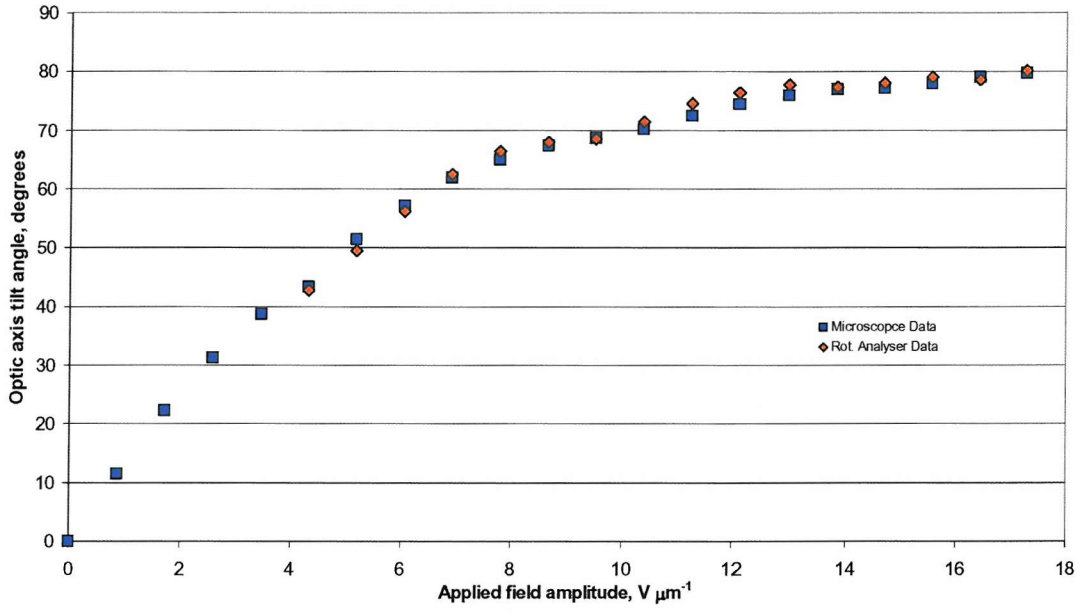

Figure 7.11 A comparison of the tilt angles measured using two different methods for the material 1.46% BDH1281 in 52% [47/53 FfE-9/11-EfF] + 48% [20/80 FfO-5/7-OCB].

The alignment of the lying helix starts to degrade when the applied field exceeds approximately 6 V/μm. However switching is still observable and this remains the case up to approximately 18 V/μm, where the alignment is severely disrupted by dielectric coupling. The maximum tilt angle measured was approximately 80°, which gives a total switching angle of 160°.

From the results in Figure 7.10 it was possible to calculate the flexo-elastic ratios. The results of which are shown in Table 7.6.

Reduced Temperature, °C (T_c = 85°C)	$\Delta\tan\phi/\Delta E$, μm V^{-1}	Pitch, nm	$\bar{e}/K$, C N^{-1} m^{-1}
-5	0.1233	568	1.36
-10	0.1353	572	1.49
-20	0.1491	584	1.60
-30	0.1680	589	1.79
-40	0.1965	616	2.00
-50	0.2326	623	2.35

Table 7.6 A comparison of the values at different reduced temperatures for the pitch and the calculated value for the ratio of the effective flexoelectric coefficient and the average of the splay and bend elastic constants. The material studied was 1.46% BDH1281 in 52% [47/53 FfE-9/11-EfF] + 48% [20/80 FfO-5/7-OCB].

It can be seen from Table 7.6 that the flexo-elastic ratio for this material is greater than that of the 3.45% BDH1281 in 50% [49/51 FfE-9/11-EfF] + 50% [19/81 FfO-5/7-OCB] material studied in Section 7.4.1. This agrees with observations made in both Chapters five and six, that when a lower concentration of chiral additive is used the measured value of the flexo-elastic ratio is greater.

7.5 Mixing the symmetric ester materials with monomesogens

In Section 7.4.1 it was theorised that it would be possible to create a liquid crystal material with good flexoelectric properties and a wide chiral nematic phase by mixing the symmetric ester materials which have large flexo-elastic coefficients, with materials possessing wide nematic phases. For the purpose of this work, it would be preferable that the new mixture is chiral nematic at room temperature and does not have an underlying smectic phase. To achieve this it was thought that using a monomesogen would be preferable to using a bimesogen, as there are an extraordinary number of monomesogenic materials available and it should be possible to find one that would be suitable for this work.

7.5.1 Mixing 7OCB with the symmetric ester bimesogens

Throughout this work the properties of the monomesogenic liquid crystal material 7OCB has been used as a reference point for comparison with the new materials that have been

investigated. As its properties are well known, 7OCB was chosen to be the first monomesogen to be mixed with the ester bimesogens. Initially, the properties of a mixture containing equal quantities of 7OCB and an ester bimesogen mixture was examined.

3.77% BDH1281 in 51% [49/51 FfE-9/11-EfF] + 49% 7OCB

This material was studied using optical microscopy and was found to exhibit the following phase sequences:

Isotropic –(65°C)-> **Blue Phases** –(61°C)-> **N*** –(>35°C)-> **Crystal** (On cooling)

Crystal –(42-56°C)-> **N*** –(63°C)-> **Blue Phases** –(65°C)-> **Isotropic** (On heating)

There appeared to be three blue phases present between the isotropic and chiral nematic phases. The material crystallises with time at lower temperatures in a manner similar to pure 7OCB. Once crystallised the material starts to melt on heating at 42°C but does melt completely until 56°C, this suggests that either the materials have not mixed completely or separation has occurred on crystallisation.

The uniformly lying helix geometry was easily achieved using the field ramping technique. The flexoelectro-optic properties were measured. The results are shown in Figure 7.12 along with the pitch, selective reflection wavelength and critical field measurements.

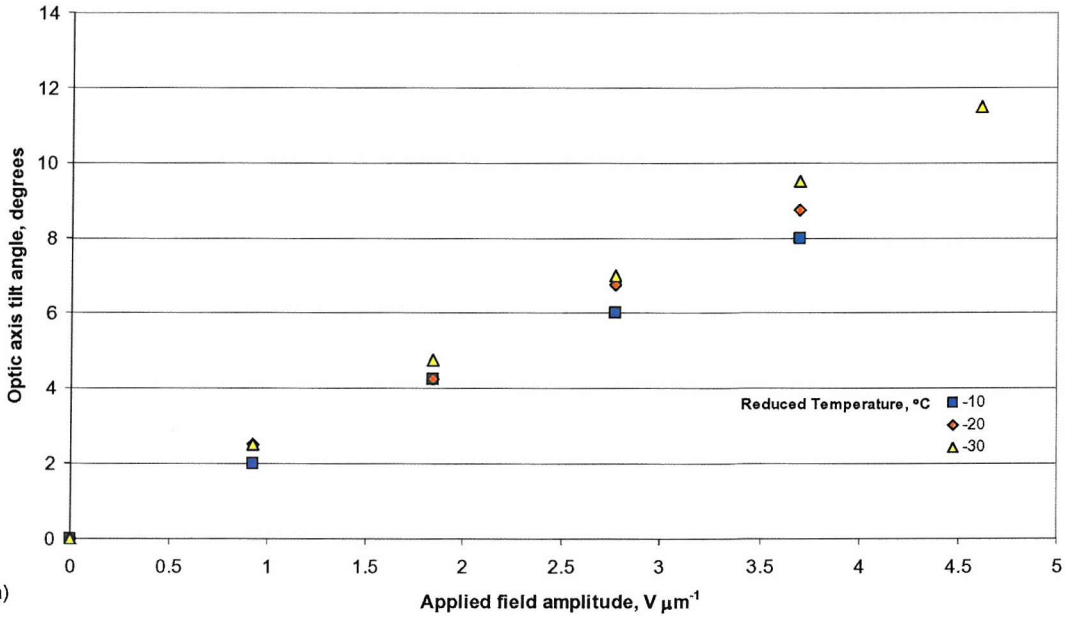

a)

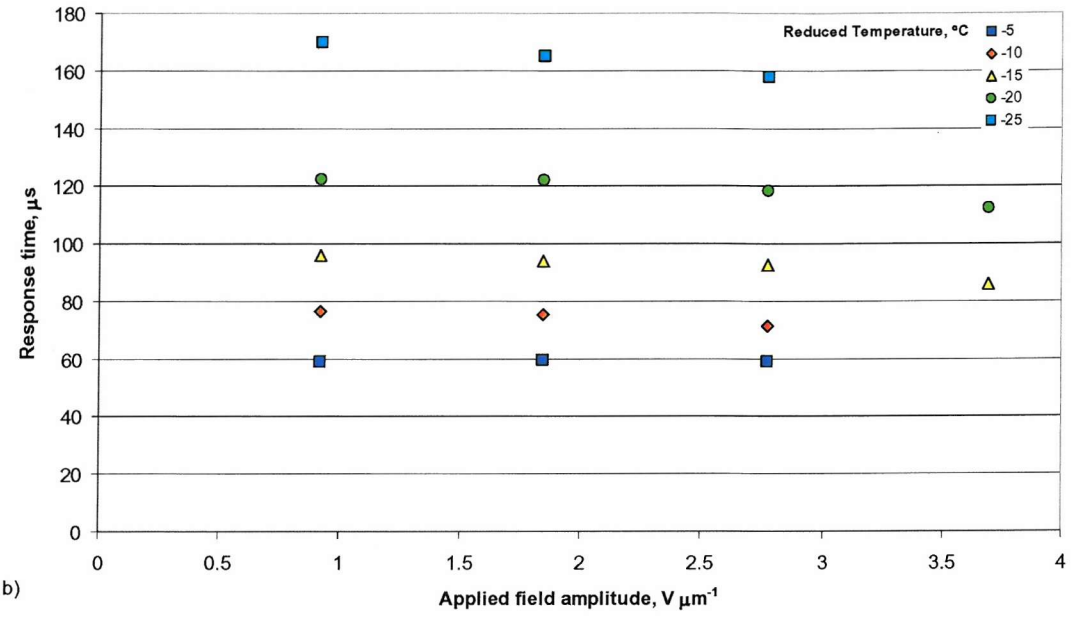
Reduced Temperature, °C
-5
-10
-15
-20
-25
Response time, µs
0
20
40
60
80
100
120
140
160
180
0
0.5
1
1.5
2
2.5
3
3.5
4
Applied field amplitude, V µm-1

b)

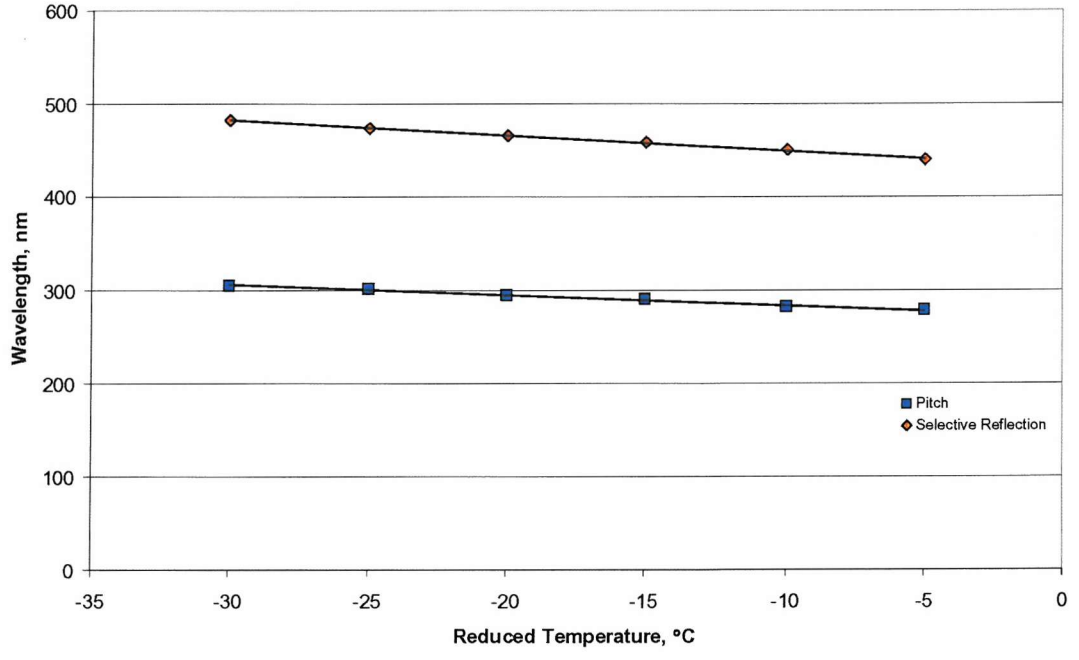
Wavelength, nm
0
100
200
300
400
500
600
-35
-30
-25
-20
-15
-10
-5
0
Reduced Temperature, °C
Pitch
Selective Reflection

c)

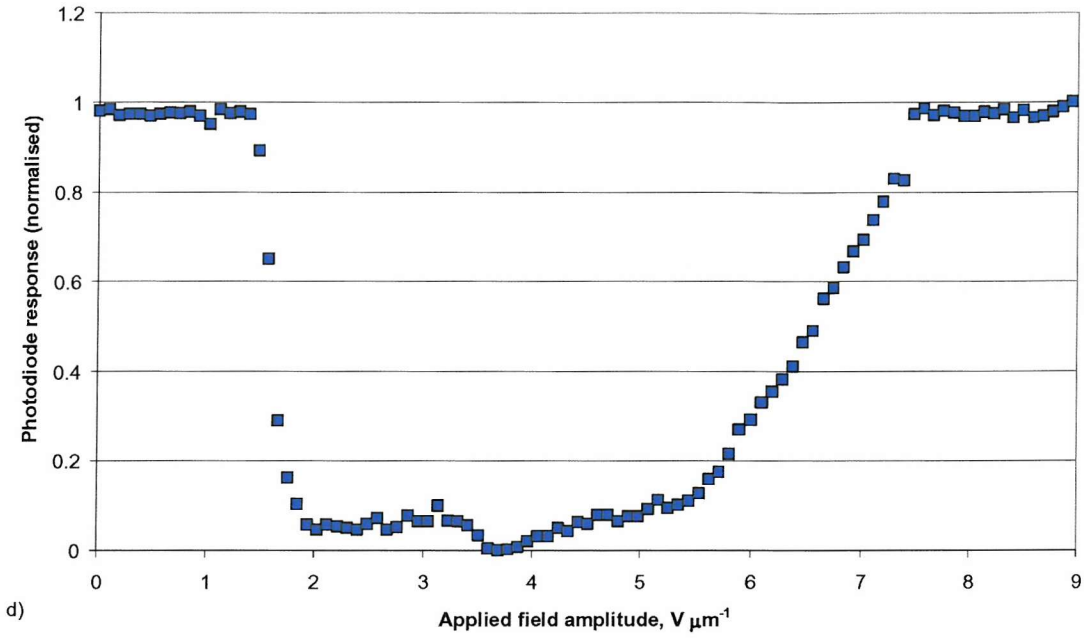

d)

Figure 7.12 The properties of a mixture of 3.77% BDH1281 in 51% [49/51 FfE-9/11-EfF] + 49% 7OCB (w/w). The graphs show a) the induced tilt angles, b) the response times, c) pitch and selective reflection wavelength, all measured across a range of reduced temperatures, and d) the critical field measurements. The response times are measured for 10-90% of the full switch of the optic axis, i.e. twice the tilt. The pitch was measured using a wedge cell of angle 0.027°. Trend-lines were added to guide the eye.

If the results in Figure 7.12 are compared with the results made using the material 3.91% BDH1281 in 7OCB, given in Section 3.6 the following observations are made:

- The maximum tilt angle measured at a reduced temperature of -30°C is 11.5° for the new material compared with 2.75° for the pure 7OCB material.
- The response times of the new material are up to 7 times slower than that of the pure 7OCB material.
- The critical field for the new material is 7.47 V/μm compared with 5.95 V/μm for the pure 7OCB material.

From the results of Figure 7.12 it is possible to calculate the flexo-elastic ratio and the average refractive index. The results are shown in Table 7.7.

Reduced Temperature, °C (T_c = 65°C)	$\Delta\tan\phi/\Delta E$, μm V^{-1}	Pitch, nm	Selective reflection wavelength, nm	$\bar{n}$	$\bar{e}/K$, C N^{-1} m^{-1}
-5	0.0342	278	440	1.58	0.77
-10	0.0381	282	451	1.60	0.85
-20	0.0415	294	466	1.58	0.89
-30	0.0449	305	483	1.58	0.92

Table 7.7 A comparison of the values at different reduced temperatures for the pitch, selective reflection and the calculated values for the average refractive index and the ratio of the effective flexoelectric coefficient and the average of the splay and bend elastic constants. The material studied was 3.77% BDH1281 in 51% [49/51 FfE-9/11-EfF] + 49% 7OCB.

From Table 7.7 it can be seen that the flexo-elastic ratio of the ester bimesogen mixture is quite high, approximately twice that of the 3.91% BDH1281 in 7OCB material, and is comparable to the values obtained for the bimesogenic material 3.93% BDH1281 in 20%/80% FfO-7/9-OfF in Chapter 5.

3.51% BDH1281 in 79% [50/50 FfE-9/11-EfF] + 21% 7OCB

The properties of a new material that contains less 7OCB were measured for comparison with the 3.77% BDH1281 in 51% [49/51 FfE-9/11-EfF] + 49% 7OCB material. This material, containing 21% 7OCB, was studied using optical microscopy and was found to exhibit the following phase sequence:

Isotropic –(65°C)-> **Blue Phases** –(61°C)-> **N*** –(34°C)-> **Crystal** (On cooling)

There appeared to be three blue phases present between the isotropic and chiral nematic phases. The material crystallises with time at lower temperatures, it tends to crystallise more rapidly than the material containing more 7OCB. On heating the crystal starts to melt in to the chiral nematic phase at 40°C but only melts completely at 69°C, which is above the nematic to isotropic phase transition. This would again suggest that the monomesogen and ester bimesogens are separating on crystallisation.

The uniformly lying helix geometry was easily achieved using the field ramping technique and the flexoelectro-optic properties were then measured. The results are shown in Figure 7.13 along with the pitch, selective reflection wavelength and critical field measurements.

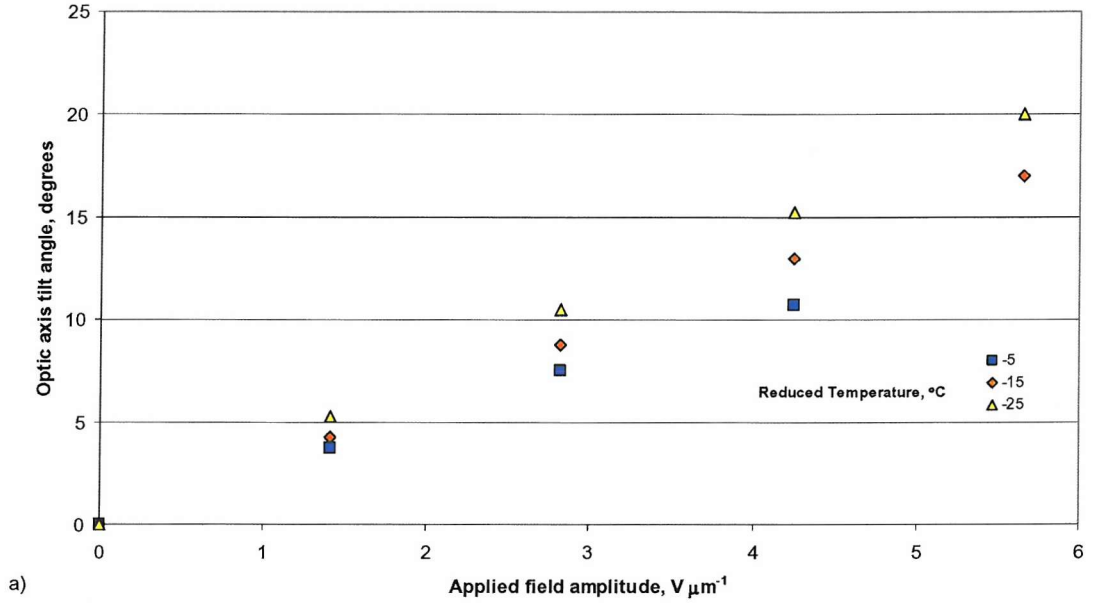

a)

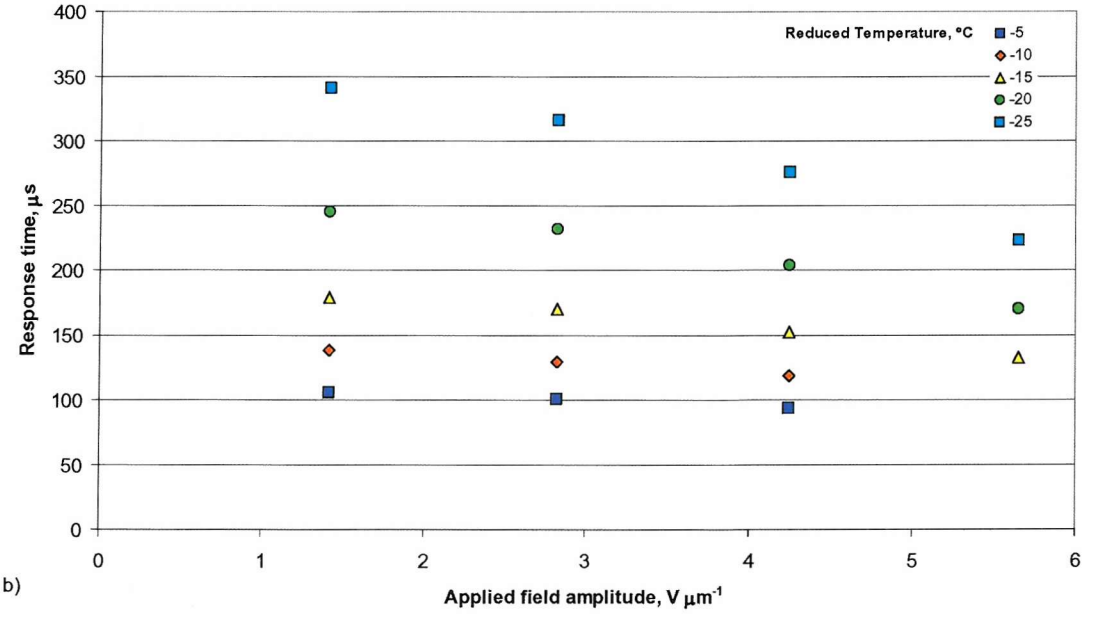

b)

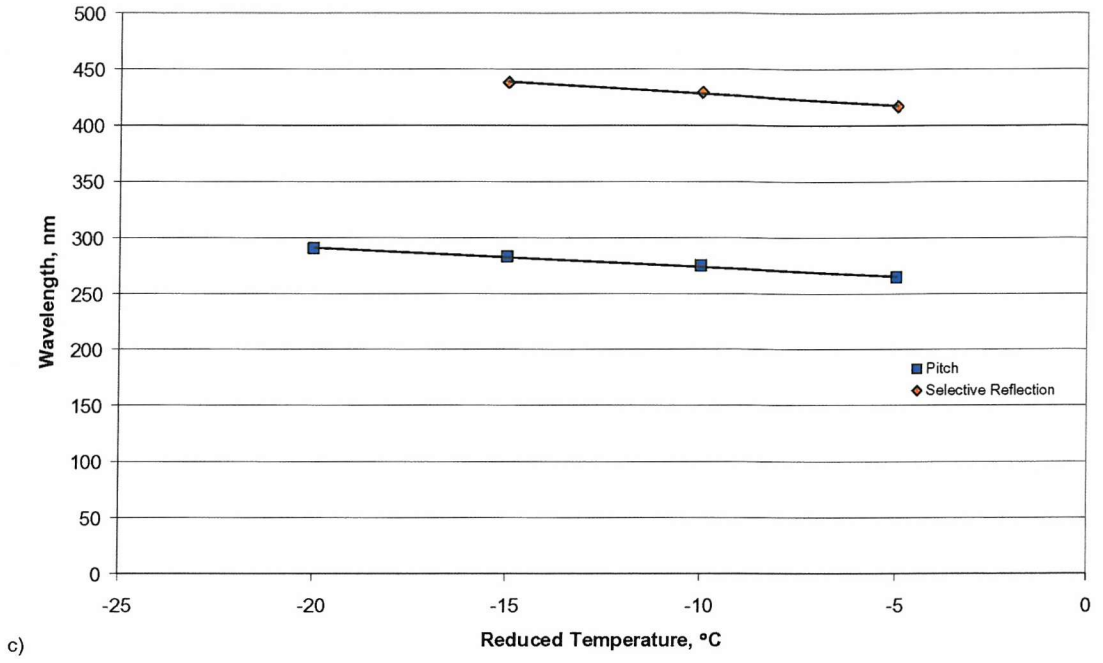

c)

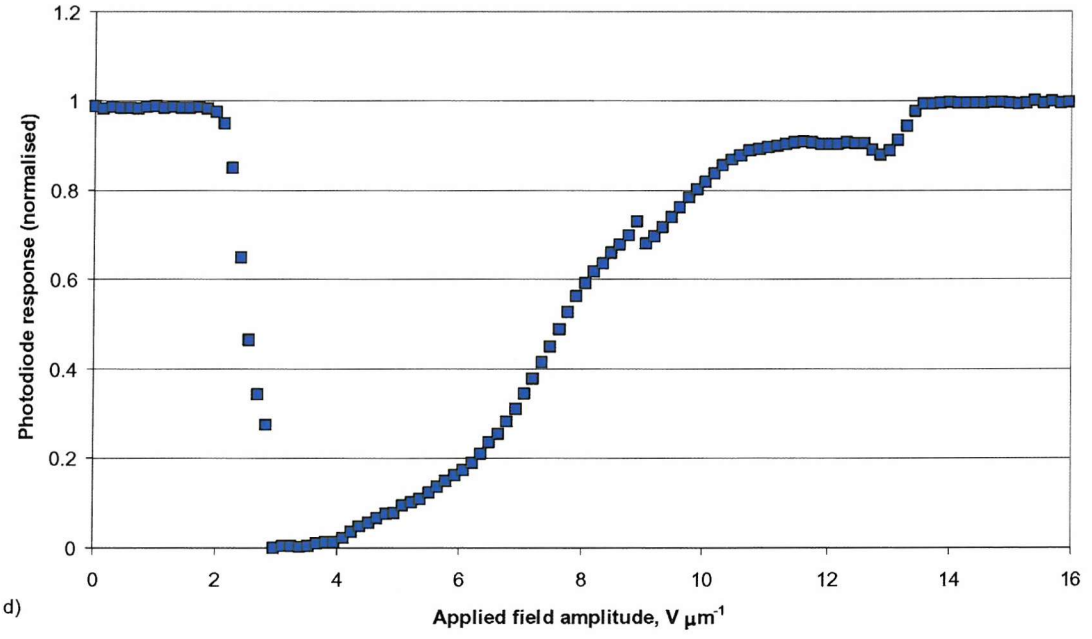

d)

Figure 7.13 The properties of a mixture of 3.51% BDH1281 in 79% [50/50 FfE-9/11-EfF] + 21% 7OCB (w/w). The graphs show a) the induced tilt angles, b) the response times, c) pitch and selective reflection wavelength, all measured across a range of reduced temperatures, and d) the critical field measurements. The response times are measured for 10-90% of the full switch of the optic axis, i.e. twice the tilt. The pitch was measured using a wedge cell of angle 0.030°. Trend-lines were added to guide the eye.

It was difficult to obtain a full set of results for the pitch and selective reflection wavelength because the material crystallises rapidly. The results show that at similar reduced temperatures, the maximum achievable tilt angles and response times are both roughly doubled (although the pitches of the mixtures are similar) when compared to the 3.77% BDH1281 in 51% [49/51 FfE-9/11-EfF] + 49% 7OCB material. From the data shown in of Figure 7.13 it was possible to calculate the flexo-elastic ratio and the average refractive index; the results are shown in Table 7.8.

Reduced Temperature, °C (T_c = 65°C)	$\Delta\tan\phi/\Delta E$, μm V^{-1}	Pitch, nm	Selective reflection wavelength, nm	$\bar{n}$	$\bar{e}/K$, C N^{-1} m^{-1}
-5	0.0450	264	417	1.58	1.07
-10	0.0501	275	430	1.56	1.14
-15	0.0544	283	438	1.55	1.21
-20	0.0585	290	-	-	1.27
-25	0.0643	299*	-	-	1.35

Table 7.8 A comparison of the values at different reduced temperatures for the pitch, selective reflection and the calculated values for the average refractive index and the ratio of the effective flexoelectric coefficient and the average of the splay and bend elastic constants. The material studied was 3.51% BDH1281 in 79% [50/50 FfE-9/11-EfF] + 21% 7OCB.

* - estimated from trend line.

From Table 7.8 it can been seen that the flexo-elastic ratio is higher than that of the previous material, which contains a higher proportion of 7OCB, and is comparable to the values for the symmetric materials and the non-symmetric materials in Chapters five and six respectively.

It was hypothesised that it would be possible to improve the liquid crystalline properties of the symmetric ester bimesogens by the addition of a monomesogen with good liquid crystalline properties and, although the test materials appear not to be completely miscible, this approach seems to be promising. The flexo-elastic ratio of the new mixtures are lower than those observed for the symmetric ester bimesogens but are significantly greater than those observed for 7OCB. The critical field of the new mixtures are less than for the

symmetric ester bimesogens and are lowest when containing a greater concentration of 7OCB as would be expected, given the higher dielectric anisotropy of the monomesogen. In contrast, the response times of the symmetric ester bimesogens decrease rapidly as a greater concentration of 7OCB is incorporated. In fact, the response of one of the bimesogen-monomesogen mixtures is over three times faster than that of the host bimesogen material (although it is slower than the response of 7OCB at similar temperatures) because the viscosity of the material is reduced by the addition of a monomesogen. The stability of the liquid crystal phase also increases in relation to the amount of the 7OCB monomesogen present.

Although the flexo-elastic ratios are comparable to those seen in Chapters five and six, the maximum tilt angles are smaller. This is because dielectric coupling occurs at a lower applied field for the materials studied in this section; since 7OCB has a significantly higher dielectric anisotropy than the bimesogens. As a result it was decided to investigate a material with a low dielectric anisotropy.

7.5.2 Mixing the symmetric ester bimesogens with a low dielectric anisotropy material

A low dielectric anisotropy material known as TL226 from Merck[3] was chosen because it has a nematic phase which crystallises below 0°C and a clearing temperature of 86°C. TL226 was known to have a dielectric anisotropy of less than 5 which is comparable to that of the non-symmetric bimesogens (see Chapter six). A mixture of 55% TL226 and 45% [48/52 FfE-9/11-EfF] doped with 3.47% BDH1281 was produced so as to allow the flexoelectric properties to be studied.

The new mixture had a clearing temperature of 73°C and was found to have a chiral nematic phase down to room temperature. A sample of the material was crystallised in a fridge (at 2°C) and then studied under the microscope to find the melting temperature. The material was found to start melting into the nematic phase at 35°C but did not completely melt until 54°C. This is similar to the observations made in the previous section (i.e. when mixing the symmetric ester bimesogens with 7OCB), which suggests that the materials used here are not completely miscible.

The material was aligned in the uniformly lying helix geometry by cooling rapidly from the isotropic phase under an applied field. The flexoelectro-optic switching properties were

measured along with the selective reflection wavelengths. The results are shown in Figure 7.14.

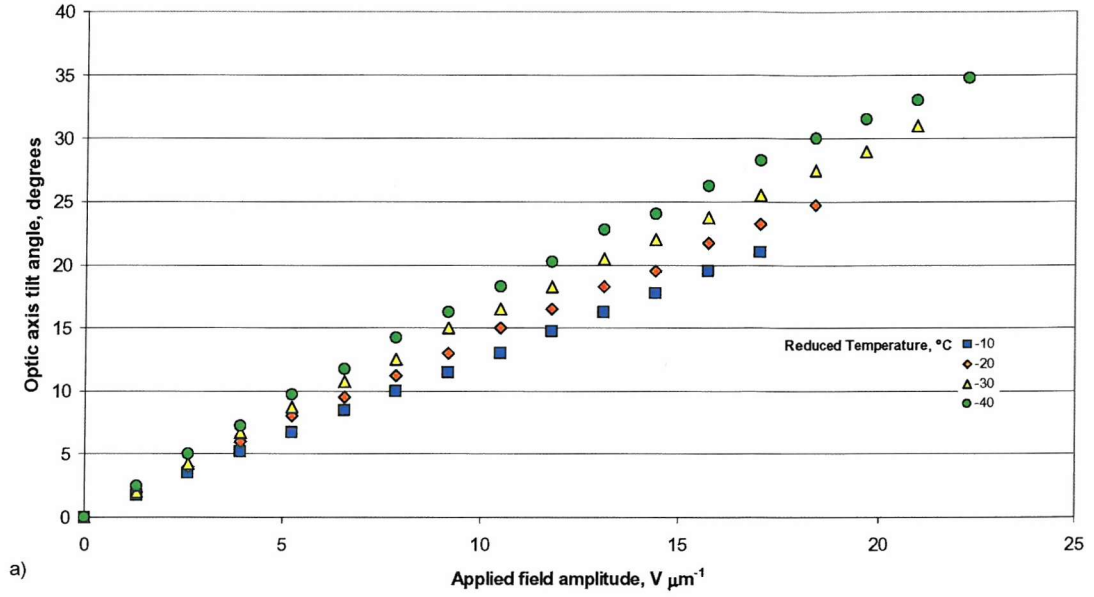

a)

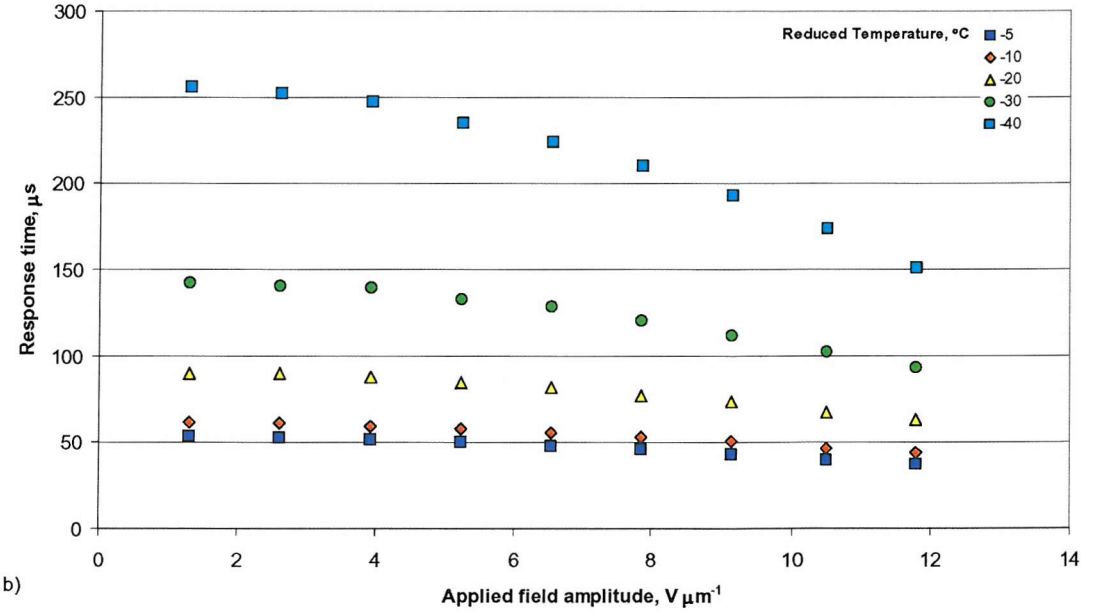

b)

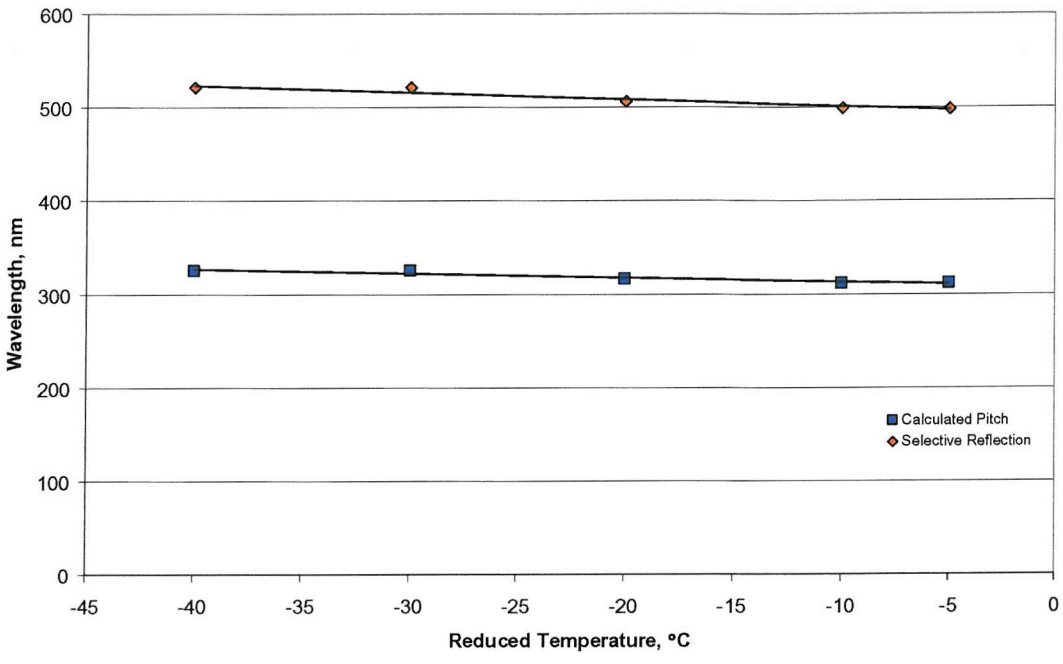

c)

Figure 7.14 The properties of a mixture of 3.47% BDH1281 in 45% [48/52 FfE-9/11-EfF] + 55% TL226 (w/w). The graphs show a) the induced tilt angles, b) the response times and c) the calculated pitch and selective reflection wavelength, all measured across a range of reduced temperatures. The response times are measured for 10-90% of the full switch of the optic axis, i.e. twice the tilt. The pitches were calculated from the selective reflection wavelengths using a value of 1.60 for the average refractive index. Trend-lines were added to guide the eye.

From Figure 7.14 it can be seen that tilt angles of up to 35° can be achieved slightly above room temperature with response times less than 300μm. Unfortunately the applied electric fields required to achieve these tilt angles are high.

The data in Figure 7.14 can be used to calculate the flexo-elastic ratio. The results of which are shown in Table 7.9.

Reduced Temperature, °C (T_c = 73°C)	$\Delta\tan\phi/\Delta E$, μm V^{-1}	Selective reflection wavelength, nm	Pitch (calculated), nm	$\bar{e}/K$, C N^{-1} m^{-1}
-5	0.0211	499	312	0.43
-10	0.0222	500	313	0.45
-20	0.0249	507	317	0.49
-30	0.0280	521	326	0.54
-40	0.0311	521	326	0.60

Table 7.9 A comparison of the values at different reduced temperatures for the selective reflection and the calculated values for the pitch and the ratio of the effective flexoelectric coefficient and the average of the splay and bend elastic constants. The material studied was 3.47% BDH1281 in 45% [48/52 FfE-9/11-EfF] + 55% TL226.

The flexo-elastic ratio of this mixture is quite low; it is comparable to that of 7OCB. As a result of the low flexo-elastic ratio the tilt angle per unit field is quite low. However because of the mixture's low dielectric anisotropy, it is possible to achieve high tilt angles because high electric fields may be applied without dielectric coupling disrupting the lying helix alignment.

It was decided to try measuring the flexoelectric properties of TL226 by doping it with the chiral additive BDH1281. It was found that TL226 exhibits barely any observable flexoelectro-optic switching. This means that TL226 dilutes the flexoelectric properties of any material it is mixed with, hence the low flexo-elastic ratio observed in Table 7.9.

7.6 Conclusions

The aim of the work presented in this chapter was to increase the flexoelectric properties of the symmetric fluorobiphenyl bimesogens (see Chapter 5) by increasing the dipole moment of the end groups. It was thought that the addition of an unsaturated ester linkage would increase the dipole moment and therefore, give improved flexoelectric properties; however it was considered likely that this addition would have a negative effect on the liquid crystallinity of the materials as it would reduce the shape anisotropy.

Five homologues of the new symmetric ester bimesogens were synthesised and it was found that only three of the homologues exhibited mesophases and that they were monotropic. The most promising course of action was to make a mixture of two of these

homologues in an attempt to increase the stability and temperature range of the mesophases. One mixture between the FfE-9-EfF and FfE-11-EfF had increased the stability, but the mixture was monotropic. The new mixture was doped with chiral additive to induce chirality in the system and the flexoelectro-optic properties were studied. The mixture showed high tilt angles (>30°) and was found to have a very high flexo-elastic ratio (1.74 C N^{-1} m^{-1}); significantly greater than that of the original symmetric fluorobiphenyl bimesogens on which these new materials were based (0.86-1.15 C N^{-1} m^{-1}). As hypothesised, the addition of unsaturated ester linkages has improved the flexoelectric properties but reduced the liquid crystallinity of the symmetric fluorobiphenyl bimesogens.

As these new symmetric ester bimesogens had low liquid crystallinity it was decided to mix them with the non-symmetric bimesogens studied in Chapter 6. It was predicted that the non-symmetric bimesogens, which had wide nematic phases and were enantiotropic, would complement the symmetric ester bimesogens and produce a mixture with high flexoelectric properties and stable nematic phases. A chiral mixture of 50% non-symmetric bimesogen and 50% symmetric ester bimesogen was found to have a nematic phase of over 40°C; however the mixture did display an underlying smectic phase. The flexoelectro-optic properties of the mixture were studied and the flexo-elastic ratio was found to increase from 1.33 C N^{-1} m^{-1} to 1.95 C N^{-1} m^{-1} as the temperature was reduced, in agreement with the observations made in Chapters 5 and 6. It was possible to measure tilt angles up to 66° near the nematic to smectic phase transition, although at this temperature the pitch of the materials is long, due to the rapid helix unwinding that occurs a few degrees above the transition.

Two new mixtures were made with different concentrations of the non-symmetric bimesogens and the symmetric ester bimesogens. One material was made with a greater concentration of the non-symmetric bimesogens and one with a greater concentration of the symmetric ester materials. The transition temperatures of these new mixtures and the mixture discussed in the previous paragraph are shown below:

1) 3.45% BDH1281 in 50% [49/51 FfE-9/11-EfF] + 50% [19/81 FfO-5/7-OCB]

Isotropic –(85°C)-> **Blue Phases** –(80°C)-> **N*** –(33°C)-> **SmX***

2) 3.47% BDH1281 in 28% [50/50 FfE-9/11-EfF] + 72% [20/80 FfO-5/7-OCB]

Isotropic –(96°C)-> **Blue Phases** –(92°C)-> **N*** –(38°C)-> **SmX***

3) 3.44% BDH1281 in 74% [50/50 FfE-9/11-EfF] + 26% [19/81 FfO-5/7-OCB]

Isotropic –(74°C)-> **Blue Phases** –(72°C)-> **N*** –(30°C)-> **SmX***

It can be seen that the clearing temperatures and smectic phase transition temperatures increase with the concentration of the non-symmetric bimesogens present. It was found that for the mixture which contained a significantly greater concentration of the symmetric ester bimesogens (in this case mixture 3) would crystallise at temperatures below 64°C and once crystallised would melt to the nematic phase above this temperature. The flexoelectric properties of the three materials were compared and it was found that the mixture containing a greater proportion of the symmetric ester bimesogens had the largest flexo-elastic ratio (see Figure 7.9) ranging from 1.41 C N^{-1} m^{-1} to 2.20 C N^{-1} m^{-1} as the temperature was reduced. This is to be expected as the symmetric ester bimesogens have a greater flexo-elastic ratio than the non-symmetric bimesogens.

It has been shown that it is possible to produce a material with a high flexo-elastic ratio and a wide nematic phase by mixing the non-symmetric bimesogens with the symmetric ester bimesogens in the right concentrations, as predicted.

In Chapters 5 and 6, it was seen that when less chiral dopant is present in a mixture the flexo-elastic ratio of the mixture is greater than when more dopant is present. If the flexo-elastic ratio is increased then the tilt angle per unit field would be increased. As a result of this, it was considered of interest to examine the 50% non-symmetric bimesogen and 50% symmetric ester bimesogen mixture previously studied, with less chiral dopant. The new mixture was seen to have the largest tilt angle per unit field of any mixture studied in this work, requiring as low as 2 V/μm for total switching angle of 45°. It was seen for the same bimesogen mixture (with a greater concentration of chiral dopant) that a few degrees above the smectic phase transition it was possible to observe a 66° tilt angle. Under the same conditions the new material was observed to exhibit an 80° switch. The flexo-elastic ratio of the new mixture was found to increase from 1.36 C N^{-1} m^{-1} to 2.35 C N^{-1} m^{-1} as the temperature was reduced.

An aim of this work was to develop a stable room temperature material with good flexoelectric properties. In an attempt to achieve this goal the symmetric ester bimesogens were mixed with a monomesogen. To examine the viability of this method 7OCB was chosen as a test material and two chiral mixtures were made. The two mixtures were

approximately a 1:1 and 1:4 mixtures of 7OCB and the symmetric ester bimesogens, respectively. Both mixtures exhibit wide nematic phases on cooling, however they both had a temperature below which they would crystallise. On heating, the 1:1 mixture was found to start melting at 42°C but not melt completely until 56°C, the 1:4 mixture was found to show similar behaviour; however it only partially melts in to the nematic phase before it enters the isotropic phase. From these observations it was hypothesised that the materials do not mix completely. The flexoelectro-optic properties of the two new mixtures were studied and it was found that their flexo-elastic ratios were comparable to that of the symmetric fluorobiphenyl bimesogens studied in Chapter 5. However the maximum achievable tilt angles are not as high as those of the symmetric fluorobiphenyl bimesogens because the dielectric anisotropy of the mixture is much greater and as a result the onset of helix unwinding occurs at low fields. The response times of the new mixtures are at least twice as fast as the symmetric ester bimesogens and at least eight times faster than the mixtures between the symmetric ester bimesogens and the non-symmetric bimesogens. The faster response times are a consequence of using monomesogens, which tend to have lower viscosities than bimesogens.

Mixing the symmetric ester bimesogen with the monomer 7OCB was a partial success; a material with a good flexo-elastic ratio was produced and was seen to be nematic below 35°C. However, the bimesogens and monomesogen do not appear to mix completely and separate on crystallisation. Another consequence of using these mixtures is that the dielectric anisotropy is quite high and as a result the onset of helix unwinding occurs at a reasonably low applied electric field.

After the study into mixing the symmetric ester bimesogens with 7OCB, it was decided to try a different monomesogen, one with a low dielectric anisotropy. A material known as TL226 was used because it has a low dielectric constant and a wide nematic phase ranging from 86°C to below 0°C. The new chiral mixture was found to exhibit a nematic phase to below room temperature. The mixture was found to have a low flexo-elastic ratio (0.43-0.60 C N^{-1} m^{-1}) and as a result the tilt angle per unit field is low. However, due to the low dielectric anisotropy of the mixture, tilt angles up to 35° were observed at close to room temperature. The response times of the new mixture are close to three times faster than for the symmetric ester bimesogens at similar temperatures. The flexo-elastic of this new mixture is low because the flexo-elastic ratio of TL226 is extremely low, so it drastically dilutes the flexoelectric properties of the symmetric ester bimesogens. As observed

previously for the mixture containing 7OCB, the symmetric ester bimesogen and TL226 were found not to be completely miscible.

References

1 Meyer, R. B., Phys. Rev. Lett., **22(18)** 918 (1969)

2 Vorlander, D., Kristalinisch-flussige Substanzen (1908)

3 Merck NB-C, Southampton, UK

4 Mettler-Toledo Thornton Inc., Bedford, MA, USA

5 Noot, C., Perkins, S., and Coles, H. J., Ferroelectrics **244** 631 (2000)

Chapter Eight

8 Concluding Remarks

8.1 Summary of the thesis

The objective of this thesis was to examine the flexoelectric[1] properties of bimesogenic liquid crystals. The method for examining the flexoelectric properties was to utilise a flexoelectric switching process known as the flexoelectro-optic effect.[2] The flexoelectro-optic effect allows the flexo-elastic ratio, $\bar{e}/K$, of a chiral nematic material to be calculated and it is the flexoelectric switching process that shows the most promise for applications.

This work is primarily concerned with the nematic phase, in particular the chiral nematic phase. The optical properties of the chiral nematic phase under a number of conditions were introduced and discussed in Chapter 2. The effects of dipolar and flexoelectric coupling of the chiral nematic phase to an electric field were discussed in some detail, with flexoelectric coupling being of primary interest. Results and theoretical treatments of flexoelectricity from the literature were introduced and discussed. The mechanism of the flexoelectro-optic switching process in the uniformly lying helix geometry was then introduced and the theoretical model for this process was discussed.

Chapter 3 introduced the experimental equipment and methods used to study the flexoelectro-optic properties and other relevant properties of the chiral nematic liquid crystal phase. In the second part of Chapter 3, the flexoelectro-optic properties of the commercially available nematic liquid crystal 7OCB were studied and related to the physical properties of the material. To study the flexoelectro-optic properties it was necessary to introduce chirality into 7OCB, this was done through the use of a high twisting power chiral additive. The flexoelectric properties of 7OCB were found to quite small and comparable to previously published literature values.

In Chapter 4, two contrasting methods for measuring the flexoelectric properties were compared. One method used the flexoelectro-optic effect that was introduced in Chapter 2

and applied in the latter part of Chapter 3. The second method used the more common hybrid aligned nematic (HAN) method.[3] The HAN method only works for achiral nematic liquid crystal materials; conversely, the flexoelectro-optic method requires a chiral nematic liquid crystal material. A selection of achiral nematic liquid crystal materials were chosen for study. It was easy to implement the HAN method to examine their flexoelectric properties. The flexoelectro-optic method for measuring their flexoelectric properties was made practical by doping the achiral nematic materials with a low concentration of high twisting power chiral dopant. In those cases where it was possible to implement both methods for determining the flexoelectric properties, it was found that the values of the measured flexoelectric parameters were comparable. In the course of this investigation, it was discovered that the HAN method could not be used to measure the flexoelectric properties of a bimesogenic-based mixture because the mixture would not adopt the alignment geometry required. In fact, it was found that none of the bimesogens studied in this work would adopt a homeotropic geometry on any of the alignment layers available. The flexoelectro-optic method was found to work for bimesogens as well as monomesogens and was found to be more sensitive.

The symmetric bimesogenic liquid crystal materials consisting of two oxy-biphenyl mesogenic groups[4] were introduced and examined in Chapter 5. A homologous series of the oxy-biphenyl bimesogens was synthesised and studied. Optical microscopy showed that the pure homologues exhibited either no mesophases or mesophases that exist over a very small temperature range. As a result of this it was decided to try mixing pairs of the homologues. Three monotropic mixtures were produced, which could be super-cooled into the nematic phase. Chirality was introduced into the bimesogenic mixtures by using a high twisting power chiral additive. The flexoelectro-optic properties of the new mixtures were studied with the material aligned in the uniformly lying helix geometry. All three mixtures showed good flexoelectro-optic properties and the flexo-elastic ratio was found to range from 0.86 to 1.15 C N^{-1} m^{-1}. Tilt angles exceeded 30° were observed. The response times of the mixtures ranged from 300μs to 2.4ms, as a function of reduced temperature.

One of the reasons for using bimesogenic liquid crystal materials was that they were expected to have low dielectric anisotropies. In the case of the chiral mixtures studied in Chapter 5, it was impossible to unwind the helix fully with the maximum available applied field. This observation indicates that the symmetric bimesogens possess a low dielectric anisotropy.

Following this work, the aim was now to synthesise a bimesogenic liquid crystal material with an enantiotropic nematic phase. Previously in the literature[5] it was shown that a symmetric oxy-cyanobiphenyl bimesogen has reasonable flexoelectric properties and a wide nematic phase. It was hypothesised that by replacing one of the oxy-fluorobiphenyl mesogenic units on the bimesogenic materials studied in Chapter 5 with an oxy-cyanobiphenyl mesogenic unit an improvement in the nematic range of the material may be produced. It was also hoped that these new materials may have greater flexoelectric properties. A homologous series based on the new molecular template was synthesised and its properties were studied in Chapter 6. By optical microscopy it was found that the new homologues exhibited enantiotropic mesophases, with temperature ranges from 2°C to 40°C wide. Chirality was introduced in the materials by doping with a high twisting power chiral additive. The mixtures were aligned into the uniformly lying helix geometry and the flexoelectro-optic properties were studied. It was found that the mixtures based on the homologues with an odd number of carbon atoms in the spacer group had a high flexo-elastic ratio (1.2 - 1.5 C N^{-1} m^{-1}), exceeding that of the symmetric bimesogens studied in Chapter 5. In contrast, it was found for the mixtures based on the homologues with an even number of carbon atoms in the spacer that the flexo-elastic ratio was much lower (0.44 - 0.55 C N^{-1} m^{-1}), which is comparable to the flexo-elastic ratio of 7OCB. It was hypothesised that the odd-even trend observed in the flexo-elastic ratio may be in part due to a significant odd-even effect in the elastic constants, as reported in the literature.[6] Measurements of the splay and twist elastic constant do show a significant odd-even trend; however, if it is assumed that $K_{11} \approx K_{33}$ then the difference is the elastic constants is not large enough to explain the difference between the flexo-elastic ratios. Thus, it is thought that there may be a difference in the average of the splay and bend flexoelectric parameters $\bar{e}$ between the homologues with an odd or even number of carbon atoms in the spacer group.

In Chapter 5 it was seen that combining pairs of bimesogenic homologues produced mixtures with larger nematic phase ranges. It was decided to try this approach using the new non-symmetric bimesogens. Four mixtures of different concentrations were made between two of the homologues. It was found that the nematic phase ranges of the new mixtures where significantly larger than those of the pure component homologues. The two pure homologues chosen for use in this study have different flexo-elastic constants. Interestingly, a graph of the flexo-elastic ratio as a function of the concentration of one of the homologues in the other does not show a smooth variation in flexo-elastic ratio but instead shows a discontinuity. Also, one of these new mixtures has a greater flexo-elastic

ratio than either of the pure component homologues on their own. Thus it would appear using mixtures can both increase the temperature range of the nematic phase and show an increased flexo-elastic ratio when compared to the component homologues.

In Chapter 7, a new series of bimesogenic materials are studied. The new materials are a molecular modification of the symmetric bimesogens, effected by introducing ester linking groups. It was hypothesised that the ester linking groups would increase the dipole moment of the mesogenic groups, thus improving the flexoelectric properties of the molecules. However, it was also thought that the addition of the ester linking groups would decrease the liquid crystallinity of the materials because the shape of the molecule is changed detrimentally.

A series of homologues was synthesised. Upon optical observation it was found that only three of the homologues exhibited mesophases and that they were monotropic and crystallised quickly. As in Chapters 5 and 6, it was decided to mix two of the homologues together to try and improve the nematic phase range. This was found to produce a slightly more stable, although still monotropic, nematic phase. As in previous chapters, chirality was introduced in to the mixture by using a high twisting power chiral additive. The mixture was aligned into the uniformly lying helix geometry and its flexoelectro-optic properties were studied. The mixture showed high tilt angles (>30°) and was found to have a very high flexo-elastic ratio (1.74 C N^{-1} m^{-1}); significantly greater than that of the original symmetric fluorobiphenyl bimesogens on which these new materials were based.

As this new symmetric ester bimesogenic mixture had a nematic phase with a small temperature range, it was decided to combine the new mixture with the mixture of two non-symmetric homologues studied in Chapter 6 to produce an enantiotropic mixture with a wide nematic temperature range and a large flexo-elastic ratio. Three different mixtures were made containing different concentrations (28%, 50% and 74% weight/weight) of the symmetric ester bimesogenic mixture in the non-symmetric bimesogen host mixture. The new mixtures exhibit nematic phases super-cooled through 40°C and have an underlying smectic phase. The new mixtures were found to have very large flexo-elastic ratios, up to 2.20 C N^{-1} m^{-1} for the mixture containing the largest concentration of symmetric ester bimesogens.

As the symmetric ester bimesogens displayed such a high flexo-elastic ratio, the effects of mixing them with a monomesogen were investigated. Two different mixtures between the symmetric ester bimesogens and 7OCB were studied. The first mixture

contained equal parts of the symmetric ester bimesogens and 7OCB and the second contained four times as much of the symmetric ester bimesogens as 7OCB. The flexoelectro-optic properties of the two mixtures were studied and it was found that their flexo-elastic ratios were comparable to that of the symmetric fluorobiphenyl bimesogens studied in Chapter 5. However, the maximum achievable tilt angles are not as high as those of the symmetric fluorobiphenyl bimesogens because the dielectric anisotropy of the mixture is much greater and as a result the onset of helix unwinding occurs at low fields. As monomesogens generally have lower viscosities than bimesogens, it is no surprise to find that the response times of the new mixtures are significantly faster than for pure bimesogenic mixtures. However, the bimesogens and monomesogen do not appear to mix completely and separate on crystallisation.

As the dielectric anisotropy of 7OCB is quite high ($\Delta\varepsilon \sim 8$), it was decided to try mixing the symmetric ester bimesogens with a different low viscosity material possessing a low dielectric anisotropy. TL226 was chosen for use because it has a low dielectric constant and a wide nematic phase ranging from 86°C to below 0°C. The mixture was found to have a low flexo-elastic ratio (0.43-0.60 C N^{-1} m^{-1}) and as a result the tilt angle per unit field is low. However, due to the low dielectric anisotropy of the mixture, very high fields could be used to induce tilt angles of up to 35°, close to room temperature. As was observed with the 7OCB mixtures, the response times of the new mixture were faster than that of a mixture containing only bimesogenic host components. The symmetric ester bimesogenic host and TL226 were found not to be completely miscible.

In Chapters 5, 6 and 7, there were two interesting observations concerning the bimesogenic mixtures: as the sample temperature was reduced, the flexo-elastic ratio increased; and the flexo-elastic ratio decreases as a greater concentration of chiral dopant is incorporated into the mixture.

The behaviour of the flexo-elastic ratio as a function of temperature does not appear to be explained fully by the simple theory that was developed to describe flexoelectro-optic switching. It is thought either the behaviour of $\bar{e}$ or K as a function of temperature deviates from varying with temperature as the square of the order parameter, as the theory predicts. In Chapter 6, this trend was only observed for mixtures based on the homologues containing an odd number of carbon atoms in the spacer group. The splay elastic constant as a function of temperature was measured for one of these homologues and was found to behave as expected, namely showing an order parameter squared dependence. This suggests that either $\bar{e}$ or the bend elastic constant has a temperature

dependence that does not rely solely on the temperature variation of the square of the order parameter.

It was observed that when the concentration of chiral additive is varied, the pitch and flexoelectro-optic properties also change. The tilt angles, response times and pitch were all found to be lower for the mixtures containing a greater concentration of chiral additive, as would be expected. However, the decrease in the flexo-elastic ratio is not expected nor is it explained by theory. It is hypothesised that the reason for this unusual behaviour is that $\bar{e}$ and K depend on the order parameter in different ways. Thus, if the concentration of chiral additive changes the order parameter (as was seen in Chapter 3 for 7OCB) then the ratio of $\bar{e}$ and K would change.

Overall, it has been seen in this work that bimesogenic based liquid crystal compounds show very promising flexoelectro-optic switching properties. For example, tilt angles of 80° and response times of less than 100μs have been measured. The ability to alter the flexoelectro-optic properties of a mixture by changing its constituent components means it is possible to tailor mixtures for use in specific applications. In a crossed polariser based birefringence device, tilt angles exceeding 22.5° are not required but fast response times are advantageous. Thus, a mixture with a short pitch may be well suited to this application: the maximum tilt angles need only be 22.5° and, owing to the short pitch, response times would be short. It would also be possible to produce dichroic flexoelectric devices by incorporating fluorescent dyes into the mixture. These devices require a tilt angle of 45°, which has been shown to be achievable for a number of mixtures in this work. Some possible applications of flexoelectro-optic switching devices are as: molecular mirrors; phase elements; analogue switching devices; and displays. Additionally, mixtures with very high tilt angles per unit field could potentially be used in Liquid Crystal on Silicon (LCoS) devices.

8.2 Future work

This work raises a number of interesting questions about the flexoelectric properties of bimesogens. As was discussed in the previous section, the behaviour of the flexo-elastic ratio as a function of temperature and as a function of concentration of chiral additive needs further examination. A thorough investigation into the behaviour of the elastic constants (the bend elastic constant in particular) as a function of temperature would help explain the behaviour of the flexo-elastic ratio and give an insight into the behaviour of $\bar{e}$ with temperature. To explain the behaviour of the flexo-elastic ratio as the amount of chiral

additive is varied will probably require a theoretical examination of the behaviour of $\bar{e}$ as a function of the order parameter.

In terms of molecular structure, the author believes the synthesis of a homologous series combining the ester mesogenic group (studied in Chapter 7) with an oxy-cyanobiphenyl would produce an interesting molecule and would be a suitable step in continuing this work. It is hypothesised that these new molecules would be similar to those examined in Chapter 6 but with higher flexoelectric properties.

The length of the spacer group was seen to have a significant effect on the flexo-elastic ratio of the non-symmetric bimesogens studied in Chapter 6. However, a study into the flexibility of the spacer group could be very interesting. The effects of replacing the alkyl chain in the spacer group with a more rigid structure could provide a useful insight into mechanism of flexoelectric coupling in bimesogenic liquid crystals by providing an indication as to how the flexibility of a molecule affects its flexoelectric properties.

It was seen in Chapter 7 that the symmetric ester bimesogens are not very miscible with monomesogens. This has also been observed by the author for the bimesogens studied in Chapters 5 and 6. It would be very useful to investigate the miscibility of bimesogens in monomesogens, as small quantities of monomesogens could help improve the properties of the host material. For example, it may be possible by the addition of suitable additives to produce a lower viscosity mixture, increase the temperature range of the nematic phase or eliminate any underlying smectic phases.

References

1 Meyer, R.B., Phys. Rev. Lett. **22(18)** 918 (1969)

2 Patel, J. S., and Meyer, R. B., Phys. Rev. Lett. **58(15)** 1538 (1987)

3 Dozov, I., Martinot-Lagarde, Ph., and Durand, G., J. Physique Lett. **43** pp. 365 (1982)

4 Coles, H. J., Coles, M. J., Perkins, S., Musgrave, B., and Coates D., Bimesogenic Compounds and Flexoelectric Devices, EU Patent EP99119114 (1999)

5 Musgrave, B., Coles M. J., Perkins, S., and Coles, H. J., Mol. Cryst. Liq. Cryst. **366** 2587 (2001)

6 Dilisi, G. A., Terentjev, E. M., Griffin, A. C., and Rosenblatt, C., J. Phys. II **3(5)** 597 (1993)